ERINDA
workshop

organized by the CERN EN-STI group on behalf of the n_TOF Collaboration

CERN, Geneva, Switzerland - 1-3 October 2013

PROCEEDINGS

ERINDA

workshop

organized by CERN EN-STI group on behalf of the n_TOF Collaboration

CERN, Geneva, Switzerland - 1-3 October 2013

PROCEEDINGS

International Advisory Committee
T. Belgya (Ek, Hungary)
E. Gonzalez (CIEMAT, Spain)
F. Gunsing (CEA, France)
F.-J. Hambsch (IRMM, Belgium)
A. Junghans (HZDR, Germany)
B. Jurado (CENBG, France)
R. Nolte (PTB, Germany)
S. Pomp (TSL, UU, Sweden)

Workshop Organizing Committee
Enrico Chiaveri (Chairman)
Eric Berthoumieux
Marco Calviani
Carlos Guerrero
Géraldine Jean
Ayse Karatepe
Roberto Losito
Vasilis Vlachoudis

FOREWORD

The Final Scientific ERINDA Workshop was held at CERN fron 1st to 3rd October 2013.

The ERINDA project (European Research Infrastructure for Nuclear Data Applications) http://www.erinda.org/ aims for coordination of European efforts to exploit up-to-date neutron beam technology for novel research on advance concepts for nuclear fission reactors and the transmutation of radioactive waste.

The aim of ERINDA is to integrate all infrastructure-related aspects of nuclear data measurements and to provide access for external users to the participating facilities.

The ERINDA Consortium groups 14 institutions (from Belgium, Czech Republic, Finland, Romania, United Kingdom, France, Germany, Hungary, Sweden, and Switzerland) equipped with nuclear data measurement infrastructures. The workshop was organized under the auspices of the ERINDA project with its speakers having the project's full financial and scientific support.

The aim of the workshop was to bring together all the ERINDA members and representatives in order to summarize the activities undertaken during the course of this program funded by European Commission and to review the status of current and future projects endorsed by or developed during programs with ERINDA contributions.
The 26 oral presentations given during the workshop covered the participating European institutions latest up-to-date achievements in the field of nuclear data measurements.

As a concluding remark, as Chairman and on behalf of the Organizing Committee, I would like, first of all, to thank the European Commission for its support in organizing this workshop.
Special thanks also to the International Advisory Committee for their invaluable scientific advice, which enabled us to set up a very effective and comprehensive program.
I would like to express my gratitude to all the speakers for their outstanding contribution to the workshop's success, for their active participation, and the quality of their talks.
Final acknowledgment goes to the Workshop Organizing Committee, in particular to our workshop secretaries, Ayse Karatepe and Géraldine Jean, who greatly contributed to the success of this final event, thanks to their very professional and competent organization.

Dr E. Chiaveri
Spokesperson of the n_TOF Collaboration

TABLE OF CONTENTS

LIST OF PARTICIPANTS

Chiaveri Enrico   *Chairman of the Workshop, CERN,* Switzerland

Prof**. Heuer** Rolf   *Director-General of CERN, CERN,* Switzerland

Barros Silvia   *CERN*, Switzerland

Belgya Tamas   *Centre for Energy Research, Hungarian Academy of Sciences*, Hungary

Berthoumieux Eric   *CEA/IRFU*, France

Calviani Marco   *CERN*, Switzerland

Carjan Nicolae   *National Institute of Physics and Nuclear Engineering*, Romania

Cerutti Francesco   *CERN*, Switzerland

Chudoba Petr   *Nuclear Physics Institute of the ASCR, v. v. i.,* Czech Republic

Garbil Roger   *European Commission*, Belgium

Gonzalez Romero Enrique   *CIEMAT*, Spain

Gorelov Dmitry   *University of Jyväskylä,* Finland

Gross Birgit   *Helmholtz-Zentrum Dresden-Rossendorf*, Germany

Grosse Ekkard   *TU Dresden*, Germany

Guerrero Sanchez Carlos   *CERN*, Switzerland

Habova Sona   *Nuclear Physics Institute AS CR v.v.i.* , Czech Republic

Hambsch Franz-Josef   *EC-JRC-IRMM*, Belgium

Hannaske Roland   *Helmholtz-Zentrum Dresden-Rossendorf*, Germany

Junghans Arnd   *Helmholtz-Zentrum Dresden Rossendorf*, Germany

Jurado Apruzzese Beatriz   *CENBG*, France

Kauwenberghs K. Josepha   *EC-JRC-IRMM*, Belgium

Kilim Stanislaw   *National Centre for Nuclear Research*, Poland

Kögler Toni   *Helmholtz-Zentrum Dresden-Rossendorf*, Germany

Lantz Mattias   *Uppsala University,* Sweden

Leal Cidoncha Esther   *Universidade de Santiago de Compostela*, Spain

Lederer Claudia	*Johann-Wolfgang-Goethe Univ.,* Germany
Losito Roberto	*CERN*, Switzerland
Manousos Athanasios	*CERN,* Switzerland
Massarczyk Ralph	*Helmhotz-Zentrum Dresden-Rossendorf*, Germany
Mattera Andrea	*Uppsala University,* Sweden
Milazzo Paolo Maria	*INFN,* Italy
Montesano Simone	*CERN*, Switzerland
Negret Alexandru Liviu	*IFIN-HH*, Romania
Nolte Ralf	*PTB,* Germany
Oberstedt Andreas	*Fundamental Physics,* Sweden
Penttilä Heikki	*JYFL, University of Jyväskylä,* Finland
Pillon Mario	*ENEA*, Italy
Plompen Arjan	*EC-JRC-IRMM,* Belgium
Pomp Stephan	*Uppsala University*, Sweden
Prokofiev Alexander	*Uppsala University,* Sweden
Rossbach Matthias	*Forschungszentrum Juelich GmbH*, Germany
Schwengner Ronald	*Helmholtz-Zentrum Dresden-Rossendorf*, Germany
Szuta Marcin	*National Centre for Nuclear Research*, Poland
Tsinganis Andrea	*CERN / NTUA*, France
Valenta Stanislav	*Charles University*, Czech Republic
Vlachoudis Vasilis	*CERN*, Switzerland
Wagner Vladimir	*Nuclear Physics Institute of CAS*, Czech Republic
Weiss Christina	*CERN*, Switzerland
Wilson Jonathan	*IPN Orsay,* France

PROGRAMME

Tuesday, October 1

Session 1 (14:30 – 18:25)

E. Chiaveri	Welcome
F. J. Hambsch	ERINDA scientific results: Transnational Access Activities, Scientific Visits
A. Mattera	Measurement of the energy spectrum from the new neutron source planned for IGISOL
R. Heuer	Welcome by Prof. R. Heuer (CERN's General Director)
M. Pillon	An intense D-T fusion source, "The New Sorgentina"
T. Kögler	Preparations of fission experiments at nELBE
R. Hannaske	Neutron total cross sections measured at nELBE
M. Lantz	Design of neutron converter for measurement of neutron induced independent fission yields
C. Guerrero-Sanchez	An outlook on "Physics at the new CERN neutron beam line"

Wednesday, October 2

Session 2 (09:00 – 12:55)

A. Oberstedt	Measurements of prompt fission γ-rays and neutrons with lanthanide halide scintillation detectors
J. Wilson	Measurements of prompt γ-rays from fast-neutron induced fission with the LICORNE directional neutron source
E. Leal-Chindoncha	Study of fission fragments angular distribution of ^{234}U(n,f) at CERN n_TOF facility
A. Tsinganis	Measurement of the ^{240,242}Pu(n,f) cross section at the CERN n_TOF facility
D. Gorelov	Measurement of the isomeric yield ratios of fission products with JYFLTRAP
P. Chudoba	Measurement of cross-sections of Yttrium(n,xn) threshold reactions by means of γ spectroscopy
V. Wagner	Studies of (n,xn) cross-section in useful neutron activation detector material by the activation method
A. L. Negret	Attempts to infer the neutron inelastic cross sections using charged particle induced reactions
R. Schwengner	Inelastic scattering of fast neutrons from excited states in ^{56}Fe

Physics at the new CERN neutron beam line

C. Guerrero[1] on behalf of the n_TOF Collaboration (www.cern.ch/nTOF)
[1]CERN, Geneva, Switzerland

Abstract

A new neutron beam line (n_TOF EAR-2) is being built at CERN within the n_TOF facility. Compared to the existing 185 meters long time-of-flight beam line, the new one (which will operate in parallel) will feature a shorter flight of 20 meters, providing a 27 times more intense neutron flux extending from thermal to 300 MeV. The scientific program is now being discussed and the first detailed proposals will be refereed by February 2014. This contribution is devoted to present and discuss the expected performance of the facility, briefly, and the details of some of the first measurements foreseen for 2014 and 2015.

1   Introduction

The European Organization for Nuclear Research (CERN) has hosted an extensive scientific program in nuclear physics. In particular, state of the art physics with white neutron beams has been carried out since 2001 at the CERN neutron time-of-flight n_TOF facility. The existing n_TOF neutron beam line, known as EAR-1 and featuring a beam line of 185 meters, provides a high instantaneous intensity pulsed neutron beam covering the energy range from thermal (25 meV) to 1 GeV. The experiments performed since 2001 are mostly aimed at measuring neutron induced cross sections of interest in nuclear technology, astrophysics, basic physics and medicine. A detailed description of the n_TOF-EAR1 facility and a comprehensive list of the experiments performed can be found in [1] and the references therein.

The increasing interest of the scientific community and the increasingly demanding measurements requests from the nuclear technology and stellar nucleosynthesis communities have triggered the upgrade of the n_TOF facility with a new neutron beam line, which is now know as n_TOF EAR-2. The main improvements with respect to the existing EAR-1, which will run in parallel to EAR-2, is that having a flight path of only 20 meters will result in a much higher neutron flux, thus allowing for measurements of lower cross sections and samples with smaller masses. A brief description is given below, but more details are given in Ref. [2].

This contribution describes the new neutron beam line and report on its construction. The expected performance and the first experiments that shall be performed along 2014 and 2015 are also summarized.

2   The new neutron beam line n_TOF EAR-2

2.1   Design and construction

The new experimental hall, at the end of a new 20 meters evacuated beam line that starts at the lead spallation target, is now under construction and is expected to be operational by Summer of 2014. The beam line will be equipped with two collimators, made of iron and polyethylene, a permanent magnet for deflecting relativistic charged particles, and a box for placing in and out neutron filters that will stop neutrons of specific energies. The second collimator, with a conical

shape of 20 mm minimal aperture, provides the desired shape to the neutron beam. The facility is sketched in Figure 1.

The experimental hall starts at 18.1 m from the spallation target as has a height of 6 meters. The ceiling holds the beam dump, which is made of concrete, iron and borated polyethylene, and has been designed in order to minimize the dose to the outside and the background from back-scattered neutrons.

The detectors and beam tubes in the experimental hall will be hold and aligned from a reinforced aluminium structure. On the bottom two neutron monitors based on gas a silicon detectors will be installed and then the samples and detectors will be installed between 1.5 and 2 meters from the floor, i.e. the end of the second collimator.
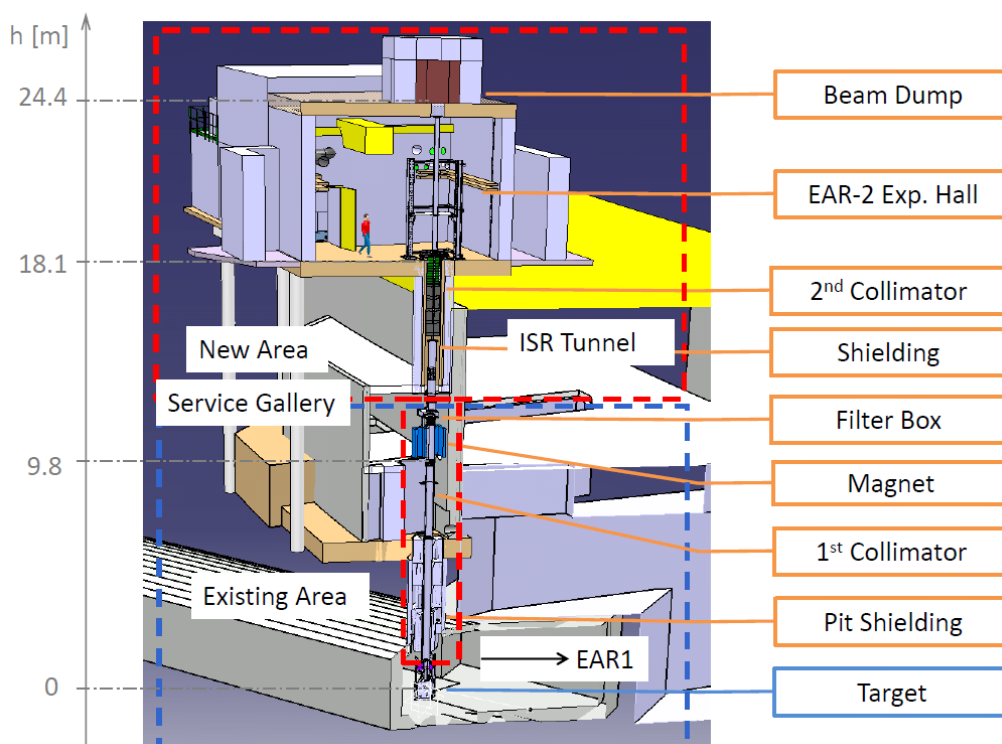
Fig. 1: Sketch of the new CERN facility n_TOF EAR-2, from the target to the measuring station and the beam dump. Details of the equipment along the beam line are also given.

2.2 Expected performance

The geometry of the facility has been implemented in detail in FLUKA and a wide range of simulations have been performed for estimating and optimizing the characteristics of the neutron beam at n_TOF EAR-2 [2]. The main quantities of interest are the intensity of the neutron beam, its spatial profile, and the neutron energy resolution. The collimators were chosen to maximize the intensity on a surface of 1 cm diameter at 1.5 meters from the ground, minimizing the halo beyond that diameter.

As a result, the expected neutron fluence is, as shown in Figure 2, a factor of 27 higher than the one in the existing EAR-1 measuring station. In addition to the increase of neutron fluence, two important differences between EAR-1 and EAR-2 are that:

- The upper energy limit will be around 300 MeV instead of 1 GeV, because of the missing relativistic forward component. This could result, to be conformed, in a reduction of the so-called g-flash (See [1]).

- The neutrons arrive in 10 times less time than in EAR-1, thus the neutrons per second are 270 times higher than in EAR-1. This should help reducing significantly the background from sample activities when measuring radioactive isotopes.
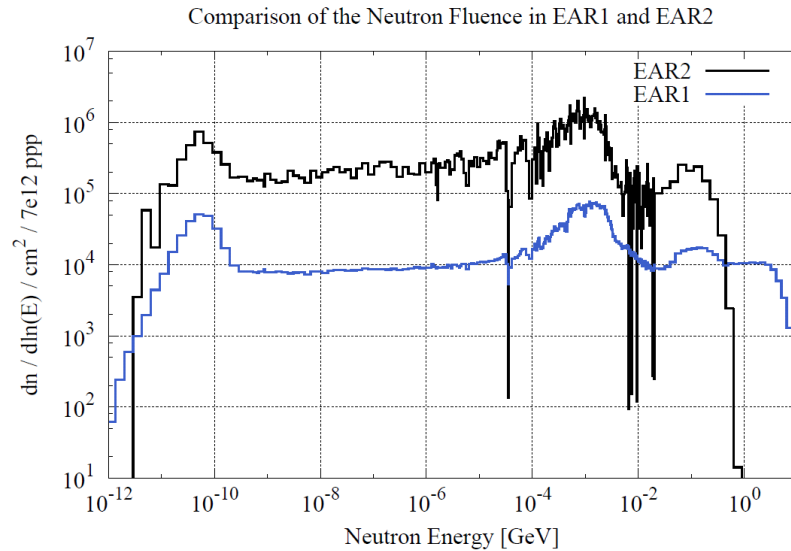
Fig. 2: Neutron fluence as function of neutron energy for the existing (EAR-1) and under construction (EAR-2) n_TOF measuring stations.

3 Measurements planned for n_TOF EAR-2 (2014-2015)

3.1 Destruction of the cosmic γ-ray emitter ^{26}Al by neutron induced reactions [3]

Observation of the cosmic g-ray emitter ^{26}Al is proof that nucleosynthesis is ongoing in our galaxy. Detailed studies in satellite telescope missions revealed that ^{26}Al is predominantly produced in massive stars. Recent sensitivity studies identified the neutron destruction reactions ^{26}Al(n,p) and ^{26}Al(n,a) as the main uncertainty to predict the galactic ^{26}Al abundance.
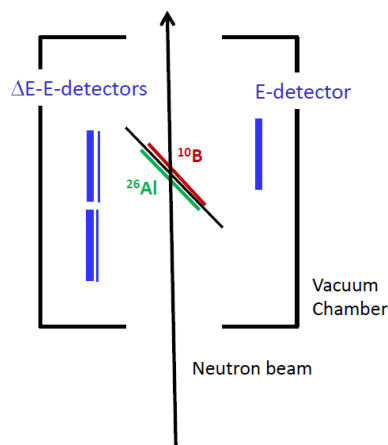
Fig. 3: Sketch of the new ΔE-E telescope made of Si strip detectors for measuring the ^{26}Al(n,p) reaction.

There are only few experimental data on these reactions and they exhibit severe discrepancies. We propose to measure ^{26}Al(n,p) and ^{26}Al(n,a) cross sections at stellar neutron energies at EAR-2 of the n TOF facility, using a highly enriched ^{26}Al sample. The charged particles emitted will be detected using a set of Silicon strip detectors arranged as ΔE-E telescopes.

3.2 g-ray energy spectra and multiplicities from ^{235}U(n,f) using STEFF [4]

An experiment is proposed to use the STEFF spectrometer at n_TOF to study fragment correlations following the neutron-induced fission of ^{235}U. The STEFF array of 12 NaI detectors will allow measurements of the single energy, the multiplicity, and the summed energy distributions as a function of the mass and charge split, and deduced excitation energy in the fission event. These data will be used to study the origin of fission-fragment angular momenta, examining angular distribution effects as a function of incident neutron energy.

The principal application of this work is in meeting the NEA high-priority request for improved g ray data from ^{235}U(n,f). To improve the detection rate and expand the range of detection angles, STEFF will be modified to include two new fission-fragment detectors each at 45 degrees to the beam direction.
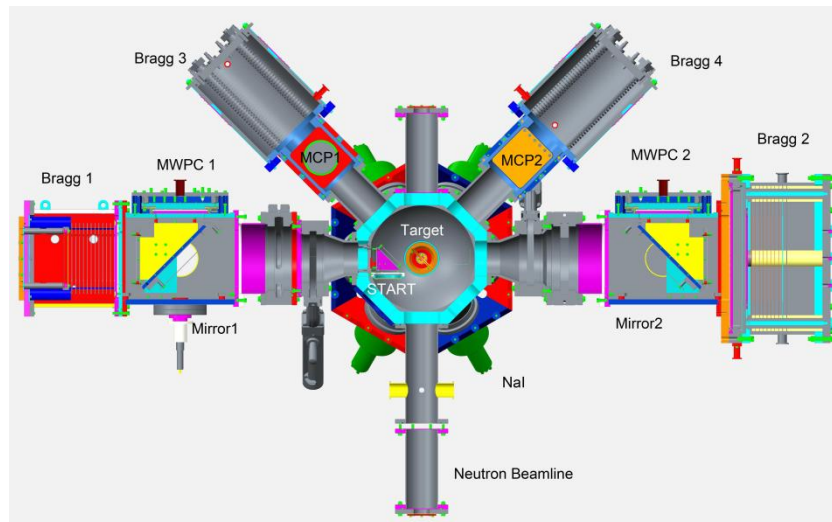
Fig. 4: The STEFF detector as it will be implemented at n_TOF EAR-2.

3.3 Measurement of the neutron capture cross-sections of ^{53}Mn [5]

We propose to measure the neutron capture cross sections of ^{53}Mn at the Experimental Area 2 (EAR-2) of the n_TOF neutron time of flight facility at CERN. This will be the first ever determination of the ^{53}Mn excitation function. These data will influence the models of explosive stage of star evolution and will serve as input data to improve nuclear reaction codes.

The ^{53}Mn target will be manufactured in the frame of the ERAWAST project at PSI. A chemical separation of manganese out of irradiated steel samples will deliver a stock solution containing $5x10^{19}$ atoms of ^{53}Mn. Due to the high amount of ^{55}Mn, the stock solution can not be used directly to prepare a target without a further treatment, but an additional depletion of ^{55}Mn must be performed in a subsequent mass separation using the ISOLDE off-line ion-source test setup. The final target will contain $5x10^{17}$ atoms of ^{53}Mn and less than $1x10^{16}$ atoms of ^{55}Mn.

The aim of this experiment is the determination of the neutron capture cross sections of ^{53}Mn from thermal neutron energies to neutron energies of about 10 keV.
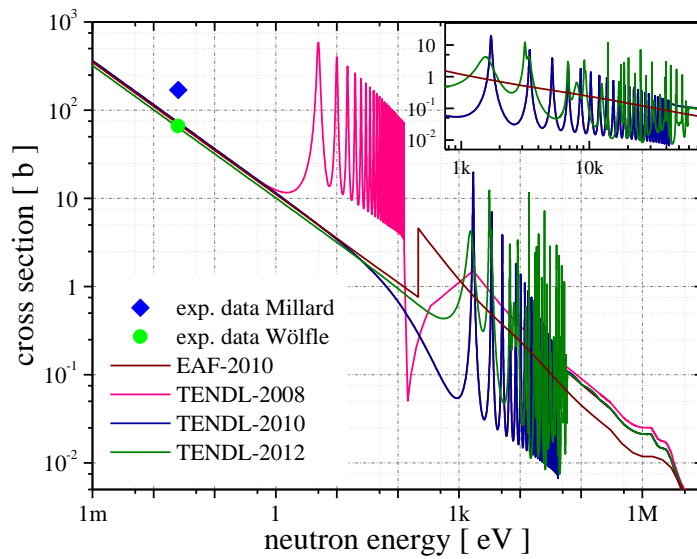
Fig. 5: Capture cross sections of ^{53}Mn, showing that only two experimental data (at thermal) are available.

3.4 Neutron capture at the s-process branching point ^{79}Se [6]

Selenium-79 is a branching point in the slow neutron capture process (s-process) with relevant implications in nucleosynthesis and in stellar models. Indeed, the products of the s-process nucleosynthesis after ^{79}Se are the s-only ^{80,82}Kr, whose solar system abundances are accurately known from chemical analysis of pre-solar grains. This information, in conjunction with the experimental CS of ^{79}Se(n,g) will allow one to extract reliable conditions for the neutron density, as well as the role of the main and weak s-process contributions to the nucleosynthesis in the A=80 mass region.

n_TOF EAR2 represents a unique place to access this experimental information, owing to the very large instantaneous neutron flux and the possibility to use the TAC-technique in order to apply specific energy cuts, reduce contaminant events from the sample activity and separate the (n,g) CS of interest from another isotopes present in the sample.
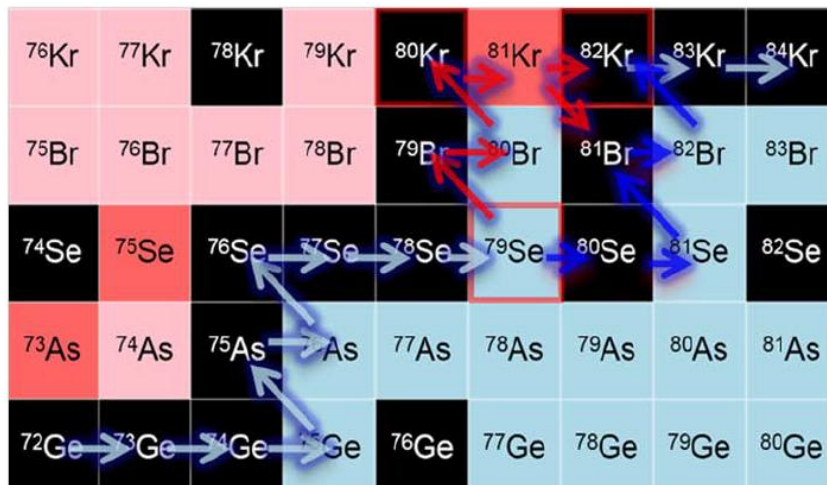
Fig. 6: s-process path around the A=80 mass region.

3.5 Test and development of a (n,p) detector for measuring ^{14}N and ^{35}Cl for BNCT [7]

We propose to study the Silicon Monitor (SiMon) and the Micromegas detector system for measuring (n,p) reactions at n_TOF. The final goal is to measure the 35Cl(n,p) and the 14N(n,p) cross-sections in a wide energy range at EAR-1 and EAR-2, respectively. These reactions are of interest in medical physics and nuclear astrophysics. SiMon is presently running at n_TOF for monitoring purposes.

This Letter of Intent can be considered as a continuation of our work related to the letter CERN-INTC-2010-023/INTC-I-092 and the subsequent proposal CERN-INTC-2012-006/INTC-P-322. In the mentioned Letter and Proposal we studied the fast ionization chamber based on Micromegas detectors, at that time running at n_TOF for monitoring purposes, with the intention to use it for measuring (n,α) cross sections. We successfully measured the 33S(n,α) cross section during the Campaign 2012 with such system. The physics motivations of the present LoI are deeply related to those of the 33S(n,α) experiment.
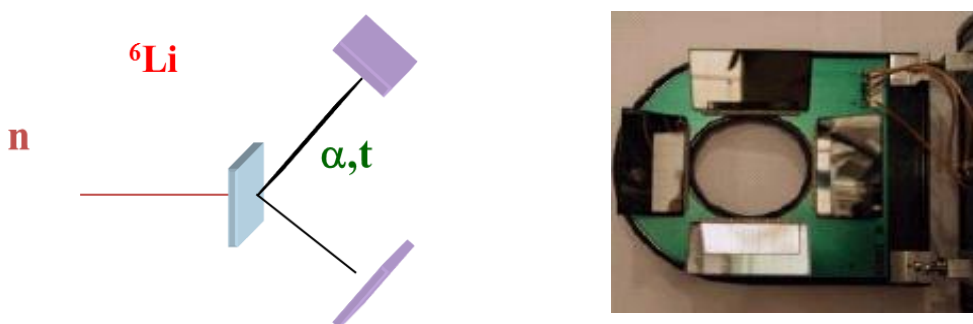
Fig. 7: The current silicon monitor for measuring (n,a) and (n,t) reactions.

3.6 Others

The current plans for future experiments include, among others, the following experiments:
- The role of ^{238}Pu and ^{244}Cm in the management of nuclear waste: (n,γ) cross sections
- Measurement of the capture (and fission) cross sections of the fissile ^{239,241}Pu and ^{245}Cm
- Measurements of (n,xn) reaction cross sections with HPGe detectors (^{197}Au, ^{181}Ta, etc.)
- Measurements of (n,n) and (n,xn) reactions cross sections with CsI+Si telescopes
- Fission cross section of the ^{230}Th, ^{231}Pa and ^{232}U reaction
- Measurement of the ^{25}Mg(n,α)^{22}Ne cross section
- Neutron capture measurement of the s-process branching point ^{147}Pm
- Measurement of ^{7}Be(n,p)^{7}Li and ^{7}Be(n,α)^{4}He cross sections, for the cosmological Li problem.

4 Summary and Outlook

A new neutron time-pf-flight measuring station, with a flight of only 20 meters, will be available at CERN n_TOF by Summer of 2014. With an increased neutron flux of a factor of 27 wit respect to the existing 200 meters beam line, the new facility will allow performing interesting and challenging experiments on neutron-induced reactions. The ones already proposed to the CERN INTC committee have been summarized in this paper, but new ones are already being discussed.

References

[1] C. Guerrero et al., "Performance of the neutron time-of-flight facility n_TOF at CERN", Eur. Phys. J. A 49:27 (2013)

[2] E. Chiaveri et al., "Proposal for n_TOF Experimental Area 2 (EAR-2)", CERN-INTC-2012-029   INTC-O-015 (2012)

[3] C. Lederer, P.J. Woods, E. Berthoumieux, E. Chiaveri, N. Colonna, T. Davinson, A. Estrade, C. Guerrero, F. Gunsing, J. Heyse, F. Kappeler, C. Massimi, W. Mondelaers, A. Musumarra, R. Reifarth, P. Schillebeeckx, G. Tagliente, C. Wagemans, A. Wallner, C. Weiss and the n_TOF Collaboration, "Destruction of the cosmic g-ray emitter ^{26}Al by neutron induced reactions", CERN-INTC-2014-006 ; INTC-P-406 (2014)

[4] A.G. Smith, T. Wright, J. Billowes, J.Ryan, S.Warren, C. Guerrero, L. Tassan-Got, A. Pollitt, O.Serot, I. Tsekhanovichz, "g-ray energy spectra and multiplicities from the neutron-induced fission of ^{235}U using STEFF", CERN-INTC-2014-004 / INTC-P-405 (2014)

[5] R. Dressler, C. Guerrero, F. Gunsing, St. Heinitz, T. Mendoza, D. Schumann, T. Stora, R. Reifarth, A. Wallner and C. Weiss, "Measurement of the neutron capture cross-sections of ^{53}Mn at EAR-2", CERN-INTC-2014-012 ; INTC-P-408 (2014)

[6] C.Domingo-Pardo, C.Guerrero, F.Käppeler, C.Lederer, R.Reifarth, D. Schumann and J.L.Tain, "First measurement of the *s*-process branching ^{79}Se(n,γ)", CERN-INTC-2014-005 / INTC-I-155 (2014)

[7] J. Praena, I. Porras, M. Sabaté-Gilarte, J. M. Quesada, B. Fernández, C. Massimi, F. Mingrone, G. Vannini, P. Woods and C. Lederer "SiMon and Micromegas tests for (n,p) measurements at n_TOF: ^{35}Cl(n,p)^{35}S and ^{14}N(n,p)^{14}C cross sections", CERN-INTC-2014-007 INTC-I-156 (2014)

ERINDA Scientific Results: Transnational Access Activities and Scientific Visits

Franz-Josef Hambsch[1]
[1]EC-JRC-IRMM, Retieseweg 111, B-2440 Geel, Belgium

Abstract

This paper gives an overview of the Transnational Access Activities and Scientific visits within the FP7 project ERINDA (European Research Infrastructures for Nuclear Data). It highlights the fact that nearly 3200 data-taking hours for external users were made available in the partner installations and 104 man weeks for scientific visits to partner institutes. This is much more than the 2500 beam hours and 80 weeks promised in the Description of Work of the project.

1   Introduction

High-quality nuclear data, in particular complete and accurate information about the nuclear reactions taking place in nuclear systems, are an essential component of such modelling capabilities. The quality of a simulation depends on many aspects, but there is a significant component that is associated with the quality of nuclear data. According to the Strategic Research Agenda (SRA), improving and completing the basic nuclear data is a necessary element to achieve the required level of prediction of the present and future simulation tools. The SRA confirms that "Availability of accurate nuclear data ... is the basis for precise reactor calculations both for current and new generation reactors. Additional experimental measurements and their detailed analysis and interpretation are required in a broad range of neutron energies and materials. This is particularly true for fuels containing minor actinides for their transmutation in fast spectra." Accurate nuclear data will help accelerating the development, at an acceptable cost, of safe and commercial advanced reactor systems.

This is why within the 7th Euratom Fission Framework Programme the ERINDA (European Research Infrastructures for Nuclear Data) project, amongst others was funded. The project was running from Nov. 1, 2010 to Oct. 31, 2013. The objective of ERINDA was to offer during the project duration of three years a total of 2500 data-taking hours for external users. This number of additional beam hours corresponds to 25 'typical experiments' for external users at the ERINDA facilities. The project was subdivided into 5 work packages. They were:

WP1 –Management of the project

WP2 - Calls for proposals and their evaluation

WP3 - Experiments at the consortium facilities

WP4 – Scientific support of experiments

WP5 - Communication and dissemination of results

The total contribution of the European Commission was just short of 1 Million Euro, of which 67% of the total budget was used for the Transnational Access Activities (TAA) of ERINDA to support the 2500 data-taking hours. About 7 % were foreseen for scientific support of experiments by providing 80 man weeks for scientific visits to partner institutions. In addition 4 scientific

workshops were organised to disseminate the results of the TAA and Scientific Visits. The total effort from the partners within the project was about a factor 2 of the EC contribution.

In order to maximise the 'scientific value for money of the available resources, all ERINDA facilities are grouped in a pool. The TAA budget is not attributed to the individual partners in advance, but the Programme Advisory Committee (PAC) steers the experimental programme and the TAA budget during the whole project.

2   Results of scientific visit

About 7% of the budget was foreseen for scientific support of experiments. This amounted to 80 weeks of support to scientists visiting the partner institutes for up to 8 weeks. The support was directly given to the visiting scientists in form of reimbursement for travel and subsistence and the host institutes benefitted from the additional manpower. In the end by shuffling remaining budget from the other work packages to the scientific visits, 18 visits with a total of 104 weeks could be financially supported by ERINDA. This is 30% more time as originally proposed in the Description of Work and can be considered as one of the success stories of ERINDA. The beneficiaries, the duration of the visit and the host institutes are mentioned in Table 1.

Name	Affiliation	ERINDA-Host	Duration (weeks)
A. Tudora	Univ. of Bucharest	JRC-IRMM	6
K.-H. Schmidt	GSI, Darmstadt	CENBG	2
M. Lantz	Univ. of Uppsala	JYFL	6
N. Carjan	Horia Hulubei National Institute of Physics and Nuclear Engineering, Bucharest	JRC-IRMM	8
L. Benedik	Jozef Stefan Institute, Slovenia	JRC-IRMM	8
A. Oberstedt	Univ. of Oerebro, Sveden	JRC-IRMM	8
A. Tudora	Univ. of Bucharest	JRC-IRMM	6
K.-H. Schmidt	GSI, Darmstadt	CENBG	2
P. Sauvan	CEA, Saclay	PTB	2
C. Lampoudis	CEA, Saclay	JRC-IRMM	4
S. Valenta	CEA, Saclay	JRC-IRMM	6
P. Archier	CEA, Cadarache	JRC-IRMM	4
N. Carjan	Horia Hulubei National Institute of Physics and Nuclear Engineering, Bucharest	JRC-IRMM	8
A. Tudora	Univ. of Bucharest	JRC-IRMM	8
K.-H. Schmidt	GSI, Darmstadt	CENBG	2
C. Rouki	Antwerp	JRC-IRMM	8
N. Carjan	Horia Hulubei National Institute of Physics and Nuclear Engineering, Bucharest	JRC-IRMM	8
C. Rouki	Antwerp	JRC-IRMM	8

Table 1: List of approved scientific visits.

Most of the scientific visit had promised output in form of refereed journal papers. This output in terms of scientific publications from those scientific visits is however delayed. It takes time to wrap up the results of the visit into a decent publication or the time the visit was too short to have enough content for a refereed journal publication. Nevertheless, I counted more than 15 publications in refereed journals as of the writing of this manuscript. This is not too bad in view of the fact that there were only 18 visits supported.

Concerning highlights of the scientific visits, I consider the work of K.-H. Schmidt as one of the most important highlight. His GEF (A General description of Fission observables) code [1-4] has been discussed in several publications and has been used by many groups in getting decent predictions of fission observables to compare the experimental results with. It is even under discussion to include the code into the TALYS code system. One of the extraordinary outcomes is the transition of e.g. symmetric to asymmetric fission fragment mass or charge distributions in the vicinity of A = 226 as illustrated in Fig. 1.
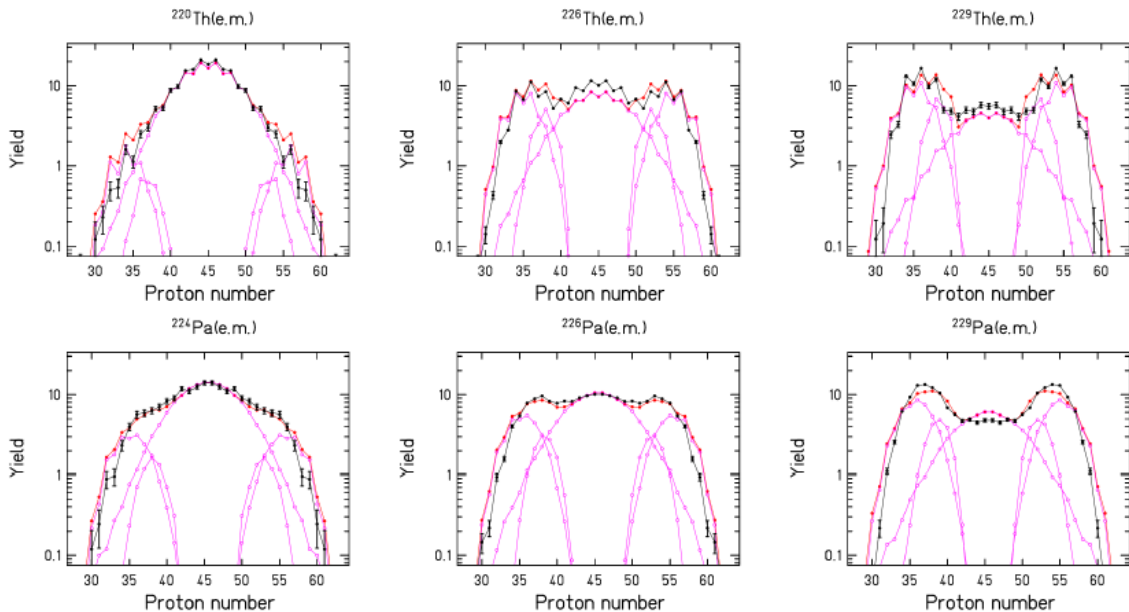
Fig.1: Charge distributions calculated with the GEF code and compared to experimental results. For details see Refs. [1-4].

The GEF code is actually able to reproduce the mass- or charge distribution over a wide range of compound system masses. Also other observables of fission (neutron multiplicities and γ-ray multiplicities) can also be calculated and are in rather good agreement with experimental data [4].

3 Results of Transnational Access to partner laboratories

In total ERINDA combined 16 partner laboratories from 11 European countries. The participating facilities of the partner laboratories are mentioned in Tab. 2. In the description of work (DoW) of ERINDA the promise was given to support 2500 data-taking hours for 25 typical experiments. At the end of the project in total 31 experiments with nearly 3200 data-taking hours were supported within the available budget. Hence nearly 30% more beam time could be delivered compared to the original proposal. This is definitely a success due to the pooling of the facilities, making it possible to allocate more beam hours to facilities which are in greater demand. As one can see

from Tab. 2 the possibilities to use partner facilities were rather widespread. The neutron energy range was from sub-thermal neutrons to neutrons with energies of several 100 MeV.

One of the key experiments I would consider among the more than 30 experiments performed was the measurement of the prompt γ-ray spectrum of ^{235}U(n$_{th}$,f) at the Budapest Research reactor facility of IKI in Hungary. Based on calculations of decay heat performed at CEA Cadarache, it has been found that an underestimation of 10-28% exists for ^{235}U and ^{239}Pu. This is a severe problem for reactor safety as about 10% of the total energy release in a standard nuclear reactor is by fission γ-rays. This has triggered two entries in the high priority request list of the OECD/NEA. Using more sophisticated γ-ray detectors based on Lanthanum halides, which have better energy resolution, improved timing resolution and larger efficiency compared to NaI detectors used in the 1970ties, new experiments have been performed in the frame of a PhD thesis (see e.g. Ref. [5] and references therein). Fig. 2 shows the prompt γ-ray spectrum of ^{235}U(n$_{th}$,f) which was measured using several different type of Lanthanum halide detectors. Two of them are compared with literature data and the ENDF/B-VII evaluation. It is obvious that the present experiment confirms the structure in the low energy part of the spectrum seen already in literature. It allows in addition to have a lower threshold which translates into a higher γ-ray multiplicity, but lower mean γ-ray energy. So in the end the total energy deposited by the prompt fission γ-rays is not so much different based on the new experimental results compared to the value in ENDF/B-VII. Hence the underestimation could not be explained in full. Other compensation effects due to the complexity of the theoretical calculations might be present as well.

nELBE	40 MeV superconducting electron linac + neutron TOF facility D-T neutron generator	FZ Dresden (Germany)
GELINA and VdG	150 MeV electron linac + neutron TOF facility 7 MV Van de Graaff accelerator	IRMM Geel (Belgium)
n_TOF	20 GeV proton beam of the PS + spallation neutron source + neutron TOF facility	CERN Geneva (Switzerland/Frai
AIFIRA	3.5 MV Van de Graaff accelerator	CENBG Bordeaux (France)
Tandem-ALTO	15 MV tandem and photo-fission source	IPN Orsay (France)
TSL	Cyclotron (180 MeV p)	UU-TSL Uppsala (Sweden)
PIAF	3.7 MV Van de Graaff accelerator Cyclotron (19 MeV p and d, α)	PTB Braunschweig (Germany)
NPI	Cyclotron (20 MeV p and d, α)	NPI Řež (Czech Republic)
BRR	10 MW research reactor	IKI Budapest (Hungary)
JYFL	130 MeV heavy ion cyclotron 30 MeV high intensity cyclotron + IGISOL	JYFL, Jyväskylä (Finland)
IFIN HH	9 MeV Tandem accelerator (p to Au)	IFIN HH, Bucharest (Romania)
NPL	3.5 MeV Tandem Van de Graaff accelerator	NPL, Teddington (Great Britain)
FRANZ	500 keV RFQ + proton linac	GUF, Frankfurt (Germany)
CEA	4 MV Van de Graaff accelerator 7 MV tandem accelerator	CEA Bruyéres-le-Chatel (France)

Table 2: Participating facilities from the partner laboratories.

. Also for the Transnational Access Activities the same hold like for the scientific visits that output in terms of publications in refereed journals is delayed. For experiments it takes even more time to analyse the acquired data, to wrap up the results of the experiment into a decent

publication and get it published in a refereed journal. Nevertheless so far nearly 30 publications in refereed journals as of the writing of this manuscript were counted.
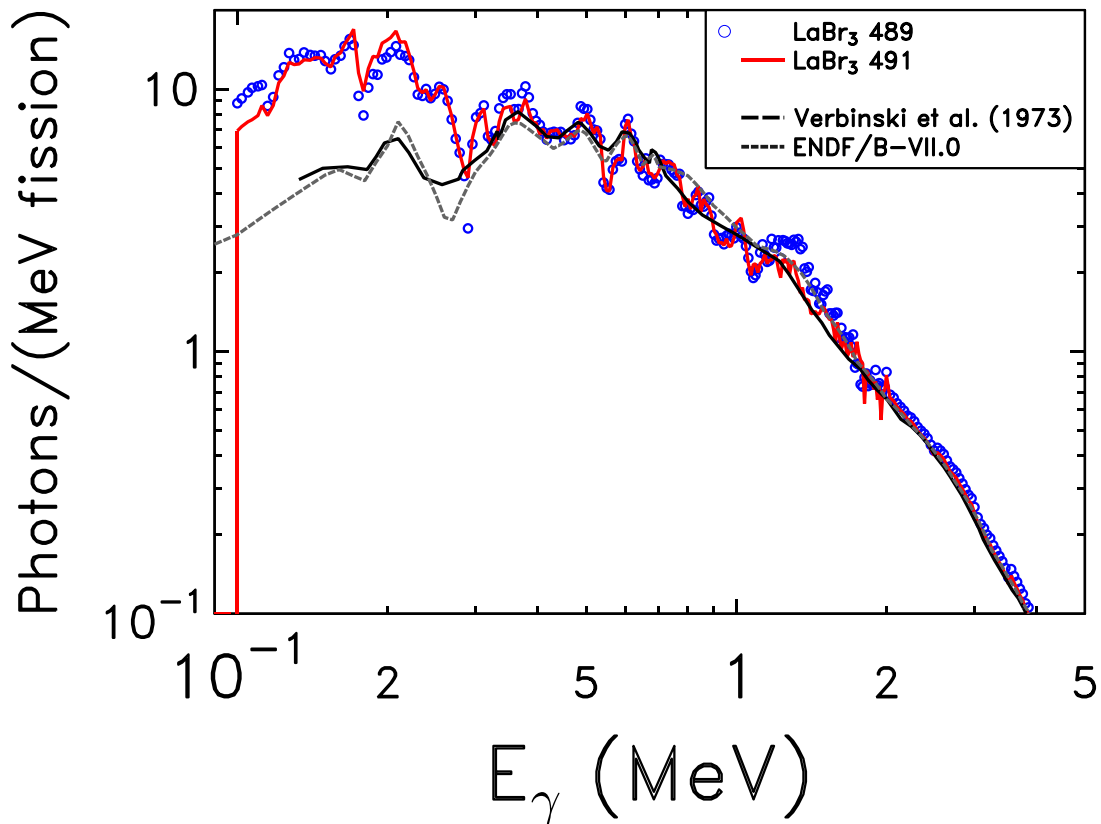
Fig. 2: Prompt g-ray emission spectrum in the fission of $^{235}U(n_{th},f)$ measured at the Budapest research reactor institute [5].

4 Outlook

ERINDA finished successfully on Oct. 31, 2013. For the next four years the next approved project called CHANDA (Challenges in Nuclear Data) will give access to partner facilities via Transnational Access. This new project has started Dec. 1, 2013 until Nov. 30, 2017. As being a much bigger project, CHANDA has 35 partners from 16 member states and Norway. The total effort of CHANDA is 770 person months (5.4 M€ EC contribution) committed to the improvement of experimental facilities and techniques and analysis, evaluation and validation methods. The activities comprise 2 work packages (WP1&2) for positioning nuclear data for energy applications in the Horizon 2020 research area, a work package (WP3) on a target preparation network, three work packages for transnational access of experimentalists and visiting scientists (WP4-6), a work package for the new neutron beam facilities at CERN and GANIL (WP6), five work packages with joint research activities (WP8-12) and one work package for the management of CHANDA (WP13). The kick-off meeting was held on Dec. 10-11, 2013 in Madrid. Hence, a first call for Transnational Access Activities and Scientific visits is expected to be launched beginning of 2014.

5   Conclusions

With nearly 3200 delivered beam hours, 31 experiments and many supported scientists, especially young scientists at the beginning of their career, the Transnational Access Activity (TAA) of ERINDA was a great success. The same is true for the Scientific visits which amounted to 104 man weeks supporting 18 different visits to partner laboratories. The money invested by the European Commission was well spent. The next project, were TAA is included is on the horizon. CHANDA (Challenges in Nuclear Data) had just had its kick-off meeting. This project will last for the next 4 years. The project scope of CHANDA is much wider than that of ERINDA and hence it has many more partners involved. More info about ERINDA and CHANDA can be found on the respective websites [6,7].

References

[1] K.H. Schmidt, B. Jurado, Entropy Driven Excitation Energy Sorting in Superfluid Fission Dynamics, Physical Review Letters, 104 (2010).
[2] K.H. Schmidt, B. Jurado, Final excitation energy of fission fragments, Physical Review C, 83 (2011).
[3] K.H. Schmidt, B. Jurado, Thermodynamics of nuclei in thermal contact, Physical Review C, 83 (2011).
[4] K.H. Schmidt, B. Jurado, JEF-DOC 1423, OECD/NEA, Paris France. http://www.khs-erzhausen.de/GEF.html
[5] A. Oberstedt, et al., Phys. Rev. C 87 (2013) 051602(R)
[6] ERINDA website (**http://www.erinda.org**),
[7] CHANDA website not yet available.

Neutron total cross section measurements of gold and tantalum at the nELBE photoneutron source[1]

Roland Hannaske*, Zoltan Elekes, Roland Beyer, Arnd Junghans[2], Daniel Bemmerer, Evert Birgersson[3], Anna Ferrari, Eckart Grosse*, Mathias Kempe*, Toni Kögler*, Michele Marta[4],
Ralph Massarczyk*, Andrija Matic[5], Georg Schramm*, Ronald Schwengner, and Andreas Wagner
Helmholtz-Zentrum Dresden-Rossendorf, Bautzner Landstr. 400, 01328 Dresden, Germany

Abstract
Neutron total cross sections of ^{197}Au and ^{nat}Ta have been measured at the nELBE photoneutron source in the energy range from 0.1 - 10 MeV with a statistical uncertainty of up to 2 % and a total systematic uncertainty of 1 %. This facility is optimized for the fast neutron energy range and combines an excellent time structure of the neutron pulses (electron bunch width 5 ps) with a short flight path of 7 m. Because of the low instantaneous neutron flux transmission measurements of neutron total cross sections are possible, that exhibit very different beam and background conditions than found at other neutron sources.

1   Introduction

Experimental neutron total cross sections as a function of neutron energy are a fundamental data set for the evaluation of nuclear data libraries. With increasing neutron energy the compound nucleus resonances cannot be resolved anymore and will start to overlap. In the energy range of fast neutrons, which is especially important for innovative nuclear applications, like accelerator driven systems for the transmutation of nuclear waste, the neutron total cross section can be described by optical model calculations (e.g. [2, 3]) where the range below 5 MeV shows a large sensitivity on the optical model parameters.

The neutron total cross section of ^{197}Au in the energy range from 5 – 200 keV is an item in the OECD NEA Nuclear Data High Priority Request list as ^{197}Au(n,γ) is an activation standard in dosimetric applications [4]. Precise total cross section data with a targeted uncertainty < 5 % will have a direct impact on future evaluations of neutron induced reactions on Au. Also an overlapping measurement from 200 keV to 2.5 MeV is of interest to check consistency.

Tantalum is a non-corrosive metal of importance as a structural material in many nuclear and high-temperature applications, e.g. it is also a component in Reduced Activation Ferritic / Martensitic steels [5]. The fast neutron cross section of tantalum has been evaluated recently [6]. In that work, a careful measurement of the neutron total cross section from several tens of keV to several MeV with an accuracy goal of ≈ 1 % has been recommended.

---

[1] This article is an updated and abridged version of Ref. [1].
* also at Technische Universität Dresden, Dresden, Germany
[2] Corresponding author: Tel. +49 351 260 3589; email: a.junghans@hzdr.de
[3] Present address: AREVA NP GmbH, 91052 Erlangen, Germany
[4] Present address: GSI Helmholtzzentrum für Schwerionenforschung GmbH, Planckstr. 1, 64291 Darmstadt, Germany
[5] Present address: IBA Particle Therapy, 45157 Essen, Germany

A comprehensive set of very precise high energy neutron total cross sections up to several hundred MeV neutron energy has previously been measured at the Weapons Neutron Research (WNR) spallation neutron source of the Los Alamos National Laboratory (LANL) [7, 8]. Due to experimental constraints these data start at 5 MeV neutron energy, but are still valuable to compare to. At lower energies precise measurements exist using neutrons from the ^{7}Li(p,n)^{7}Be reaction at the Fast Neutron Generator of Argonne National Laboratory (ANL) [9]. Neutron total cross sections of ^{197}Au in the energy region from 4 to 108 keV have been measured recently at the GELINA facility [10]. These data are complemented by the work reported here using a neutron source with very different beam and background properties.

The neutron total cross sections for tantalum of natural isotopic composition (99.95 % purity) and ^{197}Au (99.99 % purity) were determined by the transmission technique at the photoneutron source nELBE [11–13] at Helmholtz-Zentrum Dresden-Rossendorf, Germany. This is the world's only neutron time-of-flight facility driven by a superconducting electron accelerator [14] with its superior time structure definition. The very short (5 ps) electron bunches allow us to use a short flight path (7.175 m) with a good time resolution and maximize the available neutron intensity with a high repetition rate in continuous-wave (cw) operation (101.5625 kHz micropulse repetition rate). This rate is two to three orders of magnitude higher than the pulsed operation at normal-conducting accelerators. A fast plastic scintillator with low detection threshold [15] was used for the time-of-flight measurements. The neutron spectrum of this facility is characterized in a separate publication [12]. The energy range extends from $\approx$ 10 keV to 10 MeV, which essentially covers the fission neutron spectrum.

First we shortly describe the nELBE neutron time-of-flight facility and the setup for transmission measurements and then we present the data analysis and discuss the results.

2   The nELBE time-of-flight facility
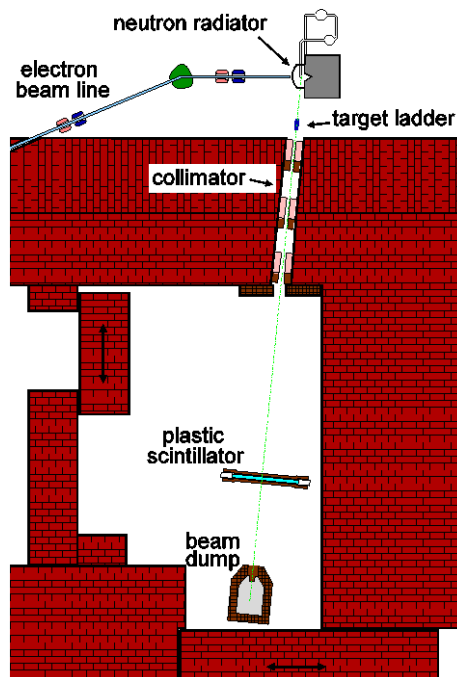
Fig. 1: Floor plan of the cave for the neutron transmission experiment at the ELBE accelerator. The neutron radiator consists of a Mo tube with rhombic cross section through which liquid lead is flowing. The target ladder is located approx. 1 m from the neutron radiator in front of the collimator tube which has a length of

2.6 m. The total flight path to the neutron detector (plastic scintillator) is 7.175 m. A beam dump behind the plastic scintillator absorbs the bremsstrahlung and neutrons.

At Helmholtz-Zentrum Dresden-Rossendorf the world's only compact photoneutron source at a superconducting electron accelerator dedicated to measurements in the fast neutron range has been built. A compact liquid lead circuit is used as a neutron-producing target. Through this technology the neutron beam intensity is not limited by the heat dissipation inside the target. The technical design including thermo-mechanical parameters of the liquid lead circuit and the beam dump is discussed in Ref. [13]. The electron beam is accelerated to 30 MeV in cw-mode by superconducting cavities. The maximum average beam current at a micropulse rate of 13 MHz is 1 mA. The neutron source strength at the nominal beam current has been calculated with the Monte Carlo N-Particle Transport Code MCNP-4C3 to be 10^{13} neutrons/s [11]. The accelerator produces high brilliance beams with variable micropulse repetition rates and duty cycles. The bunch duration is about 5 ps, so that the time-of-flight resolution is not degraded and short flight paths can be used with a high-resolution detection system.

Figure 1 shows the floor plan of the neutron time-of-flight facility. The electron beam passes through a beryllium window mounted on a stainless-steel vacuum chamber and hits the radiator, consisting of a molybdenum channel confining the liquid lead. The channel has a rhombic cross section with 11 mm side length. The electrons generate bremsstrahlung photons which release neutrons in secondary (γ,n) reactions on lead. These leave the radiator almost isotropically, whereas the angular distributions of electrons and photons are strongly forward-peaked. The collimator axis is located at 95° with respect to the electron beam direction. The collimator and the neutron beam properties at the experimental area have been optimized using MCNP-4C3 in order to maintain the correlation of time-of-flight and neutron energy [11]. The collimator of 2.6 m length contains three replaceable elements of lead and borated polyethylene that are mounted inside a precision steel tube [11].

3   Transmission

The neutron total cross sections were determined in a transmission experiment. The target samples together with bremsstrahlung absorbers were mounted in a pneumatically driven computer-controlled target ladder directly in front of the collimator entrance. The conical neutron beam collimator has an entrance aperture diameter of 20 mm increasing to 30 mm at the exit. In this geometry small diameter samples were used with a neutron transmission factor of about 0.5. The target samples were periodically moved in and out of the beam to compensate for possible long term drifts in the neutron beam intensity. The data taking time per cycle for the empty sample (3 cm thick Pb bremsstrahlung absorber only) was 600 s, for the Au and Ta samples it was 900 s. The total measurement time was about 78 hours. The order of the cycle was empty-Au-Ta-Pb in the first half of the experiment whereas it was empty-Au-empty-Ta-empty-Pb in the second half with 300 s duration for empty, to increase the frequency of empty target measurements. Each sample was combined with a 3 cm thick Pb absorber to reduce the bremsstrahlung count rate. All Pb absorbers and the Pb sample were made from a technical lead alloy (PbSb4). The data from the Pb sample have been used to determine the energy resolution of the time-of-flight measurement.

The transmitted neutrons were detected using a plastic scintillator (Eljen EJ-200, 1000 mm x 42 mm x 11 mm) that was read out on both ends using high-gain Hamamatsu R2059-01 photomultiplier tubes (PMT). The scintillator is surrounded by a 1 cm thick lead shield to reduce the background count rate. The detection threshold for recoil protons in this detector is at about 10 keV [15]. The overlap neutron energy for the given micropulse repetition rate and flight path is 2.8 keV. This is below the detection threshold of the plastic scintillator used in the transmission measurement. The electron beam intensity was reduced to the sub μA range to have a detector

count rate of ≈ 10 kHz (empty sample beam). This corresponds to a neutron count rate of ≈ 250 n/s. On average, only every tenth accelerator bunch is registered by the scintillator.

The time-of-flight of the transmitted neutrons was measured in list mode with the Multi-Branch-System (MBS) real-time data acquisition developed at GSI, Darmstadt. This setup is optimized to control several VME bus crates with several front-end processors using a real-time operating system. The PMT output signals were fed into a CAEN V874B 4 Channel BaF$_2$-Calorimeter Read-Out Unit housing charge to digital converter (QDC) and constant fraction discriminator (CFD) sections. An internal constant veto time of ≈ 2.7 μs in this module helps to suppress the rate of afterpulses that may occur in high-gain PMTs. The CFD output signals were fed into a SIS 3820 scaler module to determine the detector count rate and into the multi-hit multi-event time-to-digital converter (TDC) CAEN V1190A to determine the time information with a dispersion of 97.6 ps/channel. The accelerator radiofrequency (rf)-signal serves as reference for the time-of-flight determination. A CAEN V1495 FPGA module was used to produce the logical AND of the CFD signals from both PMTs to trigger the data acquisition (DAQ). The coincident signals from the TDC that triggered the data acquisition were analysed for this transmission measurement. The time sum signal of both PMTs is used to measure the time-of-flight, while a software condition on the time difference signal was used to select events that occurred in the central beam spot region of the scintillator bar. The absolute scale of time-of-flight is determined using the bremsstrahlung peak and the known flight path. The flight path has been verified by resonant structures that appear in the neutron spectrum [12]: Several absorption minima appear due to resonances with strong elastic neutron scattering in ^{208}Pb. Emission peaks appear in the neutron spectrum from nuclear levels just above the neutron separation energy mainly in ^{208}Pb that can be excited via (γ,n) or $(e,e'n)$ reactions.

The transmission T is given by the relation

$$T = \frac{R_{in}}{R_{out}} = \exp(-nl\sigma_{tot}) \ , \tag{1}$$

$$\sigma_{tot} = -\frac{1}{nl}\ln\left(\frac{R_{in}}{R_{out}}\right) = -\frac{1}{nl}\ln(T) \ , \tag{2}$$

where R_{in}, R_{out} are the background and dead-time corrected count rates in the detector with the sample in and out of the beam, respectively. The areal density nl is given by the product of the number density of atoms and the thickness and σ_{tot} is the neutron total cross section. The Au and Ta samples used are characterized in Table 1. The areal density nl is known to a relative uncertainty of $6\cdot10^{-3}$.

The spectra of transmitted neutrons measured as a function of time-of-flight are shown in Fig. 2. The flight path from the centre of the neutron radiator to the centre of the plastic scintillator was determined by geometrical survey to be 717.5 ± 0.2 cm. The bremsstrahlung peak from the neutron radiator has a time-of-flight of 23.9 ns. The fastest neutrons arrive at about 100 ns after this peak. Measurements with a ^{235}U fission chamber, which is sensitive down to the thermal region, show that the neutron energy range extends down to about 10 keV [12].

Table 1: Ta and Au sample characteristics. The samples had cylindrical shape. The density has been calculated from the measured dimensions and mass of the sample to show agreement with the standard density within the relative uncertainty of $6 \cdot 10^{-3}$ or better. The Ta corresponds to ASTM B365 Grade RO5200, the gold to standard fine gold. The bremsstrahlung absorbers consisted of technical lead alloy (PbSb4) machined to a cylinder (diameter 25.0 ± 0.1 mm, length 30.0 ± 0.1 mm).

Sample	Diameter (mm)	Length (mm)	Mass (g)	Density (g/cm³)	Standard Density (g/cm³)	Purity (weight %)	Areal Density nl (atoms/barn)
Ta	25.1 ± 0.1	25.5 ± 0.1	210.419 ± 0.001	16.68 ± 0.09	16.65	99.95	0.1413 ± 0.0006
Au	26.0 ± 0.1	16.0 ± 0.1	163.760 ± 0.001	19.28 ± 0.12	19.32	99.99	0.0945 ± 0.0006
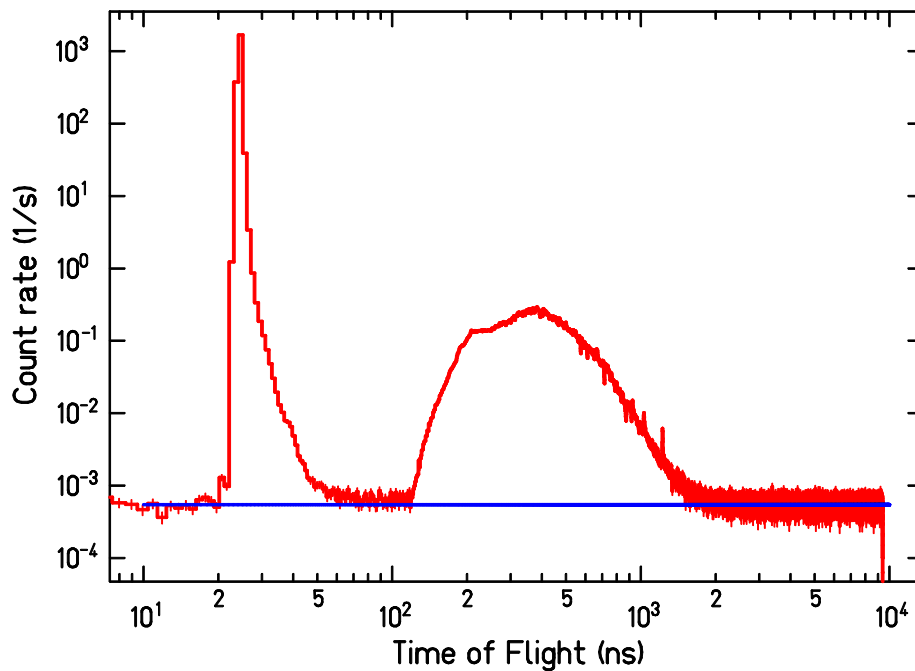
Fig. 2: Typical time-of-flight spectrum for the transmission measurement at nELBE. The dead-time corrected count rate is shown as a function of time-of-flight for the transmission through the Au sample + Pb absorber. A narrow gate was set on the time difference of the two PMTs to select the region, where the transmitted neutron beam passes through the scintillator. The random background rate (blue line) was fitted in the time interval from 8500 ns – 9350 ns. The time resolution of the detection system is characterized by the width of the bremsstrahlung peak and amounts to 0.46 ns.

4 Data analysis and experimental uncertainties

To determine the neutron transmission and the total cross section from the measured time-of-flight distribution several corrections have to be done:

1. Correction for a time-of-flight dependent dead time

2. Subtraction of a constant random background in the time-of-flight spectra

3. Neutron beam intensity fluctuations

4. In-scattering of neutrons

5. Resonant self shielding in thick transmission samples

Random background and dead-time corrections are very important. The remaining neutron beam intensity fluctuations were measured in the target cycle and found to have a small influence. In-scattering of neutrons was minimized by using a "good" geometry. Resonant self shielding can be an important correction at low neutron energy, where the total cross section can have strong, separated resonances [9]. Above 100 keV neutron energy this correction is found to be negligible.

A detailed discussion of all corrections as well of the energy resolution and the uncertainty budget can be found in Ref. [1].

5 Results

The neutron total cross sections of Ta and Au have been measured in the energy range from about 0.1 MeV to 10 MeV. The energy resolution $\Delta E/E$ over this energy range increases from 1.4 % to 7.4 % (FWHM). The energy resolution is mostly due to the scattering of neutrons in the lead shield of the plastic scintillator. The resolution is sufficient for average cross sections that can be compared with optical model calculations.

In Fig. 3 the neutron total cross section of Au is shown in comparison with the data from Poenitz *et al.* [9, 16] and Abfalterer *et al.* [8]. The nELBE data are systematically about 2 % higher than the other two experiments. The typical statistical uncertainty is smaller than 5 % for Au data at 100 keV and above as was asked for in the High Priority Request List of the Nuclear Energy Agency [4]. Also our measurement extends up to the very accurate data of Abfalterer *et al.* [8] and thus demonstrates good consistency. The calculated total cross section of the Talys 1.4 reaction code [17] shows good agreement with the data to within 4 %. The Talys code was used with the default options, using the optical model parameters from Koning and Delaroche [2]. Concerning the neutron total cross section of [197]Au all current evaluations are quite similar. The JEFF-3.1.2 and CENDL-3.1 evaluations are about 2-3 % lower than the experimental data. The corresponding ENDF/B-VI.8, ENDF/B-VII.0, and ENDF/B-VII.1 evaluations are identical to JEFF-3.1.2. The JENDL-4.0 evaluation is up to 5 % higher than the evaluations mentioned before.
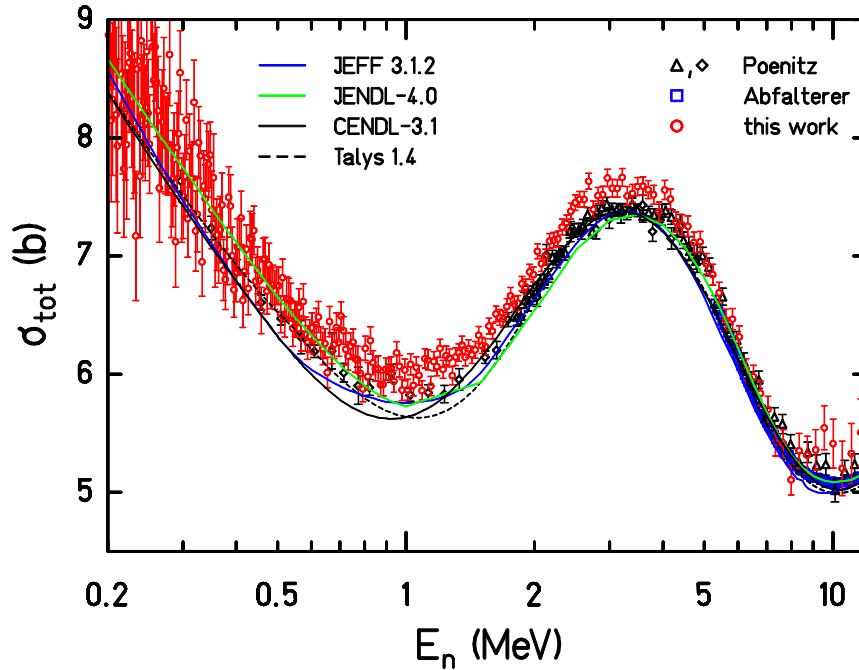
Fig. 3: The experimental neutron total cross section of ^{197}Au as a function of the neutron energy from 0.2 MeV to 10 MeV (this work, red circles). The data from Abfalterer *et al.* [8] from the LANL WNR spallation neutron source are shown as blue squares. The black symbols denote results from Poenitz *et al.* [9, 16] from the ANL fast neutron generator. The nELBE data have an equidistant binning in time of 3.9 ns to decrease statistical uncertainties and to increase the readability of the figure. The dashed line shows a result from the Talys code [17]. The JEFF-3.1.2 evaluation is shown by a blue line. The JENDL-4.0 evaluation is shown as a green line and the CENDL-3.1 evaluation as a black line.

Figure 4 shows the neutron total cross section of Ta. In the energy range from 0.2 MeV to 10 MeV our data are about 3 % higher than results from Finlay *et al.* [7] and Poenitz *et al.* [9, 16] that covered only a part of this energy range. Older data by A.B. Smith [18] are very close in the absolute normalization. A small gap from 0.6 MeV to 1.0 MeV where no high resolution data existed before has been filled. The Talys 1.4 reaction code does not describe the neutron total cross section correctly in the energy range below 2 MeV.
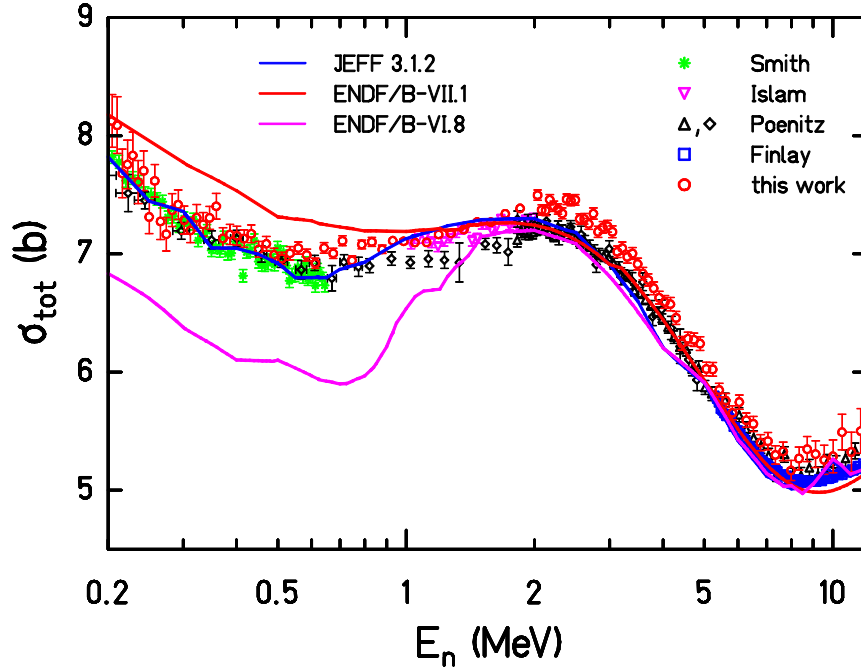
Fig. 4: The neutron total cross section for ^{nat}Ta as a function of the neutron energy from 0.2 MeV to 10 MeV (this work, red circles). The data from Finlay *et al.* [7] at the LANL WNR spallation neutron source are shown as blue squares. The black symbols denote results from Poenitz *et al.* [9, 16] from the ANL fast neutron generator. The green and purple symbols denote data from Refs. [18] and [19], respectively. The ENDF/B-VII.1 evaluation is shown by a red curve; the ENDF/B VI.8 evaluation by a purple line. The JEFF-3.1.2 evaluation is shown by a blue line. The experimental data of Refs. [18, 19] and this work below 2 MeV have been rebinned to increase readability.

The neutron total cross section of Ta is also compared to different recent nuclear data evaluations in Fig. 4. The JEFF-3.1.2 evaluation is in good agreement with the experimental data, as are the nearly identical curves from RUSFOND 2010 and JENDL-4.0. The ENDF/B-VI.8 and the identical ENDF/B-VII.0 evaluations are below the data. The ENDF/B-VII.1 evaluation is above the data in the energy range below 1 MeV. These discrepancies show again the importance of neutron-total cross section measurements in the fast-energy range covered in this work. This work allows us to base nuclear data evaluations on experimental neutron total cross sections in the energy range below 5 MeV, which is especially sensitive on the optical model parameters used. A careful measurement as recommended in [6] has been done.

Additional figures of the measured neutron total cross sections of ^{197}Au and ^{nat}Ta with different binning or in a different energy range can be found in Ref. [1].

The present results with a systematic uncertainty of 1 % might be an indication that the total cross section could be slightly higher than the ones measured before at LANL and ANL. Our detection system had a low detection threshold and good efficiency; however the PMT afterpulsing caused high single count rates that cause additional dead time. To investigate systematic uncertainties in future transmission measurements a data acquisition with much smaller

dead-time correction is in preparation. The data measured in this work will be made available through the EXFOR data base. A table of cross sections has been added as electronic supplementary material to Ref. [1].

An improved time-of-flight facility is currently under construction in the National Center for High Power Radiation Sources of HZDR Dresden, which includes a 6 m x 6 m x 9 m time-of-flight hall with reduced background from scattering on the walls. This facility will also allow improved measurements of neutron total cross sections to assist future nuclear data evaluations [20].

References

[1] R. Hannaske *et al.*, *Eur. Phys. J.* **A 49** (2013) 137.

[2] A. Koning and J. Delaroche, *Nucl. Phys.* **A 713** (2003) 231.

[3] P. Pereslavtsev and U. Fischer, *Nucl. Inst. Meth.* **B 248** (2006) 225.

[4] NEA Nuclear Data High Priority Request List (HPRL)
Available online: http://www.oecd-nea.org/dbdata/hprl/hprlview.pl?ID=428.

[5] R.L. Klueh, Oak Ridge National Laboratory Report (2004) ORNL/TM-2004/176.

[6] A.B. Smith, *Ann. Nucl. Ene.* **32** (2005) 1926.

[7] R.W. Finlay *et al.*, *Phys. Rev.* **C 47** (1993) 237.

[8] W.P. Abfalterer *et al.*, *Phys. Rev.* **C 63** (2001) 044608.

[9] W. Poenitz, J. Whalen and A. Smith, *Nucl. Sci. Eng.* **78** (1981) 333.

[10] I. Sirakov *et al.*, *Eur. Phys. J.* **A 49** (2013) 144.

[11] J. Klug *et al.*, *Nucl. Inst. Meth.* **A 577** (2007) 641.

[12] R. Beyer *et al.*, *Nucl. Inst. Meth.* **A 723** (2013) 151.

[13] E. Altstadt *et al.*, *Ann. Nucl. Ene.* **34** (2007) 36.

[14] F. Gabriel *et al.*, *Nucl. Inst. Meth.* **B 161** (2000) 1143.

[15] R. Beyer *et al.*, *Nucl. Inst. Meth.* **A 575** (2007) 449.

[16] W. Poenitz and J. Whalen, Argonne National Laboratory (1983) ANL/NDM-80.

[17] A. Koning, S. Hilaire and M. Duijvestijn, Proc. Int. Conf. Nucl. Data Science and Tech., April 22-27, 2007 Nice, France, EDP Sciences (2008) 211.

[18] A.B. Smith, P.T. Guenther and J.F. Whalen, *Phys. Rev.* **168** (1968) 1344.

[19] E. Islam *et al.*, *Nucl. Phys.* **A 209** (1973) 189.

[20] A.R. Junghans, Proc. Int. Conf. Nucl. Data Science and Tech., New York, 2013, to be published in *Nucl. Data Sheets* (2014).

The *n*ELBE (*n*,fis) experiment

T. Kögler[1,2], *R. Beyer*[1], *R. Hannaske*[1,2], *A. R. Junghans*[1], *R. Massarczyk*[1,2], *R. Schwengner*[1] *and A. Wagner*[1]

[1] Institute of Radiation Physics, Helmholtz-Zentrum Dresden-Rossendorf, 01328 Dresden, Germany
[2] Technische Universität Dresden, 01062 Dresden, Germany

Abstract

Simulations of the *n*ELBE ^{235}U and ^{242}Pu parallel plate fission ionization chambers are presented using finite element methods and extensive GEANT4 simulations. The homogeneity of the electrical field was improved and the optimal amount of target material determined. Pile-up effects due to the high α activity of the plutonium targets have been considered in a realistic geometry.

1 Introduction

The simulation of transmutation in innovative reactor systems or accelerator driven systems (ADS) requires accurate nuclear data [1]. Sensitivity studies [2, 3] show that the total uncertainty of cross section data has to be reduced below 5 % to enable reliable neutron physical simulations. However, neutron-induced fission cross sections of plutonium and minor actinides in part show high uncertainties in the fast-neutron range. For example, available data on ^{242}Pu are discrepant by about 21 % (see for example Fig. 1), where the target uncertainties are in the order of 7 %.
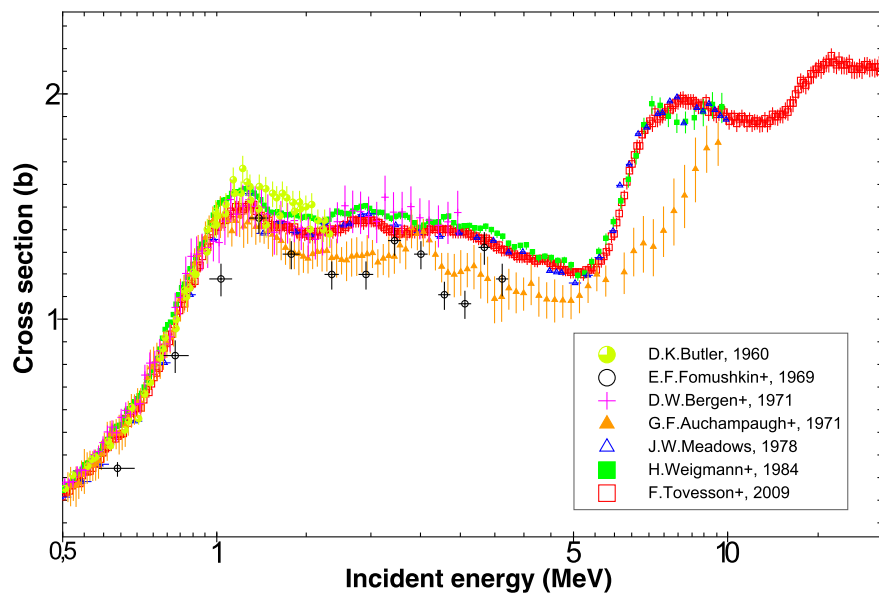
Fig. 1: Selected fast neutron-induced fission cross sections on ^{242}Pu taken from the EXFOR database [4] (graph taken from Janis 3.4 [5]). Large discrepancies are visible above the fission threshold at around 2 MeV.

The *n*ELBE neutron time-of-flight facility at the new National Center for High-Power Radiation Sources at Helmholtz-Zentrum Dresden-Rossendorf (HZDR) will be used to face the challenging task of reducing nuclear data uncertainties. Improved experimental conditions (low-scattering environment) and beam power, paired with the adequate spectral shape of the neutron beam will provide excellent conditions to achieve this aim.

Table 1: Isotopic composition of the targets.

(a) Plutonium target		(b) Uranium target	
Isotope	rel. abundance (%)	Isotope	rel. abundance (%)
^{238}Pu	0.003	^{234}U	0.0100
^{239}Pu	0.005	^{235}U	87.9600
^{240}Pu	0.022	^{236}U	0.0039
^{241}Pu	0.009	^{238}U	12.0261
^{242}Pu	99.959		
^{244}Pu	0.002		

2 Design of the *n*ELBE fission chambers

Two parallel-plate fission ionization chambers are currently under development at the HZDR. The fission chambers will measure fission fragments from thin and homogeneous (cf. Fig. 2) minor actinide layers.

The target material is deposited on eight 400 μm silicon wafers by molecular plating [6]. To ensure good electric conductivity, the wafers will be coated with a 100 nm titanium layer. The target diameter (74 mm) was chosen to be larger than the neutron beam diameter to avoid uncertainties related to beam profile effects.

Eight uranium targets with a total amount of 160 mg ($n_A \approx 450$ μg/cm^2) uranium (the isotopic composition is shown in Table 1) have already been produced at the Institute for Nuclear Chemistry of the University of Mainz. With the neutron flux of *n*ELBE a neutron-induced fission count rate of 2-5 per second can be achieved. The production of the plutonium targets ($m_{Pu} \approx 50$ mg, $n_A \approx 150$ μg/cm^2) is still in progress.
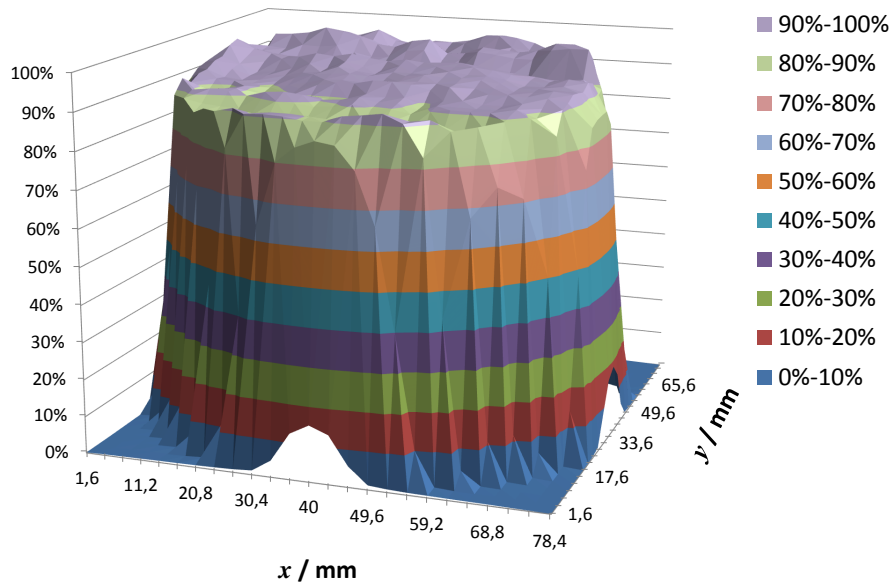
Fig. 2: Radiographic image of an ^{235}U target produced by the Institute for Nuclear Chemistry of the University of Mainz. The image plate is sensitive to the α activity of the target isotopes and reflects the distribution of uranium within the sample. A homogeneous target is important for the precise examination of neutron induced fission cross sections.

Due to the high radiotoxicity, the plutonium samples will be placed in a metal-sealed vacuum chamber (Fig. 3). A continuous gas flow of P10 (90 % Argon + 10 % Methane) gas at 1 atm will be

applied in combination with ultra high purity gas ceramic filters. Sealing and filtering are necessary to protect against release of radioactive particles with the counting gas flow.
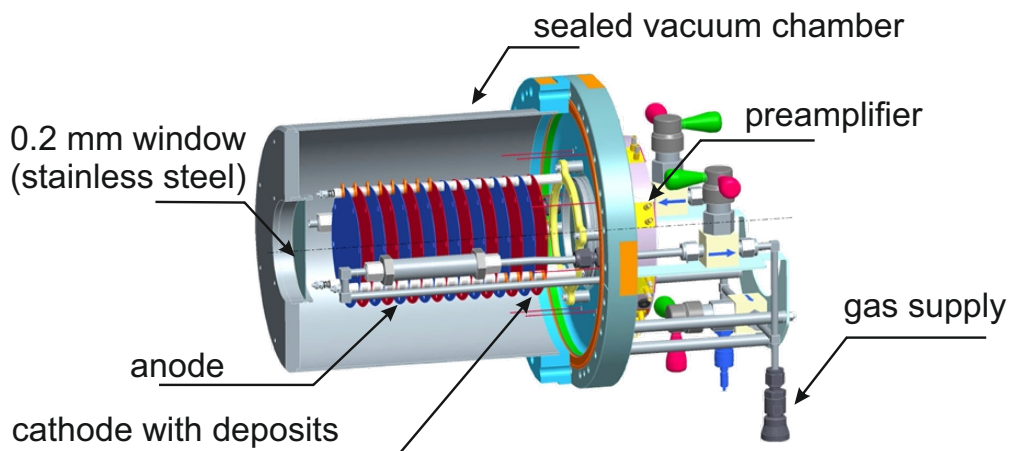
Fig. 3: Computer-aided design of the fission chamber.

The influence of the stainless steel filter housing on the electrical field homogeneity was examined using the finite element simulation COMSOL Multiphysics®. Small perturbations of the field are clearly visible in Fig. 4. An optimization was achieved by a re-arrangement of the filters and an improvement in the design of the support rods and the copper clamps used to contact the layers with the voltage supply and the preamplifier.
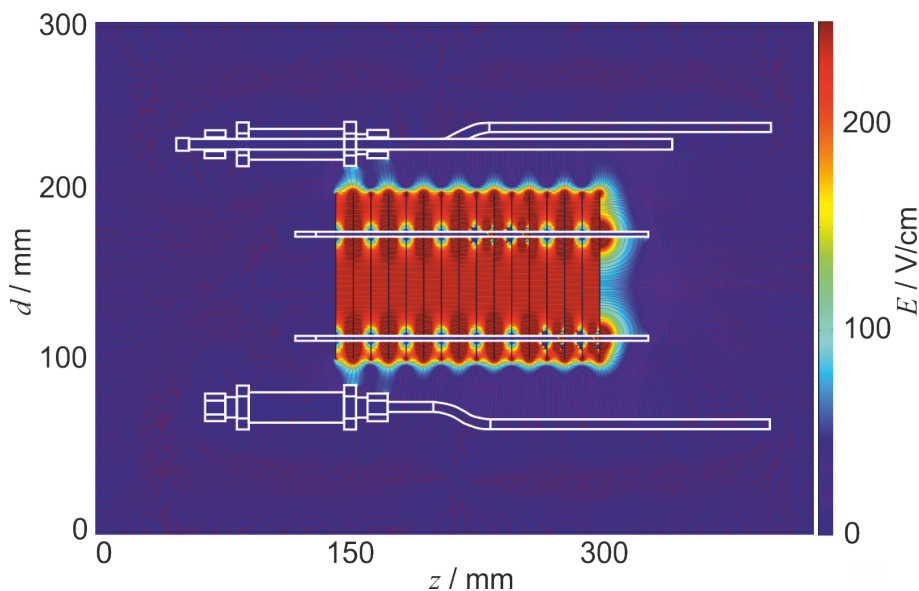
Fig. 4: Finite element simulation of the electric field within the fission chamber. The stainless steel ultra high purity gas filters and support rods are framed in white. Small perturbations of the field homogeneity are clearly visible arising from the small distance between filters and electrodes.

3 Simulations of pile-up

To handle the high specific α activity of the Pu targets, a combination of fast preamplifiers and digital signal processing has been developed to suppress pile-up effects. A fast charge-sensitive preamplifier

was developed at HZDR that produces total signal times in the order of 300 ns and shows identical performance in terms of time and energy resolution compared to conventional preamplifiers with $10 - 100\,\mu s$ decay constants. Nevertheless, pile-up events related to the α decay will influence the measurement. The α-decay rate per sample is expected to be 1.51 million per second. Occurring within a time window of typical signal rise-times of 110 ns, the probability of higher (2nd, 3rd and even 4th) order pile-up is not negligible. This could lead to a misinterpretation of fission events. To optimize the target thickness and total mass, simulations have been performed using the GEANT4 framework [7].

To use an accurate distribution of fission fragments in the GEANT4 simulation, the charge, mass and kinetic energies of the fission fragments were simulated using the General Description of Fission Observables (GEF) code [8]. Accurate data describing the α decay of plutonium was provided by the radioactive decay package of GEANT4 (G4RadioactiveDecay).

The probability P_n of detecting n additional α particles to the primary particle is given by

$$P_n(R,\tau) = \frac{(R\tau)^n e^{R\tau}}{n!},\tag{1}$$

where R denotes the expected detection rate and τ the time window, in which these events should occur. The fission rate was scaled with respect to a measurement at nELBE using the ^{235}U fission chamber H19 [9] of the Physikalisch-Technische Bundesanstalt (PTB) Braunschweig. Within the simulation, pile-up up to the 4th order was considered.

To create a realistic charge spectrum one also has to include the signal generation process into the simulation. The generated charged particle looses energy in the counting gas of the chamber and produces electron-ion pairs. Applying an electrical field between to electrodes, these charge carriers starting to drift in opposite directions. The induced charge on the anode [10] can be calculated by:

$$Q = \int_0^D \frac{n_e(z)ez}{D}\mathrm{d}z \qquad \text{with:} \qquad n_e(z) = \frac{1}{W}\int_0^D \left(-\frac{\mathrm{d}E}{\mathrm{d}z}\right)\mathrm{d}z$$

$$= \frac{e}{WD}\int_0^D \left(-\frac{\mathrm{d}E}{\mathrm{d}z}\right)z\mathrm{d}z\tag{2}$$

Discretization:

$$= \sum_i \frac{e}{WD}E_i \begin{cases} (D - z_i) & \text{forward bias (anode readout)} \\ z_i & \text{reverse bias (cathode readout)} \end{cases}\tag{3}$$

Equation 3 is a sum over all steps of a simulated event and sums the created charge at position z ($n_e(z)e$) multiplied by the ratio of their travel length to the anode and the distance (D) between anode and cathode. The number of produced electron-ion pairs can be calculated by dividing the locally deposited energy E_i by the average energy per ion pair (W) [11]. The outcome of this procedure is given in Fig. 5.

With 50 mg of plutonium and an electrode distance of 5 mm, a separation of α-induced background events from the main part of the fission fragment distribution is only possible for the reverse bias case, where the amount of fission events below the threshold is higher than for the forward one and the induced charge is much smaller. An increase of the layer spacing to 7 or 9 mm (cf. Fig. 6) will be performed, if this will not worsen the time resolution too much. Simulations with this spacing predicted the number of fission fragments below a threshold of $Q_{FF} \leq 100$ fC to be less then 0.9%. The distribution of fission fragments in the low energy range drops firstly linearly to rise again below 15 fC.
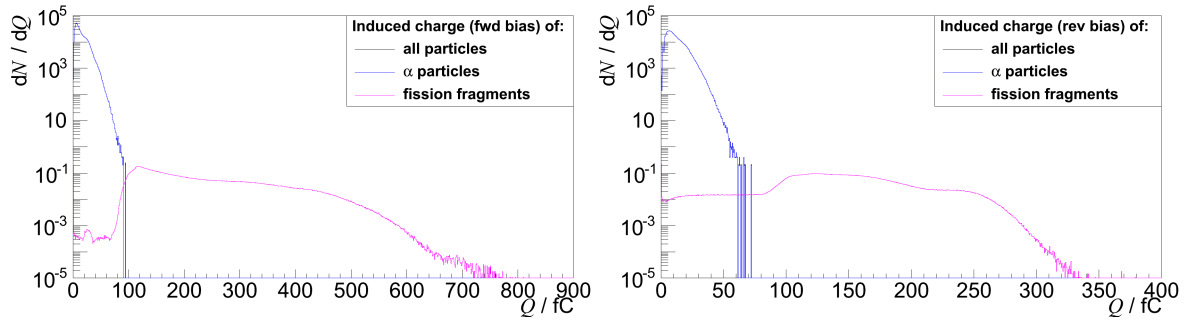
Fig. 5: GEANT4 simulated pulse height spectra of the decay products (blue) and fission fragments (magenta) from neutron-induced fission of the *n*ELBE plutonium target material in P10 counter gas. On the left side the forward biased case and on the right hand side the reverse biased case. The distance between anode and cathode was 5 mm.
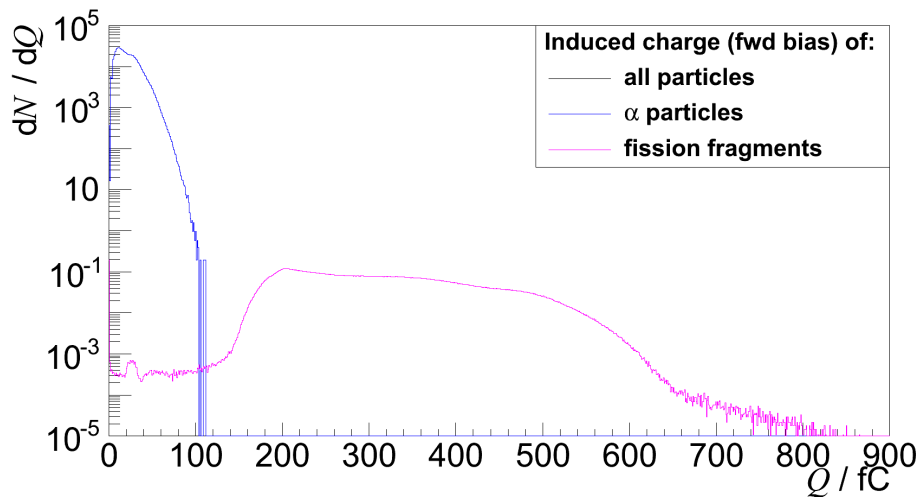
Fig. 6: Simulated forward biased charge spectrum for an electrode spacing of 9 mm. The used colour code is identical to Fig. 5.

4 Conclusions

Fast neutron-induced fission experiments on ^{235}U and ^{242}Pu will be performed at the neutron time-of-flight facility *n*ELBE in the near future. Fission cross sections will be examined using a parallel-plate fission ionization chamber. Different chamber parameters have been optimized by using extensive GEANT4 simulations and finite element methods. For the announced 50 mg of plutonium and the resulting target thickness, the loss of fission events below the trigger threshold is negligible low ($\approx 0.7\%$) and the calculated neutron-induced fission rate is high enough to perform experiments with sufficient statistics in less than one week. The construction of the uranium chamber was successfully completed and the analysis of the first *n*ELBE data is ongoing.

References

[1] M. Salvatores, G. Palmiotti, PROG. PART. NUCL. PHYS. **66**, 144 (2011).

[2] Working Party on International Evaluation Co-operation, THE HIGH PRIORITY REQUEST LIST FOR NUCLEAR DATA (HPRL) (2011). `http://www.nea.fr/html/dbdata/hprl/`.

[3] Working Party on International Evaluation Co-operation, UNCERTAINTY AND TARGET ACCURACY ASSESMENT FOR INNOVATIVE SYSTEMS USING RECENT COVARIANCE DATA EVALUATIONS (2008). `http://www.nea.fr/html/science/wpec/volume26/volume26.pdf`

[4] Nuclear Reaction Data Centres Network - The EXFOR database, IAEA **NDS**, 206 (2008). `http://www-nds.iaea.org/nrdc/nrdc_doc/iaea-nds-0206-200806.pdf`

[5] N. Soppera *et al*., J. KOREAN PHYS. SOC. **59**, 1329 (2011).

[6] A. Vascon *et al*., NUCL. INSTRUM. METHODS **A 696**, 180 (2012).

[7] The GEANT4 Collaboration, NUCL. INSTRUM. METHODS **A 506**, 250 (2003).

[8] K.-H. Schmidt, B. Jurado, PHYS. REV. C **83**, 014607 (2011).

[9] R. Nolte *et al*., NUCL. SCI. ENG. **156**, 197 (2007).

[10] G. F. Knoll, *Radiation Detection and Measurement*, (John Wiley & Sons, Inc., New York, 1999) Vol. III, p. 151.

[11] J. Beringer *et al*. (Particle Data Group), PHYS. REV. **D 86**, 010001 (2012)

Development of a neutron converter for studies of neutron-induced fission fragments at the IGISOL facility

M. Lantz[1], *D. Gorelov*[2], *A. Al-Adili*[1], *A. Jokinen*[2], *V. Kolhinen*[2], *A. Mattera*[1], *S. Rinta-Antila*[2],
H. Penttilä[2], *S. Pomp*[1], *V. Rakopoulos*[1], *V. Simutkin*[1] *and A. Solders*[1]

[1] Uppsala University, Uppsala, Sweden
[2] University of Jyväskylä, Jyväskylä, Finland

Abstract

The ERINDA funded scientific visit has enabled the groups at Uppsala University and University of Jyväskylä to work closer together on the design of a neutron converter that will be used as neutron source in fission yield studies at the IGISOL-JYFLTRAP facility at the University of Jyväskylä. The design is based on simulations with both deterministic codes and Monte Carlo codes, and an ERINDA funded benchmark measurement. In order to obtain a competitive count rate the fission targets will be placed very close to the neutron converter. The intention is to have a flexible design that will enable neutron fields with different energy distributions. In this report the progression and the present status of the design work will be discussed, together with an outlook of the future plans.

1 Background

The IGISOL-JYFLTRAP facility was recently moved to a new location within the accelerator laboratory at the University of Jyväskylä. A high intensity MCC30/15 cyclotron that gives 100 μA protons in the energy range 18-30 MeV, and about 50 μA deuterons of 9-15 MeV, has been installed, eventually the intensities can be increased even further. The high intensity beams of charged particles allow the production of a high neutron flux through some (p,xn) or (d,xn) reaction by using a suitable material as neutron production target. The resulting neutron field can be used for high precision studies of neutron-induced fission-fragment distributions, where the Ion Guide Separator On-Line (IGISOL) technique is combined with the JYFLTRAP Penning trap. The method has been successfully used for proton-induced fission yields [1, 2] and it is therefore of interest to extend the use with a neutron source. This opens up new possibilities for fundamental research on nuclides far from stability, and for systematic studies of fission yield distributions in view of present and future nuclear fuel cycles.

2 Objectives

The aim of the ERINDA scientific visit was to allow closer interaction between the groups at Uppsala university and University of Jyväskylä with the purpose of determining a feasible design for a neutron production target, a so called neutron converter. The converter is to be used for measurements of neutron-induced independent fission yields at the new IGISOL-JYFLTRAP facility.

It should be mentioned that there are two seemingly conflicting goals that need to be fulfilled for the neutron converter:

– The Jyväskylä group has a long and proud history of fundamental research with radioactive nuclides, and the intention is to perform nuclear structure studies on neutron-induced fission-fragments far from the stability line. In order to be competitive with other experimental facilities the neutron converter should be able to deliver 10^{12} fast neutrons (E > 1 MeV) per second on a ^{238}U target.

– The mutual interest of the Jyväskylä and Uppsala groups to provide nuclear data of relevance for society, in particular within the objectives of the ERINDA framework, requires neutron fields with

energy distributions that resemble those in nuclear reactors, i.e. thermal spectra as well as fast reactor spectra.

There are also some other boundary conditions that have to be fulfilled:

– The use of a 30 MeV proton beam with 100 μA intensity that fully stop in the neutron converter means that about 3 kW of heat is deposited in a very small volume of material. Cooling requirements may limit the options for suitable materials and geometries.

– Activation of the neutron converter will have to be handled. The IGISOL experimental chamber will also be used for other experiments so it is important to find a solution where the induced activation does not reduce access too much. There is also the concern that the neutron converter may suffer problems with structural integrity due to hydrogen buildup from the absorbed protons or deuterons.

With these goals and constraints in mind the aim has been to reach a flexible design that is relatively easy to assemble and remove, that allows different neutron fields, that will maintain its structural integrity, and that will not compromise safety when it comes to induced radioactivity and chemical toxicity.

3 Initial approach and some lessons learned

Some preliminary studies were initiated by the Uppsala group during 2010, before the ERINDA funded scientific visit had been approved. The initial approach was to start from the geometry of the ANITA white neutron source that is available at TSL [3]. The ANITA target is made of tungsten, which has a very high melting point, high thermal conductivity and give relatively little residual radioactivity at the proton energies of interest [4]. The dimensions of the ANITA target is a cylindrical disc with 5.0 cm diameter and 2.5 cm thickness.

The initial studies with Monte Carlo codes started with characterizing the neutron flux with respect to energy and angular distributions. The geometry was varied in different ways and moderator materials were introduced in order to imitate light water reactor spectra. There were also studies with different geometries of the fission target and heavy metal reflectors in order to enhance the neutron flux on the fission target. Focus was on tungsten as converter material although studies on beryllium were performed for comparison. Only protons were considered due to the ambition of maximising the neutron flux and the difficulty of properly simulating the (d,xn) reaction with the Monte Carlo codes. Below are some conclusions drawn from the initial studies [4, 5]:

– The neutron flux does not vary significantly with the geometry of the target. Incident projectile energy and neutron scattering angle determines the flux roughly within a factor of two, no matter which geometry is used.

– The flexibility with the target geometry allows for enough surface area to be in contact with some sort of cooling circuit in order to provide sufficient cooling.

– It is relatively easy to imitate a light water reactor spectra by introducing layers of water or polyethylene as moderator, while a fast reactor spectra can only be approximated very roughly. In both cases there will be an excess of fast neutrons depending on the incident proton energy and neutron scattering angle, see Fig. 1.

– The excess of fast neutrons can be reduced by using protons at lower incident energy, or deuterons, though with the consequence of reducing the total number of fast neutrons.

– The goal of 10^{12} fast neutrons on a fission target can be fulfilled with tungsten by placing a foil of ^{238}U in the forward direction, spanning a cross sectional area of about 10 cm x 10 cm approximately 10 cm from the neutron converter.
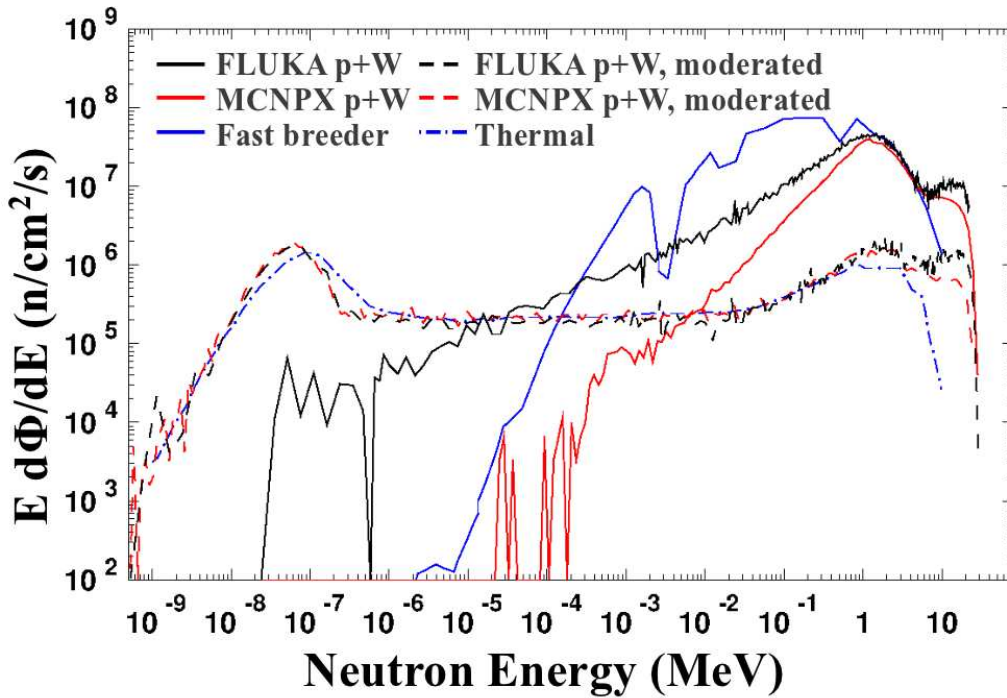
Fig. 1: Simulated neutron spectra for 30 MeV protons on a thick tungsten targets, with and without 10 cm of moderator, compared with typical spectra for light water (thermal) and fast breeder reactors. The discrepancy between MCNPX and FLUKA is clearly seen for the unmoderated spectra. There is an excess of high energy neutrons in comparison with the reactor spectra, due to the high energy of the incident protons.

- The use of heavy metal reflectors behind the fission target only slightly increases the effective neutron flux, and mainly at low energies. Furthermore it means that more material will be exposed to neutron activation, increasing the radiotoxicity of the assembly.
- The use of beryllium instead of tungsten increases the fast neutron flux with about a factor of seven, and the total neutron flux with about a factor of four.

The simulations of neutron production were initially performed with MCNPX [6], and later on the work was cross checked through independent simulations with FLUKA [7, 8]. FLUKA has also been used for determining the geometrical distribution of the heat deposition within the target, and for calculations of induced radioactivity within the target and surrounding material. Heat transfer and the need for cooling has been studied with COMSOL Multiphysics [9].

Some discrepancies between MCNPX and FLUKA have been observed both in the shape of the neutron fields and in their absolute magnitude, see Fig. 1 for an example with 30 MeV protons on tungsten. So far, the reasons for the discrepancies have not been fully sorted out, but it should be pointed out that incident proton energies below 50 MeV are relatively challenging for the models used in the Monte Carlo codes. Whatever the reason, the discrepancies do not change any conclusions regarding the design of the neutron converter, but may impact the information used for normalization of experimental results. The reference measurement (see Sec. 5) and comparison with other measurements will help to reduce these uncertainties.

4 Towards a final design

The option of using beryllium was initially discarded due to concerns about its toxicity, but when it became clear that it would significantly increase the fast neutron flux the issue was reconsidered. It was decided to aim for a design where factory made pieces of beryllium can be used in a flexible target holder without any further machining, and where the structural integrity would be preserved as far as possible.

When the development of the LENS target at Indiana University Cyclotron Facility [10] came to our knowledge a similar approach was pursued. In brief, the idea is to make the target slightly thinner than the full stopping length, and to have the cooling media (water) directly on the back side of the target plate. The effect is that the noninteracting protons stop in the cooling water instead of in the target, thus significantly reducing hydrogen buildup. Furthermore the main part of the Bragg peak will occur in the cooling water, reducing the need of a high flow rate of cooling water. The neutron production will only be reduced by less than 10% as the energy of the outgoing protons are near the neutron production threshold.

A design has been proposed and decided upon, where the beryllium disc is pressed against an O-ring that ensures a vacuum tight assembly where no water will leak into the beam pipe, see Fig. 2. The risk can be further reduced by having the beam pipe ending with a thin window of havar or steel in front of the target assembly [11]. With such a design the target assembly can be positioned relatively freely within the IGISOL experimental chamber, without any need of tight attachement to the beam pipe [12]. This will speed up the procedure of removing the assembly, thus reducing exposure of personnel to radioactivity.

The design will allow the use of different target materials and target thicknesses. It may be feasible to construct several identical target assemblies, if need be one can then quickly replace the entire assembly instead of wasting time with opening the assembly for exchange of the target disc. By using thinner beryllium targets, or targets of other materials, different neutron fields can be used for intercomparison.
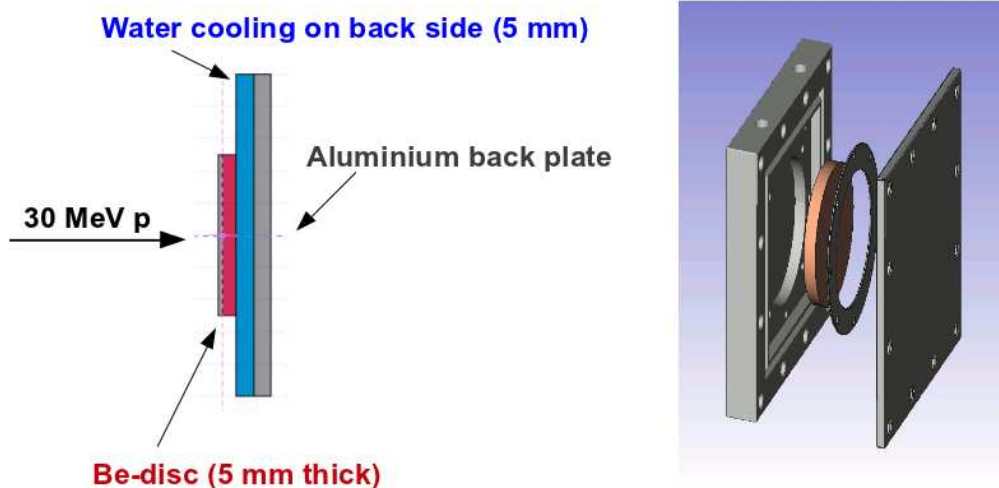
Fig. 2: Principle drawing (left) of a beryllium neutron converter for the IGISOL project. Protons will loose most of their energy within the target, the neutrons that do not cause any nuclear reaction will be fully stopped in the water layer behind the target. CAD drawing of the target assembly (right) by D. Gorelov.

5 Reference measurement at TSL

Besides sorting out the observed discrepancy between the predicted neutron fields from the Monte Carlo codes MCNPX and FLUKA, it is of importance to have a reference measurement from a target assembly of similar design as the one that will be used at the IGISOL facility. Therefore an ERINDA funded experiment [13] was performed with a mockup of the target assembly. The neutron field in the forward direction was measured, varying several parameters. Two different measurement methods were used, Bonner Sphere Spectrometers (BSS) for energies from the thermal range up to about 20 MeV, and a Time-of-Flight measurement with a liquid scintillator for the energy range 5-30 MeV. Analysis is approaching the final stages and some preliminary results and status reports have been reported at different occasions [14–16]. More details are given elsewhere in these proceedings [17].

6 Present status and outlook

In June 2013 the first experiment with the new IGISOL-JYFLTRAP facility was performed, where isomeric yield radios from selected proton-induced fission products were measured in an ERINDA funded experiment [18, 19]. This was an important first step of improving the performance of the JYFLTRAP, and the experimental results will be assessed before introducing the neutron converter, which is being constructed during the winter 2014.

   Although a the general design and the selection of beryllium as target material has been decided, there are still a number of issues to look closer at:

- Activation of the target and surrounding material: Preliminary studies were initally performed using FLUKA and are now being followed up in more detail. This is of importance in order to work out strategies for how to handle the target and planning for other experimental work in the IGISOL chamber.

- Radiation protection during experimental runs: The IGISOL experimental hall is situated behind heavy concrete shielding, with the data taking area being on the outside of the concrete, adjacent to the JYFLTRAP. Due to the high intensities from the new MCC30/15 cyclotron the neutron flux in the full geometry of the experimental facility is being simulated as a precaution.

- The MCNPX/FLUKA discrepancy: We are performing a systematic intercomparison between the two codes, varying different parameters in order to try to pinpoint the reasons for the discrepancy. Earlier discussions with members of the FLUKA development team did not reveal any user error, but a close scrutiny of how both codes are handled will be performed. If no reason is found the issue will be brought up again with the FLUKA and MCNPX development teams in order to find out the reason. It should be mentioned that both development teams expect better agreement between the two codes.

- Neutron background: The neutron flux within the IGISOL chamber will have a background that is dominated by scattering from the chamber itself. To a smaller extent there will be a contributions from different objects and surrounding concrete in the IGISOL experimental hall. The magnitude of these background sources will have to be assessed and eventually corrected for, depending on the type of experiment. In Fig. 3 is an example from FLUKA simulations where the neutron field from the bare target assembly (both options of beryllium and tungsten are shown) is compared with the same target inside the IGISOL chamber. The figure also show the effect of introducing a polyethylene moderator between the target assembly and the fission target. As seen there will be a thermal neutron peak due to scattering in the IGISOL chamber itself. In spite of this, a moderator material may still be useful in order to modify the neutron spectrum.

- Gamma-induced effects: So far only rough estimates have been made on the effects of intense gamma flux from the converter, mainly on the fission rate. The contribution is relatively small but not negligible and needs to be assessed.
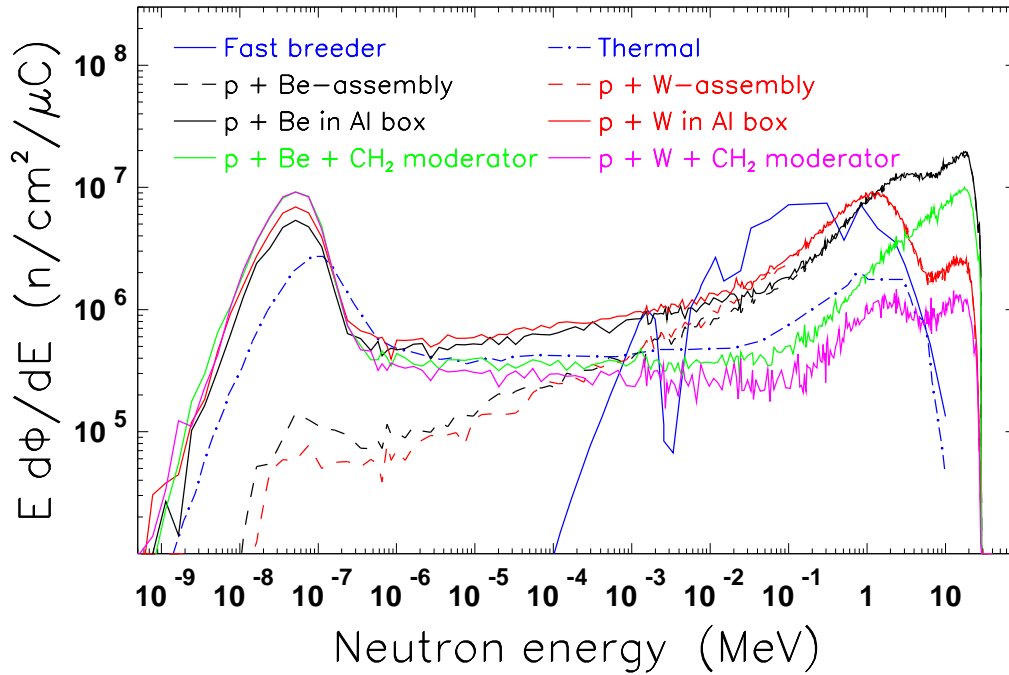
Fig. 3: FLUKA simulation with example of how the neutron spectrum from the target assembly (dashed lines) is affected by the IGISOL target chamber (solid lines) and the inclusion of a 10 cm thick CH_2 moderator block (solid green and magenta lines). The difference in neutron spectra between beryllium (black and green lines) and tungsten (red and magenta lines) is also shown.

– Varying beam and geometries: With a relatively flexible target assembly one can use deuteron beams in order to vary the neutron spectrum. Reduction of proton energy is also a possibility in order to vary the neutron energy distribution. One can also consider placing the fission target at a different angle with respect to the beam direction, within the geometrical constraints given by the ion guide and the IGISOL chamber. These options need to be studied closer before being implemented.

It should be noted that a neutron converter with the suggested design can be constructed and used for measurement campaigns with relatively short notice, disregarding some of the study areas mentioned above. But for absolute normalization and disentangling of the energy dependence of the fission yields, there is plenty of work left to do, both through simulations and through further analysis of the experimental data from the measurement at TSL. It may also be fruitful to verify the actual neutron field within the IGISOL experimental chamber. Thin-film breakdown counters (TFBC) [20] in combination with neutron activation methods, similar to how they were used in another ERINDA funded experiment [21] could be a suitable solution. The use of TFBCs may also be considered as a permanent monitor of the actual neutron flux as they are small and rather radiation resistant.

7 Deliverables

The preliminary designs have been presented at various scientific meetings, one purpose being to obtain feedback from other researchers based on their experiences. References [5, 11, 12] discuss directly technical details around the design of the neutron converter, while refs. [14–17] are status reports on the analysis work of the data from the measurement on a mock-up target at the ERINDA funded experiment at TSL in June 2012 [13]. A more extensive article on the design is being prepared [22]. The ERINDA

scientific visit has also enabled members of the Uppsala group to participate in stable ion-beam tests at IGISOL-JYFLTRAP as part of the recommisioning of the new facility [23].

8 Conclusions

The objective of the scientific visit to Jyväskylä has been met as the basic properties for the design of a neutron converter have been determined. A flexible design has been proposed that can fulfil some essential boundary conditions and the somewhat contradictory requirements for fundamental research versus nuclear data taking in view of applications. Further work is necessary in order to obtain better knowledge of the neutron flux and other properties, but most of these issues are of importance mainly in the analysis step. Therefore the neutron converter is ready to be constructed.

Acknowledgements

References

[1] H. Penttilä, P. Karvonen, T. Eronen *et al.*, Determining isotopic distributions of fission products with a Penning trap, *Eur. Phys.* J. A **44** (2010) 147.

[2] H. Penttilä, V.-V. Elomaa, T. Eronen *et al.*, Fission yield studies at the IGISOL facility, *Eur. Phys. J. A* **48** (2012) 43.

[3] Y. Naitou, Y. Watanabe, S. Hirayama *et al.*, Measurement of the spectral neutron flux at the ANITA facility at TSL, *Proceedings of the 2009 Annual Symposium on Nuclear Data*, Ricotti, Tokai, Japan (2009).

[4] M. Lantz, D. Gorelov, B. Lourdel *et al.*, Neutron-induced fission studies at the IGISOL facility, *Proceedings of NEMEA-6*, Krakow, Poland, 25-28 October 2010, NEA/NSC/DOC(2011)4.

[5] M. Lantz, D. Gorelov, A. Mattera *et al.*, Design of a neutron converter for fission studies at the IGISOL facility, *Phys. Scr.* **T150** (2012) 014020.

[6] G.W. McKinney *et al.*, MCNPX features for 2006, *Proceedings of the 2006 ANS Winter Meeting*, Albuquerque, NM (2006).

[7] G. Battistoni *et al.*, The FLUKA code: Description and benchmarking, *AIP Conf. Proc.* **896** (2007) 31.

[8] A. Fassò *et al.*, FLUKA: A Multi-Particle Transport Code, Reports CERN-2005-10, INFN/TC05/11, SLAC-R-773 (2005).

[9] COMSOL Multiphysics ®, ©1997-2013 Comsol AB. Url: http://www.comsol.com.

[10] C.M. Lavelle, D.V. Baxter, A. Bogdanov *et al.*, Neutronic design and measured performance of the Low Energy Neutron Source (LENS) target moderator reflector assembly, *Nucl. Instrum. Meth.* **A 587** (2008) 324.

[11] M. Lantz, D. Gorelov, A. Jokinen *et al.*, Design of a High Intensity Neutron Source for Neutron-Induced Fission Yield Studies, *Proceedings of the IAEA Technical Meeting on the use of Neutron Beams for High Precision Nuclear Data Measurements* (2013), IAEA-F1-TM-42752.

[12] A. Solders, D. Gorelov, A. Jokinen *et al.*, Accurate Fission Data for Nuclear Safety, *Nuclear Data Sheets*, accepted for publication, arXiv: 1303-2829 [nucl-ex].

[13] R. Bedogni, D. Bortot, A. Esposito. *et al.*, Measurement of the energy spectrum from the new neutron source planned for IGISOL, *ERINDA PAC proposal PAC 3/9*, 15 March 2012.

[14] A. Mattera, P. Andersson, A. Hjalmarsson *et al.*, Characterization of a Be(p,xn) neutron source for fission yields measurements, *Proc. International Conference on Nuclear Data for Science and Technology*, New York, U.S.A., 4-8 March 2013, arXiv: 1304-0547 [nucl-ex].

[15] A. Mattera, R. Bedogni, P. Andersson *et al.*, Neutron energy spectra from a Be(p,xn) source for fission yield measurements, *Proc. NEUDOS-12*, Aix-en-Provence, France, 3-7 June 2013.

[16] V. Rakopoulos, M. Lantz, A. Solders *et al.*, Target thickness dependence of the Be(p,xn) neutron energy spectrum, *Proc. International Nuclear Physics Conference 2013*, Firenze, Italy, 2-7 June 2013.

[17] A. Mattera, R. Bedogni, V. Rakopoulos *et al.*, Measurement of the energy spectrum from the neutron source planned for IGISOL, *These proceedings*.

[18] M. Lantz, A. Mattera, S. Pomp *et al.*, Isomeric yield ratios of fission products in 25 MeV proton induced fission of ^{238}U, *ERINDA PAC proposal PAC 3/8*, 15 March 2012.

[19] D. Gorelov, J. Hakala, A. Jokinen *et al.*, Measurement of the Isomeric Yield Ratios of Fission Products with the JYFLTRAP, *These proceedings*.

[20] V.P. Eismont, A. Prokofiev, A.N. Smirnov, Thin-film Breakdown counters and their applications, *Radiat. Meas.* **25** (1995) 151.

[21] A. Wallner, Fe(n,x) and Th(n,x) reactions at energies up to 60 MeV measured with AMS, *ERINDA PAC proposal PAC 4/10*, 16 October 2012.

[22] M. Lantz, D. Gorelov, A. Mattera *et al.*, manuscript in preparation.

[23] V.S. Kolhinen, T. Eronen, D. Gorelov *et al.*, Recommissioning of JYFLTRAP at the new IGISOL-4 facility, *Nucl. Instrum. Meth.* **B 317** (2013) 506.

Measurement of the energy spectrum from the neutron source planned for IGISOL

A. Mattera[1], R. Bedogni[2], V. Rakopoulos[1], M. Lantz[1], S. Pomp[1], A. Solders[1], A. Al-Adili[1],
P. Andersson[1], A. Hjalmarsson[1], J. Valldor-Blücher[1], A. Prokofiev[1], E. Passoth[1], A. Gentile[2],
D. Bortot[2], A. Esposito[2], M.V. Introini[2], A. Pola[2], H. Penttilä[3], D. Gorelov[3], S. Rinta-Antila[3]

[1] Uppsala University, Sweden
[2] Laboratori Nazionali di Frascati (INFN), Italy
[3] University of Jyväskylä, Finland

Abstract

We report on the characterisation measurements of the energy spectra from a $Be(p,xn)$ neutron source to be installed at the IGISOL-JYFLTRAP facility for studies of neutron-induced independent fission yields.

The measurements were performed at The Svedberg Laboratory (Uppsala, Sweden), during 50 hours of beam-time in June, 2012. A 30 MeV proton beam impinged on a mock-up of the proton-neutron converter; this was a 5 mm-thick beryllium disc inserted in an aluminium holder, with a 1-cm thick layer of cooling water on the backside. The geometry of the mock-up has been chosen to reproduce the one that will be used as the IGISOL-JYFLTRAP source.

During the experiment, two configurations for the neutron source have been used: a fast neutron field, produced using the bare target; and a moderated field, obtained adding a 10 cm-thick Polyethylene block after the target assembly.

The neutron fields have been measured using an Extended Range Bonner Sphere Spectrometer (ERBSS), able to simultaneously determine all energy components of the spectrum from thermal energies up to tens of MeV. In addition to that, a Time of Flight (TOF) system was used to study more in detail the high-energy component of the neutron fields ($E \gtrsim 5$ MeV).

1 Introduction

We report on the measurements that took place at The Svedberg Laboratory (TSL) in June 2012 in order to characterize a $Be(p,xn)$ neutron source to be used for neutron-induced independent fission yield measurements at the upgraded IGISOL-JYFLTRAP facility in Jyväskylä, Finland.

Neutron-induced independent fission yields are an important quantity for both fundamental and applied nuclear physics. In view of the extension of the life-time of current nuclear reactors for power production, as well as the use of new fuel-cycles and Generation IV reactor designs, high-quality measurements of independent fission yields are desired. This is true both to provide data for neutron energies and actinides that are not available in evaluated nuclear data libraries and for those isotopes for which data exist, but are reported with large uncertainties [1].

The IGISOL-JYFLTRAP facility was successfully used in the past years to measure proton-induced fission yields from several actinides [2]. The setup has been recently upgraded, relocated and equipped with a high-current cyclotron MCC30/15, that can deliver proton (deuteron) beams up to 30 MeV (15 MeV) in energy and 100 μA (50 μA) in current. The isotope selection is done using a Penning trap, where isotopes' mass can be identified with a mass resolving power larger than $M/\Delta M \approx 10^5$. The upgraded beam-line has been used for the first time for measurements of proton-induced fission yields in June, 2013 [3].

The neutron source that will be used at IGISOL consists of a 5 mm-thick water-cooled beryllium target embedded in an aluminium case. Since the thickness of the beryllium disc is less than the stopping

range of 30 MeV protons, they will penetrate the target and stop in the subsequent 1 cm layer of cooling water. This makes the cooling easier and avoids the problem of hydrogen build-up in the target, at the cost of a small reduction ($\approx 5\%$) in the neutron output.

The energy of the produced neutrons was studied by Monte Carlo simulations with Fluka and MCNP [1,4]. The two codes, however, show some disagreement in the neutron spectra. Given the strong energy dependence of the fission yield with the neutron energy, a direct measurement of the neutron fields was then required, in order to investigate this discrepancy and validate the Monte Carlo calculations.

2   Materials and Methods

The measurement on a mock-up of the Be(p,xn) source that will be used at IGISOL-JYFLTRAP was performed at the Paula facility [5] at TSL. A sketch of the experimental setup is shown in Fig. 1. The initial proton energy of 37.3 MeV was reduced to 29.8 MeV with a 1.015-mm aluminium tile and a path in air. The period of the cyclotron was 44.25 ns.

Two configurations of the target were used: i) the mock-up of the target assembly (5 mm beryllium + 10 mm cooling water in an aluminium case), later referred to as "total field"; ii) the same target assembly to which a 10 cm Polyethylene moderator is applied, "attenuated field" in the following.

The neutrons from both these sources were measured with two independent and complementary techniques: an extended-range Bonner sphere spectrometer (ERBSS) and a time of flight (TOF) system.
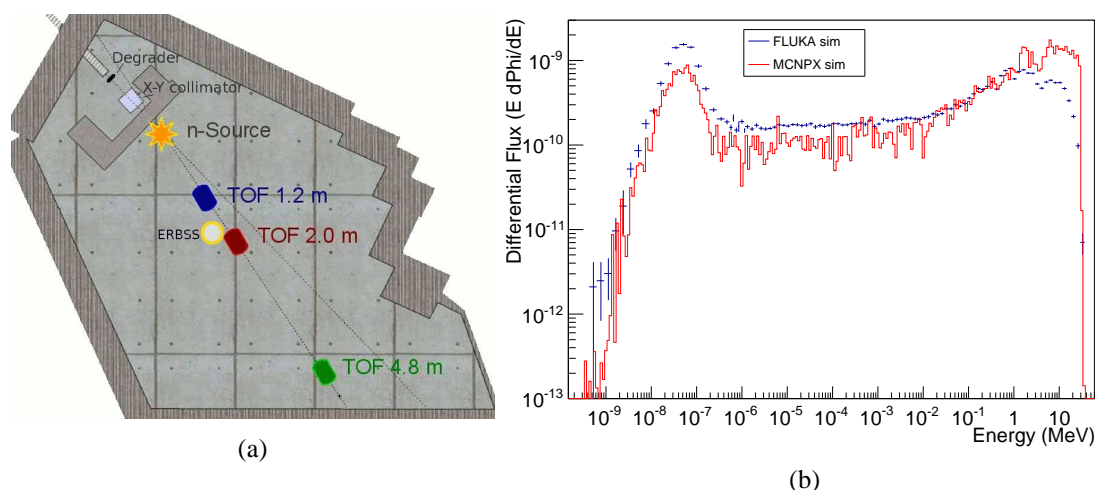

Fig. 1: (a) Experimental setup at the Paula facility, TSL; (b) Fluka and MCNPX simulation of the experimental setup. The two spectra have been used as guess for the FRUIT unfolding procedure.

2.1   Extended-range Bonner sphere spectrometer

The ERBSS was composed of fourteen spheres of different radii of moderator material, ranging from 0 (no moderation) to 12 inches. Three of the spheres also included a metal layer to increase the response at higher energies and extend the range of applicability of the ERBSS up to the expected end-point of the neutron spectrum (30 MeV).

The thermal neutron detector was a cylindrical 4 mm$\times$4 mm ^{6}LiI(Eu) scintillator. The gamma-background was rejected using a cut on the signals pulse height.

The data collected with the ERBSS was analysed using the deconvolution code FRUIT [6–8]. This can be used with a guess-spectrum or in parametric mode. In the first case, a guess spectrum is provided, typically derived from Monte Carlo simulations and possibly as close as possible to the spectrum to

be determined. In the second case, the neutron spectrum is modelled as a superposition of elementary functions, covering the different energy domains and fully described by a reduced number (less than ten) of physically meaningful parameters.

A statistical package within the code propagates uncertainties of input quantities (sphere counts, response matrix, monitor instrument uncertainty) through the unfolding process, thus obtaining distribution probabilities for all spectrum-integrated quantities (such as fluence and ambient dose equivalent) as well as for the neutron spectrum, on a bin-per-bin basis. Uncertainties are derived on this basis.

The fourteen spheres were exposed in sequence at the point of test (180 cm from the neutron-emitting target in forward direction) for both "total field" and "moderated field" scenarios. Their readings were normalized to the time-integrated indication of a fixed instrument (proton telescope), thus obtaining the so-called "normalized ERBSS counts".

The normalized ERBSS counts were unfolded using the FRUIT code in "guess spectrum" mode (FRUIT-SGM). Fluka and MCNPX simulations implementing the same simplified geometry of the experimental setup were performed to obtain pre-information suitable for the unfolding code. The spectra (Fig. 2) show two main structures, namely an evaporation peak at about 1 MeV and a high-energy peak at about 10 MeV. MCNPX produces a more intense high-E peak than Fluka.

2.2 Time of flight

The TOF system consists of a 3.3 litres BC-501 liquid scintillator from the NORDBALL array [9]. Measurements were performed with the detector at 3 different distances (1.2, 2.0 and 4.8 m) from the beryllium, in order to optimize the energy resolution vs. the effect of the wrap-around, both increasing with the source-to-detector distance. The pulse-shape discrimination (PSD) capabilities of the liquid scintillator allowed to reduce the gamma background.

Two data-acquisition (DAQ) systems were used simultaneously. An analog system, where the TOF was acquired and digitized with a TDC. Here the PSD was obtained from a dedicated electronics module and stored on an event-by-event basis along with the TOF information. The settings for the PSD were optimised before the experimental run with a ^{252}Cf neutron source and tested with the neutrons from the Be converter. The hardware threshold was varied between 3 values (corresponding to approximately 2, 3 and 7 MeV neutrons). And a digital system, where the pulse shapes were saved with a Multi Channel Analyser (SP Devices ADQ412 High-speed Digitizer) for off-line PSD. In this case, the threshold was kept constant at ≈ 2 MeV, since further cuts in pulse-height can be applied off-line.

In both DAQ systems, the trigger was provided by an event above-threshold detected in the scintillator (start of the TOF), while the TOF information was obtained from the radio-frequency pulse from the cyclotron (stop of the TOF). The calibration of the TOF and the identification of t_0, i.e. the time at which protons hit the beryllium target, was done by analysing the gamma peaks produced when protons hit elements along the beam-line.

3 Results

3.1 ERBSS

The experimental data obtained with FRUIT-SGM are more coherent with Fluka than with MCNPX. As far as the E > 10 keV region is concerned, FRUIT-SGM alters much more the MCNPX-based guess spectrum than the Fluka-based one. However, final unfolded spectra from both methods satisfactorily agree within the uncertainties provided (Fig. 4). These are generally < 15% (E < 5 MeV), 15-30% (5 - 20 MeV) and approximately 30% (E > 20 MeV).

Higher uncertainties above 20 MeV reflect the poor resolving power in this energy-range. The agreement between the Fluka- or MCNPX-based unfolded data is highly satisfactory. Obtaining the same final spectrum when different guess spectra are used is a robust indication about the code reliability.

These considerations are valid for both total field and moderated field scenarios (Fig. 5).
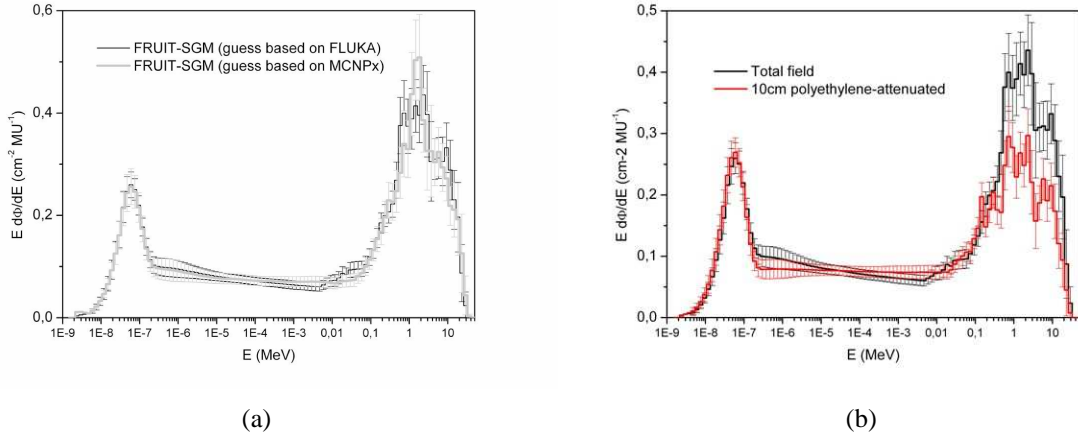

(a)

(b)

Fig. 2: Energy spectrum (a) unfolded with FRUIT compared with the Fluka-based guess spectrum and (b) ERBSS result of the total v. attenuated field.

3.2   TOF

The analysis of the TOF data have been performed in parallel for the two different DAQ systems. In the first step, the TOF has been converted to energy for each of the 3 source-to-detector distances. The background from neutrons scattered in the measurement room has been measured using the Shadow Cones technique. Still not implemented is a correction for the efficiency of the scintillator as a function of the neutron energies, that is currently being investigated using Monte Carlo calculations.

3.2.1   *Analog DAQ*

The effect of the on-line PSD can be observed in Fig. 7. From this basic plot it can already be seen that in correspondence of the gamma peaks (produced by protons hitting the collimators and the target), the online PSD misclassifies some of the photons as neutrons. This is also evident when TOF is converted to energy (Fig. 8).

The information from the measurements at the 3 distances has been merged to obtain a plot over the wider energy range, trying to reduce the effect of the wrap-around, still keeping the best available energy resolution for that energy range. The result of this attempt is shown in Fig. 9, where the TOF data are compared with ERBSS results.

3.2.2   *Digital DAQ*

The method used for the off-line PSD is the charge integration method that compares the total charge of the pulse with the charge obtained by a partial integration of the peak and the tail of the pulse. The full integration represents both the fast and the slow component (peak and tail) A_1, while the partial range (A_2) covers the fast component. The difference between these corresponds to the integral of the tail. The integrals are expressed in units of (V·ns). The optimal sample points for defining the start and the end of the integrals are depicted in Fig. 10. The area ratio R is defined as

$$R = \frac{A_1 - A_2}{A_1}.$$ (1)

Neutron pulses generally have a larger ratio R, as the magnitude of the slow component integral is larger for neutrons than for γ-rays. A classification point R_c must be chosen, in order to classify the
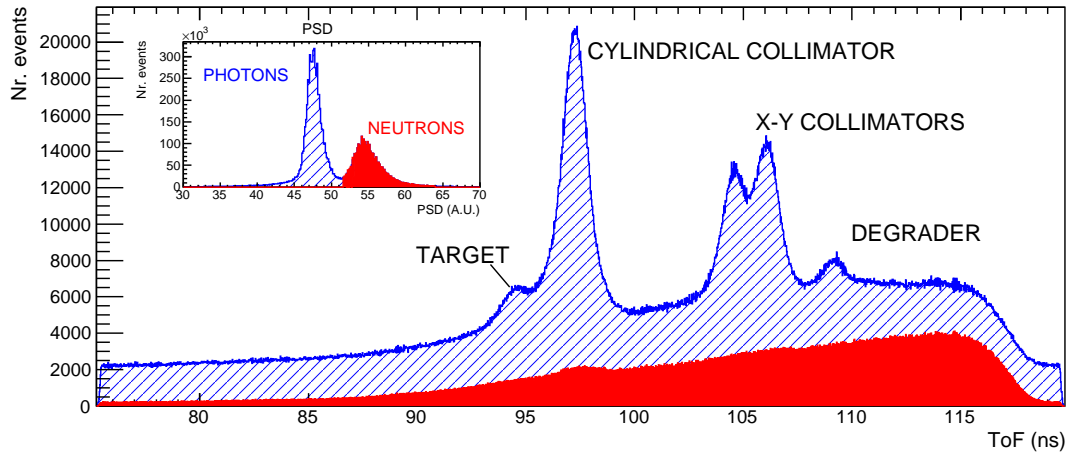
Fig. 3: Time of Flight spectrum from the analog DAQ showing the effect of the on-line PSD that allows to separate neutrons (solid red) from the gamma background (hatched blue).
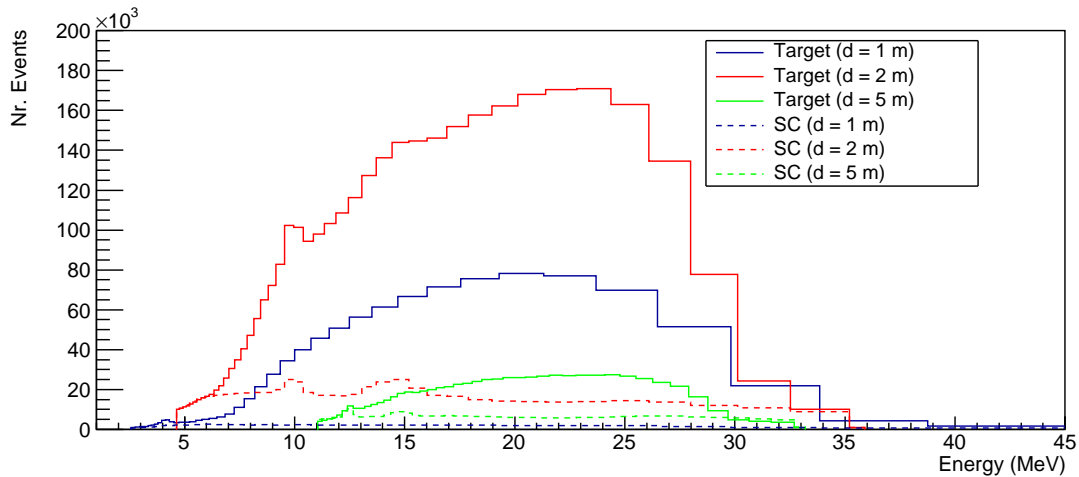

Fig. 4: Reconstructed energy spectrum from the TOF measurement with analog DAQ and online PSD without and with Shadow Cones (Target and SC, respectively). The proton current was changed between the runs at the 3 distances.

detected particles. Above this point, pulses are classified as neutrons, while below they are classified as γ-rays. An example of the one dimensional discrimination is shown in Fig. 11, with $R_c = 0.248$.

The optimization of the PSD has been further investigated in order to improve the results of the n-γ separation. For this reason a 2D-plot similar to the one shown in Fig. 13 has been used. The red line represents the two-dimensional cut that takes into account also the pulse height information. Some pulses, especially those corresponding to the low energy neutrons, are misclassified, but applying a 2D gate can improve the discrimination (Fig. 14) [10].

4   Conclusion

The energy spectra from a $\mathrm{Be}(p,xn)$ source for studies of neutron induced fission yields have been measured with two techniques: an ERBSS to measure from thermal energies up to 30 MeV and a TOF system, to focus on the high-energy part of the spectrum.

As far as the BSS is concerned, separate unfolding procedures have been performed by using both
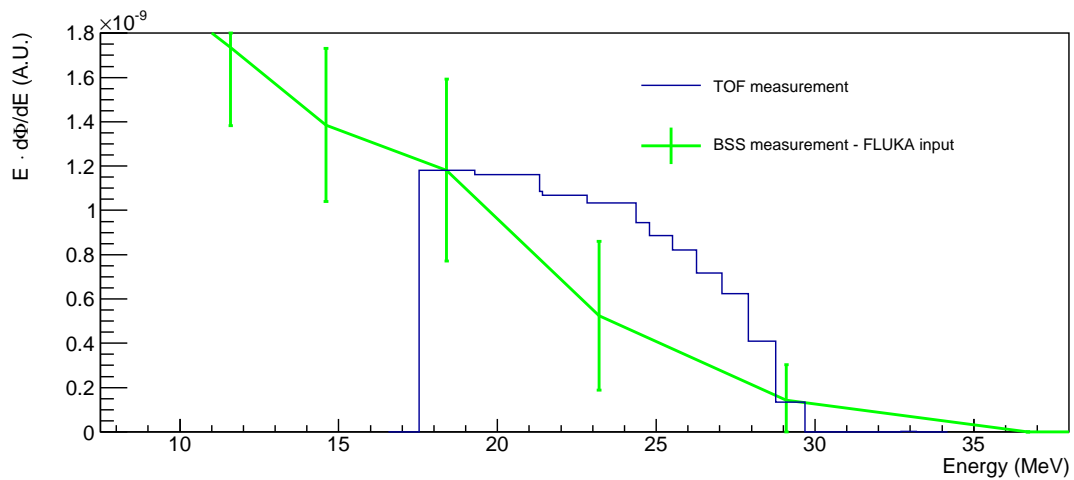
Fig. 5: Energy distribution obtained combining the measurements at the 3 different distances. The TOF distribution is compared with the BSS result.

(a)

(b)

Fig. 6: (a) Integration of pulse over different time ranges and (b) resulting 1D-plot of the off-line PSD.

(a)

(b)

Fig. 7: (a) off-line n-γ PSD taking into account also the pulse height information and (b) result of the cut before (blue line) and after (red line) the 2D cut for the PSD. In particular, the peak due to misclassified photons (black arrow) is removed.

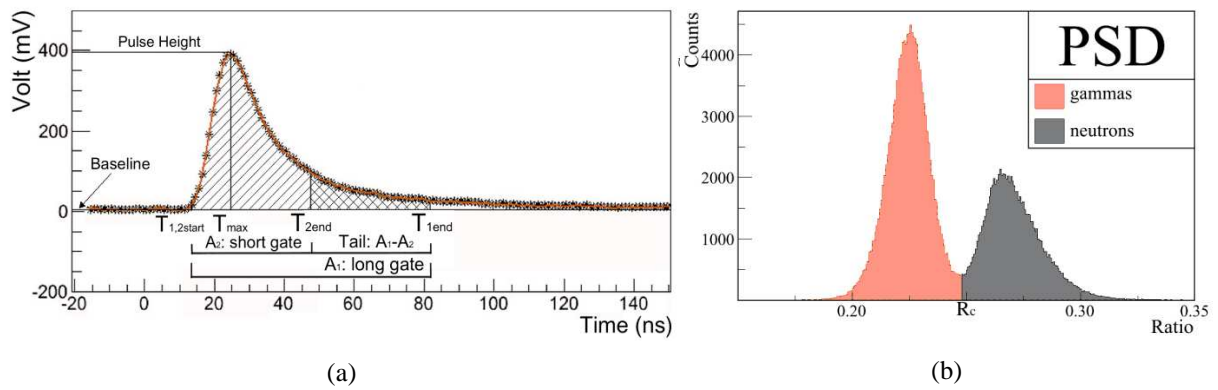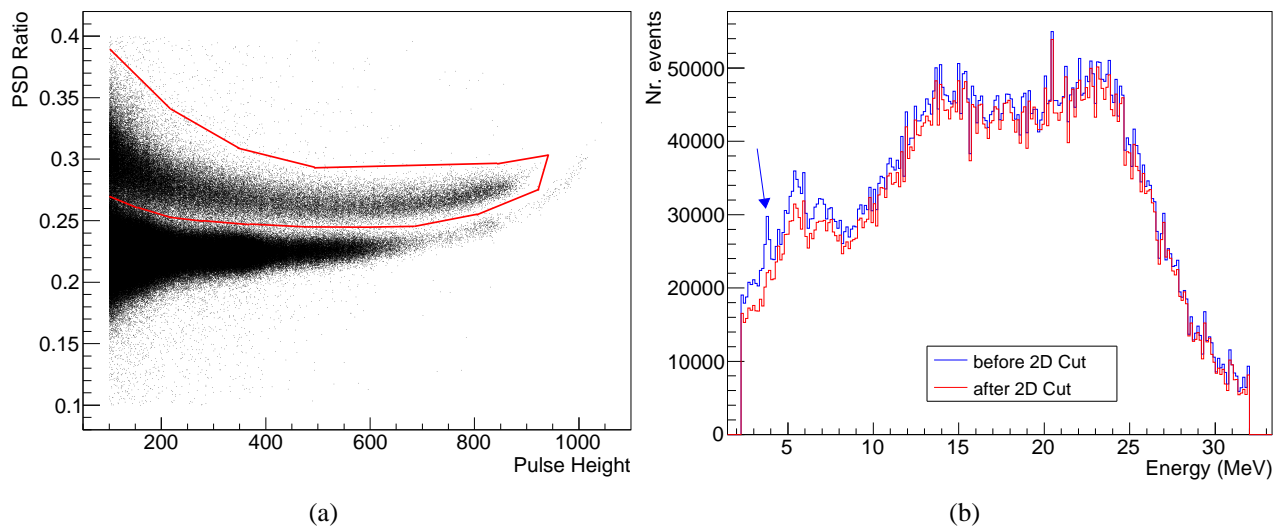a Fluka- and MCNPX-based guess spectra in the FRUIT-SGM code. Comparable spectra were obtained in both total or moderated field scenarios. The high-energy part of the BSS spectrum has been compared with the spectrum calculated with the TOF technique. The results are still preliminary, since an accurate correction for the response function of the TOF detector still has to be implemented; nevertheless a general agreement of the two techniques within the uncertainties provided can be observed.

The future work will focus on the estimation of the neutrons scattered in the experimental hall, that contribute to the low-energy peaks in the BSS spectra. This will help to investigate the disagreement that was found between the MCNPX and Fluka simulations. A realistic response function for the TOF technique will also be extracted combining Monte Carlo simulations and the pulse height information collected with the digital DAQ.

Acknowledgements

References

[1] A. Solders *et al.* (2013) Accurate fission data for nuclear safety. *Nuclear Data Sheets*. Accepted for Publication.

[2] H. Penttilä *et al.* (2012) Fission yield studies at the IGISOL facility. *The Eur. Phys. J. A* 48:43.

[3] D. Gorelov *et al.* (2013) Measurement of the Isomeric Yield Ratios of Fission Products with the JYFLTRAP. *These Proceedings*.

[4] M. Lantz *et al.* (2013) Design of a High Intensity Neutron Source for Neutron-Induced Fission Yield Studies. *Proceedings of the IAEA Technical Meeting on Use of Neutron Beams for High Precision Nuclear Data Measurements*.

[5] The Paula proton beam facility (Nov. 2013). `http://www.tsl.uu.se/ irradiation-facilities-tsl/PAULA-proton-beam-facility`.

[6] S. Agosteo *et al.* (2012) Characterization of extended range Bonner Sphere Spectrometers in the CERF high-energy broad neutron field at CERN. *Nucl. Instr. Meth. Phys. Res. A*694, 55.

[7] R. Bedogni *et al.* (2007) FRUIT: an operational tool for multisphere neutron spectrometry in workplaces. *Nucl. Instr. Meth. Phys. Res. A*580, 3.

[8] R. Bedogni *et al.* (2010) A parametric model to describe neutron spectra around high-energy electron accelerators and its application in neutron spectrometry with Bonner Spheres. *Nucl. Instr. Meth. Phys. Res. A*615, 78.

[9] S.E. Arnell *et al.* (1991) A 2π neutron and γ-ray multiplicity filter for the NORDBALL detection system. *Nucl. Instr. Meth. Phys. Res. A*300, 303.

[10] V. Rakopoulos *et al.* (2013) Target thickness dependence of the Be(p,xn) neutron energy spectrum. *Proceedings of INPC*. Accepted for Publication.

A Project for High Fluence 14 MeV Neutron Source

Mario Pillon[1], Maurizio Angelone[1], Aldo Pizzuto[1], Antonino Pietropaolo[1]
[1]Associazione ENEA-EURATOM Sulla Fusione, ENEA C.R. Frascati, via E. Fermi, 45, 00044 Frascati (Rome) Italy

Abstract
The international community agrees on the importance to build a large facility devoted to test and validate materials to be used in harsh neutron environments. Such a facility, proposed by ENEA, reconsiders a previous study known as "Sorgentina" but takes into account new technological development so far attained. The "New Sorgentina" Fusion Source (NSFS) project is based upon an intense D-T 14 MeV neutron source achievable with T and D ion beams impinging on 2 m radius rotating targets. NSFS produces about 1×10^{13} n cm^{-2} s^{-1} over about 50 cm^3. The NSFS facility will use the ion source and accelerating system technology developed for the Positive Ion Injectors (PII) used to heat the plasma in the fusion experiments,. NSFS, to be intended as an European facility, may be realized in a few years, once provided a preliminary technological program devote to study the operation of the ion source in continuous mode, target heat loading/removal, target and tritium handling, inventory as well as site licensing. In this contribution, the main characteristics of NSFS project will be presented.

1   Introduction

In the context of the development of future fusion machines, such as DEMO, the availability of a intense 14 MeV neutrons source is of paramount importance to address important issues, e.g. verify the influence of nuclear transmutation on the electric characteristics of ceramic insulators and window materials, experimentally select low activation materials, thus avoiding the uncertainties of numerical calculations, carry out basic studies on neutron damage to materials. In this respect, the feasibility study of the intense 14 MeV source named "The New Sorgentina Fusion Source (NSFS)" is a necessary step toward its full design and realization to serve as a large scale facility for the fusion community.

2   Performances and main feature of NSFS

The performances and main features of NSFS rely on those already stated at the European Workshop on the Requirements of a High-Energy Neutron Source for Fusion Materials Testing and Development held in Rome from 20 - 22 October 1988 [1], where the preliminary study of a single-target high flux fusion source was discussed. The performances were determined as follows: A 14-MeV neutron flux production, $\geq 10^{13}$ cm^{-2} s^{-1} in a volume (for irradiation) ≤ 0.5 dm^3, with a low flux gradient. It must also be possible to carry out simple experiments on materials during irradiation (e.g., heating and cooling of specimens). With the minimum flux required, specimen damage would be equal to 2 dpa over roughly a year's continuous irradiation. The main features should be neutron production with D-T reaction by irradiating a solid target containing tritium, with deuterium ions accelerated to 100-600 keV. Target with high heat dissipation

capability, e.g., water-cooled rotating disk made of copper alloy with Ti, Y, or Er coating loaded with T; increased target lifetime against T-loss, e.g., by using a mixed beam (D+T) and thereby continuously reloading the target. The technological feasibility of the above features has partly been demonstrated, and they have been proposed with the aim of constructing Sorgentina possibly within a short period of time , say 3-4 years, as many of these features are already typical of the Rotating Target Neutron Source (RTNS II) [2], that reached a maximum neutron intensity of about 10^{13} s^{-1} As a comparison, the intensity of the NSFS can be two orders of magnitude higher, in the order of 10^{15} s^{-1}. A neutron source that is based on the D-T fusion reaction basically consists of a vacuum vessel containing a T-saturated metal target, a D-ion source, and an electrostatic accelerator. The deuterium ions produced by the source are accelerated to energies of 100 - 600 keV and then hit the target. Here, a small fraction (8×10^{-5} n/deuteron) produces the 14-MeV neutrons through the T(d,n)^{4}He reaction, while the largest fraction is slowed down by collisions, without giving rise to nuclear reactions, and releases all its energy to the target (2.5×10^3 MeV/neutron). Under ion irradiation, the target releases tritium, and the neutron yield decreases with time. When the neutron yield is reduced a great deal, the target is replaced by another saturated with T. NSFS should have a rotating water-cooled target with a good capability for heat dissipation and a mixed D+T ion beam to reload the target with tritium and thus maintain the neutron yield constant for as long as possible. The conditions to insure this fact is to maintain the surface temperature of the target below about 300°C otherwise the deuterium and the tritium loaded by the impinging beams are released at a rate higher then the loading rate [3].

2.1   Consideration on the feasibility study of NSFS

The NSFS project is based upon two intense D-T 14 MeV rotating targets facing each-other. Two beams of 160 keV, 25A each provide 50-50% Deuterons and Tritons on a 2 m radius rotating target. Deuterium and Tritium are implanted during the beams bombardment on a Titanium layer covering the rotating targets. The Titanium layer, spattered by the beams bombardment, is continuous reformed using a Titanium sputtering source. Figure 1 shows a schematic of the target station.
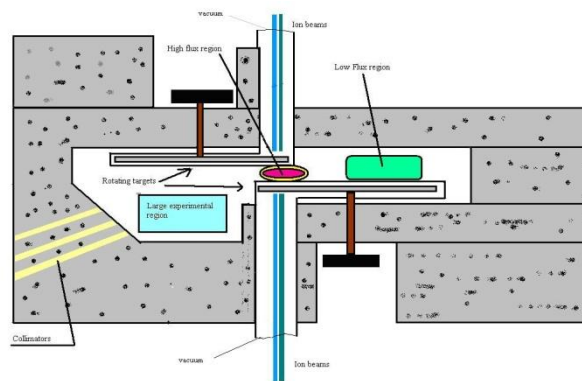
Fig. 1: Schematic of the NSFS' target station.

Figure 2 shows a 3D CAD-based picture of the double rotating target, while in figure 3 is shown the proposed configuration with the primary shielding.
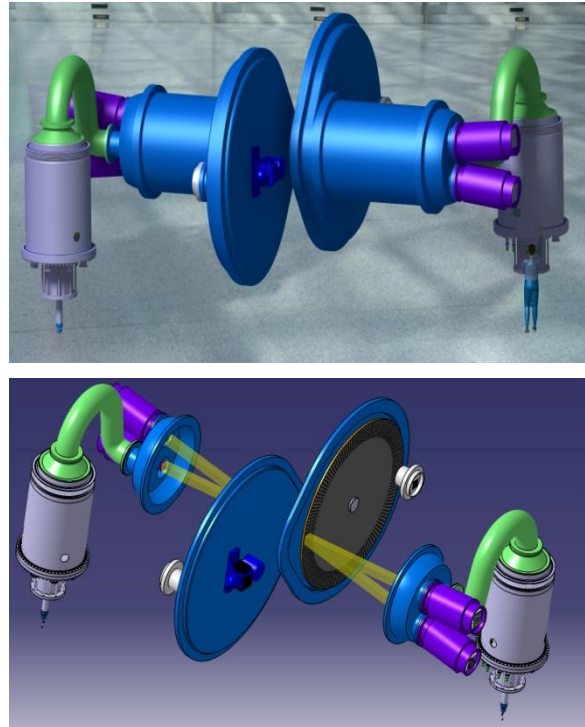
Fig. 2: CAD-based picture of the NSFS' rotating target.

One basic aspect of the proposed neutron source is the use of available and tested technology, e.g. the intense beams are produced by 4x4 MW power Deuterons and Tritons Positive Ion Injectors adapted to produce a rectangular spot of 10x20 cm2 on each rotating target.
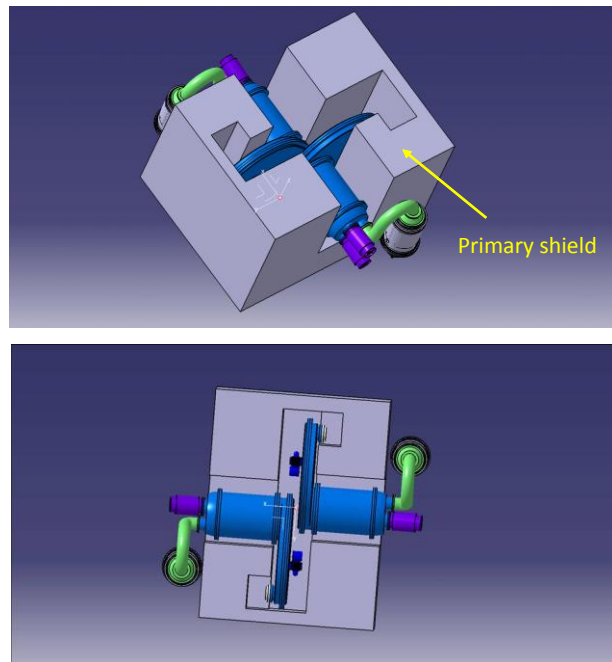
Fig. 3: CAD-based picture of the two rotating target inside the primary shield.

The main design parameters of the rotating targets can be found in Ref. 4. One important issue to be addressed is the thermal analysis on the target that should support an intense power load. Figure 4 shows the target temperature time evolution in one cycle for a beam power of 8 MW.
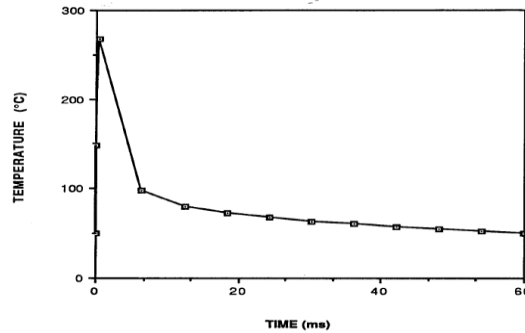

Fig. 4: Temperature of the Titanium surface as a function of time (radius= 2 m, frequency= 1000 rpm, incident beam power density= 40 kW/cm^2 ,one cycle).

The feasibility to load with hydrogen isotopes the titanium surface of the target has been investigated with and "ad hoc" experiment performed using the neutral beam test bed at JET. A deuteron beam has been used to implant, at high fluence rate, deuterium in a mock-up of NSFS target.

The mock-up of the target had a 1.6 ±0.1 µm tick Ti coating whose surface temperature was measured with an infrared thermometer while the bulk target was cooled with pressurized water flowing in apposite channels. A set of calibrated neutron detectors was used to determine the neutron source strength of the D-D reactions which occur during the deuteron bombardment. The measured neutron rate was converted in the amount of deuterium implanted using a neutron yield code developed for the Sorgentina project [4]. The results of these measurements is gathered in figure 5 where the measured deuterium concentration is shown versus the deuteron fluence also at different Titanium surface temperature demonstrating the feasibility of the deuterium implantation also for temperature around 400 °C.
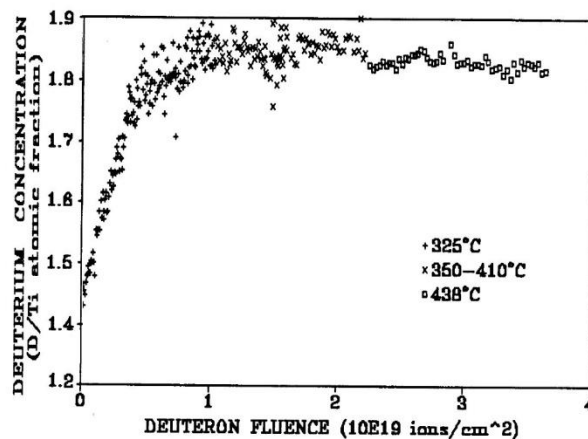
Fig. 5: Measurements of the deuterium implantation during deuteron bombardment in target mock-up.

3   Neutron Yield calculation

As a matter of fact, the neutron production depends on the impinging deuterons energy and the concentration level of D and T into the Ti lattice matrix. This is shown in figure 6, where the number of neutron per deposited power per second is plotted against beam energy. The data in figure 6 were calculated with a dedicated code developed for the Sorgentina project using the procedure suggested by Kim [5], assuming different hydrides content into the Ti matrix.
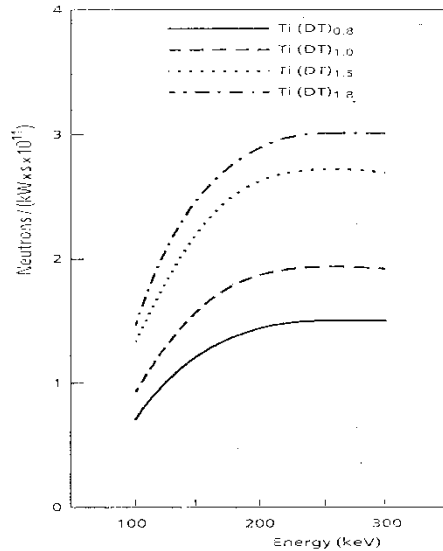
Fig. 6: Neutron yield per kW vs. beam energy from a 50-50% D-T beam striking a Titanium target versus different hydride load calculated with a dedicated code [4].

New Sorgentina Fusion Source is able to produce an high neutron flux region ($\sim 7 \times 10^{12}$ n/cm^2/s) of about 1200 cm^3. In a restricted volume of 50 cm^3 the neutron flux is $\sim 1 \times 10^{13}$ n/cm^2/s corresponding to 2 dpa/year in iron. With the target configuration sketched in figures 1,2 and 3, the flux is higher and the iso-flux surfaces, obtained by means of a MCNPX simulation using the modeled configuration in figure 7, are shown in figure 8.
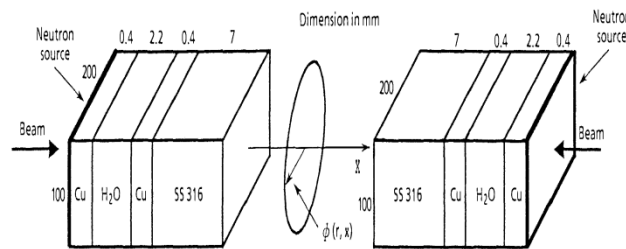
Fig. 7: Simplified MCNPX model used to calculate neutron flux within the region comprised between the two rotating targets.
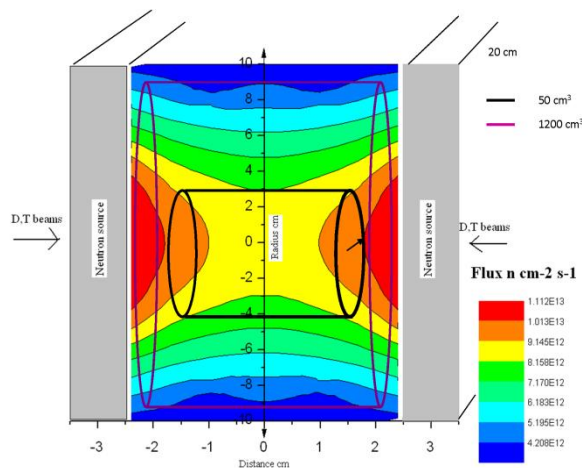
Fig. 8: Iso-flux surfaces in the region between the two rotating target obtained by means of MCNPX simulation.

4. Conclusions

The NSFS facility was described and its main design parameters and expected performances in term of neutron production were discussed. A 14 MeV neutron source like the NSFS may be considered of strategic importance for the fusion community for the experimental activity towards the DEMO machine. Indeed NSFS envisaged activity could be devoted to :

a) carry-out basic studies on 14 MeV neutrons induced damage into irradiated materials in turn validating damage calculation codes (~ 1- 2 dpa/y);

b) verify the influence of nuclear transmutation on the electric characteristics of   ceramic insulators, optical fibers and window materials;

c) provide a neutron field were damage cross sections can be tested and/or measured;

d) address basic experimental information for the selection of low activation materials;

e) furnish reliable data about the radiation hardness of materials to be used for diagnostics.

References

[1] EUR FU Brussels / XII - 230/88 Matia 12 lEA Paris.

[2] C.M. Logan and D.W. Heikkinen, Nucl. Instr. Meth. 200 (1982) 105-111.

[3] M. Martone et al. High Flux High Energy Deuterium Ion Implantation, in High Temperature titanium (Preliminary Experimental Tests for sn Intermediate Intensity Neutron Source, Sorgentina) ENEA internal report (June 1992)

[4] M. Martone et al. Feasibility Study of a 14-MeV Neutron Source (Sorgentina) , ENEA internal report (1990)

[5] J. Kim, Neutron Sources Using D-T Mixed Beams Driven into Solid Target, Nucl. Instrum. Methods 145 (1977) 9-17.

Measurement of cross-sections of yttrium (n,xn) threshold reactions by means of gamma spectroscopy

Petr Chudoba[1,2], S. Kilim[3], V. Wagner[1], J. Vrzalova1, 4, O. Svoboda[1], M. Majerle[1], M. Stefanik[1], M. Suchopar1, 4, A. Kugler[1], M. Bielewicz[3], E. Strugalska-Gola[3], M. Szuta[3], D. Hervas[1], T. Herman[1], B. Geier[1]

[1] Nuclear Physics Institute of the ASCR, v. v. i., Rez 130, 250 68 Rez, Czech Republic

[2] Charles University in Prague, Faculty of Mathematics and Physics, Ke Karlovu 3, 121 16 Praha 2, Czech Republic

[3] National Centre for Nuclear Research, Otwock-Swierk 05-400, Poland

[4] Faculty of Nuclear Sciences and Physical Engineering, Czech Technical University in Prague, Brehova 7, 11519 Praha, Czech Republic

Abstract

Neutron activation and gamma spectrometry are usable also for the determination of cross-sections of different neutron reactions. We have studied the cross-sections of yttrium (n,xn) threshold reactions using quasi-monoenergetic neutron source based on the reaction on ^{7}Li target at Nuclear Physics Institute of ASCR in Rez. Yttrium (n,xn) threshold reactions are suitable candidates for fast neutron field measurement by activation detectors. Fast neutron field monitoring is necessary already today at a wide range of accelerator facilities and will gain on importance in future fast reactors of generation IV, accelerator transmutation systems or fusion reactors. The knowledge of the cross-sections is crucial for such purpose. Unfortunately, the cross-section is sufficiently known only for ^{89}Y(n,2n)^{88}Y reaction. For higher orders of reactions there are almost no experimental data. Special attention was paid to the ^{89}Y(n,3n)^{87}Y reaction. The cross-sections of both ^{89}Y(n,2n)^{88}Y and ^{89}Y(n,3n)^{87}Y reactions were analyzed.

1 Introduction and motivation

For future advanced reactor systems same as for fusion reactors and advanced spallation sources of neutrons, the suitable activation neutron detectors will be necessary. During the experiments of the international collaboration 'Energy and Transmutation of RadioActive Waste' it was shown that yttrium is good candidate for monitoring of neutron fields with activation samples, mainly because of its (n,xn) threshold reactions, whose products are easily identifiable and with good half-life for γ-spectrometry. Unfortunately the knowledge of cross-sections of these reactions is insufficient. So we decided to measure cross-section of yttrium (n,xn) reactions at different neutron energies. Quasi-monoenergetic (QM) neutron source at Nuclear Physics Institute (NPI) of the Academy of Sciences of the Czech Republic in Rez [1] was used as the neutron source. The source is based on ^{7}Li(p,n)^{7}Be reaction. This series of measurements is continuation of previous measurements [2] made by our group using NPI source and quasi-monoenergetic neutron source at The Svedberg Laboratory in Uppsala, Sweden [3].

2 Samples and measurements

The measurements were done using six different proton energies. Four irradiations were part of ERINDA project and two next irradiations were on base of CANAM. Positions of QM peak were 17.4, 24.5, 24.8, 27.9, 28.7 and 33.5 MeV. Two of them were almost the same, so there is a good opportunity to check the consistency of evaluation procedure and systematic uncertainty sources. Two types of samples were used: 'YN' samples which were made of solid yttrium foil with dimensions $25 \times 25 \times 0.64$ mm^3, with

weight ~ 1.8 g and 'YO' samples which had form of pills made of compressed yttrium powder with dimensions $\oslash 9 \times 1.5$ mm^3, with weight $\sim 0.6 - 0.8$ g. The samples were fixed on a paper attached to an aluminum holder which was mounted behind the neutron source. Gold samples were irradiated together with the yttrium samples. Both samples were on the same position on the holder. The yttrium sample was placed on top of the gold sample. The gold samples with much better known cross-sections of neutron reactions were used as the experimental condition monitors. Figures 1 (a) and (b) shows the arrangement of samples and neutron source. Both pictures were made using VISED [4] program. For each irradiated sample, the neutron spectrum was calculated by means of MCNPX [5] simulation.
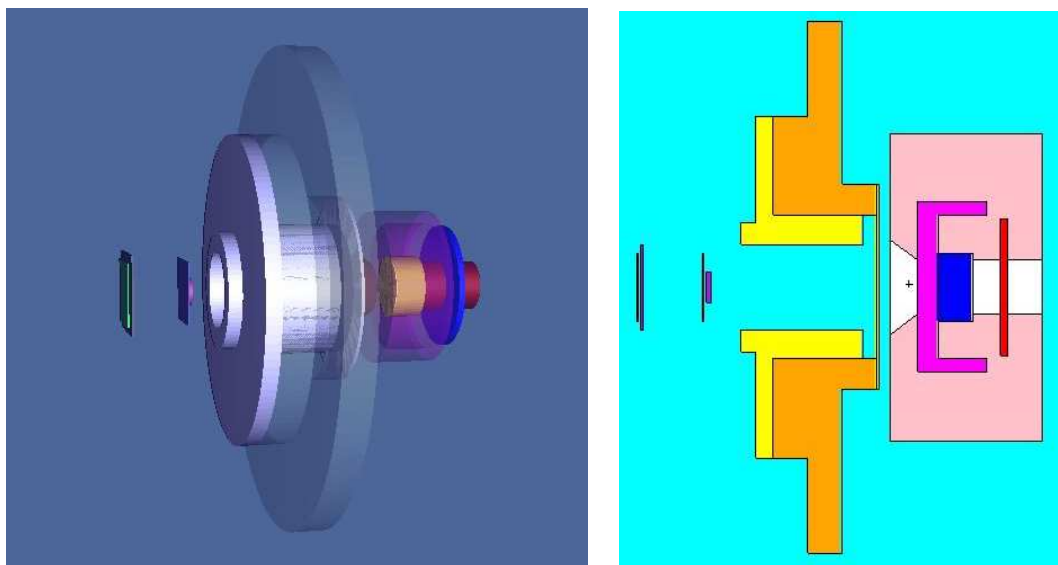
Fig. 1: (a) 3D model of neutron source with samples; (b) visualization of neutron source with samples for MCNPX

2.1 Evaluation of cross-section

The evaluation procedure consists in the calculation of number of produced nuclei N_{yield} for each isotope. Then using this value the cross-section is calculated. The N_{yield} is calculated accordingly to formula

$$N_{yield} = \frac{S_{peak} \cdot C_{abs}(E)}{I_\gamma \cdot \varepsilon_p(E) \cdot COI_E \cdot C_{area}} \frac{t_{real}}{t_{live}} \frac{e^{\lambda \cdot t_0}}{1 - e^{-\lambda \cdot t_{real}}} \frac{\lambda \cdot t_{irr}}{1 - e^{-\lambda \cdot t_{irr}}}, \tag{1}$$

where S_{peak} - peak area, $C_{abs}(E)$ - self-absorption correction, I_γ - gamma emission probability, $\varepsilon_p(E)$ - detector efficiency, COI_E - true coincidences correction, C_{area} - square emitter correction, t_{real} - real time of measurement, t_{live} - live time of measurement, t_0 - cooling time, t_{irr} - irradiation time, λ - decay constant. The last three fractions represent respectively dead time correction, correction for decay during cooling and measurement and correction for decay during irradiation. The peak area was determined using Canberra's Genie 2000 software. The uncertainties of peak areas were between 0.5% and 3%. The uncertainties brought in by corrections are about 1%, except the detector efficiency which has uncertainty not worst then 3%. Using formula (1) to get the number of produced nuclei it is possible to use formula (2) to calculate the cross-section. This formula has the form

$$\sigma = \frac{N_{yield} \cdot S \cdot A \cdot B_a}{N_n \cdot N_A \cdot m}, \tag{2}$$

where S - foil area, A - molar mass, B_a - beam instability correction, N_n - number of neutrons in peak, N_A - Avogadro's number, m - foil mass. The character of neutron spectra forces to involve one more correction. Since almost half of the produced neutrons are in low energy background tail, it is necessary to involve background subtraction correction.

2.2 Background subtraction method

The quasi-monoenergetic neutron source based on ^{7}Li(p,n)^{7}Be reaction has the energy spectrum with contributions from monoenergetic peak and continuum at lower energies. Fig. 2 shows an example of the neutron spectrum with the cross-sections for (n,2n) and (n,3n) reactions on yttrium. The neutron background is negligible only in case, when the threshold energy is just under the energy of the peak, for other cases subtraction procedure [6] was involved. This procedure is based on the ratio between the folding of calculated cross-section $\sigma(E)$ and neutron spectrum $N(E)$ in the peak energy interval and the same convolution in the whole spectrum interval. Since the neutron spectrum is binned, the integral operators are replaced by sum operators. The background subtraction correction factor is defined accordingly to formula (3). Using this coefficient it is possible to correct the number of produced nuclei for the ones produced by background neutrons accordingly to (4).

$$C_{bgr} = \frac{\int\limits_{Peak} \sigma(E) \cdot N(E)\, \mathrm{d}E}{\int\limits_{Spectrum} \sigma(E) \cdot N(E)\, \mathrm{d}E} \longrightarrow \frac{\sum\limits_{i \in Peak} \sigma_i \cdot N_i}{\sum\limits_{i} \sigma_i \cdot N_i} \tag{3}$$

$$N_{yield} \longrightarrow N_{yield,peak} = N_{yield} \cdot C_{bgr} \tag{4}$$

Cross-sections are calculated using TALYS 1.4 [7]. The background subtraction procedure is independent on the absolute value of cross-section. It is dependent only on the shape of the cross-section. The advantage of it will be seen in discussion of results. If the shape wouldn't be accurate, then the values for higher energies would diverge from it. Direction of divergence would be opposite than the difference between the correct shape and the used one. In order to validate simulated neutron flux by MCNPX, the gold samples were irradiated together with yttrium samples. Difference between simulated and calculated neutron fluency is not exceeding 2 %. Two uncertainties are brought in the final cross-section by the background subtraction procedure: 1) uncertainty of the used cross-sections below QM peak, 2) uncertainty of the used neutron spectra. We estimate the sum of these two uncertainties to be around 10%.
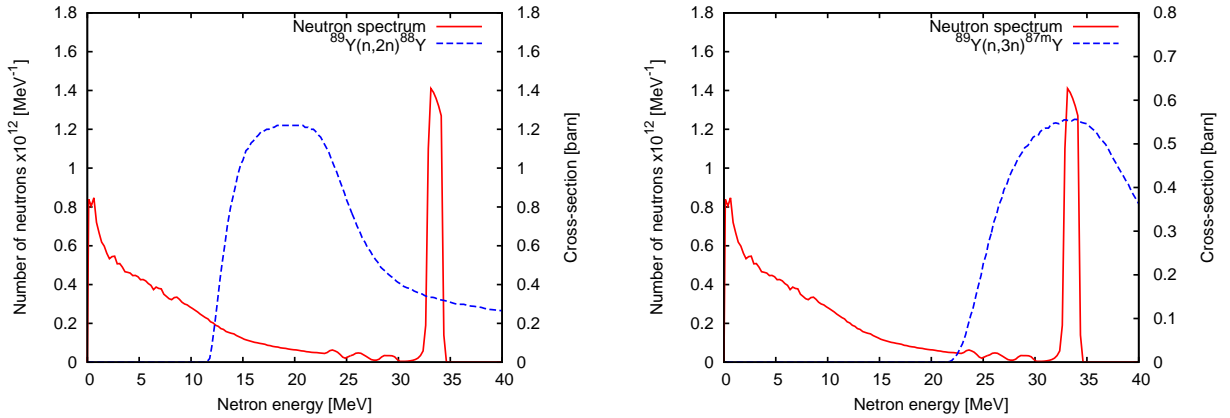
Fig. 2: Neutron spectrum and cross-section for (a) (n,2n) reaction; (b) (n,3n) reaction

3 Cross-section results

Currently the experimental cross-section data of yttrium (n,xn) reactions for higher are almost nonexistent. Only for (n,2n) reaction there are enough experimental points in the EXFOR database. For (n,3n) and higher order reactions, there are almost no experimental data. The data in this work are still preliminary, but they are in good agreement with the current experimental data in EXFOR. The cross-sections of the reaction ^{89}Y(n,3n)^{87m}Y are available only in [2] for neutron energies from 59.0 to 89.3 MeV, in

bachelor thesis [8] for neutron energy 32 MeV and in this contribution for neutron energies from 24.5 to 33.5 MeV. The results together with data from [8] marked as 'Rez 2011', TALYS calculations and EXFOR data are shown in Figs. 3 and 4.
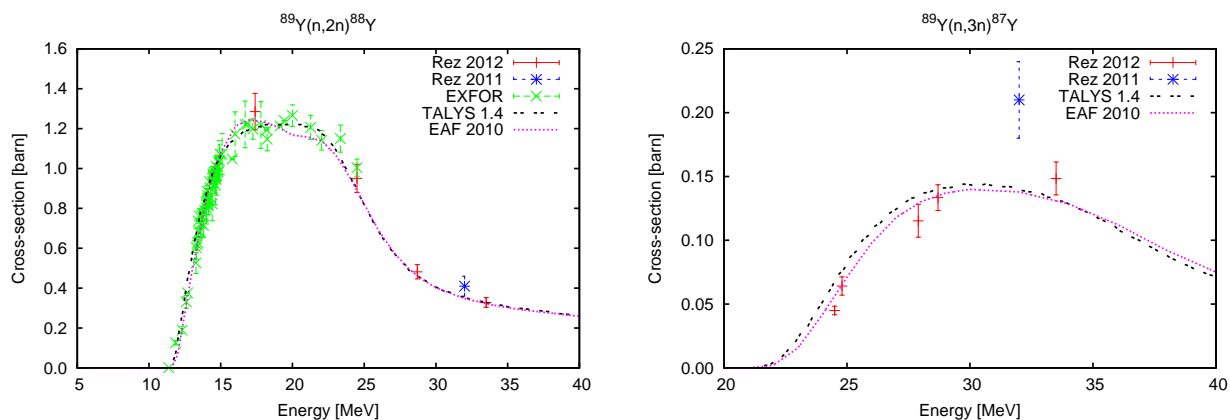
Fig. 3: Cross-sections for (a) ^{89}Y(n,2n)^{88}Y reaction; (b) ^{89}Y(n,3n)^{87}Y reaction
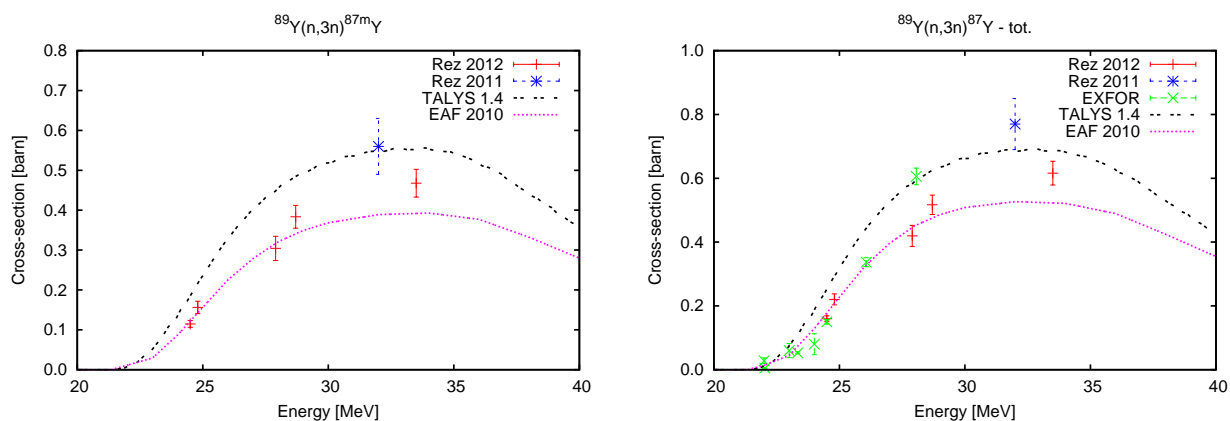
Fig. 4: Cross-sections for (a) ^{89}Y(n,3n)^{87m}Y reaction; (b) ^{89}Y(n,3n)^{87}Y reaction - total production

The data shows good agreement both with the TALYS and EAF 2010 [9] cross-sections. For ^{89}Y(n,3n)^{87m}Y reaction there is a shift in absolute value, but the shape agrees very well with the TALYS calculations. In case of the EAF 2010 library and reaction ^{89}Y(n,3n)^{87m}Y, there is possible to see difference even in shape. Fortunately, except of the highest energy, all the measured neutron energies were so close to the threshold, that the effect of the background subtraction was less or equal than 1 %. Due to this fact, it is possible to expect accurate description of the cross-section behavior in the measured region of energies. Difference between background subtraction using TALYS results and EAF 2010 library are negligible in our accuracy, so we kept to use TALYS, due to the better agreement with the shape in case of ^{89}Y(n,3n)^{87m}Y reaction.

4 Conclusion

Using the NPI quasi-monoenergetic ^{7}Li(p,n)^{7}Be neutron source, six irradiation of yttrium samples with neutron energies 17.4, 24.5, 24.8, 27.9, 28.7 and 33.5 MeV were made. Obtained cross-sections are in this contribution. The agreement of obtained ^{89}Y(n,2n)^{88}Y cross-sections and the cross-sections from EXFOR shows good applicability of the discussed method of background subtraction. The systematic shift between the data 'Rez 2012' and 'Rez 2011' is most probably due to different method of obtaining

the neutron spectra. The difference will be subject of further analysis. The data are still preliminary, but there should not be significant changes in the results.

Acknowledgements

References

[1] P. Bem, V. Burjan, J. Dobes, U. Fischer, M. Gotz, M. Honusek, V. Kroha, J. Novak, S. Simakov, E. Simeckova, The npi cyclotron-based fast neutron facility, in: International Conference on Nuclear Data for Science and Technology 2007, 2007.

[2] J. Vrzalova, O. Svoboda, A. Krasa, A. Kugler, M. Majerle, M. Suchopar, V. Wagner, Studies of (n,xn) cross-sections in al, au, bi, cu, fe, i, in, mg, ni, ta, y, and zn by the activation method, Nuclear Instruments and Methods in Physics Research Section A: Accelerators, Spectrometers, Detectors and Associated Equipment vol. 726 (2013) 84–90.

[3] A. V. Prokofiev, J. Blomgren, O. Bystrom, C. Ekstrom, S. Pomp, U. Tippawan, V. Ziemann, M. Osterlund, The tsl neutron beam facility, Radiation Protection Dosimetry vol. 126 (1-4) (2007-05-13) 18–22.

[4] R. A. Schwarz, L. L. Carter, Visual editor to create and display mcnp input files, Journal Name: Transactions of the American Nuclear Society.

[5] G. X-6, Mcnpx 2.3.0 - monte carlo n-particle transport code system for multipraticle and high energy application (2002).

[6] O. Svoboda, Experimental study of neutron production and transport for adtt, Dissertation thesis, Czech Technical University in Prague (2011),
http://ojs.ujf.cas.cz/~wagner/transmutace/diplomky/PHD_Svoboda.pdf.

[7] A. J. Koning, S. Hilaire, M. C. Duijvestijn, Talys-1.0, in: O. Bersillon, F. Gunsing, E. Bauge, R. Jacqmin, S. Leray (Eds.), Proceedings of the International Conference on Nuclear Data for Science and Technology, April 22 to April 27, 2007, Nice, France, EDP Sciences, 2008, pp. 211–214.

[8] B. Geier, Experimental determination of neutron cross sections of yttrium by activation method, Bachelor thesis, Graz University of Technology (2011),
http://ojs.ujf.cas.cz/~wagner/transmutace/diplomky/BakkArbeit_last.pdf.

[9] J.-Ch. Sublet, L. W. Packer, J. Kopecky, R. A. Forrest, A. J. Koning, D. A. Rochman, The European Activation File: EAF-2010 neutron-induced cross section library, CCFE Report, 2010, CCFE-R (10) 05.

Measurement of the isomeric yield ratios of fission products with JYFLTRAP

D. Gorelov[1], A. Al-Adili[3], J. Hakala[1], A. Jokinen[1], V. S. Kolhinen[1], J. Koponen[1], M. Lantz[3],
A. Mattera[3], I. Moore[1], H. Penttilä[1], I. Pohjalainen[1], S. Pomp[3], V. Rakopoulos[3], M. Reponen[1],
S. Rinta-Antilav[1], V. Schonnenschein[1], V. Simutkin[3], A. Solders[3], A. Voss[1] and J. Äystö[2]
[1]University of Jyväskylä, Jyväskylä, Finland
[2]Helsinki Institute of Physics, Helsinki, Finland
[3]Uppsala University, Uppsala, Sweden

Abstract

Several isomeric yield ratios of fission products in 25 MeV proton-induced fission of ^{238}U were measured recently at the JYFLTRAP facility. The ion-guide separator on-line method was utilized to produce radioactive ions. The double Penning-trap mass spectrometer was used to separate isomeric and ground states by their masses. To verify the new experimental technique γ-spectroscopy method was used to obtain the same isomeric ratios.

1 Introduction

Nuclei having the same charge and mass numbers but could be distinguished only by other properties, particularly radioactive ones are called isomeric nuclei. A nuclear isomerism happens due to structural effects. In terms of a shell model isomeric states exist when major shells occupied by particles of high angular momentum are preceded by closely lying subshells occupied by particles of low angular momentum [1]. In these cases electromagnetic transition probabilities are strongly reduced because the multipolarity of γ-quanta is quite high and emitted energy is relatively small.

As result, the isomeric states have a wide range of lifetimes. In Ref. [2] the range from $\sim 10^{-6}$ to $\sim 10^{10}$ s is mentioned. Thus, the population of isomeric states can dramatically change the time dependent description of some physical processes. For example, the time development of the decay energy release following binary fission depends on the initial relative populations between isomeric and ground states [2]. Thus, experimental data on the isomeric yield ratios are very important for decay heat calculations for reactors.

Different techniques exist to measure the independent isomeric yield ratios. They include isotope separator [3], recoil mass separator [4] or radiochemical methods in combination with γ-ray spectroscopy. The bottleneck all of this methods is the detection of isomeric and ground states by their decays. To estimate the initial ratio between population of the isomeric and the ground state, information about the decay scheme, the branching ratios etc. is required.

A complitely different method to measure isomeric yield ratios of fission products was proposed at the Accelerator Laboratory of the University of Jyväskylä [5]. The main idea is to combine the ion guide technique and the unique capabilities of JYFLTRAP [6] to separate the isomeric and the ground state [7,8]. In this method two states are distinguished due to the mass difference. Previous experiments have already demonstrated that the resolving power of the facility is enough to perform isomeric yield ratio measurements for several cases [7,9–11].

2 Experimental method

The experimental measurement of independent isomeric yield ratios of fission products recently has been carried out at JYFL. The isomeric yield ratios have been determined in 25 MeV proton-induced fission of ^{238}U. Two different methods have been utilized in the experiment. First technique is based on isobaric

separation of the fission products and detection of the isomeric and the ground state by their γ-decays. The main idea of the second method is to separate the isomeric and the ground state with JYFLTRAP and count ions with microchannel plate (MCP) detector.

The schematic view of the experimental facility is presented on the Fig. 1. The uranium target,
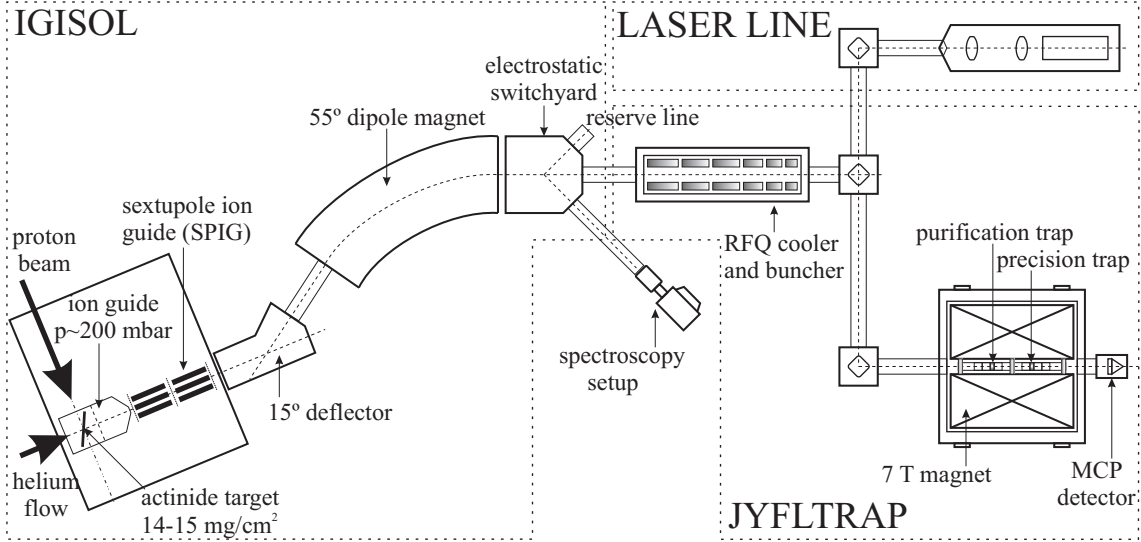
Fig. 1: A schematic view of the IGISOL-4 facility. Due to new layout it is possible to make various experiments employing different setups and techniques. The double Penning trap and γ-spectroscopy system were used in the present work.

15 mg/cm^2 thick, is placed in the fission ion-guide. Ions produced in nuclear fission are stopped in the ion-guide filled with helium gas at a pressure of around 200 mbar. Due to high ionization potential of the buffer gas, after slowing down a considerable fraction of ions aquires charge state +1. The ions are extracted from the gas cell by differential pumping and transported futher with a sextupole ion-guide (SPIG) [12]. After an acceleration to 30 kV the continuous ion beam is separated with a 55° dipole magnet. As result, the isobaric chain with certain mass number A is selected.

The new construction of the IGISOL facility at JYFL [13] gives the opportunity to distribute separated beams between different setups. After the electrostatic switchyard the beam can be send towards JYFLTRAP or it can be directed to the γ-spectroscopy setup.

The Penning trap measurements require specially prepared beam. For this purpose ions are injected into a gas-filled radio-frequency quadrupole cooler and buncher (RFQ) [14]. The RFQ system cools ions and releases them as short bunches to JYFLTRAP.

JYFLTRAP [6,16] consists of two cylindrical Penning traps inside a 7-T superconducting solenoid. The fact that there are two traps in one magnet is very important. It allows us to utilize two stage purification technique [17] and achive a mass resolving power about $m/\Delta m \approx 10^6$. However in the present experiment the isomeric and the ground states were separated by the purification trap with a buffer gas cooling technique [15, 18].

When ions are inside the trap, dipole excitation is applied to the electrods. As result, all ions regardsless at their mass are moved to a large radius. After that, applying a quadrupole radio-frequency field will center only ions whose cyclotron frequency $f_c(m)$ matches with applied frequency. The cyclotron frequency f_c of an ion with a mass m and a charge q is given as:

$$f_c = \frac{1}{2\pi}\frac{q}{m}B \tag{1}$$

where B is the magnetic field.

Recentered ions are released from the trap through a 2 mm diameter diaphragm and registered by MCP detector. In the present measurements full cycle has been chosen 660 milliseconds. The final spectrum shows how many ions were detected for each quadrupole excitation frequency.

To test the new method and compare results, γ-spectroscopy mesurement was done in the same experiment. The constant beam after the dipole magnet (see Fig. 1) was directed to the spectroscopic station. Ions were implanted on the aluminium foil, which was placed in front of the detector. The single γ-spectrum was collected in several hours.

3 Results

In the present experiment isomeric yield ratios were measured for several cases utilizing the Penning trap technique and the γ-spectroscopy. Data analysis is still on going. That's why only preliminary data on ^{81}Ge are presented in this report.

On the Fig. 2 the quadrupole frequency spectrum is presented for Ge and As ions. Black circles are
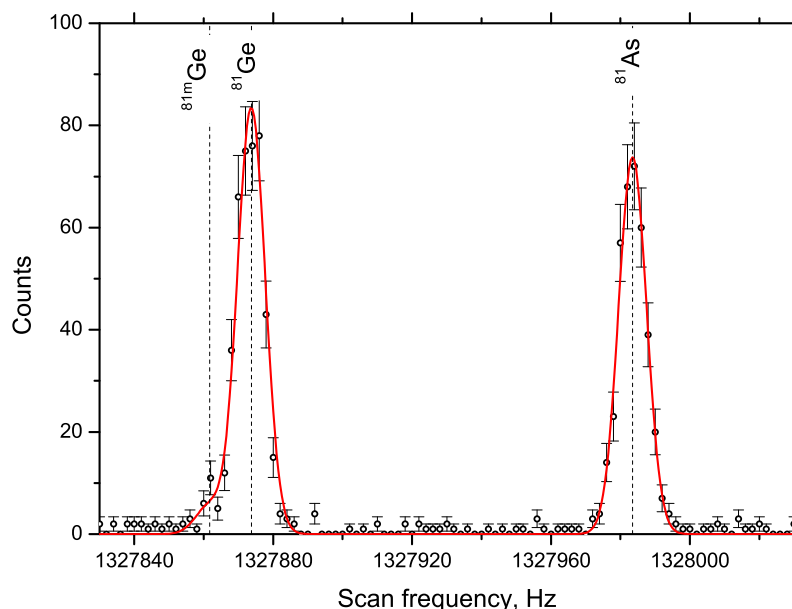
Fig. 2: The quadrupole frequency spectrum collected after the Penning trap. Black circles are experimental points with statistical error bars. Red line is gaussian fit of the spectrum. Position of peaks was calculated according to ion masses.

experimental points with statistical error bars. The difference between the isomeric and the ground state of ^{81}Ge is 679 keV. This value is very close to maximum resolving power of the purification trap. That's why the peak position for ^{81m}Ge and ^{81}Ge were calculated according to their masses. The peak position of ^{81}As was taken as a reference. Peak width was chosen equal for all peaks. Using this assumptions experimental data were fitted by gaussian function (red line on the Fig. 2). The ratio between respective peak areas gives us the isomeric yield ratio for ^{81}Ge. It is around 0.07 in the case of ^{81}Ge. The uncertainty has not been estimated yet.

Another way to get the same parameter is to measure γ-decays of the isomeric and the ground state

of ^{81}Ge. Such measurement was done in the same experiment. A spectrum of γ-rays from isobaric chain with mass number A=81 is presented on the Fig. 3. It is more difficult to extract data from γ-spectrum
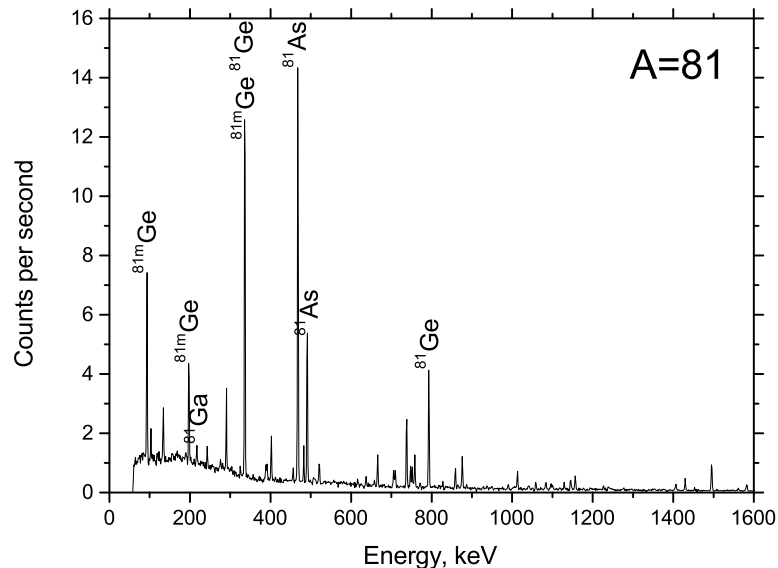
Fig. 3: Spectrum from the decay of all elements produced in 25 MeV proton-induced fission of ^{238}U with mass number 81. Laboratory background was subtracted from the spectrum. Several peaks related to the mass spectrum are identified.

than from data obtained with the Penning trap. In the case of γ-spectroscopy it is necessary to account for detector efficiency, branching ratio of decays, feeding decays of elements which have the same mass number etc.

Nevertheless, γ-spectroscopy was only the way to perform such measurements in the past. A very similar experiment utilizing the IGISOL method and γ-spectroscopy technique was done by M. Tanikawa et al. [3]. Data analysis is in progress and comparison between two different methods and literature values will be performed in future.

Acknowledgements

References

[1] E. Segre and A. C. Helmholz, *Rev. of Mod. Phys.* **21** (1949) 271.

[2] D. G. Madland and T. R. England, *Nucl. Sci. and Eng.* **64** (1977) 859.

[3] M. Tanikawa *et al.*, *Z. Phys. A* **347** (1993) 53.

[4] F. Gönnenwein *et al.*, *Int. J. of Mod. Phys. E* **16** (2007) 410.

[5] D. Gorelov *et al.*, *Proc. of ICFN5*, Sanibel Island, USA, 2012

[6] T. Eronen *et al.*, *Eur. Phys. J. A* **48: 46** (2012).

[7] H. Penttilä *et al.*, *Eur. Phys. J. A* **44** (2010) 147.

[8] H. Penttilä *et al.*, *Eur. Phys. J. A* **48** (2012) 43.

[9] K. Peräjärvi *et al.*, *App. Rad. Isot.* **68** (2010) 450.

[10] K. Peräjärvi *et al.*, *App. Rad. Isot.* **71** (2013) 34.

[11] A. Kankainen *et al.*, *Phys. Rev. C.* **87** (2013) 024307.

[12] P. Karvonen *et al.*, *Nucl. Instr. and Meth. B* **266** (2008) 4794.

[13] I. D. Moore *et al.*, *Nucl. Instrum and Meth. B* **317** (2013) 208.

[14] A. Nieminen *et al.*, *Nucl. Instr. and Meth. A* **469** (2001) 244.

[15] V. S. Kolhinen *et al.*, *Nucl. Instr. and Meth. A* **528** (2004) 776.

[16] V. S. Kolhinen *et al.*, *Nucl. Instr. and Meth. B* **317** (2013) 506.

[17] T. Eronen *et al.*, *Nucl. Instr. and Meth. B* **266** (2008) 4527.

[18] G. Savard *et al.*, *Physics Letters A* **158** (1991) 247.

Study of the ^{234}U(n,f) fission fragment angular distribution at the CERN n_TOF facility

E. Leal-Cidoncha[1], I. Durán[1], C. Paradela[1], D. Tarrío[1,33], L.S. Leong[2], L. Audouin[2], L.Tassan-Got[2], S. Altstadt[3], J. Andrzejewski[4], M. Barbagallo[5], V. Bécares[6], F. Bečvář[7], F. Belloni[8], E. Berthoumieux[8,9], J. Billowes[10], V. Boccone[9], D. Bosnar[11], M. Brugger[9], M. Calviani[9], F. Calviño[12], D. Cano-Ott[6], C. Carrapiço[13], F. Cerutti[9], E. Chiaveri[8,9], M. Chin[9], N. Colonna[5], G. Cortés[12], M.A. Cortés-Giraldo[14], M. Diakaki[15], C. Domingo-Pardo[16], R. Dressler[17], N. Dzysiuk[18], C. Eleftheriadis[19], A. Ferrari[9], K. Fraval[8], S. Ganesan[20], A.R. García[6], G. Giubrone[16], M.B. Gómez-Hornillos[12], I.F. Gonçalves[13], E. González-Romero[6], E. Griesmayer[21], C. Guerrero[9], F. Gunsing[8], P. Gurusamy[20], A. Hernández-Prieto[9,12], D.G. Jenkins[22], E. Jericha[21], Y. Kadi[9], F. Käppeler[23], D. Karadimos[15], N. Kivel[17], P. Koehler[24], M. Kokkoris[15], M. Krtička[7], J. Kroll[7], C. Lampoudis[8], C. Langer[3], C. Lederer[3,25], H. Leeb[21], R. Losito[9], A. Mallick[20], A. Manousos[19], J. Marganiec[4], T. Martínez[6], C. Massimi[26], P.F. Mastinu[18], M. Mastromarco[5], M. Meaze[5], E. Mendoza[6], A. Mengoni[27], P.M. Milazzo[28], F. Mingrone[26], M. Mirea[29], W. Mondalaers[30], A. Pavlik[25], J. Perkowski[4], A. Plompen[30], J. Praena[14], J.M. Quesada[14], T. Rauscher[31], R. Reifarth[3], A. Riego[12], M.S. Robles[1], F. Roman[9,29], C. Rubbia[9,32], M. Sabaté-Gilarte[14], R. Sarmento[13], A. Saxena[20], P. Schillebeeckx[30], S. Schmidt[3], D. Schumann[17], G. Tagliente[5], J.L. Tain[16], A. Tsinganis[9], S. Valenta[7], G. Vannini[26], V. Variale[5], P. Vaz[13], A. Ventura[27], R. Versaci[9], M.J. Vermeulen[22], V. Vlachoudis[9], R. Vlastou[15], A. Wallner[25], T. Ware[10], M. Weigand[3], C. Weiß[9], T. Wright[10], P. Žugec[11]

[1]Universidade de Santiago de Compostela (USC), Spain
[2]Centre National de la Recherche Scientif que/IN2P3 - IPN, Orsay, France
[3]Johann-Wolfgang-Goethe Universität, Frankfurt, Germany
[4]Uniwersytet Lódzki, Lodz, Poland
[5]Istituto Nazionale di Fisica Nucleare, Bari, Italy
[6]Centro de Investigaciones Energeticas Medioambientales y Tecnológicas (CIEMAT), Madrid, Spain
[7]Charles University, Prague, Czech Republic
[8]Commissariat à l'Énergie Atomique (CEA) Saclay - Irfu, Gif-sur-Yvette, France
[9]European Organization for Nuclear Research (CERN), Geneva, Switzerland
[10]University of Manchester, Oxford Road, Manchester, UK
[11]Department of Physics, Faculty of Science, University of Zagreb, Croatia
[12]Universitat Politecnica de Catalunya, Barcelona, Spain
[13]Instituto Tecnológico e Nuclear, Instituto Superior Técnico, Universidade Técnica de Lisboa, Lisboa, Portugal
[14]Universidad de Sevilla, Spain
[15]National Technical University of Athens (NTUA), Greece
[16]Instituto de Física Corpuscular, CSIC-Universidad de Valencia, Spain
[17]Paul Scherrer Institut, Villigen PSI, Switzerland
[18]Istituto Nazionale di Fisica Nucleare, Laboratori Nazionali di Legnaro, Italy
[19]Aristotle University of Thessaloniki, Thessaloniki, Greece
[20]Bhabha Atomic Research Centre (BARC), Mumbai, India
[21]Atominstitut, Technische Universität Wien, Austria
[22]University of York, Heslington, York, UK
[23]Karlsruhe Institute of Technology, Campus Nord, Institut für Kernphysik, Karlsruhe, Germany
[24]Department of Physics, University of Oslo, N-0316 Oslo, Norway
[25]University of Vienna, Faculty of Physics, Austria
[26]Dipartimento di Fisica, Università di Bologna, and Sezione INFN di Bologna, Italy
[27]Agenzia nazionale per le nuove tecnologie, l'energia e lo sviluppo economico sostenibile (ENEA), Bologna, Italy

[28]Istituto Nazionale di Fisica Nucleare, Trieste, Italy

[29]Horia Hulubei National Institute of Physics and Nuclear Engineering - IFIN HH, Bucharest - Magurele, Romania

[30]European Commission JRC, Institute for Reference Materials and Measurements, Retieseweg 111, B-2440 Geel, Belgium

[31]Department of Physics and Astronomy - University of Basel, Basel, Switzerland

[32]Laboratori Nazionali del Gran Sasso dell'INFN, Assergi (AQ),Italy

[33] Department of Physics and Astronomy, Uppsala University, Sweden

Abstract

The angular distribution of the fission fragments (FFAD) produced in neutron-induced reactions of actinides have been measured with a fission detection setup based on parallel-plate avalanche counters (PPACs) at the Neutron Time-Of-Flight (n_TOF) facility at CERN. The main features of the setup and preliminary results are reported here for the ^{234}U(n,f) reaction measurement showing a high concordance with previous data, while providing new results up to 100 MeV.

1 Introduction

A deeper knowledge on the reaction cross sections related to the Thorium-Uranium fuel cycle, such as the ^{234}U isotope, is crucial for the development of New Generation nuclear reactors and the Accelerator Driven Systems (ADS). An accurate cross section of this nucleus is required for a detailed investigation of its fission barrier parameters, shedding some light on the Triple Humped Fission Barrier controversy.

The angular distribution of the fragments (FFAD) produced in the fission of an excited nucleus plays a role to achieve more accurate measurements of the fission cross sections. This is also an important observable to investigate the properties of transition levels close to the fission threshold [1, 2]. The directional dependence of fission fragments (FF) as a result from a transition state is related with its quantum numbers J, K and M (total spin and its projections on the nuclear symmetry axis and on a space-fixed axis). Since the ^{234}U has zero spin and the neutron spin is $\frac{1}{2}$, only two values of M are allowed, which makes this nucleus a simple case to study.

The behaviour of the FFAD is of particular interest above several tens of MeV, where it has been predicted almost isotropic similarly to the case of proton-induced fission. However, recent experimental results [3] suggest a revision of this assertion.

In order to provide accurate data of neutron-induced reactions, a broad program of measurements is being performed at the CERN Neutron Time-of-Flight (n_TOF) facility. As a part of this program, measurements of neutron-induced reactions in ^{234}U, ^{235}U, ^{238}U and ^{237}Np have been carried out at the last campaign (2012) using a fission detection setup based on parallel-plate avalanche counters (PPACs) developed and built at the IPN-Orsay (France). Previous measurements with several isotopes were performed during the Phase I (2002 to 2003) and the Phase II (2010 to 2011) of the n_TOF project [4, 5]. The angular arrangement of the detectors and targets has been modified for the Phase II experiments with respect to the Phase I to cover all the angular range in the emission of the FF.

The results obtained for ^{232}Th(n,f) with this new setup in the last campaigns of the Phase II confirmed large variations of the anisotropy around the fission chances [6]. The ^{234}U(n,f) cross section is higher than the ^{232}Th(n,f), which makes this isotope a good candidate to study the vibrational resonances in the sub-threshold region, where the existing data show large anisotropy values. Above the threshold, the bibliography is scarce and only Leachman provides information up to 15 MeV [7–11].

This work presents the preliminary results of the FFAD analysis of the ^{234}U(n,f) data. The anisotropy parameter has been calculated and compared with the available data up to 15 MeV, extending the analysis up to 100 MeV.

2 Experimental setup

The Neutron Time-of-Flight (n_TOF) facility at CERN is characterized by a white neutron source produced by spallation on a lead target of 20 GeV/c protons provided by the Proton Synchrotron (PS), covering the energy range from thermal up to 1 GeV. The long f ight path (183.4 m) from the spallation target to the chamber containing the detectors and targets, located in the experimental area, offers the possibility to obtain high resolution measurements. Charged particles produced in the spallation reaction are removed from the beam using a sweeping magnet and two collimators are placed in the neutron path, the second of which, for f ssion reactions measures 8 cm diameter, def ning the neutron beam prof le. More detailed information about the n_TOF facility can be found in Ref. [12].

2.1 Parallel Plate Avalanche Counter detectors

The detection setup used to perform the measurements was constituted by parallel-plate avalanche counters (PPACs). Each PPAC consist in three electrodes, one central anode sided by two cathodes. The 3.2 mm gaps between the electrodes are f lled with the non f ammable gas Octaf uoropropane (C_3F_8) at 4 mbar pressure.

The electrodes are composed of 1.7 μm Mylar foils covered by an aluminum layer. The anode is characterized by a very fast signal response, providing a time resolution better than 500 ps. Each cathode is segmented in parallel aluminum strips connected to a delay line in order to provide information about the position of the f ssion fragment hit in one dimension. Through the combination of two cathodes, with the strips placed perpendiculary between them, we can reconstruct the two dimensional position of the hit in the detector.

2.2 Targets

The targets used in this experiment consisted in a thin radioactive layer (~ 0.3 mg/cm^2) deposited as a 8 cm diameter disk in an aluminum foil of 2.5 μm (the f rst six targets) or 0.7 μm (the last three targets) thickness built at the IPN-Orsay. The deposition of the samples compounds in the aluminum backing was performed by electro-deposition. Three samples of ^{234}U, one of ^{237}Np and, as reference samples, two of ^{235}U and three of ^{238}U were used in this campaign.

The thickness and the mass distribution of the thick backing samples were measured by α spectroscopy and by Rutherford Backscattering Spectroscopy (RBS).
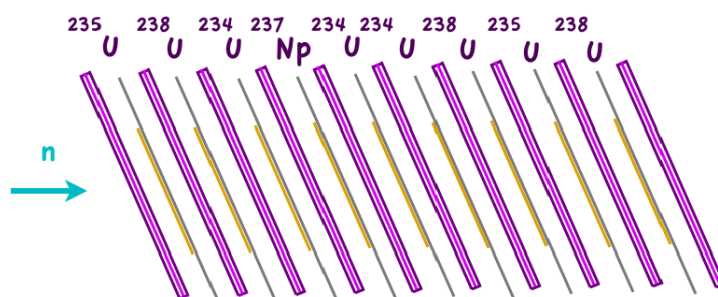
Fig. 1: Schematic top view of the PPACs and targets (2012 campaign).

The f ssion chamber containing the ten PPACs and nine targets in between consisted in a stainless steel cylinder f lled with the gas at low pressure. The detectors and targets inside the chamber were tilted 45° with respect to the incident neutron beam in order to cover all the angular range (from 0° to 90°) and placed in an aluminum bottom supporting them, which distribution is shown in Fig. 1.

3 Data Analysis

The f ssion event identif cation is determined by the coincidence detection of the two FF by the PPACs f anking the target where the f ssion reaction takes place. The fast signal of the anodes is used for this coincidence technique, which allows to discriminate the α background and the spallation reaction products. The PPAC detectors are almost insensitive to gamma rays. The cathode signals were used to calculate the emission angle of the FF by means of the knowledge of the hit position in the detector. As was mentioned before, when the fragment reaches the cathode, the signal produced in one of the parallel aluminum strips is directed to the delay line and propagated along it in both directions. Because every PPAC is composed of two cathodes, with perpendicular strips between them, in the X and Y directions, we can obtain the two dimensional position of the FF hit in the detector. Since each target is f anked by two PPACs, knowing the points of both FF hits in each one of them and assuming that both fragments are emitted with 180° between them, we can design a vector $\vec{V}_{FF}$, and the beam direction is def ned by the vector $\vec{V}_{beam}$, see Fig. 2.
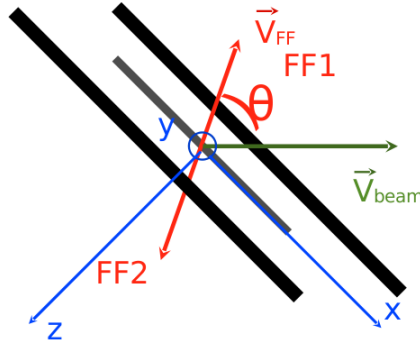
Fig. 2: Scheme of the reference frame used to reconstruct the trajectories of the FF, as is explained in Refs. [5, 6].

The assumption that both FF are emitted back to back with an angle of 180° between them is valid because the error introduced by the momentum transfer in the angle measurement at large neutron energies is negligible as explained in Ref. [6].

Hence, the emission angle of the FF can be expressed through its cosine ($cos\theta$), which is calculated as the scalar product of both vectors, as given by equation (1).

$$cos\theta = \frac{\vec{V}_{FF} \cdot \vec{V}_{beam}}{|\vec{V}_{FF}| \cdot |\vec{V}_{beam}|} \tag{1}$$

3.1 Fission Fragment Angular Distribution (FFAD)

The number of emitted FF with an angle θ for a particular neutron energy is given by the expression:

$$W(E_n, \theta)_{emitted} = \Phi(E_n) \cdot N \cdot \frac{d\sigma(E_n, \theta)}{d\Omega} \tag{2}$$

while the number of detected FF is def ned as:

$$W(E_n, \theta)_{detected} = \Phi(E_n) \cdot N \cdot \frac{d\sigma(E_n, \theta)}{d\Omega} \cdot \epsilon(\theta, \phi) \tag{3}$$

where $\Phi(E_n)$ is the time-integrated neutron f uence over the full measuring time, N is the number of atoms in the sample, $d\sigma(E_n, \theta)/d\Omega$ is the differential cross section and $\epsilon(\theta, \phi)$ is the detection eff ciency.

The FFAD for different energy intervals can be expressed in terms of cosθ, however to study the angular behaviour, an accurate value of the detection efficiency is required. Assuming that the efficiency is independent of the energy range and that the FFAD is isotropic in the resonance region, we can substract the dependence on the efficiency factor in the last equation dividing the angular distribution for each energy interval by that obtained below 1 keV.

The experimental FFAD (W(θ)/W(90°)) can been fitted by a sum of Legendre polynomials:

$$W(\theta)/W(90°) = A_0 \cdot \left[1 + \sum_{L_2}^{L_{max}} A_L \cdot P_L(cos\theta) \right] \qquad (4)$$

where L is the order of the polynomial (only even terms are considered) and A_L are the coefficients, which are considered up to 4th order. The best fit to the data has been chosen for every energy range depending on the $\mathcal{X}^2$ value.

3.2 The anisotropy parameter

The angular distribution behaviour in the edges depending on the neutron energy can be studied by means of the anisotropy parameter (W(0°)/W(90°)) which is defined in this case as:

$$W(0°)/W(90°) = \frac{1 + A_2 + A_4}{1 - \frac{1}{2} \cdot A_2 + \frac{3}{8} \cdot A_4} \qquad (5)$$

where the coefficients are obtained from the previous Legendre polynomial fit to the FFAD data.

Although this parameter does not provide a complete description of the angular distribution, it is a simple way of comparing our results with the existing experimental data.

4 Preliminary results

The present results correspond to the preliminary analysis of one of the three ^{234}U targets.
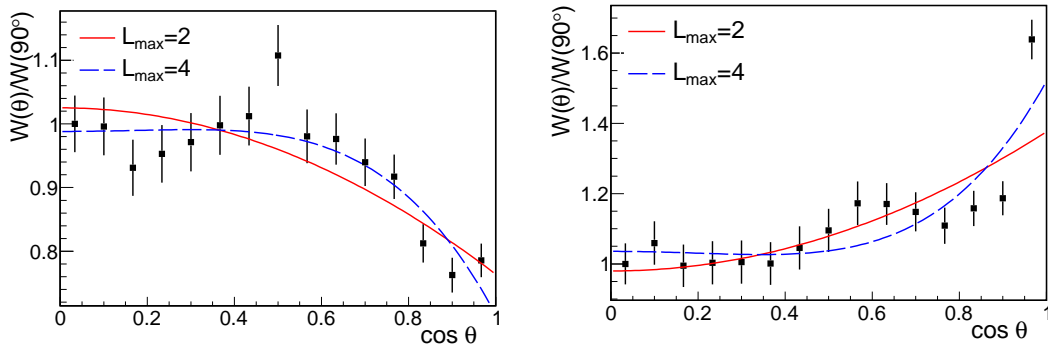
Fig. 3: Experimental FFAD of ^{234}U(n,f) for the energy range E$_n$= $(0.46, 0.56)$ MeV (left panel) and for E$_n$= $(6.31, 7.08)$ MeV (right panel) fitted to the Legendre polynomials up to 4th order.

The experimental FFAD fitted to the Legendre polynomials of 2th and 4th order are shown in Fig. 3 for two energy ranges. The error bars are related to the statistical uncertainty. The figure on the left panel corresponds to the energy range from 0.46 to 0.56 MeV. This distribution is side peaked, showing a minimum at the cosine equal to one. Otherwise, in the energy range from 6.31 to 7.08 MeV, the angular distribution is peaked at the cosine of the angle equal to one, which means that fragments are predominantly emitted in the beam direction.
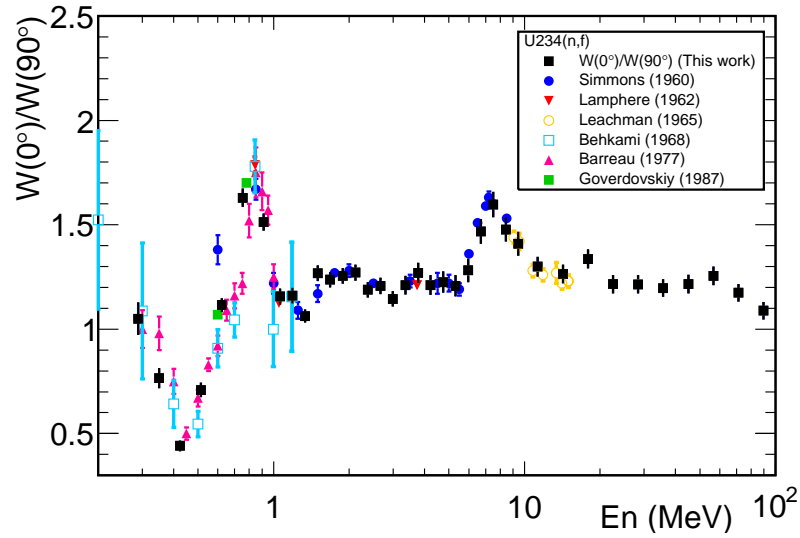
Fig. 4: Anisotropy parameter obtained in this work up to E_n=100 MeV for the ^{234}U(n,f) reaction compared with previous measurements, Refs. [7–11].

The anisotropy parameter has been calculated for neutron energies up to 100 MeV and compared with other works, which provide data below 15 MeV, showing a good agreement with the previous measurements, as can be seen in Fig. 4.
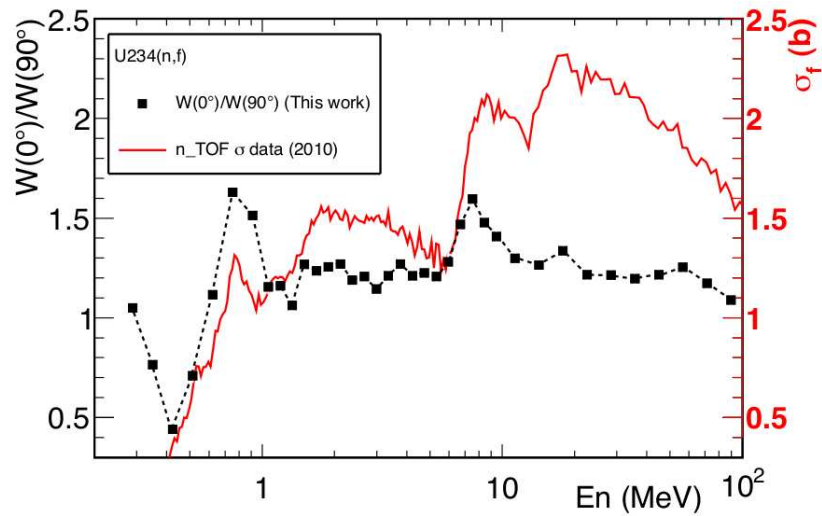
Fig. 5: Comparison between the anisotropy parameter obtained in this work up to E_n=100 MeV and the cross section data obtained in the n_TOF Phase I previous measurement by C. Paradela et al (2010), [4]

The comparison between the anisotropy parameter calculated in this campaign and the cross section data obtained in the n_TOF Phase I previous measurement by C. Paradela et al. [4], is shown in the Fig. 5. It can be seen that the main FFAD variations occurs at the openning of the f rst and second f ssion chances.

5 Conclusions and outlook

The method used in the present analysis was successfully proved with ^{232}Th by D. Tarrío et al. in the earlier Phase II experiment at n_TOF [5, 6]. Preliminary results hold here correspond only to one target of ^{234}U, showing a good agreement with the literature, which provide data of the previous experimental measurements up to 15 MeV, and extending them up to 100 MeV.

The analysis of the two ^{234}U samples is in progress and it will continue with the ^{235}U, ^{238}U, and ^{237}Np targets. The complete experimental data of the three ^{234}U samples will increase the statistics providing a more detailed description of the FFAD. This will allow us to obtain a more precise value of the ^{234}U(n,f) cross sections.

Experimental program on the thorium cycle isotopes will follow with the ^{231}Pa measurement which is planned for the next f ssion campaign. It is expected during 2015, depending on target manufacture.

References

[1] R. Vandenbosch and J.R. Huizenga, *Nuclear Fission*, Academic Press (1973).

[2] A. Goverdovsky, *Workshop on Nuclear Reaction Data and Nuclear Reactors* (Trieste, 2002).

[3] L. S. Leong, *PhD dissertation*, Université de Paris Sud (2013).

[4] C. Paradela et al., *Phys. Rev. C 82, 034601* (2010).

[5] D. Tarrío et al., Submitted to *Nucl. Instrum. Meth. A* (2013).

[6] D. Tarrío, *PhD dissertation*, Universidade de Santiago de Compostela (USC) (2012).

[7] J. E. Simmons and R. L. Henkel, *Phys. Rev. 120, 198* (1960).

[8] R. W. Lamphere et al., *Nucl. Phys. 38, 561-589* (1962).

[9] A. N. Behkami et al., *Phys. Rev. 171, No 4, 1267* (1968).

[10] G. Barreau, *PhD dissertation* CEN(BG) (1977).

[11] R. B. Leachman and L. Blumberg, *Phys. Rev. 137, B814* (1965).

[12] C. Guerrero, A. Tsinganis, E. Berthoumieux, the n_TOF Collaboration, *Eur. Phys. Journ. A 49, 27* (2003).

Attempts to infer the neutron inelastic cross sections using charged particle induced reactions

A. Negret[1], A. Bacquias[2], C. Borcea[1], D. Bucurescu[1], D. Deleanu[1], Ph. Dessagne[2],D. Filipescu[1], D. Ghita[1], T. Glodariu[1], M. Kerveno[2], N. Marginean[1], R. Marginean[1], C. Mihai[1], A. Olacel[1], S. Pascu[1], A.J.M. Plompen[3], T. Sava[1], L. Stroe[1], G. Suliman[1] and R. Suvaila[1]

[1] Horia Hulubei National Institute for Physics and Nuclear Engineering, Bucharest, Romania

[2] CNRS, Université de Strasbourg, UMR7178, IPHC, Strasbourg, France

[3] European Commission, Joint Research Center, Institute for Reference Materials and Measurements, Geel, Belgium

Abstract

Two experiments were performed at the Tandem accelerator of the Horia Hulubei National Institute for Physics and Nuclear Engineering, IFIN-HH with the purpose to investigate the possibility to use alpha-induced reactions for the calculation of neutron inelastic cross sections based on the Bohr hypothesis of the compound nucleus. A first experiment compared the gamma production cross sections excited in the ^{25}Mg$(\alpha, n\gamma)^{28}$Si and the ^{28}Si$(n, n'\gamma)^{28}$Si reactions. A second measurement, supported by the ERINDA project, was dedicated to the measurement of ^{70}Zn$(\alpha, n\gamma)^{73}$Ge cross sections with the purpose of inferring the neutron inelastic cross sections on ^{73}Ge.

1 Introduction

The future nuclear facilities are expected to have a crucial impact on the economical development of the human civilization. In this context, the current request for precise measurements of neutron-induced reaction data on specific materials is increasingly significant.

A particular emphasis is made on the specific cases where the direct measurement of cross sections is difficult or impossible, like in the case of radioactive targets. During the past decade numerous attempts were made to use the so-called *surrogate method* which relies on the use of charged-particle beams to mimic the neutron-induced reactions. In particular the *surrogate ratio method* proved rather successful in several studies being applied to neutron induced capture and fission reactions [1–6].

We intend therefore to investigate the possibility of inferring neutron inelastic cross sections from charged particle induced reactions based on the well-known Bohr hypothesis [7]. Two such attempts were performed using the experimental setups presented in the second section of this paper. The first attempt, dedicated to the comparison of the ^{25}Mg$(\alpha, n\gamma)^{28}$Si and the ^{28}Si$(n, n'\gamma)^{28}$Si reactions is described in Ref. [12]. We will give here an overview of this work in the third section. A second experiment, supported by the ERINDA project, consisted in the measurement of the gamma production cross sections in the ^{70}Zn$(\alpha, n\gamma)^{73}$Ge reaction. These data are currently under analysis and preliminary results will be shown in the fourth section.

2 Experimental details

Two experimental facilities were used in the present work. The neutron inelastic cross sections on ^{28}Si were measured using the spectrometer GAINS (Gamma Array for Inelastic Neutron Scattering) at GELINA (Geel Linear Accelerator), the neutron source of EC-JRC-IRMM, Belgium. The ^{25}Mg$(\alpha, n\gamma)^{28}$Si and the ^{70}Zn$(\alpha, n\gamma)^{73}$Ge reactions were investigated at the Tandem accelerator of IFIN-HH, Romania. In both cases we used HPGe detectors to determine the gamma production cross section for the strongest transitions of in the final nucleus.

Fig. 1: The GAINS array used at EC-JRC-IRMM to determine the neutron inelastic cross sections on ^{28}Si.

2.1 The GAINS setup at the GELINA neutron source of IRMM

The GELINA neutron source operated by EC-JRC-IRMM produces a white neutron flux with energies ranging from $\approx$70 keV to $\approx$18 MeV at a repetition rate of 800 Hz. Neutron pulses are produced within 1 ns following an intense gamma flash. Multiple flight paths are available. The energy of the neutrons is determined using the time-of-flight technique [8].

The GAINS array (Fig. 1) used to detect the gamma rays emitted during the inelastic scattering of neutrons on ^{28}Si is located in a cabin 200 m away from the neutron source [9, 10]. It consists of eight HPGe detectors placed at $110°$ and $150°$ with respect to the beam (the neutron flux is collimated so that in the 200 m cabin it constitutes a beam with a diameter of 61 mm). The special choice of the detection angles allows a precise integration of the angular distribution of the gamma rays emitted in the reaction. The beam was monitored with a ^{235}U fission chamber [11].

The ^{nat}Si sample of 1.326(1) g/cm^2 was irradiated for about 1000 h.

2.2 The gamma array at the Tandem accelerator of IFIN-HH

We used the Tandem facility operated by IFIN-HH to accelerate alpha particles to energies ranging between 5 MeV and 23 MeV.

During the ^{25}Mg$(\alpha, n\gamma)^{28}$Si experiment a simple setup was used (Fig. 2-(b)) consisting of two HPGe detectors placed at $30°$ and $70°$ respectively with respect to the beam axis. The beam was integrated using a Faraday cup placed after the target. The self-supported ^{25}Mg sample had an areal density of 0.63(2) mg/cm^2. We used an irradiation time of 3-4 h for each alpha energy.

The ^{70}Zn$(\alpha, n\gamma)^{73}$Ge reaction was investigated using the same accelerator but an upgraded detection setup. This was RoSphere, an array able to hold up to 25 HPGe detectors or a combination of HPGe and LaBr$_3$ detectors (Fig.2-(a)). We used 11 detectors placed at $37°$, $70°$, and $90°$. The ^{70}Zn enriched sample of 2 mg/cm^2 was placed inside a Faraday cup serving as beam integrator.
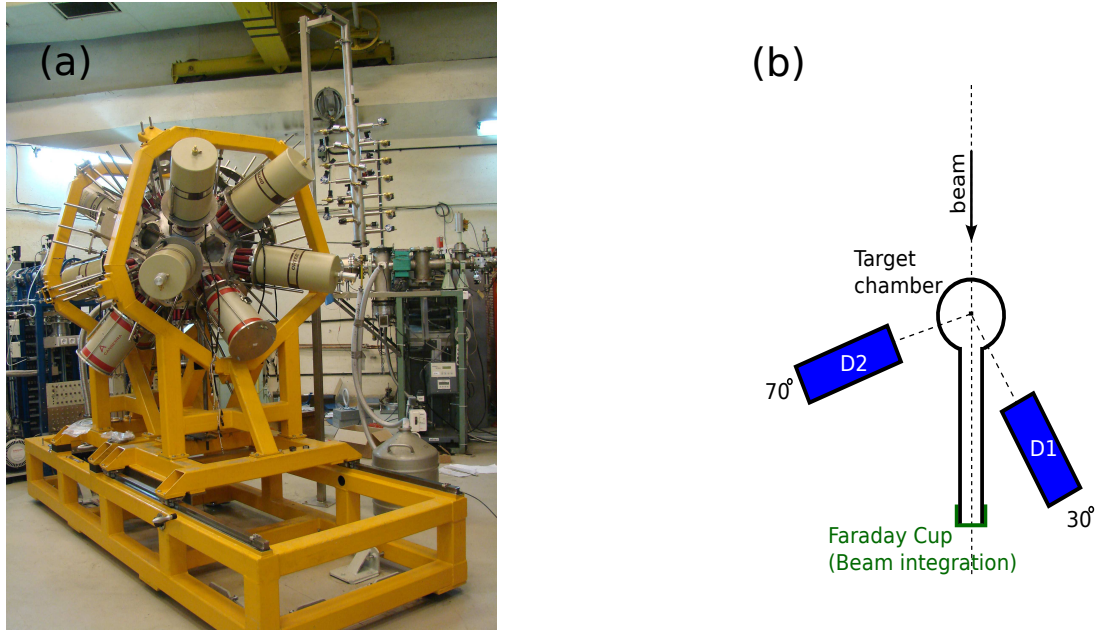
Fig. 2: (a) RoSphere, the gamma array used for the investigation of the ^{70}Zn(α, $n\gamma$)^{73}Ge reaction. (b) Scheme of the detection setup used for the determination of gamma production cross sections excited in the ^{25}Mg(α, $n\gamma$)^{28}Si reaction at the Tandem accelerator of IFIN-HH

3 Comparison of the gamma production cross sections in ^{28}Si excited through the (α, n) and the (n, n') reactions

The basic idea of the comparison presented in Fig. 3 relies on the hypothesis formulated by N. Bohr in Ref. [7]: due to the fact that the projectile/ejectile needs a short time to cross the target/recoil nucleus compared to lifetime of the compound nucleus, the final channel should not depend - in a first approximation - on the input channel. We compare indeed two cases where the compound nucleus is the same (^{29}Si) and the final channel coincides as well.

However, as discussed in Ref. [12], several aspects should be addressed while doing such a comparison:

- The Q-value is different in the two cases. Therefore in order to perform a meaningful comparison the gamma production cross sections from Fig. 3 are displayed as a function of the total excitation energy in the compound nucleus ^{29}Si.
- The Coulomb barrier in case of the alpha-induced reaction limits the energy range where the cross sections can be compared to values larger than E*(^{29}Si)$\approx$17 MeV.
- The total angular momentum available in the compound nucleus is also different in the two cases because the initial participants to the reaction have different spins: the ground state of ^{28}Si has J^{π}=0$^+$ while the ground state of ^{25}Mg has J^{π}=5/2$^+$.
- As a consequence of the previous argument, the interplay of various reaction mechanisms - direct, preequilibrium and compound nucleus - may be different in the two reactions.

Fig. 3 shows that the gamma production cross sections excited in the two reactions have the same order of magnitude but may differ by about 50%. The TALYS calculations reproduce acceptably well the (n, $n'\gamma$) data but the first two transitions excited through the (α, $n\gamma$) reaction are poorly described.
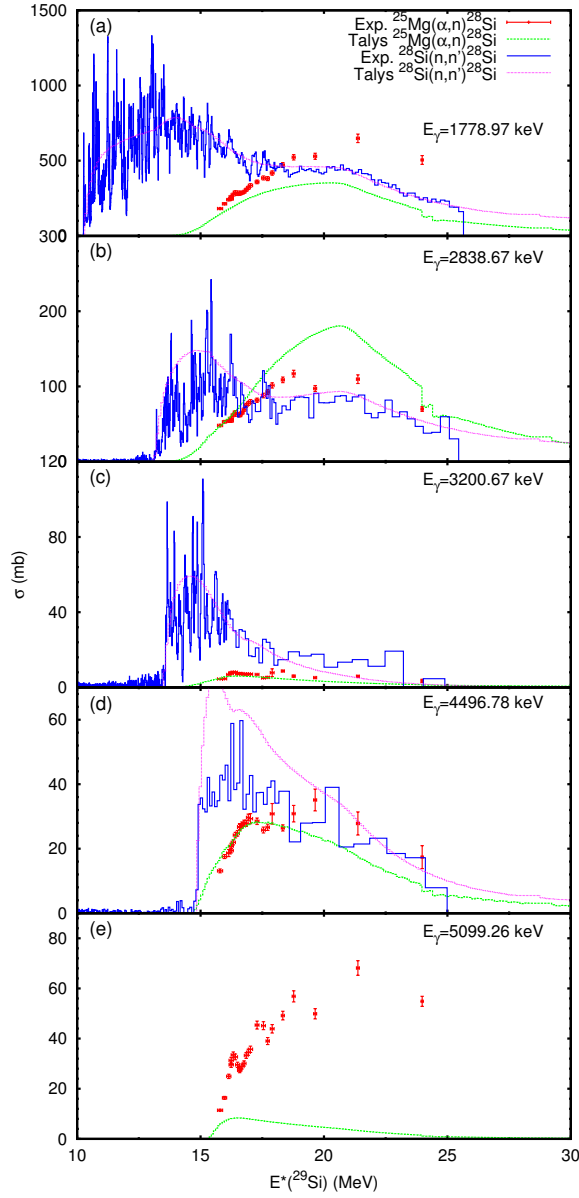
Fig. 3: Comparison of the gamma production cross sections in ^{28}Si excited through the ^{28}Si(n, $n'\gamma$)^{28}Si and the ^{25}Mg(α, $n\gamma$)^{28}Si reactions [12].

4 Preliminary results of the ^{70}Zn(α, $n\gamma$)^{73}Ge experiment

As already mentioned, the ^{70}Zn(α, $n\gamma$)^{73}Ge data are currently under analysis. The reaction was not previously investigated with the purpose to determine cross sections. An experiment was performed with Ge(Li) detectors in the seventies at E_α=14.2 MeV aiming at the investigation of the structure of ^{73}Ge [13]. The improved resolution of our HPGe detectors allows the identification of an increased number of transitions.

Unfortunately, the first gamma transitions in ^{73}Ge (E_γ=13.3 keV, 53.4 keV, 68.7 keV) could not be detected with our system. However we identified using the evaluated level scheme from Ref. [14] a large number of transitions in the energy range 200-1000 keV coming from ^{73}Ge, although the coincidence matrices were not yet investigated.

Fig. 4 displays the production cross sections of the gamma rays of 284.9, 297.3, 325.7 and
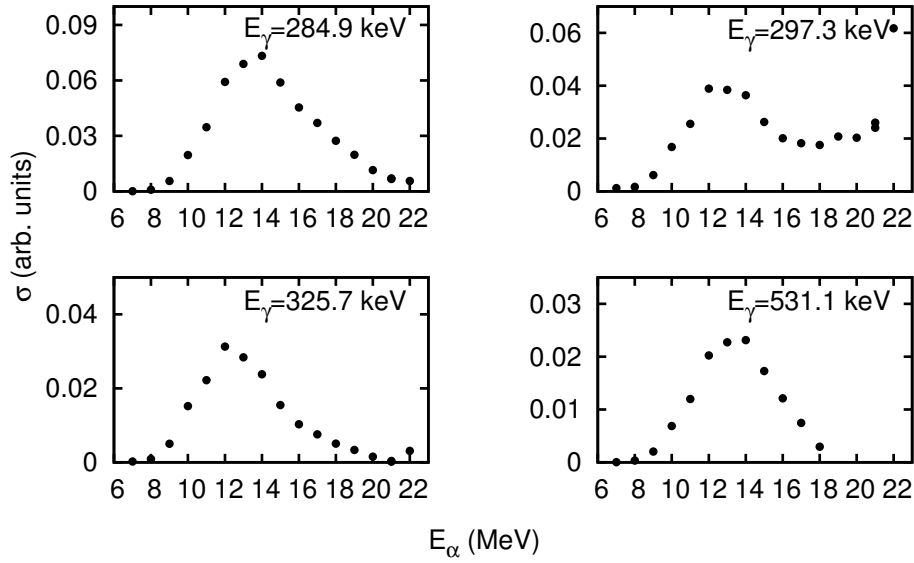
Fig. 4: Production cross sections for gammas excited through the ^{70}Zn$(\alpha, n\gamma)^{73}$Ge. Preliminary results. On the x-axis the energy of the incoming alphas is plotted, not corrected for the energy lost in the target.

531.1 keV decaying from the 4th, 5th, 6th and 11th excited level in ^{73}Ge. However the absolute values of the cross sections were not yet determined and these data should be considered as preliminary, unchecked results. Moreover the alpha energies were not corrected for the energy lost in the target.

5 Conclusions

An experimental effort is ongoing with the purpose of investigating to which extent the Bohr hypothesis could be employed to infer neutron inelastic cross sections from charged particle induced reactions. The first comparison was performed for the case of the ^{28}Si nucleus excited through the $(n, n'\gamma)$ and $(\alpha, n\gamma)$ reactions. The analysis for an experiment investigating the ^{70}Zn$(\alpha, n\gamma)^{73}$Ge reaction is ongoing.

References

[1] C. Plettner *et al.*, Phys. Rev. C**71**, 051602 (2005).

[2] J.T. Burke *et al.*, Phys. Rev. C**73**, 054604 (2006).

[3] B.L. Goldblum *et al.*, Phys. Rev. C**78**, 064606 (2008).

[4] M. Petit *et al.*, Nucl. Phys. A**735**, 345 (2004).

[5] S. Boyer *et al.*, Nucl. Phys. A**775**, 175 (2006).

[6] J.M. Allmond *et al.*, Phys. Rev. C**79**, 054610 (2009).

[7] N. Bohr, Nature **137**, 344 (1936).

[8] D. Ene, C. Borcea, S. Kopecky, W. Mondelaers, A. Negret, A.J.M. Plompen, Nucl. Instrum. Meth. Phys. Research A618, 54 (2010).

[9] A. Negret, C. Borcea, J.C. Drohe, L.C. Mihailescu, A.J.M. Plompen and R. Wynants, Proceedings of the International Conference on Nuclear Data for Science and Technology ND2007, April 22-27 2007, Nice, France (2008).

[10] D. Deleanu, C. Borcea, Ph. Dessagne, M. Kerveno, A. Negret, A.J.M Plompen, J.C. Thiry, Nucl. Instrum. Meth. Phys. Research A624, 130 (2010).

[11] A.J.M. Plompen *et al.*, J. Korean Phys. Soc. 59, 1581 (2011).

[12] A. Negret *et al.*, Phys. Rev. C**88**, 034604 (2013).

[13] K. Forssten, A. Hasselgren, Ph. Monseu and A. Nilsson, Physica Scripta **10**, 51 (1974).

[14] B. Singh, Nucl. Data Sheets **101**, 193 (2004).

Measurements of prompt fission gamma-rays and neutrons with lanthanide halide scintillation detectors

A. Oberstedt [1], T. Belgya [2], R. Billnert [3], [1], R. Borcea [3], T. Bryś [3], C. Chaves [3], T. Gamboni [3], W. Geerts [3], A. Göök [4], C. Guerrero [5], F.-J. Hambsch [3], Z. Kis [2], T. Martinez [6], S. Oberstedt [3], L. Szentmiklosi [2], K. Takács [2], M. Vidali [3]

[1] Fundamental Physics, Chalmers University of Technology, 41296 Göteborg, Sweden

[2] Centre for Energy Research, Hungarian Academy of Sciences, 1121 Budapest, Hungary

[3] European Commission, Joint Research Centre (IRMM), 2440 Geel, Belgium

[4] Institut für Kernphysik,Technische Universität Darmstadt, 64289 Darmstadt, Germany

[5] CERN Physics Department, 1211 Genève, Switzerland

[6] Nuclear Innovation Group, Department of Energy, CIEMAT, 28040 Madrid, Spain

Abstract

Photons have been measured with lanthanide halide scintillation detectors in coincidence with fission fragments. Using the time-of-flight information, reactions from γ-rays and neutrons could easily be distinguished. In several experiments on ^{252}Cf(sf), ^{235}U(n$_{th}$,f) and ^{241}Pu(n$_{th}$,f) prompt fission γ-ray spectra characteristics were determined with high precision and the results are presented here. Moreover, a measured prompt fission neutron spectrum for ^{235}U(n$_{th}$,f) is shown in order to demonstrate a new detection technique.

1 Introduction

A good knowledge of particle emission in fission is essential for the peaceful use of nuclear power. Prompt gamma-rays contribute considerably to the fission heat in a reaction core, whereas prompt neutrons are responsible for maintaining a chain reaction. The precision, with which their characteristics are known, is of course important for both safety reasons and economy. Apart from the technological aspects, there are also indications that in particular prompt fission gamma-rays reveal detailed information on the dynamics of the fission process.

A coordinated research program for the experimental investigation of prompt fission neutron spectra (PFNS) from major actinides, induced by fast neutrons, was launched by the IAEA [1], while new measurements of prompt fission γ-ray spectra (PFGS), in particular for the reactions ^{235}U(n,f) and ^{239}Pu(n,f), have been included in OECD-NEA's high priority request list for prompt fission γ-ray data [2]. In recent studies we developed a technique, which allows in principle to measure simultaneously both prompt neutrons and γ-rays emitted in fission, and applied it to the reactions ^{252}Cf(sf), ^{235}U(n$_{th}$,f) and ^{241}Pu(n$_{th}$,f). Below we report on the experiments, recently performed in the framework of ERINDA, and present results that were obtained so far.

2 Experiments

All experiments described in this paper have in common that γ-rays were measured in coincidence with fission fragments. The photons were detected with novel lanthanide halide scintillation detectors, based on cerium-doped lanthanum-chloride (LaCl$_3$:Ce) [3], cerium-doped lanthanum-bromide (LaBr$_3$:Ce) [4] and cerium-bromide (CeBr$_3$) [5, 6] crystals, respectively, which combine an excellent timing resolution with a reasonably good energy resolution. The trigger was provided by the fission fragments, which were detected by either an ultra-fast polycrystalline chemical vapor deposited (pcCVD) diamond detector [7] in conjunction with the fission fragment spectrometer VERDI [8] or a Frisch-grid ionization chamber. In all experiments both energy and time-of-flight (TOF) of the photons were recorded. Figure 1 shows a typical two-dimensional presentation of photons measured with a 2 in. $\times$ 2 in. LaBr$_3$:Ce detector in
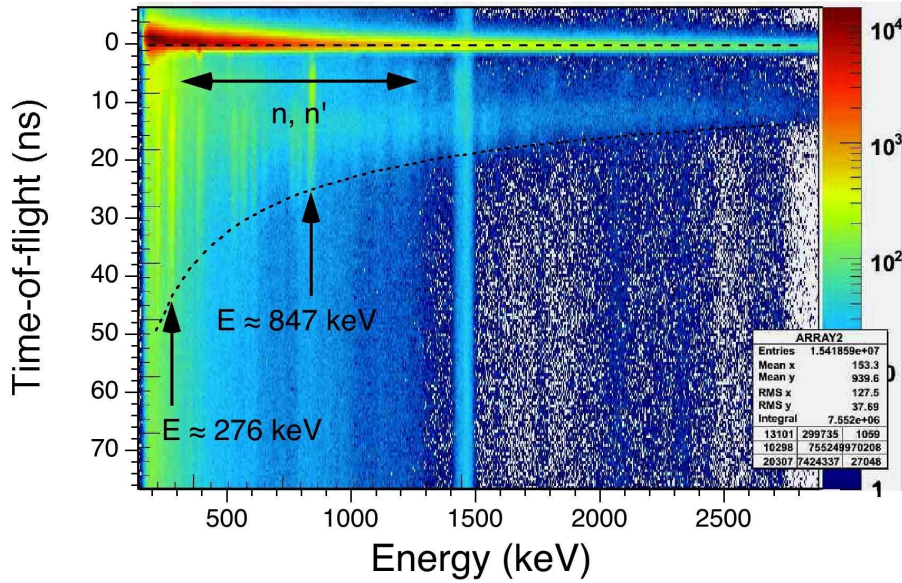
Fig. 1: Distribution of γ-rays by time-of-flight vs. energy. Prompt fission γ-rays are represented by a horizontal area (dashed line), while the vertical lines represent γ-rays from reactions induced by prompt fission neutrons, preferably inelastic scattering (see text for details).

coincidence with fission fragments, here from the spontaneous fission of ^{252}Cf, investigated at the DG Research Centre Institute for Reference Materials and Measurements (IRMM). The region of prompt fission γ-rays is indicated by the dashed line, while the many vertical lines between the dashed and the dotted lines correspond to de-excitations after inelastic neutron scattering in the detector or in structural materials in the vicinity of the experimental set-up. E.g., the line at 847 keV corresponds to the first excited state in ^{56}Fe, whereas the one at 276 keV corresponds to the first excited state in ^{81}Br present in the detector. The time-of-flight distribution of the latter one is converted into an energy spectrum and used to determine the neutron detection efficiency, as described in Ref. [9]. Below we show results from an experiment on ^{235}U(n_{th},f), obtained by applying this neutron efficiency to data taken at the 10 MW research reactor of the Centre for Energy Research in Budapest.

The prompt fission γ-rays were selected by choosing a narrow TOF window, the background from other reactions was assessed and subtracted, and the obtained energy spectrum was normalized with the number of fission events. In order to deduce the emitted prompt fission γ-ray spectrum, the measured spectrum has to be corrected with the response function of the used detectors, which were determined by means of Monte Carlo simulations with the computer code PENELOPE2011 [12], folded with the energy resolution of the corresponding detector. More detailed information on the actual extraction of the emission spectrum is described e.g. in Ref. [4]. In this manner we obtained PFGS characteristics, i.e. the average γ-ray multiplicity $\overline{\nu}_\gamma$, the average energy per photon ϵ_γ and the total γ-ray energy $E_{\gamma,tot}$, which are presented below.

3 Results

In this section an overview of experimental results is given for our prompt fission neutron and γ-ray measurements performed so far. The results are compared to other experimental and calculated values, where available. The reactions that were investigated are ^{252}Cf(sf), ^{235}U(n_{th},f) and ^{241}Pu(n_{th},f).

$T_{fit} = (1.3 \pm 0.5)$ MeV
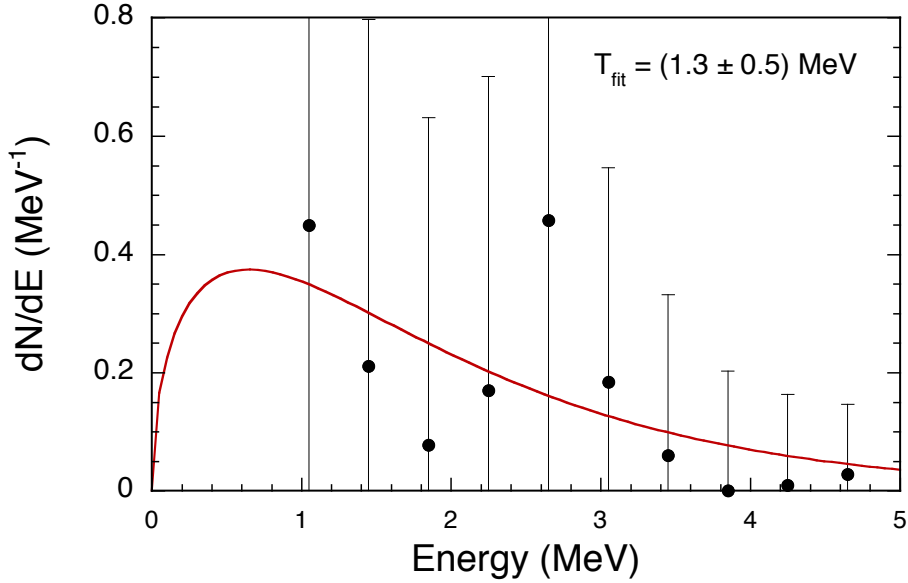
Fig. 2: Energy spectrum of neutrons from the reaction ^{235}U(n$_{th}$, f). The experimental values are fitted to a Maxwell-Boltzmann distribution in order to extract a temperature parameter and the distribution was normalized to 1.

3.1 PFNS from the reaction ^{235}U(n$_{th}$,f)

In an experiment performed at the 10 MW research reactor of the Centre for Energy Research in Budapest, the reaction ^{235}U(n$_{th}$,f) was investigated with the same set-up as used to determine the neutron efficiency mentioned above (see Ref. [10] for details). Fig. 2 shows the obtained neutron energy probability distribution, normalized to one. Due to several experimental problems, leading to the loss of an unknown number of events it was not possible to extract an average number of prompt fission neutrons $\overline{\nu}$. As a consequence of the poor statistics, we had to restrict ourselves to neutron energies above 1 MeV due to uncertainties in assessing the constant background. However, it was at least possible to extend the energy range to 5 MeV. Although the statistical accuracy is quite poor, indicated by the large error bars (containing both statistical uncertainties and those from background determination as well as efficiency), we fitted a Maxwell-Boltzmann distribution to the data. It results in a temperature parameter $T_{fit} = (1.3 \pm 0.5)$ MeV, which agrees well with documented values like e.g. 1.33 MeV from Ref. [11]. Admittedly, the experimental data presented here is of poor quality and the shape of the neutron spectrum - a Maxwell-Boltzmann distribution - was assumed to be known beforehand; still, perfect agreement with previously published values for the temperature parameter was achieved. This result might serve at least to illustrate the applicability of the neutron detection technique mentioned above.

3.2 PFGS characteristics from the reactions ^{252}Cf(sf), ^{235}U(n$_{th}$,f) and ^{241}Pu(n$_{th}$,f)

Several experiments were performed to measure prompt fission γ-ray spectra (PFGS). The investigation of the spontaneous fission of ^{252}Cf was carried out at the DG Research Centre IRMM in Geel, while the thermal neutron-induced fission of both ^{235}U and ^{241}Pu was studied at the 10 MW research reactor of the Centre for Energy Research in Budapest. The experiments were conducted according to the brief description in Sect. 2. More information on the particular instrumentation and experimental set-ups for each measurement as well as details about the data treatment are given in Refs. [4, 13–15], where also the obtained emission spectra are shown. An overview of the determined PFGS characteristics from our measurements, denoted by the individual detector that was used, are displayed in Fig. 3 for ^{252}Cf(sf), in Fig. 4 for ^{235}U(n$_{th}$,f) and in Fig. 5 for ^{241}Pu(n$_{th}$,f). Mean photon multiplicity, mean photon energy per
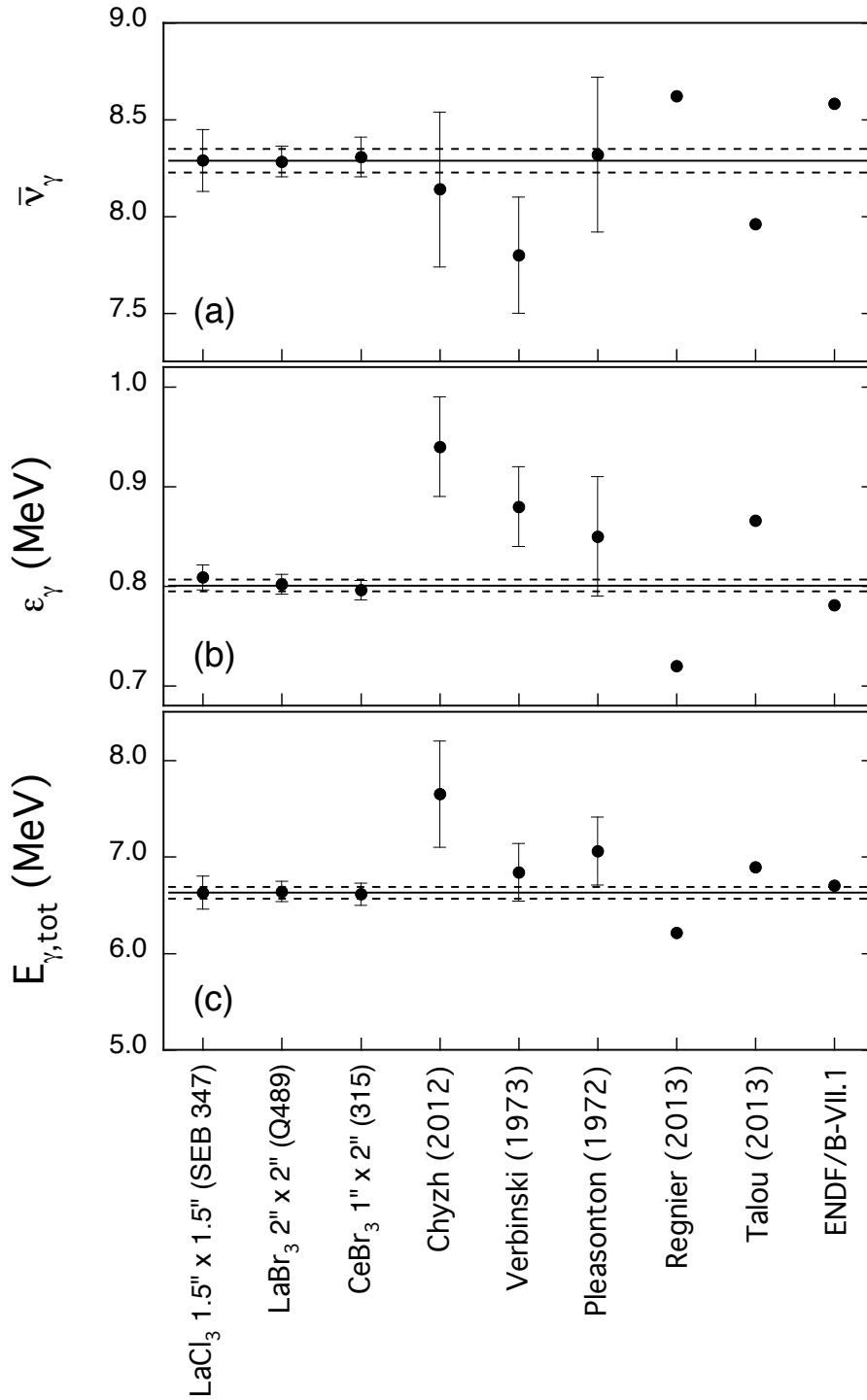
Fig. 3: Overview of measured PFGS characteristics for the spontaneous fission of ^{252}Cf: (a) Mean photon multiplicity, (b) mean photon energy per fission and (c) total released photon energy from our work, denoted by the detectors in use. Average values and their uncertainties are displayed as full drawn and dashed lines, respectively. They are compared to results from other experiments and model calculations (see Refs. [4, 13] and references therein.
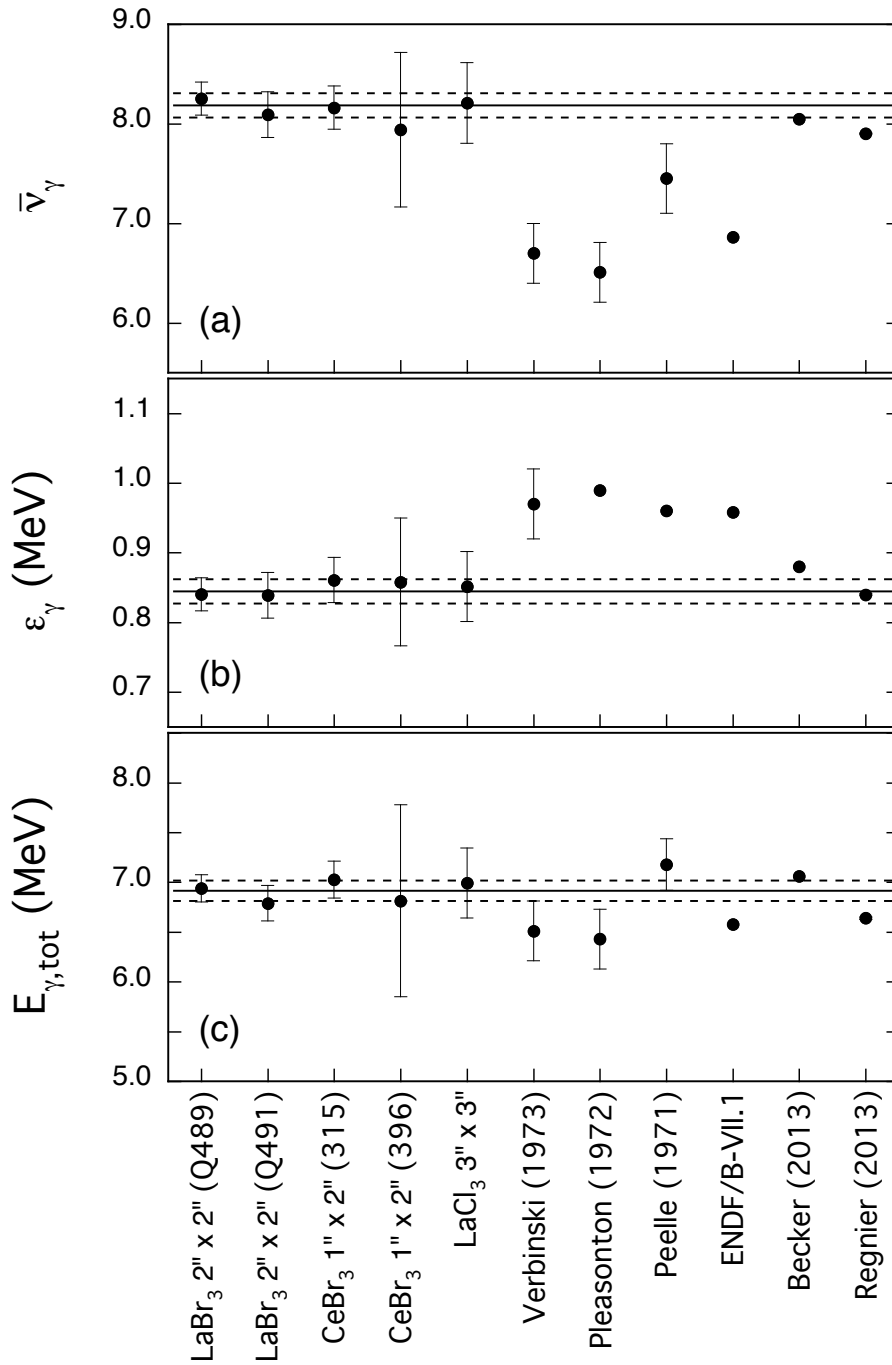
Fig. 4: Overview of measured PFGS characteristics for the thermal neutron-induced fission of ^{235}U: (a) Mean photon multiplicity, (b) mean photon energy per fission and (c) total released photon energy from our work, denoted by the detectors in use. Average values and their uncertainties are displayed as full drawn and dashed lines, respectively. They are compared to results from other experiments and model calculations (see Ref. [14] and references therein).
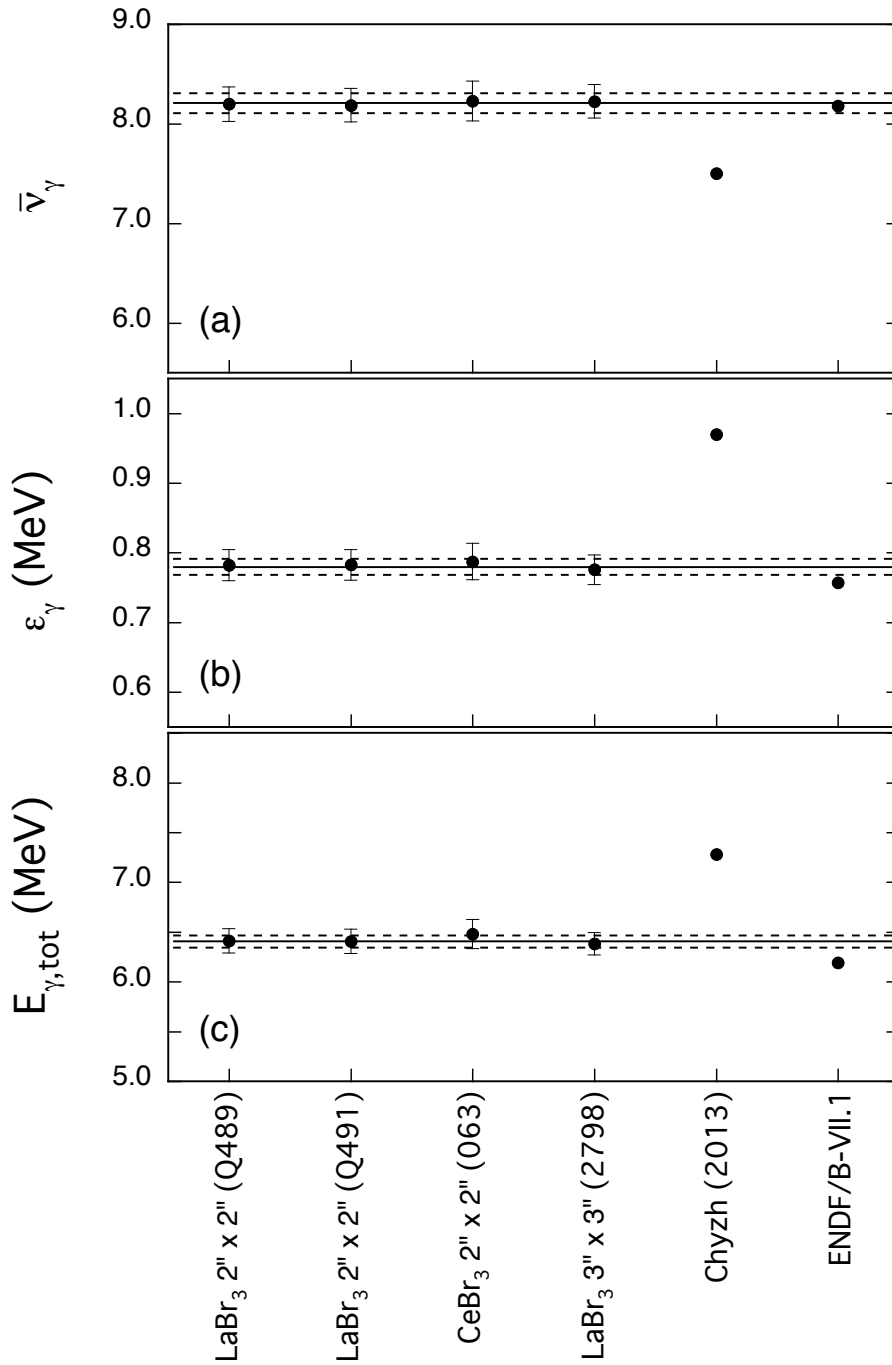
Fig. 5: Overview of measured PFGS characteristics for the thermal neutron-induced fission of ^{241}Pu: (a) Mean photon multiplicity, (b) mean photon energy per fission and (c) total released photon energy from our work, denoted by the detectors in use. Average values and their uncertainties are displayed as full drawn and dashed lines, respectively. They are compared to results from other experiments and model calculations (see Ref. [15] and references therein.
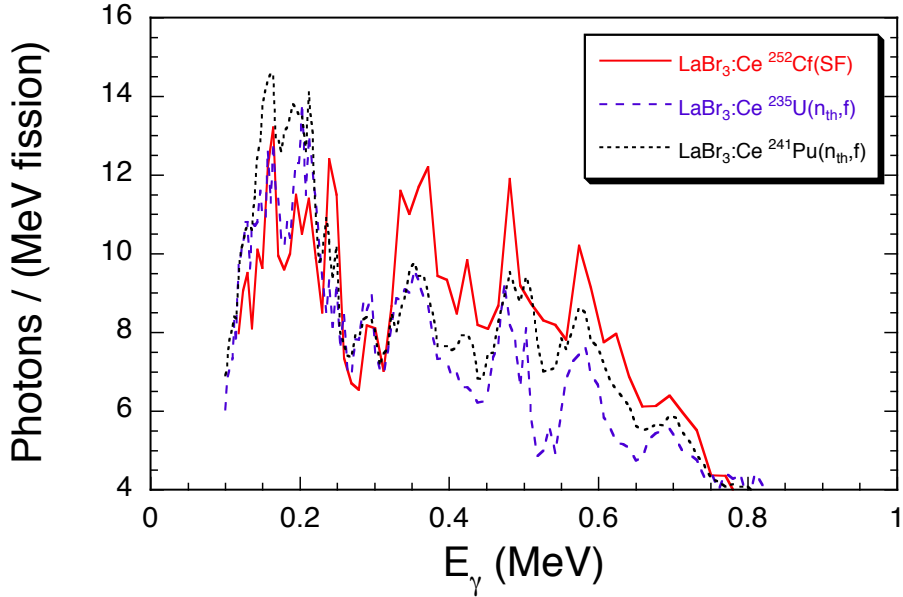
Fig. 6: Low energy part of PFGS for the fissioning systems reported about in this work. The distinct peak structures exhibit obvious similarities.

fission and total released photon energy are plotted in the upper, middle and lower part of the figures, respectively. Values averaged over our results and their uncertainties are shown as as full drawn and dashed lines. Corresponding values from other measurements as well as from theoretical calculations and an evaluated data library are shown for comparison. References to those studies are given in the references mentioned above. A brief discussion of our findings follows below.

4 Summary and discussion

From the overviews presented in the previous section we may conclude that all our measurements gave very consistent results independent of the particular detector in use. That made it possible to determine average values for the PFGS characteristics with hitherto unprecedented accuracy for all fissioning systems investigated so far. Other recent experimental results, taken with the detector system DANCE and published during the years 2012 and 2013, exhibit average multiplicities, which are lower than ours, and a total γ-ray energy released in fission that is too high compared to our results. An explanation for this discrepancy is given by absorption effects for low energy γ-rays as addressed in Ref. [4]. A comparison of the low energy regions of the PFGS for the fissioning systems reported about in this work, exhibits distinct and very similar peak structures (see Fig. 6). We believe that their origin is de-excitation of rotational states in mainly heavy fission fragments. A possible confirmation for that is the topic of our efforts in the next future.

We have also demonstrated a technique to measure PFNS with lanthanum bromide detectors by evaluating γ-rays produced in inelastic neutron scattering off bromine nuclei, even if the obtained data for ^{235}U is affected by very low statistics. Since the energy of the considered excited state is equal to the minimum kinetic energy of the detectable neutrons, the low energy threshold in this work should be in principle at about 280 keV. This is much lower than the 500 and 1000 keV, which is reported for standard neutron detectors. In order to prove that we have to apply this technique to experimental data taken with better statistics, which is in progress.

Acknowledgements

References

[1] R. Capote, V. Maslov, E. Bauge, T. Ohsawa, A. Vorobyev, M. Chadwick, S. Oberstedt, Consultants' Meeting on Prompt Fission Neutron Spectra of Major Actinides, Summary Report, IAEA-INDC International Nuclear Data Committee, INDC(NDS)-0541 (January 2009).

[2] Nuclear Data High Priority Request List of the NEA (Req. ID: H.3, H.4), www.oecd-nea.org/dbdata/hprl/hprlview.pl?ID=421 and www.oecd-nea.org/dbdata/hprl/hprlview.pl?ID=422.

[3] A. Oberstedt, S. Oberstedt, R. Billnert, W. Geerts, F.-J. Hambsch, J. Karlsson, Nucl. Instr. and Meth. A668 (2012) 14.

[4] R. Billnert, F.-J. Hambsch, A. Oberstedt, and S. Oberstedt, Phys. Rev. C 87 (2013) 024601.

[5] R. Billnert, S. Oberstedt, E. Andreotti, M. Hult, G. Marissens, and A. Oberstedt, Nucl. Instr. and Meth. A647 (2011) 94.

[6] G. Lutter, M. Hult, R. Billnert, A. Oberstedt, S. Oberstedt, E. Andreotti, G. Marissens, U. Rosengård and F. Tzika, Nucl. Instr. and Meth. A703 (2013) 158.

[7] S. Oberstedt, R. Borcea, T. Brys, Th. Gamboni, W. Geerts, F.-J. Hambsch, A. Oberstedt, and M. Vidali, Nucl. Instr. and Meth. A714 (2013) 31.

[8] S. Oberstedt, R. Borcea, F.-J. Hambsch, Sh. Zeynalov, A. Oberstedt, A. Göök, T. Belgya, Z. Kis, L. Szentmiklosi, K. Takács, T. Martinez-Perez, Proceedings of Seminar on Fission VII, Het Pand, Gent, Belgium, May 16-20, 2010, eds. C. Wagemans, J. Wagemans and P. D'hondt, ISBN-13 978-981-4322-73-7 (2010) 207.

[9] A. Oberstedt, R. Billnert, S. Oberstedt, Nucl. Instr. and Meth. A708 (2012) 7.

[10] A. Oberstedt, R. Billnert, S. Oberstedt, Phys. Proc. 31 (2012) 21.

[11] N. Kornilov, F.-J. Hambsch, I. Fabry, S. Oberstedt, T. Belgya, Z. Kis, L. Szentmiklosi and S. Simakov, Nucl. Sci. Eng. 165 (2010) 117.

[12] http://www.oecd-nea.org/tools/abstract/detail/nea-1525.

[13] A. Oberstedt, R. Billnert, F.-J. Hambsch, and S. Oberstedt, to appear in Phys. Rev. C.

[14] A. Oberstedt, T. Belgya, R. Billnert, R. Borcea, T. Bryś, W. Geerts, A. Göök, F.-J. Hambsch, Z. Kis, T. Martinez, S. Oberstedt, L. Szentmiklosi, K. Takàcs, and M. Vidali, Phys. Rev. C87, 051602(R) (2013).

[15] R. Billnert, T. Belgya, T. Bryś, W. Geerts, C. Guerrero, F.-J. Hambsch, Z. Kis, A. Moens, A. Oberstedt, S. Oberstedt, G. Sibbens, L. Szentmiklosi, D. Vanleeuw, and M. Vidali, to appear in Phys. Rev. C.

Inelastic scattering of fast neutrons from ^{56}Fe

R. Beyer[1], R. Schwengner[1], R. Hannaske[1,2], A. R. Junghans[1], R. Massarczyk[1,2], M. Anders[1,2],
D. Bemmerer[1], A. Ferrari[1], T. Kögler[1,2], M. Röder[1,2], K. Schmidt[1,2] and A. Wagner[1]
[1]Institute of Radiation Physics, Helmholtz-Zentrum Dresden-Rossendorf, 01328 Dresden, Germany
[2]Technische Universität Dresden, 01062 Dresden, Germany

Abstract

Inelastic scattering of fast neutrons from ^{56}Fe was studied at the photoneutron source nELBE. The neutron energies were determined on the basis of a time-of-flight measurement. Gamma-ray spectra were measured with a high-purity germanium detector. The total scattering cross sections deduced from the present experiment in an energy range from 0.8 to 9.6 MeV agree within 15% with earlier data and with predictions of the statistical-reaction code Talys.

1   Introduction

Cross sections of neutron-induced reactions attract growing interest in the context of future nuclear technologies. In particular, there is a need of data with high accuracy for neutron capture and fission induced by fast neutrons for isotopes of uranium, plutonium, and minor actinoids. In addition, cross sections of inelastic scattering of fast neutrons from structural materials, such as sodium, iron, and lead are of great interest [1].

The present work describes experiments studying the inelastic scattering of neutrons in the energy range from 0.8 to 9.6 MeV using the photoneutron source nELBE at the superconducting electron accelerator ELBE of the Helmholtz-Zentrum Dresden-Rossendorf (HZDR), Germany.

2   The photoneutron source nELBE

The photoneutron source nELBE consists of a circuit of liquid lead. The electron beam of about 3 mm in diameter passes a beryllium window and hits the liquid lead circulating in a molybdenum channel of 11.2 mm width. The intersection of the beam with the lead channel defines a volume of 0.6 cm^3. Liquid lead was chosen as the radiator material because the thermal load deposited by the electron beam (up to 25 kW) is too high to be dissipated from a solid target of such small size by gas cooling and heat radiation. Cooling with water is unfavorable because of neutron scattering and moderation. A detailed description of nELBE is given in Ref. [2].

The neutrons travelling at an angle of 95° relative to the incident electron beam enter the experimental area after passing a collimator in the concrete wall of 2.40 m thickness, followed by a 10 cm thick lead wall. The collimator consists of a combination of borated polyethylene and lead cylinders [2]. The experimental setup is schematically shown in Fig. 1. The neutron intensity was monitored with a calibrated ^{235}U fission chamber [3] delivered by the Physikalisch-Technische Bundesanstalt (PTB) Braunschweig. As no moderation was applied, the short accelerator beam pulses of about 5 ps provided the basis for a good time resolution for time-of-flight experiments at a flight path of 6.2 m. The neutron intensity at the target position was about 2×10^4 cm^{-2} s^{-1} using an electron bunch charge of 77 pC and a pulse repetition rate of (13 MHz)/64 = 203.125 kHz. Details of the neutron-beam profile, the determination of the neutron flux and the neutron spectrum are given in Ref. [4].

3   Experimental methods at the time-of-flight setup

The target consisted of a disk of natural iron with a diameter of 20 mm and a thickness of 8 mm with a mass of 19.787 g. This results in an areal density of $6.211 \cdot 10^{-2}$ ^{56}Fe atoms per barn. A high-purity
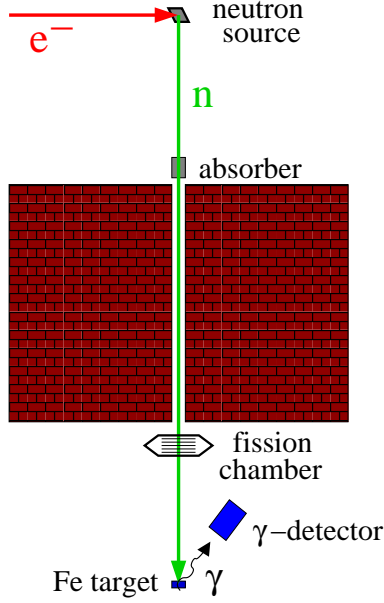
Fig. 1: (Color online.) Time-of-flight setup at the photoneutron source nELBE.

germanium (HPGe) detector with an efficiency of 100% relative to a NaI detector of 7.6 cm in diameter and in length was used to measure γ rays from states in ^{56}Fe. The detector was positioned at a distance of 20 cm from the target and at an angle of 125° relative to the beam direction. An energy and efficiency calibration of the detector was performed using ^{22}Na, ^{60}Co and ^{226}Ra standard calibration sources. The experiment was carried out with an electron beam energy of 30 MeV and an average current of 15 μA. The measurement was performed by cyclically placing the target in and out of the beam every hour to reduce long-term fluctuations of the beam current. The total live time of the measurement was 23 h for each case. The time of flight was measured as the time difference between the accelerator pulse and the signal of the HPGe detector. With this detector, a time resolution of 10 ns (FWHM) was achieved. The data acquisition recorded list-mode data containing signals of the fission chamber, the time-of-flight signal and the energy signal of the HPGe detector. Details of the system and of the dead-time correction are given in Ref. [4].

The calibration of the time-of-flight spectrum was performed as described in Ref. [4]. The time of flight was calculated according to

$$t_n = f \cdot (ch_n - ch_\gamma) + s/c, \tag{1}$$

where $f = 0.9766$ ns/channel, ch_n is the channel number in the time-of-flight spectrum, ch_γ is the channel number of the peak produced by bremsstrahlung scattered from the sample, $s = 6175$ mm is the flight path and c is the speed of light. Time-of-flight spectra for the measurements with and without target are shown in Fig. 2. The kinetic neutron energy E_n was derived as

$$E_n = m_n c^2 \left[\frac{1}{\sqrt{1 - s^2/(t_n c)^2}} - 1 \right], \tag{2}$$

where $m_n c^2$ is the neutron rest energy. The measured events containing time-of-flight and γ-ray energy were corrected for dead time and sorted into coincidence matrices for the measurements with and without target. The matrix containing events without target was subtracted from the one with target to reduce background events. Gamma-ray spectra were extracted by setting gates of 12 channels width, corresponding to 11.72 ns, on the time axis in the net matrix after background subtraction. An example
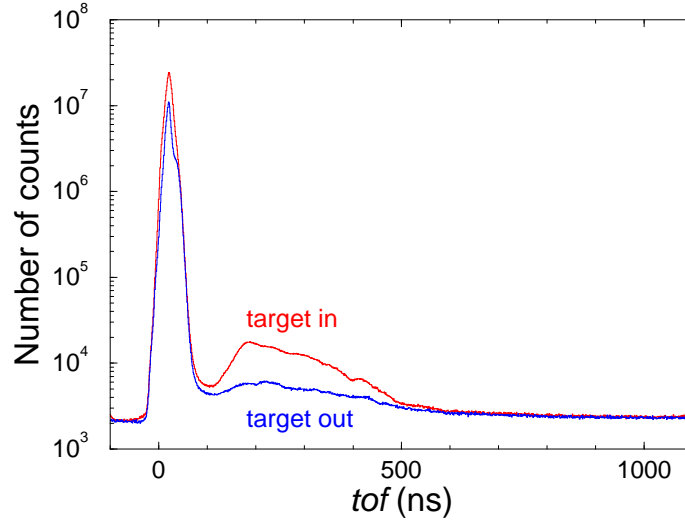
Fig. 2: Time-of-flight spectra with and without target containing events registered in the HPGe detector relative to the accelerator pulse.
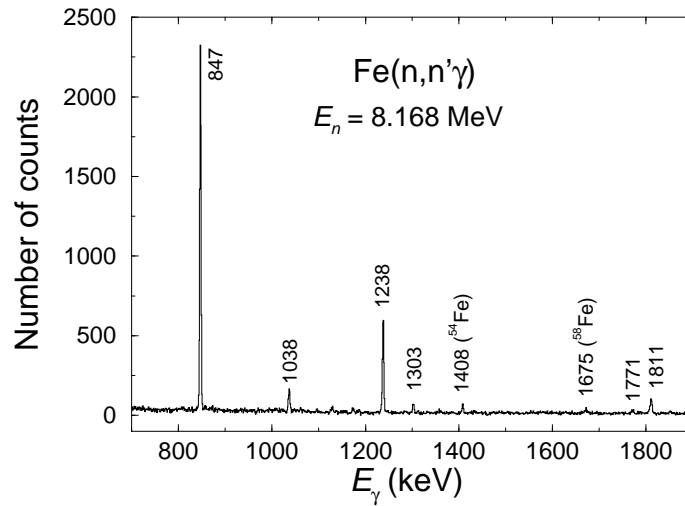
Fig. 3: Gamma-ray spectrum measured in the Fe$(n, n'\gamma)$ reaction for a neutron energy around E_n = 8.168 MeV. The time-of-flight gate width of 11.72 ns corresponds to a neutron-energy gate width of ΔE_n = 1.229 MeV. The labels denote energies of transitions in ^{56}Fe unless given otherwise.

of a resulting γ-ray spectrum is shown in Fig 3. The spectrum shows transitions between excited states in ^{56}Fe and, in addition the $2_1^+ \rightarrow 0_1^+$ transitions in ^{54}Fe and ^{58}Fe.

The neutron fluence (time-integrated flux) determined with the fission chamber for the present measuring time is shown in Fig. 4. The neutron flux was corrected for attenuation of the neutron beam in the target. The determination of the neutron flux using the fission chamber is described in detail in Ref. [4].
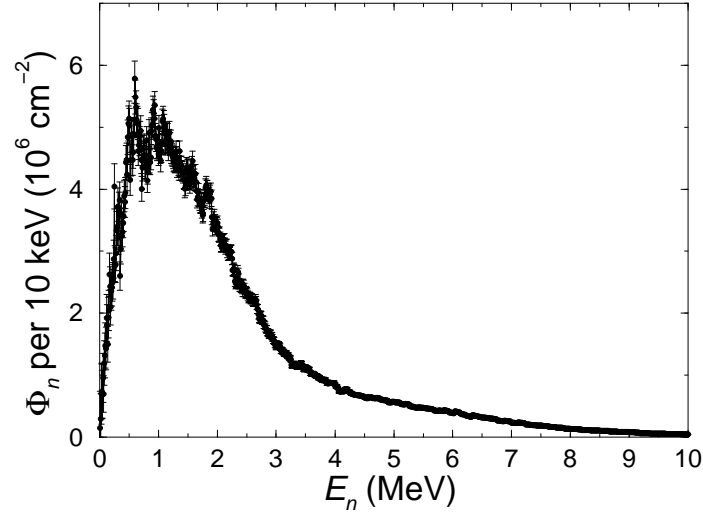
Fig. 4: Neutron fluence determined for the present experiment according to the procedure described in Ref. [4].

4   Experimental results

The reaction cross sections σ for excited states with energies E_i emitting γ rays of energy E_γ were calculated using the relation

$$\sigma(E_i, E_n) = \frac{N(E_\gamma, E_n)}{\varepsilon(E_\gamma)\Phi(E_n)N_{\mathrm{at}}}, \tag{3}$$

where $N(E_\gamma, E_n)$ is the number of dead-time corrected events in the peak at E_γ observed at a neutron energy E_n, $\varepsilon(E_\gamma)$ is the absolute efficiency of the HPGe detector at E_γ, $\Phi(E_n)$ is the neutron fluence at E_n, and N_{at} is the number of atoms in the target.

The cross sections obtained in this way were corrected for the attenuation of the emitted γ rays in the target material. The attenuation was simulated for γ rays emitted isotropically from the target. The start positions of the γ rays were distributed uniformly perpendicular to the beam direction and exponentially in beam direction because of the decreasing neutron intensity. For γ rays moving in the direction toward the detector the path length through the target l_{path} was calculated. The attenuation of the γ rays was described by an exponential distribution using the attenuation factors μ/ρ taken from Ref. [5] as mean values. From this distribution an attenuation length l_{att} was randomly sampled for each photon. If $l_{\mathrm{att}} < l_{\mathrm{path}}$, then the photon is absorbed in the target. The correction factors C applied to the cross sections are the ratios of started photons to absorbed photons. The mean value of the path lengths was 5.16 mm assuming an average total cross section of 4 b for calculation of the attenuation of the neutron intensity. A change of this value by $\pm$ 4 b resulted in a change of C by less than 1%.

For high-energy neutrons, there exists a certain probability that they can be inelastically scattered more than once inside the target. This multiple scattering increases the cross section of an excited state at a certain neutron energy, although the multiply scattered neutron has an energy different from the incident energy. The increase is expected to be considerable in particular for the lowest excited state, namely the first 2^+ state in ^{56}Fe. The probability P for multiple scattering with the detection of the 847 keV γ ray in a subsequent scattering step was simulated with the code GEANT4 [6]. The cross section of the 2^+ state was corrected with the factor $(1 - P)$.

At the angle of $\theta = 125°$ between detector and neutron beam direction, the term $A_2 P_2(\cos\theta)$ of the expression for the angular distribution approaches zero. Nevertheless, the term $A_4 P_4(\cos\theta)$ may produce a deviation of the angular distribution from unity, for example for a $2 \to 0$ transition. Feeding

from higher lying states attenuates the angular distribution. This means, the term may be applied to the 847 keV transition at energies below the next higher state, i.e. below about 2.1 MeV. Angular distributions of the 847 keV γ rays emitted in the ^{56}Fe reaction were measured in Ref. [7]. The coefficients A_2 and A_4 deduced from these measurements are listed in Table 1.

Table 1: Angular distribution coefficients of the 847 keV γ ray at various neutron energies, taken from Ref. [7].

| E_n (MeV)[a]	A_2^b	A_4^b	$W(125°)^c$
0.93	0.521(30)	–0.511(33)	1.193(13)
0.98	0.539(13)	–0.302(14)	1.113(5)
1.08	0.435(17)	–0.144(19)	1.053(7)
1.18	0.398(39)	–0.331(44)	1.125(17)
1.28	0.312(31)	+0.020(4)	0.990(2)
1.38	0.396(18)	+0.039(20)	0.982(8)
1.59	0.319(22)	–0.167(25)	1.062(10)
1.68	0.226(12)	–0.155(15)	1.058(6)
1.79	0.216(10)	–0.082(13)	1.030(5)
1.85	0.245(31)	–0.089(36)	1.033(14)
2.03	0.190(18)	–0.023(21)	1.008(8)

[a] Neutron energy.
[b] Coefficients of the angular distribution $W(\theta) = 1 + A_2 P_2(\cos\theta) + A_4 P_4(\cos\theta)$ taken from Ref. [7].
[c] Angular distribution $W(\theta = 125°)$ calculated using the given A_2 and A_4 values.

The largest A_4 value was found at the lowest neutron energy. This value amounts to 30% of the maximum value of $A_4^{\max} = -1.714$ predicted for a $2 \rightarrow 0$ transition [8]. This attenuation may be caused by the reaction mechanism. The further values generally decrease with increasing neutron energy. However, the values at $E_n = 1.28$ and 1.38 MeV do not follow the general behavior and have an unpredicted sign, which may indicate uncertainties of the values not covered by the given errors. Therefore, a correction of the total scattering cross section deduced from the 847 keV transition for the angular distribution has not been applied. This concerns the values for neutron energies below 2.1 MeV. At higher energies, feeding from higher-lying states occurs and the angular distribution is further attenuated. For the $4 \rightarrow 2$ and $6 \rightarrow 4$ transitions the $A_4^{\max}$ values are -0.367 and -0.242, respectively. Assuming also an attenuation of about 30%, the contribution of $A_4 P_4(\cos 125°)$ to the angular distribution at 125° is 4.0% and 2.5%, respectively. For the 4^+ state, also feeding has been taken into account, which reduces the value of 4% further. For the 6^+ state, the mentioned value of 2.5% has also not been applied to the values shown in the following. The contribution of $A_4 P_4(\cos 125°)$ to the $2 \rightarrow 2$ transitions feeding the 2^+ state at 847 keV is less than 0.5%, also if taking into account a mixing ratio of $\delta = 0.25$ as recommended for the 2113 and 2523 keV γ rays [9].

The total inelastic scattering cross section can be deduced from the intensity of the respective $2_1^+ \rightarrow 0_1^+$ transition that collects all intensity from higher-lying states, whereas the intensities of other ground-state transitions can be neglected [9]. The total scattering cross section deduced in this way for ^{56}Fe is shown in Fig. 5. The error bars include statistical uncertainties of the γ-ray intensities and the total uncertainty of the neutron flux. Possible systematic uncertainties of the neutron flux are discussed in Ref. [4]. The cross section shows resonance-like structures at 1.2, 1.6 and 2.4 MeV and a flattening above about 6 MeV.

Total inelastic neutron-scattering cross sections calculated with the code Talys [10] on the basis of the statistical reaction model are compared with the present experimental values in Fig. 5. It can be seen that the calculations describe magnitude and gross behavior of the experimental cross section. However, the resonance-like structures observed at about 1.2, 1.6 and 2.4 MeV are not included in the statistical model.
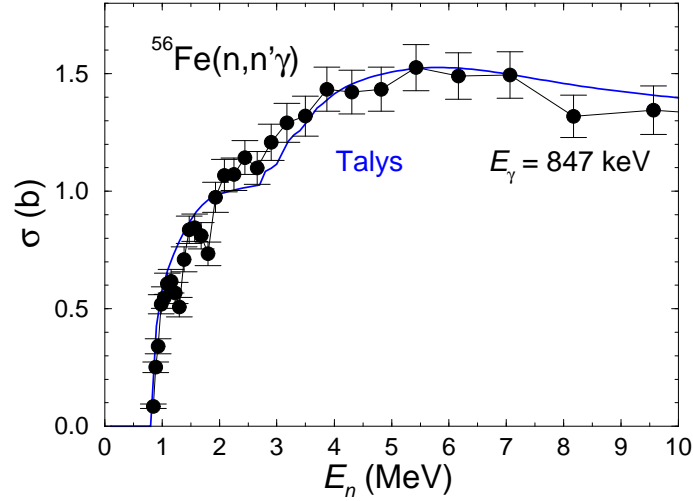
Fig. 5: (Color online) Total neutron-scattering cross section of ^{56}Fe deduced from the measured intensities of the 847 keV transition (black circles) and calculated with Talys (blue solid line).
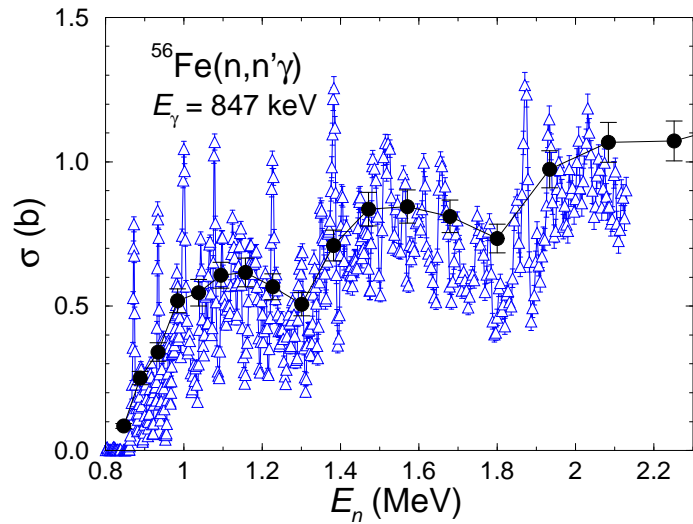
Fig. 6: (Color online) Total neutron-scattering cross section of ^{56}Fe deduced from the measured intensities of the 847 keV transition of the present work (black circles) and of Ref. [11] (blue triangles).

The total inelastic scattering cross section deduced in an earlier experiment [11] is compared with the present one in Fig. 6. The smaller steps in neutron energy resulting from a better time resolution at a longer flight path reveal fluctuations in the cross section not resolved in the present measurement. The present data tend to be greater than the data of Ref. [11]. For a better comparison of the absolute values of the data of Refs. [11] and the evaluated data of Ref. [12] with the present ones, the data of Refs. [11, 12] were rebinned according to the present conditions and are compared with the present data in Fig. 7. This comparison shows that the present data tend to exceed the data of Ref. [11] by up to about 15% and the data of Ref. [12] by up to about 20%.
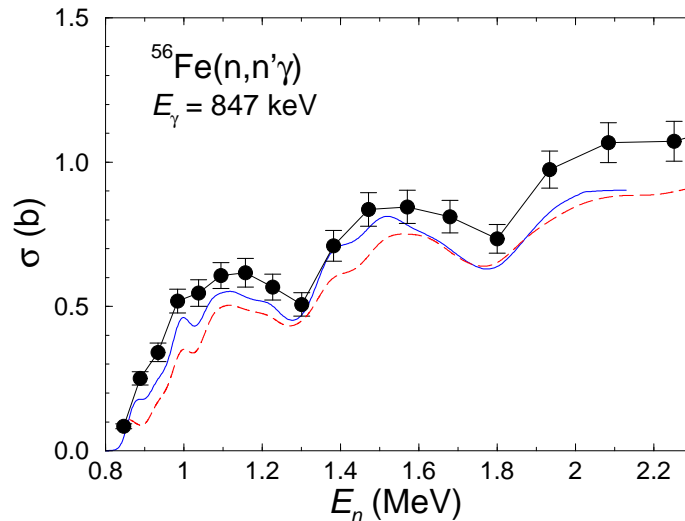
Fig. 7: (Color online) Total neutron-scattering cross section of ^{56}Fe deduced from the present data (black circles) in comparison with rebinned data of Ref. [11] (blue solid line) and of Ref. [12] (red dashed line).

5 Acknowledgments

References

[1] M. Salvatores, NEA/WPEC-26, OECD (2008); http://www.nea.fr/html/science/wpec/volume26/volume26.pdf.

[2] J. Klug, E. Altstadt, C. Beckert, R. Beyer, H. Freiesleben, V. Galindo, E. Grosse, A. R. Junghans, D. Legrady, B. Naumann, K. Noack, G. Rusev, K. D. Schilling, R. Schlenk, S. Schneider, A. Wagner, and F.-P. Weiss, Nucl. Instr. Meth. A 577 (2007) 641.

[3] R. Nolte, M. S. Allie, F. D. Brooks, A. Buffler, V. Dangendorf, J. P. Meulders, H.Schuhmacher, F. D. Smith, and M. Weierganz, Nucl. Sci. Eng. 156 (2007) 197.

[4] R. Beyer, E. Birgersson, Z. Elekes, A. Ferrari, E. Grosse, R. Hannaske, A. R. Junghans, T. Kögler, R. Massarczyk, A. Matic, R. Nolte, R. Schwengner, and A. Wagner, Nucl. Instr. Meth. A 723 (2013) 151.

[5] J. H. Hubbell and S. M. Seltzer, NIST Standard Reference Database 126 (2004).

[6] S. Agostinelli *et al.*, Nucl. Instr. Meth. A 506 (2003) 250.

[7] D. L. Smith, Argonne National Laboratory, report ANL/NDM-20, 1976.

[8] T. Yamazaki, Nucl. Data A **3** (1967) 1.

[9] H. Junde, H. Su, and Y. Dong, Nucl. Data Sheets 112 (2011) 1513.

[10] A. J. Koning, S. Hilaire, and M. C. Duijvestijn, AIP Conf. Proc. 769 (2005) 1154.

[11] F. G. Perey, W. E. Kinney, and R. L. Macklin, 3rd Conf. Neutron Cross-Sections + Technology, Knoxville 1971, vol. 1, p. 191.

[12] JEFF-3.1 evaluated data library; http://www.oecd-nea.org/dbforms/data/eva/evatapes/jeff_31/

Measurement of the ^{240,242}Pu(n,f) cross section at the CERN n_TOF facility

A. Tsinganis[,1,2], *E. Berthoumieux*[3], *C. Guerrero*[2], *N. Colonna*[4], *M. Calviani*[2], *R. Vlastou*[1], *S. Andriamonje*[2], *V. Vlachoudis*[2], *F. Gunsing*[3], *C. Massimi*[5], *S. Altstadt*[6], *J. Andrzejewski*[7], *L. Audouin*[8], *M. Barbagallo*[4], *V. Bécares*[9], *F. Bečvář*[10], *F. Belloni*[3], *J. Billowes*[11], *V. Boccone*[2], *D. Bosnar*[12], *M. Brugger*[2], *F. Calviño*[13], *D. Cano-Ott*[9], *C. Carrapiço*[14], *F. Cerutti*[2], *M. Chin*[2], *G. Cortés*[13], *M.A. Cortés-Giraldo*[15], *M. Diakaki*[1], *C. Domingo-Pardo*[16], *I. Duran*[17], *R. Dressler*[18], *N. Dzysiuk*[19], *C. Eleftheriadis*[20], *A. Ferrari*[2], *K. Fraval*[3], *S. Ganesan*[21], *A.R. García*[9], *G. Giubrone*[16], *M.B. Gómez-Hornillos*[13], *I.F. Gonçalves*[14], *E. González-Romero*[9], *E. Griesmayer*[22], *P. Gurusamy*[20], *A. Hernández-Prieto*[2,13], *D.G. Jenkins*[23], *E. Jericha*[22], *Y. Kadi*[2], *F. Käppeler*[24], *D. Karadimos*[1], *N. Kivel*[18], *P. Koehler*[25], *M. Kokkoris*[1], *M. Krtička*[26], *J. Kroll*[26], *C. Lampoudis*[3], *C. Langer*[6], *E. Leal-Cidoncha*[16], *C. Lederer*[6,27], *H. Leeb*[22], *L.S. Leong*[8], *R. Losito*[2], *A. Mallick*[21], *A. Manousos*[20], *J. Marganiec*[7], *T. Martínez*[9], *P.F. Mastinu*[19], *M. Mastromarco*[4], *M. Meaze*[4], *E. Mendoza*[9], *A. Mengoni*[28], *P.M. Milazzo*[29], *F. Mingrone*[5], *M. Mirea*[30], *W. Mondalaers*[31], *C. Paradela*[17], *A. Pavlik*[27], *J. Perkowski*[7], *A. Plompen*[31], *J. Praena*[14], *J.M. Quesada*[14], *T. Rauscher*[32], *R. Reifarth*[6], *A. Riego*[13], *M.S. Robles*[17], *F. Roman*[2,30], *C. Rubbia*[2,33], *M. Sabaté-Gilarte*[14], *R. Sarmento*[14], *A. Saxena*[21], *P. Schillebeeckx*[31], *S. Schmidt*[6], *D. Schumann*[18], *G. Tagliente*[4], *J.L. Tain*[16], *D. Tarrío*[17], *L. Tassan-Got*[8], *S. Valenta*[26], *G. Vannini*[5], *V. Variale*[4], *P. Vaz*[14], *A. Ventura*[28], *R. Versaci*[2], *M.J. Vermeulen*[23], *A. Wallner*[27], *T. Ware*[11], *M. Weigand*[6], *C. Weiss*[22], *T. Wright*[11], and *P. Žugec*[12]

[1]National Technical University of Athens (NTUA), Greece
[2]European Organisation for Nuclear Research (CERN), Geneva, Switzerland
[3]Commissariat à l'Énergie Atomique (CEA) Saclay - Irfu, Gif-sur-Yvette, France
[4]Istituto Nazionale di Fisica Nucleare, Bari, Italy
[5]Dipartimento di Fisica e Astronomia, Universita' di Bologna, and Sezione INFN di Bologna, Italy
[6]Johann-Wolfgang-Goethe Universität, Frankfurt, Germany
[7]Uniwersytet Łódzki, Lodz, Poland
[8]Centre National de la Recherche Scientif que/IN2P3 - IPN, Orsay, France
[9]Centro de Investigaciones Energeticas Medioambientales y Tecnológicas (CIEMAT), Madrid, Spain
[10]Charles University, Prague, Czech Republic
[11]University of Manchester, Oxford Road, Manchester, UK
[12]Department of Physics, Faculty of Science, University of Zagreb, Croatia
[13]Universitat Politecnica de Catalunya, Barcelona, Spain
[14]Instituto Tecnológico e Nuclear, Instituto Superior Técnico, Universidade Técnica de Lisboa, Portugal
[15]Universidad de Sevilla, Spain
[16]Instituto de Física Corpuscular, CSIC-Universidad de Valencia, Spain
[17]Universidade de Santiago de Compostela, Spain
[18]Paul Scherrer Institut, Villigen PSI, Switzerland
[19]Istituto Nazionale di Fisica Nucleare, Laboratori Nazionali di Legnaro, Italy
[20]Aristotle University of Thessaloniki, Thessaloniki, Greece
[21]Bhabha Atomic Research Centre (BARC), Mumbai, India
[22]Atominstitut, Technische Universität Wien, Austria
[23]University of York, Heslington, York, UK
[24]Karlsruhe Institute of Technology, Campus Nord, Institut für Kernphysik, Karlsruhe, Germany
[25]Department of Physics, University of Oslo, Norway
[26]Charles University, Prague, Czech Republic
[27]University of Vienna, Faculty of Physics, Austria
[28]Agenzia nazionale per le nuove tecnologie, l'energia e lo sviluppo economico sostenibile (ENEA), Bologna, Italy

[29]Istituto Nazionale di Fisica Nucleare, Trieste, Italy

[30]Horia Hulubei National Institute of Physics and Nuclear Engineering - IFIN HH, Bucharest - Magurele, Romania

[31]European Commission JRC, Institute for Reference Materials and Measurements, Geel, Belgium

[32]Department of Physics and Astronomy - University of Basel, Basel, Switzerland

[33]Laboratori Nazionali del Gran Sasso dell'INFN, Assergi (AQ),Italy

Abstract

Knowledge of neutron cross sections of various plutonium isotopes and other minor actinides is crucial for the design of advanced nuclear systems. The ^{240,242}Pu(n,f) cross sections were measured at the CERN n_TOF facility, taking advantage of the wide energy range (from thermal to GeV) and the high instantaneous flux of the neutron beam. In this work, preliminary results for ^{242}Pu are presented along with a theoretical cross section calculation performed with the EMPIRE code.

1 Introduction

The sustainable use of nuclear energy as a means of reducing reliance on fossil-fuel for energy production has motivated the development of nuclear systems characterised by a more efficient use of nuclear fuels, a lower production of nuclear waste, economic viability and competitiveness and minimal risk of proliferation of nuclear material and is being pursued by international collaborations [1, 2]. The accurate knowledge of relevant nuclear data, including neutron cross sections of a variety of plutonium isotopes and other minor actinides, is crucial for feasibility and performance studies of advanced nuclear systems.

In particular, the ^{240}Pu and ^{242}Pu isotopes are produced in thermal and fast reactors by successive neutron captures and β- or α- decays. Both isotopes are non-fissile and therefore unsuitable for recycling in a thermal reactor, due to their low fission cross-section. Furthermore, they are typically produced faster than they are transmuted due to their relatively long half-life. A more efficient burning via fission would occur with the harder neutron spectrum of a fast reactor.

In this context, the ^{240,242}Pu(n,f) cross sections were measured at n_TOF relative to the well-known ^{235}U(n,f) cross section. These isotopes are included in the Nuclear Energy Agency (NEA) High Priority List [3] and the NEA WPEC Subgroup 26 Report on the accuracy of nuclear data for advanced reactor design [4].

The high α-activity ($\sim$6.5 MBq/sample) of the ^{240}Pu samples significantly complicates the analysis of the obtained data. The very high α-pile-up probability affects the pulse-height spectrum and significantly reduces the quality of the separation of α-particles and fission fragments. Furthermore, a significant deterioration of the detector performance was observed in the detectors exposed to the ^{240}Pu samples. For the above reasons, only preliminary results for the ^{242}Pu(n,f) measurement are presented in this work.

2 Experimental setup

2.1 The n_TOF facility

The experiment was carried out at the CERN n_TOF facility [5–7]. At n_TOF, neutrons are produced through spallation induced by a 20 GeV/c bunched proton beam impinging on a massive lead target and subsequent moderation in a few centimetres thick layer of (borated) water. The produced neutrons have energies starting from thermal and up to over 10 GeV and travel along an approximately 185 m long path to reach the experimental area. This allows to cover a very extended energy region in a single experiment, thus reducing uncertainties related to different measurements performed in separate neutron

energy ranges. The high instantaneous f ux of the n_TOF neutron beam mitigates the adverse effects of the strong α-particle background produced by the samples and the low f ssion cross section below and near the f ssion threshold.

2.2 Samples

Eight plutonium oxide (PuO_2) samples manufactured at IRMM, Geel, were used [8] (4 × $^{240}PuO_2$, 4 × $^{242}PuO_2$), for a total mass of 3.1 mg of ^{240}Pu (∼0.11 mg/cm^2 per sample, 99.90% purity) and 3.6 mg of ^{242}Pu (∼0.13 mg/cm^2 per sample, 99.97% purity). The material was electro-deposited on an aluminium backing 0.25 mm thick and 5 cm in diameter, while the deposit itself had a diameter of 3 cm. Various contaminants were present, mainly in the form of other plutonium isotopes, such as ^{238}Pu, ^{239}Pu, ^{241}Pu and ^{244}Pu. While these impurities are present in very small amounts, the high f ssion cross sections of f ssile contaminants compared to the isotopes of interest dominate in parts of the energy range studied.

Additionally, a ^{235}U sample (UF_4) with a mass of 18 mg deposited on a 0.2 mm thick aluminium backing was used as reference. Since this sample had a diameter of 7 cm, its active area was reduced with a thin aluminium mask to match the diameter of the plutonium samples. The active mass was therefore reduced to 3.3 mg of ^{235}U (∼0.47 mg/cm^2).

2.3 Detectors and data acquisition

The measurements were performed with Micromegas (Micro-MEsh GAseous Structure) gas detectors [9, 10]. The gas volume of the Micromegas is separated into a charge collection region (several mm) and an amplif cation region (typically tens of μm) by a thin "micromesh" with 35 μm diameter holes on its surface. The amplif cation that takes place in the amplif cation region signif cantly improves the signal-to-noise ratio of the detector. This is of special importance for the high neutron energy region, where the f ssion signals are recorded within a few μs of the γ-f ash (see section 3.2). A chamber capable of holding up to 10 sample-detector modules was constructed and used to house the plutonium and uranium samples. The chamber was f lled with an Ar:CF_4:isoC_4H_{10} gas mixture (88:10:2) at a pressure of 1 bar and under constant circulation.

Existing electronics from previous f ssion measurements were used for signal shaping. Additional electronic protection was added to the pre-amplif er channels to prevent breakage, while the mesh voltage value was chosen to minimize the number of sparks and subsequent trips. Furthermore, the shielding of the pre-amplif er module was improved to mitigate the baseline oscillation observed following the prompt γ-f ash. The standard n_TOF Data Acquisition System [5] based on 8-bit Acqiris f ash-ADCs was used for recording and storing the raw data collected by the detectors at a sampling rate of 100 MHz.

Due to the low expected count rate for the measurement, the chamber was placed in the n_TOF experimental area for several months and in parallel with other measurements performed at n_TOF. Throughout the measurement, beam-off data were acquired in order to record the α- and spontaneous f ssion background produced by the samples.

2.4 Experimental issues

The analysis of the experimental data is complicated by certain features of the experimental setup and by sample-induced backgrounds. These include the baseline oscillation induced by the prompt "γ-f ash" which is discussed in section 3.2 and the spontaneous f ssion background, particularly in the case of ^{242}Pu.

While the above factors can be dealt with, an unexpected effect of the high α-activity of the samples (>6 MBq for ^{240}Pu) was encountered. After the end of the measurement, a visual inspection of the detectors used with the ^{240}Pu samples revealed a remarkable feature. As seen in f g. 1 (left panel), an obvious circular discolouration of the mesh whose dimension and position exactly matched those of the samples was observed. Upon closer inspection with a microscope (f g. 1, right panel), it became clear
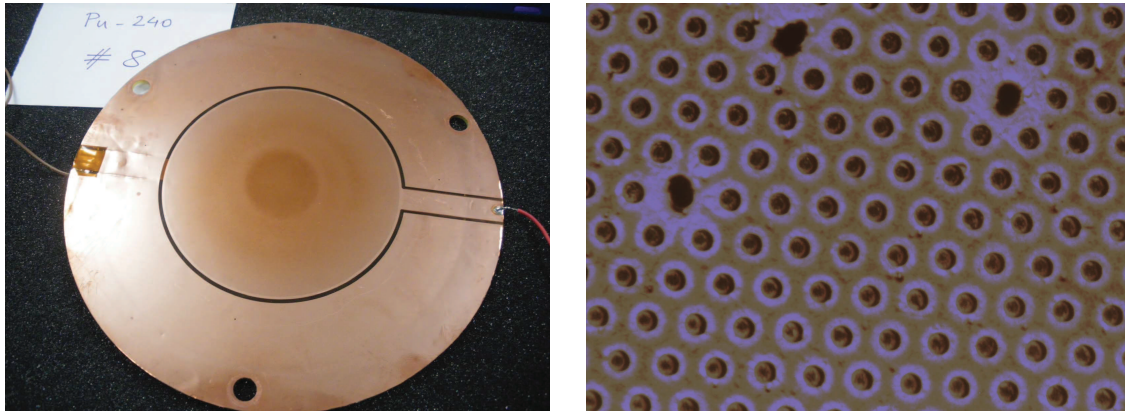
Fig. 1: Left: One of the Micromegas detectors used with a ^{240}Pu sample pictured after the end of the measurement. A 3 cm diameter discolouration is visible on the micromesh. Right: Picture of the micromesh taken with an electronic microscope. Mechanical damage around the rims of the holes can be observed. This leads to a severe deterioration of the detector gain and performance.

that the micromesh had suffered serious mechanical damage, particularly around the rims of the holes which were evidently deformed.

The mechanical damage suffered by the detectors must lead to a deterioration of the electrical f eld and therefore of the detector gain and overall performance. Indeed, this was clearly observed in the ^{240}Pu data, where f ssion fragment and α-particle signals eventually became virtually indistinguishable in the obtained pulse height spectra. Because of this, a considerable part of the ^{240}Pu data must be discarded, partially compromising the measurement. Although there was no visible damage, a similar but less pronounced effect was observed in the ^{242}Pu data, in the form of a slow but non-negligible gain shift throughout the duration of the measurement. The data, therefore, need to be analysed in smaller subsets where the gain can be considered constant.

For the above reasons, preliminary results on ^{242}Pu only are being presented in this report.

3 ANALYSIS AND RESULTS

3.1 Raw data analysis

The raw data from each detector are analysed by means of a pulse recognition routine that determines the amplitude and position in time of the detected signals, among other quantities. The signal baseline is determined by analysing the pre-trigger and post-acquisition window data, accounting for possible signals (α or spontaneous f ssion) that may be present. Since the Pu samples are in the same chamber as the ^{235}U it can be assumed that they receive the same neutron f ux, while the f ssion count rates are suff ciently low to ignore pile-up effects.

3.2 The high neutron energy region

The interactions of the proton beam with the spallation target lead to a signif cant production of prompt γ-rays and other relativistic particles that travel to the experimental area at (nearly) the speed of light and constitute the bulk of what is commonly termed the "γ-f ash". In Micromegas detectors, this causes an initial signal lasting a few hundred ns, followed by a baseline oscillation that lasts for several μs or, in terms of neutron energy, down to 1-2 MeV. This behaviour can be observed in f g. 2 (top panel), where the baseline oscillations are clearly visible.

This problem can be mitigated by applying a software "compensation" technique [11] to the digitally recorded data. This method is based on the observation that the oscillations recorded in adjacent
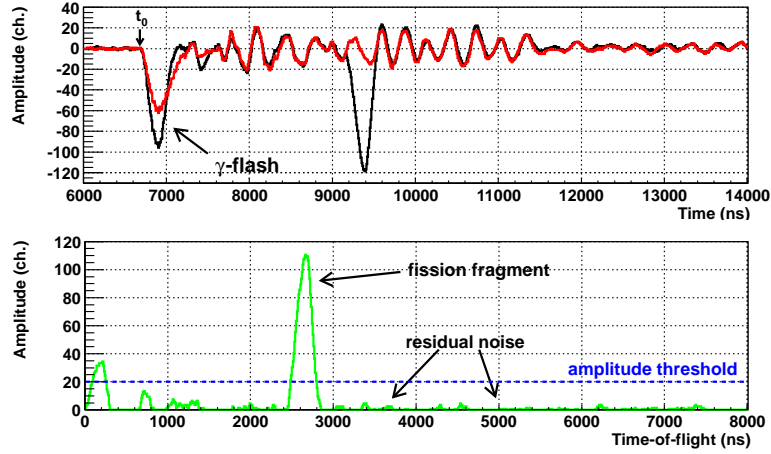
Fig. 2: Top panel: The beginning (first few μs) of the recorded signals during the same proton bunch from two adjacent detectors. The γ-flash signal and the baseline oscillations are clearly visible. Bottom panel: the residual signal after the subtraction of the two signals above. The oscillation is almost entirely suppressed.
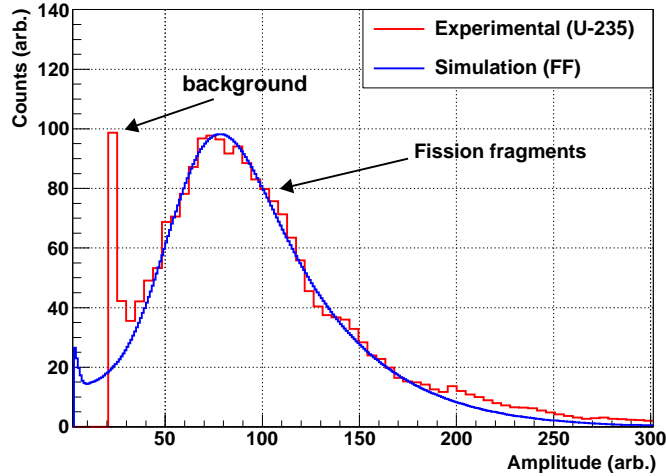
Fig. 3: Experimental (red) and simulated (blue) pulse height spectra for ^{235}U. The cut-off of the low-amplitude signals is due to the threshold set in the peak-search routine.

detectors for the same proton bunch are almost identical. This can be seen by comparing the recorded signals from two detectors placed consecutively in the chamber (fig. 2, top panel). The subtraction of the output of adjacent detectors causes the oscillations to largely cancel each other out, leaving a residual signal that consists primarily of signals attributable either to fission fragments or α-particles (fig. 2, bottom panel). This signal is then analysed with the peak search routine used for the lower energy region, thus extracting the desired pulse height spectra. The small residual of electronic noise is generally well below the amplitude threshold for fission fragment detection.

3.3 Monte-Carlo simulations

The behaviour of the detectors was studied by means of Monte Carlo simulations performed with the FLUKA code [12, 13], focusing particularly on the reproduction of the pulse height spectra of α-particles and fission fragments for the evaluation of the detector efficiency and the quality of the peak-search routine. In fig. 3, an experimental pulse height spectrum obtained from ^{235}U and a simulated fission
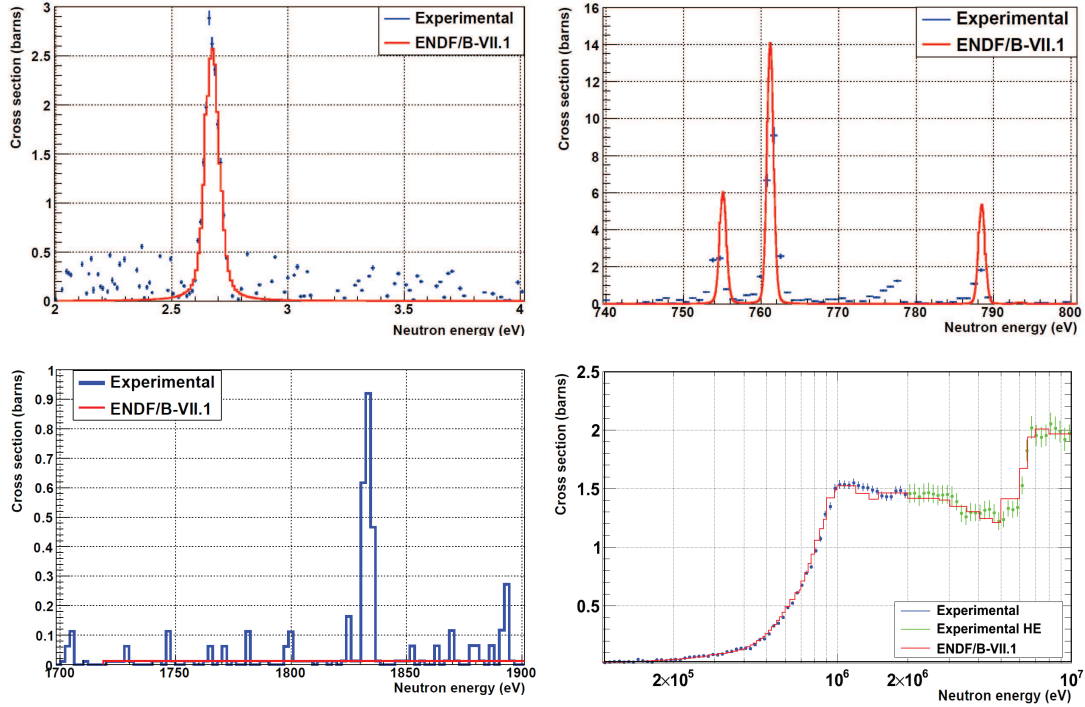
Fig. 4: The first ^{242}Pu resonance at 2.7 eV (top left panel) and resolved resonances between 750 and 800 eV (top right) and around 1800 eV (bottom left). Data above the fission threshold (bottom right). Above 2 MeV, data are treated with the method described in section 3.2. The use of this CPU-intensive method means only a subset of the available statistics has been processed, hence the larger uncertainties pictured here.

fragment spectrum can be compared.

3.4 Present results

The spontaneous fission background dominates the low energy region and remains visible up to about 10 keV. Still, several resonances can be observed above this background. The first ^{242}Pu resonance at $\sim$2.7 eV can be seen in the top left panel of Fig. 4, after subtraction of the spontaneous fission background, as determined with a fit of the beam-off data. The top right and bottom left panels panel show resolved resonances in the 700-800 eV region and up to approximately 1900 eV, including one at $\sim$780 eV and one at $\sim$1830 eV not present in the evaluated libraries and, at a preliminary analysis, not attributable to any of the stated sample impurities. Additional resonance candidates at higher energies have been observed. Data above 1 keV are shown in the bottom right panel of Fig. 4. The data displayed are combined from the two analysis methods; the conventional "straightforward" analysis, which fails above about 2 MeV due to the baseline oscillations, and the high-energy analysis described in section 3.2. The analysis of the high energy region will be extended up to several tens of MeV.

4 THEORETICAL CALCULATIONS

A theoretical calculation of the ^{242}Pu(n,f) cross section was performed with the EMPIRE nuclear reaction model code [14] (version 3.1). The level densities of the nuclei involved in the calculations were treated within the framework of the Enhanced Generalised Superfuid Model (EGSM). The initial values used
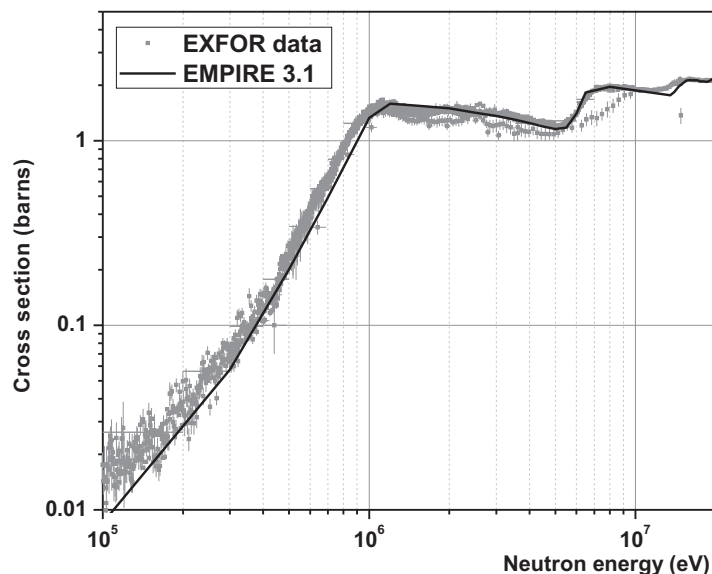
Fig. 5: Theoretical calculation of the ^{242}Pu(n,f) cross section performed with the EMPIRE code, with experimental data retrieved from the EXFOR database.

for the fission barrier parameters (barrier height and width) were retrieved from the RIPL-3 library [15] and subsequently adjusted to better reproduce the experimental data. Preliminary results can be seen in Fig. 5.

5 CONCLUSIONS

Preliminary results from the ^{242}Pu(n,f) experiment performed at the CERN n_TOF facility are presented. The experimental setup and analysis method is described, including auxiliary Monte-Carlo simulations and an off-line technique to recover high-neutron energy data affected by the prompt γ-flash.

Analysis of the ^{242}Pu(n,f) data is well under way and is only complicated by the gradual detector gain shift. Among the issues still to be addressed are the exact determination of the detector efficiency and the amplitude threshold correction, the accurate subtraction of the spontaneous fission background and the estimation of all uncertainties involved. The analysis of the high-energy region data is particularly CPU-intensive and is therefore proceeding at a relatively slow pace, given the amount of data acquired during the measurement.

Finally, a significant part of the ^{240}Pu(n,f) was discarded due to the damage suffered by the detectors, as explained in section 2.4. Even under normal detector operation, the high α-pileup probability (>30%) produces a long tail in the amplitude spectra that adversely affects the α - fission fragment separation. In order not to set a very high amplitude threshold that would further reduce the statistics, an alternative approach – characterising and subtracting the α-background – will be employed.

References

[1] Generation-IV International Forum, `www.gen-4.org/`

[2] International Framework for Nuclear Energy Cooperation (IFNEC), `www.ifnec.org/`

[3] NEA Nuclear Data High Priority Request List, `www.nea.fr/html/dbdata/hprl/`

[4] OECD/NEA WPEC Subgroup 26 Final Report, `www.nea.fr/html/science/wpec/volume26/volume26.pdf/`

[5] U. Abbondanno, Tech. Rep. CERN-SL-2002-053 ECT, CERN, Geneva (2002)

[6] C. Guerrero et al., Eur. Phys. J. A **49**, 1 (2013)

[7] E. Berthoumieux, `cds.cern.ch/record/1514680?ln=en`

[8] G. Sibbens et al., J. Radioanal. Nucl. Chem. (2013) `dx.doi.org/10.1007/s10967-013-2668-7`

[9] Y. Giomataris et al., Nucl. Instrum. Meth. A **376**, 29 (1996)

[10] S. Andriamonje et al., J. Instrum. **5**, P02001 (2010)

[11] N. Colonna et al., *A software compensation technique for fission measurements at spallation neutron sources*, Under preparation

[12] A. Ferrari et al., Tech. Rep. CERN 2005-10, INFN/TC_05/11, SLAC-R-773 (2005)

[13] G. Battistoni et al., AIP Conf. Proc. **896**, 31 (2007)

[14] M. Herman et al., Nucl. Data Sheets **108**, 2655 (2007)

[15] R. Capote et al., Nucl. Data Sheets **110**, 3107–3214 (2009)

Cross-section studies of relativistic deuteron reactions obtained by activation method.

V. Wagner[1,2], M. Suchopár[1,2], O. Svoboda[1], J. Vrzalová[1,2,4], M. Majerle[1], A. Krása[1], P. Chudoba[1,2], M. Honusek[1], A. Kugler[1], J. Adam[4], A. Baldin[4], W. Furman[4], M. Kadykov[4], J. Khushvaktov[4], A. Sol-nyskhin[4], V. Tsoupko-Sitnikov[4]. L. Závorka[2,4], S. Tyutyunnikov[4], N. Vladimirova[4]

[1] Nuclear Physics Institute of the ASCR v.v.i., Řež 130, 250 68 Řež, Czech Republic

[2] Faculty of Nuclear Sciences and Physical Engineering, Czech Technical University in Prague, Břehová 7, 115 19 Prague, Czech Republic

[3] Faculty of Mathematics and Physics, Charles University in Prague, Ke Karlovu 3, 121 16 Praha 2, Czech Republic

[4] Joint Institute for Nuclear Research, Joliot-Curie 6, 141 980 Dubna, Russia

Abstract

The cross-sections of relativistic deuteron reactions on natural copper were studied in detail by means of activation method. The copper foils were irradiated during experiments with the big Quinta uranium target at Joint Institute for Nuclear Research (JINR) in Dubna, Russia. The deuteron beams with energies ranging from 1 GeV up to 8 GeV were produced by JINR Nuclotron. Residual nuclides were identified by the gamma spectrometry. Lack of such experimental cross-section values prevents the usage of copper foils from beam integral monitoring.

1   Introduction and motivation

The international collaboration "Energy and Transmutation of RadioActive Waste" (E&T RAW) at Joint Institute for Nuclear Research in Dubna (JINR Dubna), Russia, performed intensive studies of simple ADS set-ups irradiated by proton and deuteron beams during past years [1-6]. We use ^{24}Na production reaction in aluminium foils for beam monitoring. However, the foils have to be placed in large distance from irradiated set-up due to production of ^{24}Na also by spallation neutrons emitted from thick target studied. On the other hand, the production of radionuclides on copper monitor foils by deuteron beam is not affected by MeV spallation neutrons reactions and hence copper foils can be placed near the set-up under study. Therefore we measured partial cross-sections of different radionuclides production by deuterons on copper. The obtained data will improve possibility to use copper monitors during ADS studies. The second main goal of these studies is to provide a database for evaluation of models used for prediction of the production of different radionuclides by relativistic deuterons in various fields of application.

An extensive set of experimental partial cross-section data is in EXFOR data base for different radionuclide production by relativistic proton beam on copper. However, on the other hand, there is only one partial cross-section value for such type of reaction for relativistic deuteron beam. The production of ^{24}Na on copper by 7.3 GeV deuterons was described by R. Brandt et al. [7]. An improvement of our knowledge of excitation functions of different radionuclide production on copper by relativistic deuterons is necessary.

2   Experimental method

The measurements were performed in the frame of E&T RAW collaboration during irradiations of QUINTA and GAMMA-3 set-ups with deuterons from Nuclotron accelerator at JINR Dubna [8,

9]. Typical irradiation lasted about ten hours. Sixteen irradiations were performed during five sets of experiments carried on from 2011 to 2013. Our new data were measured relatively to the monitoring reaction ^{27}Al(d,X)^{24}Na. The aluminium and copper foils had the same sizes (10×10 cm) and thicknesses of copper and aluminium were 0.0128 cm and 0.0196 cm, respectively. The used copper foils have natural isotope composition (69.15 % of ^{63}Cu and 30.85 % of ^{65}Cu). Both foils were placed in the same position. The distance from the set-up was sufficient to neglect the possible influence of neutrons and other particles produced by the set-up to the direction of the beam monitors.

Unfortunately, there are only three experimental cross-section values for ^{27}Al(d,3p2n)^{24}Na reaction in GeV energy range. One value is from J. Bainaigs et al (15.25 ± 1.5 mbarn at 2.33 GeV) [10] and two are from P. Kozma et al (14.1 ± 1.3 mbarn at 6.0 GeV and 14.7 ± 1.2 mbarn at 7.3 GeV) [11]. The uncertainties of beam monitoring reaction cross-sections are the main source of systematic uncertainties of obtained absolute cross-section values. We made a fit between experimental points and calculated the cross-section value for the given energies between the points from database. We got value 16.4 mbarn for 1 GeV, value 15.4 mbarn for 2 GeV, value 14.5 mbarn for 4 GeV and value 13.6 mbarn for 8 GeV (error is about 10%).
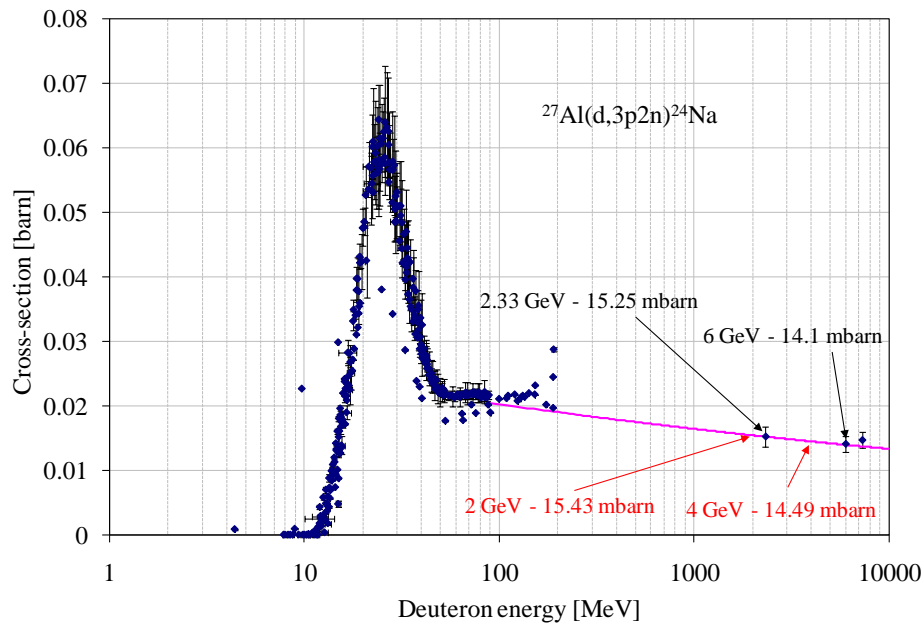
Fig. 1: Cross-section of ^{27}Al(d,3p2n)^{24}Na reaction – experimental data taken from EXFOR data base and examples of point fits.

The activation method exploiting gamma-ray spectrometry was used for the cross-section determination. The foils were packed from original size to a smaller one with dimensions 2.5×2.5×0.3 cm^3 for the spectroscopy measurement. Several high purity germanium detectors were used. More different geometries were also used. Distances of measured sample from detector ranged from 4 cm up to 10 cm. Every radioactive sample was measured many times to detect and identify short lived and also long lived radioisotopes. First measurements were started only a few hours after end of irradiation and even very short lived radionuclides (half-lives only a few hours) were detected. The measured gamma spectra were analysed by the DEIMOS code [12]. The yield of activated material was calculated after identification of the isotope by means of gamma peaks. All necessary spectroscopic corrections and related sources of uncertainties were taken into account. All uncertainties were quadratically added according to the laws of uncertainty propagation. The cross-sections were determined taking into account the number of atoms in a sample and deuteron beam integral, see [13, 14] for details.

Gamma lines of more than twenty different radioisotopes were identified (for example ^{24}Na, ^{42}K, ^{43}K, ^{43}Sc, ^{44}Sc+ ^{44m}Sc, ^{46}Sc, ^{47}Sc, ^{48}Sc, ^{48}V, ^{48}Cr, ^{51}Cr, ^{52}Mn, ^{54}Mn, ^{56}Mn, ^{52}Fe, ^{59}Fe, ^{55}Co, ^{56}Co, ^{57}Co, ^{58}Co + ^{58m}Co, ^{57}Ni, ^{61}Cu, ^{64}Cu and ^{62}Zn). Some couples of radionuclides decayed to the same daughter nucleus and therefore it was necessary to analyze decay curves to distinguish separate radionuclides (for example ^{43}Sc and ^{43}K, ^{48}Sc and ^{48}V, ^{56}Mn and ^{56}Co). The complex analyzes of decay curves were necessary also in the case of decay sequences and study of isomeric state population (^{44m}Sc). More detailed description of the used procedures is in [15, 16].
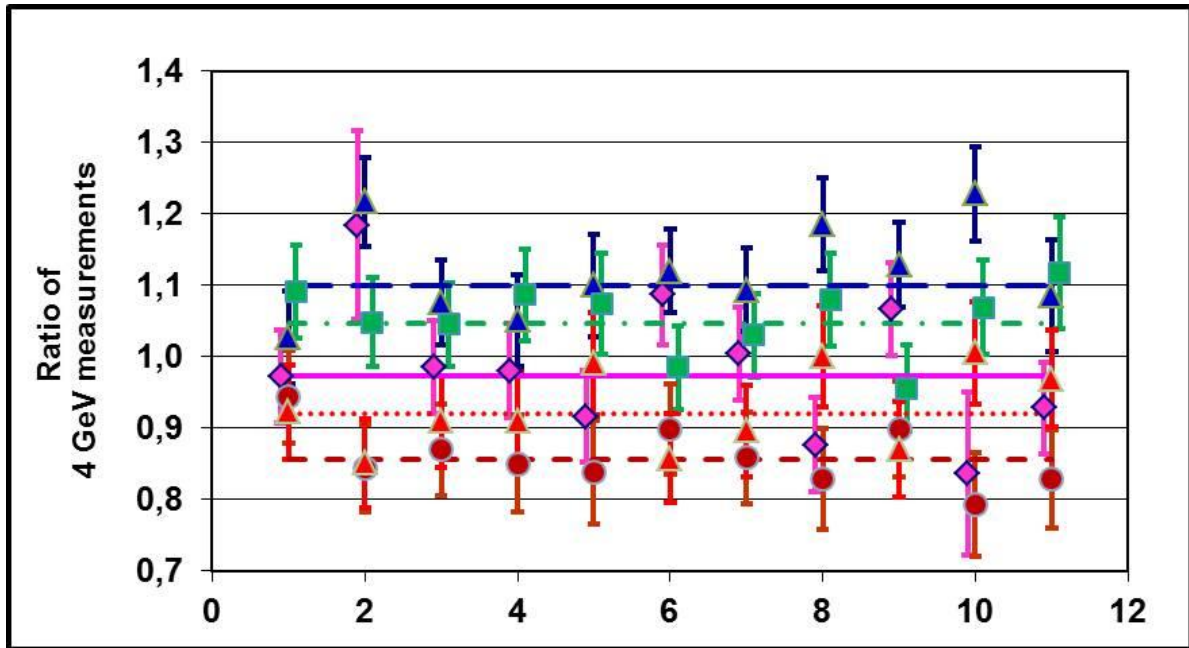
Fig. 2: Five measurements with 4 GeV deuterons were done. Ratio of cross-section determined during individual measurement and mean weighted average of all five measurements. Order of isotopes is ^{58}Co, ^{56}Co, ^{52}Mn, ^{48}Sc, ^{44m}Sc, ^{57}Ni, ^{48}V, ^{47}Sc, ^{55}Co, ^{48}Cr and ^{43}K. Used signs are: March 2011 – violet diamond, December 2011 – blue triangle, March 2012 – green square, December 2012 – red ring and March 2013 – red triangle.

More irradiations were done for some energy. For example, we obtained five independent values of cross-sections for deuteron energy 4 GeV (see Fig. 2). The systematic uncertainties of beam integral determination were estimated by means of these data. It is noted that all measurements are within 20 % range and within expected uncertainties of single irradiations. The similar situation, even better, was for other deuteron energies which were measured more times. The detailed analysis of different sources of systematic uncertainties was performed.

The more detailed study whether or not the given cross-sections are independent or do contain uncorrectable contributions from radioactive progenitors will be done in near future.

3 Obtained results

Examples of the new experimental data for deuteron reactions are presented in Figs 3-7 (left) together with EXFOR data for relativistic proton reactions (right figures). The excitation functions of lighter radionuclides (^{24}Na, ^{42}K) production show sharp rise starting below 1 GeV and continuing to about 3 GeV (see Figs 3 and 4), above which slow decrease starts. Excitation functions of radionuclides between nucleon numbers 44 and 48 have constant value for energies

ranged from 1 to 3 GeV. The slow decrease is visible for higher energies. Decrease with rising energy is observable for excitation functions of radionuclides with nucleon number higher than 52 (see Fig. 5). There are set of partial cross-sections of proton production of different radionuclides on copper in EXFOR data base. The excitation functions of relativistic deuteron reactions on copper show very similar trends as excitation functions of relativistic proton reactions. The absolute values of the relativistic proton reaction partial cross-sections are lower by about 30 % than the same partial cross-sections for deuteron reactions.
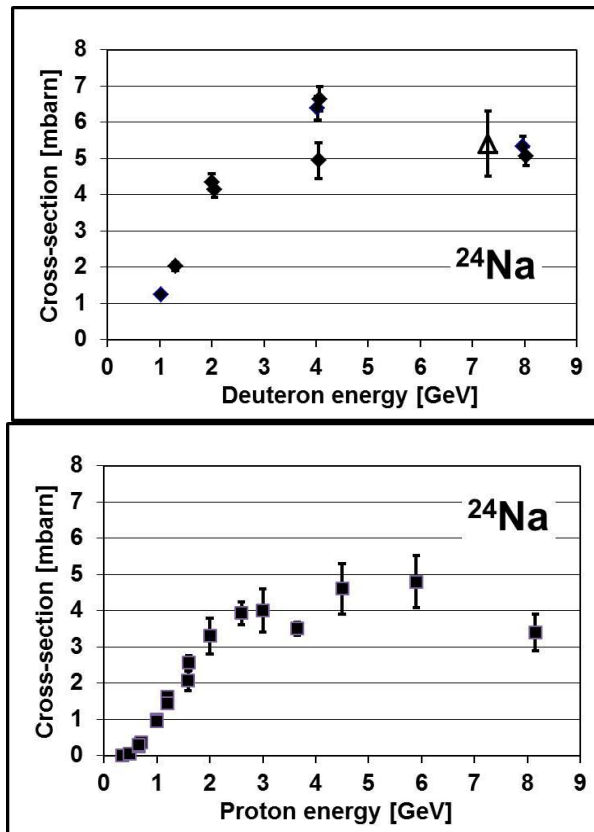
Fig. 3: Cross-sections of $^{nat}Cu(d,x)^{24}Na$ reaction measured by us, open triangle shows only one existing experimental value from EXFOR data base (left figure). Existing experimental cross-sections of $^{nat}Cu(p,x)^{24}Na$ reaction induced by proton beam obtained from EXFOR data base (right figure).
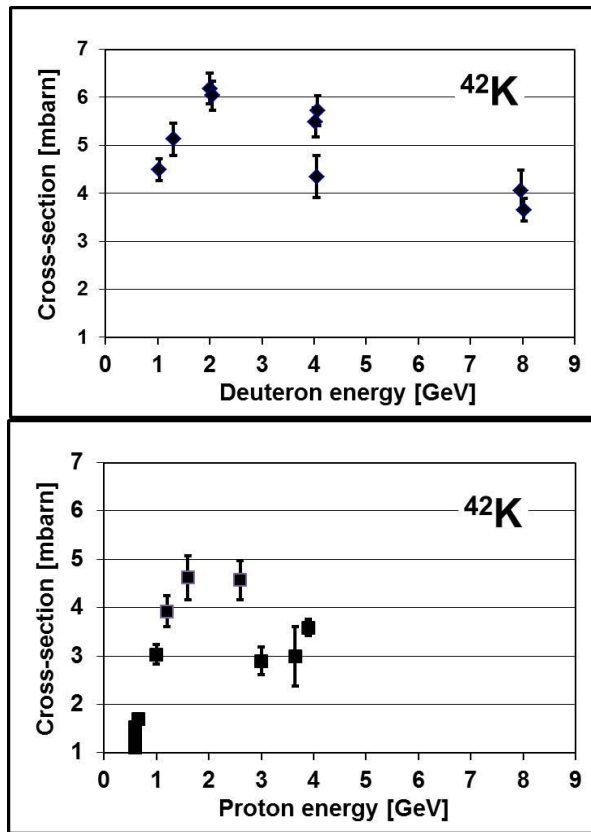
Fig. 4: Cross-sections of $^{nat}Cu(d,x)^{42}K$ reaction induced by deuteron beam measured by us (left figure). Existing experimental cross-sections of $^{nat}Cu(p,x)^{24}Na$ reaction induced by proton beam obtained from EXFOR data base (right figure).

Some measured partial cross-sections have rather high values by approximately 30 mbarn (for example ^{51}Cr, ^{54}Mn, ^{57}Co, ^{58}Co and ^{64}Cu). Some values are about few milibarns (for example ^{43}K, ^{43}Sc, ^{47}Sc, ^{52}Mn, ^{56}Mn, ^{56}Co and others) and smallest values are up to fraction of milibarn (for example ^{52}Fe and ^{62}Zn). The production of ^{62}Zn is very special and interesting case. The proton from deuteron should be stopped at copper nucleus and only a few neutrons should be emitted in this case. The probability of such development is very small and the partial cross-section of ^{62}Zn production is very small, only about 0.6 mbarn.
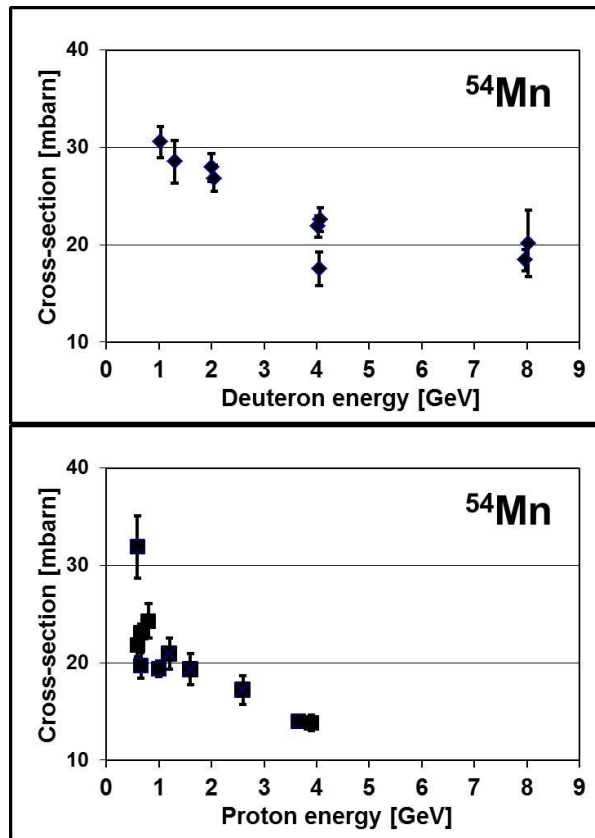
Fig. 5: Cross-sections of $^{nat}Cu(d,x)^{54}Mn$ reaction induced by deuteron beam measured by us (left figure). Existing experimental cross-sections of $^{nat}Cu(p,x)^{54}Mn$ reaction induced by proton beam obtained from EXFOR data base (right figure).
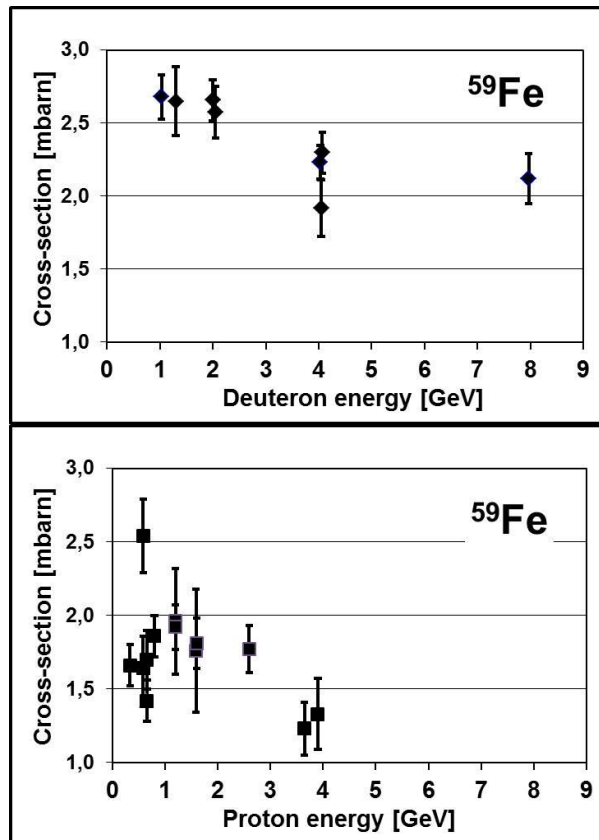
Fig. 6: Cross-sections of $^{nat}Cu(d,x)^{59}Fe$ reaction induced by deuteron beam measured by us (left figure). Existing experimental cross-sections of $^{nat}Cu(p,x)^{59}Fe$ reaction induced by proton beam obtained from EXFOR data base (right figure).
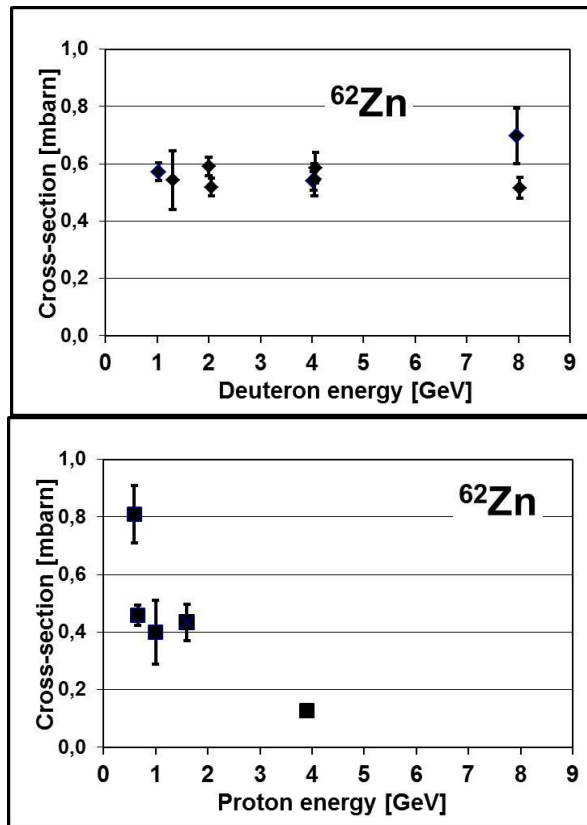
Fig. 7: Cross-sections of $^{nat}Cu(d,x)^{62}Zn$ reaction induced by deuteron beam measured by us (left figure). Existing experimental cross-sections of $^{nat}Cu(p,x)^{62}Zn$ reaction induced by proton beam obtained from EXFOR data base (right figure).

4   Conclusions

In this work, the excitation functions of relativistic deuteron reactions on copper were studied. The partial cross-sections of more than twenty different radionuclide productions were determined. The residual nuclides investigated cover gamma emitting radionuclides with half-lives between 2 hours and almost 300 days. The shape of excitation function for light fragment production is initially sharply increasing up to 3 GeV and after wide maximum the excitation function starts to decrease slowly. Fragments with the nucleon number around 46 have constant value of partial cross-section up to deuteron energy 3 GeV and the slow decrease of cross-section value starts for higher deuteron energies. The excitation function is monotonically decreasing for nucleon number higher than 52. Our newly obtained data for ^{24}Na production partial cross-sections nicely agree with only one measured value of such cross-section placed in EXFOR data base. The shapes of the excitation functions obtained by us for relativistic deuteron reactions are similar as shapes of excitation functions for relativistic proton reactions taken from EXFOR data base. The absolute values of partial cross-sections for deuteron reactions are more than 20 % higher than for proton reactions

The new consistent set of experimental partial cross-sections measured by us will be used to test nuclear reaction models of high-energy reactions such as spallation and fragmentation. Mainly we want to test different models used by MCNPX. The obtained cross-sections will be also useful for monitoring of deuteron beam by copper foil.

110

The measurements of cross-sections of neutron threshold reactions with energies ranging from 10 MeV to 100 MeV are second main field of our studies. We use quasi-monoenergetic neutron sources based on the reaction on [7]Li target at Nuclear Physics Institute of ASCR in Řež and at The Svedberg Laboratory Uppsala. The last study of yttrium (n,xn) threshold reactions is described by Petr Chudoba in these proceedings and overview of our results obtained by us is in [13]. Both these studies were supported by EFNUDAT and ERINDA projects.

Acknowledgements

References

[1] M. I. Krivopustov et al, First experiments with a large uranium blanket within the installation "Energy plus Transmutation" exposed to 1.5 GeV protons, Kerntechnik 68 (2003) 48

[2] F. Křížek et al, The study of spallation reactions, neutron production, and transport in a thick lead target and a uranium blanket during 1.5 GeV proton irradiation, Czech. Journal of Physics 56 (2006) 243

[3] A. Krása et al, Neutron production in a Pb/U-setup irradiated with 0.7-2.5 GeV protons and deuterons, Nucl. Instr. and Meth. in Phys. Res. A615 (2010) 70

[4] M.I. Krivopustov et al, First results studying transmutation of [129]I, [237]Np, [238]Pu and [239]Pu in the irradiation of extended [nat]U/Pb-assembly with 2.52 GeV deuterons, Journal of Radioanalytical and Nuclear Chemistry, 279 (2009) 567

[5] M. Zamani-Valasiadou et al, Performance of a Pb-spallation target surrounded by a U-blanket during irradiations with 1.6 and 2.5 GeV deuteron beams: Comparison with relativistic proton beams, Annals of Nuclear Energy 37 (2010) 241

[6] J.J. Borger et al, Spatial distribution of thorium fission rate in a fast spallation and fission neutron field: An experimental and Monte Carlo study, Nucl. Instr. and Meth. in Phys. Res. A664 (2010) 70

[7] R. Brandt et al, Enhanced production of 24Na by wide-angle secondaries produced in the interaction of relativistic carbon ions with copper, Phys. Review C45 (1992) 1194

[8] W. Furman et al, Recent results of the study of ADS with 500 kg natural uranium target assembly QUINTA irradiated by deuterons with energies from 1 to 8 GeV at JINR NUCLOTRON, Proceedings of Science (Baldin ISHEPP XXI **086**) http://pos.sissa.it/archive/conferences/173/086/Baldin%20ISHEPP%20XXI_086.pdf

[9] M. Suchopár et al, Monte Carlo simulations of natural uranium setups irradiated with relativistic deuterons by means of MCNPX code, Proceedings of Science (Baldin ISHEPP XXI **091**) http://pos.sissa.it/archive/conferences/173/091/Baldin%20ISHEPP%20XXI_091.pdf

[10] J. Banaigs et al, Determination De L„Intensite D„Un Faisceau De Deutons Extrait D"Un Synchrotron Et Mesure Des Sections Efficaces Des Reactions C-12(D,P2N)C-11 Et Al-27(D,3P2N)Na-24 a 2.33 GeV, Nuclear Instruments and Methods in Physics Research 95 (1971) 307-311

[11] P. Kozma and V. V. Yanovski, Application of BaF2 scintillator to off-line gamma ray spectroscopy, Czech Journal of Physics, 40 (1990) 393

[12] J. Frána, Program DEIMOS32 for gamma-ray spectra evaluation, Journal of Radioanalytical

and Nuclear Chemistry 257 (2003) 583

[13] J. Vrzalová et al, Studies of (n,xn) cross-sections in Al, Au, Bi, Cu, Fe, I, In, Mg, Ni, Ta, Y, Zn by the activation method, Nucl. Instr. and Meth. in Phys. Res. A726 (2013) 84

[14] O. Svoboda, Experimental Study of Neutron Production and Transport for ADTT, Disertation Thesis, Czech Technical University, Faculty of Nuclear Sciences and Physical Engineering, Prague (2011), [http://ojs.ujf.cas.cz/~wagner/transmutace/diplomky/PHD_Svoboda.pdf]

[15] V. Wagner et al, Studies of deuteron and neutron cross-sections important for ADS research, Proceedings of Science (Baldin ISHEPP XXI 090) http://pos.sissa.it/archive/conferences/173/090/Baldin%20ISHEPP%20XXI_090.pdf

[16] V. Wagner et al, Cross-section studies of important neutron and relativistic deuteron reactions, XX International School on Nuclear Physics, Neutron Physics and Aplications (VARNA 2013)

Measurements of prompt gamma-rays from fast-neutron induced fission with the LICORNE directional neutron source

J.N. Wilson[1], M. Lebois[1], P. Halipre[1], S. Oberstedt[2], A. Oberstedt[3]
1 IPN Orsay, Bat. 100, 15 rue G. Clemenceau, 91406 Orsay, France
2 European Commission, DG Joint Research Centre IRMM, Retieseweg 111, B-2440 Geel,Belgium
3 Fundamental Fysik, Chalmers Tekniska Högskola, S-41296 Göteborg, Sweden

Abstract
At the IPN Orsay we have developed a unique, directional, fast neutron source called LICORNE, intended initially to facilitate prompt fission gamma measurements. The ability of the IPN Orsay tandem accelerator to produce intense beams of ^{7}Li is exploited to produce quasi-monoenergetic neutrons between 0.5 - 4 MeV using the p(^{7}Li,^{7}Be)n inverse reaction. The available fluxes of up to 7×10^7 neutrons/second/steradian for the thickest hydrogen-rich targets are comparable to similar installations, but with two added advantages: (i) The kinematic focusing produces a natural neutron beam collimation which allows placement of gamma detectors adjacent to the irradiated sample unimpeded by source neutrons. (ii) The background of scattered neutrons in the experimental hall is drastically reduced. The dedicated neutron converter was commissioned in June 2013.

Some preliminary results from the first experiment using the LICORNE neutron source at the IPN Orsay are presented. Prompt fission gamma rays from fast-neutron induced fission of ^{238}U, ^{232}Th and ^{235}U were measured by two different techniques. An ionisation chamber containing 10 mg samples of ^{238}U and ^{235}U to provide a fission trigger was used in conjunction with BaF$_2$ and LaBr$_3$ scintillator gamma detectors to detect fission fragment-gamma-ray coincidences. In the second part of the experiment thick targets of around 50g of ^{238}U and ^{232}Th were used, with a high efficiency calorimeter to tag on fission events by requiring both high sum energy and multiplicity.

1   Introduction

Conventional quasi-mono-energetic neutron sources produce neutrons isotropically via direct reactions on light nuclei (e.g. d(d,p)n or ^{7}Li(p,n)^{7}Be). The lack of directionality means the typically less than 1 percent of the source neutrons produced can be used for irradiating samples, the vast majority instead contributing to the room background. However, natural collimation of neutron beams can be achieved if the neutrons are produced using a reaction in inverse kinematics where the projectile is much heavier than the target. Neutron production via this method thus combines the best features of white neutron sources (collimated beams) and conventional quasi-mono-energetic neutron sources (high neutron fluxes at short distances).

The LICORNE neutron source is based on the p(^{7}Li,^{7}Be) reaction in inverse kinematics[1]. It has been initially developed for performing fundamental studies of the nuclear fission process and associated nuclear data measurements related to 4th generation nuclear reactors. A first experimental program will involve the study of prompt gamma-ray emission in

fission since the directional neutron beam will allows placement of gamma-ray detectors out-of-flux but adjacent to the sample to be irradiated. However, other potential uses of LICORNE span several different research fields and include gamma-spectroscopy of neutron-induced reactions, measurements of capture and inelastic scattering cross sections, non-destructive assay of nuclear waste and irradiation for the aerospace industry.

The main advantage of inverse kinematics is the natural forward collimation of the reaction ejectiles. This opens up the possibility of placing gamma detectors very close to the source without them being irradiated with source neutrons. In addition, the lack of emission at most angles means that the source is a very low background source.

For reactions which eject neutrons this will induce large enhancements of neutron fluxes at 0 degrees in the laboratory frame. The p(7Li,7Be)n reaction is one of the most commonly used in direct kinematics to produce mono energetic neutrons, especially below 0.7 MeV. However, in inverse kinematics with a Li-beam a mono-energetic neutron of 1.5 MeV is produced at bombarding energies at the reaction threshold of 13.09 MeV.

The gain from the focusing and natural collimation can be expressed in terms of neutron flux enhancement over the non-inverse reaction. Near the threshold the enhancement factor is maximal (> 100) since the emitted neutrons move with the centre of mass of the system which follows the ^{7}Li beam direction. As a consequence, close to the threshold energy, it is possible to produce very narrow (< 5 degrees) cones of neutrons. With increasing ^{7}Li bombarding energy, the cone broadens and the number of neutrons in a given solid angle decreases so the enhancement factor drops to around 20 at 16.5 MeV. However, the huge gain in intensity due to the kinematic focusing is offset by corresponding losses from two other factors. Firstly, the available beam current of ^{7}Li is much lower than that available for protons in the non-inverse reaction because of the relative difficulty of extraction of ^{7}Li-ions from the ion source. Secondly, the energy loss of ^{7}Li across a given target will be higher than that for protons due to its higher atomic number.

The current sputter source of the IPN tandem can produce ^{7}Li beam currents of up to 200 nA, but currents greater than 500 nA may be achievable with source improvements. The maximum available fluxes from LICORNE are therefore expected to around 10^7 neutrons/second/steradian for a thin polypropylene target (4μm) and $7x10^7$ neutrons/second/steradian for a thick (28μm) polypropylene target. These fluxes are comparable with other accelerator-based neutrons sources, but LICORNE has the added advantages of a natural directionality and a much lower background.

The LICORNE neutron converter sits in an aluminium chamber of diameter approximately 17 cm. It is designed with a rotating polypropylene target of 4 μm thickness and a diameter of 8 cm. The rotation is necessary to increase the irradiated surface area by a factor of 25 with respect to a fixed target. Polypropylene is not very resistant to radiation damage, and therefore the rotating target prolongs the lifetime of the target by a similar factor. Even so, it has been shown that at maximum 7Li beam currents the targets loses hydrogen fairly rapidly and may need to be changed every few hours to maintain maximum neutron fluxes. Between one and 10 polypropylene targets can be stacked on the target wheel. The discs are self-supporting due to the surface tension of the polypropylene between the outer and inner zone made of epoxy, so the target wheel has no arms which have to pass through the ^{7}Li beam.

The beam current and time structure can be measured at the beam stop, which consists of a 50μm gold foil. This measurement coupled to neutron flux measurement in the experimental area can serve as an online monitoring of hydrogen content in the target and can indicate the appropriate time to change targets before significant quantities of hydrogen are lost. The exit window of the LICORNE convertor front face is made of aluminium and is only 0.3 mm thick. A mini camera, illuminating LED are included for beam-tuning and inspecting the targets from inside without having to break the vacuum of 10^{-5} bar. The beam spot is tuned by placing a retractable

phosphorescent quartz target in the path of the beam to ensure that the beam spot is sufficiently diffuse (typically 8 mm diameter).
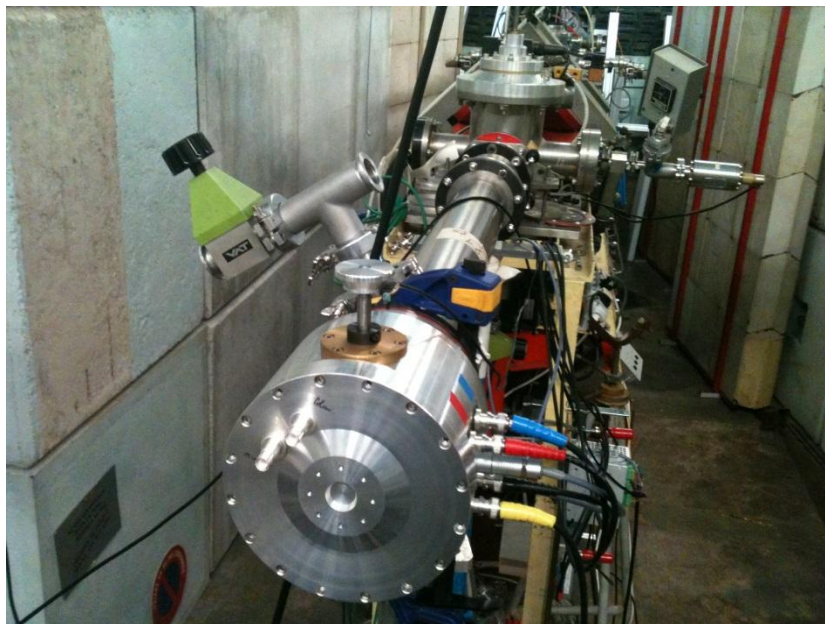
Fig. 1: The LICORNE neutron convertor

This ensures that the power density in the polypropylene is sufficiently low to keep temperature rises to only a few degrees since the polypropylene is very sensitive to heating with a melting point of 160℃. Macroscopic structural changes almost certainly occur at lower temperatures than that and it is currently an open question how much the polypropylene deforms and/or becomes thinner under a combination of surface tension, heating effects and radiation damage.

2   First experiment

A first experiment using LICORNE was conducted in July 2013 over a period of two weeks to measure prompt fission gamma ray spectra of ^{232}Th, ^{238}U, ^{235}U and ^{252}Cf. The experiment was financed by ERINDA and was split into two parts with around 100 h of beam time allocated to each part.

The first part used a cylindrical twin Frisch grid ionization chamber of 28 cm diameter and 20 cm length. The chamber was filled with P10 counting gas (90% argon, 10% methane) to detect fission fragments with an efficiency of almost 100%. Two targets of ^{235}U and ^{238}U were placed back to back at the central cathode position and signals from the cathode and anode were digitized and recorded to disk. The targets consisted of approximately 10 mg of uranium, forming circular deposits of 6.5 cm diameter on aluminium backings of 30 μm thickness. Fission fragments emitted from the surface of the targets were identified by measuring the anode and cathode signals in coincidence and placing a constraint on the minimum pulse heights recorded to reject intrinsic alpha activity.

For gamma detection 14 hexagonal BaF$_2$ scintillator crystals were configured into two independent clusters of seven detectors. Each crystal measured 10 cm diameter and 14 cm in length for a total

mass of scintillator of 62 kg. The two clusters were placed at 29 cm from the target position at angles of +/- 62 degrees to the beam axis. In such a configuration, the total geometric efficiency of the two clusters was estimated to be ~7%. MCNP simulations of the clusters and targets show that each cluster has a high photopeak efficiency of 2.1% and a peak-to-total ratio of 75% for gamma rays of energy 1 MeV. Figure 2 shows a schematic diagram of the setup for the first part of the experiment.
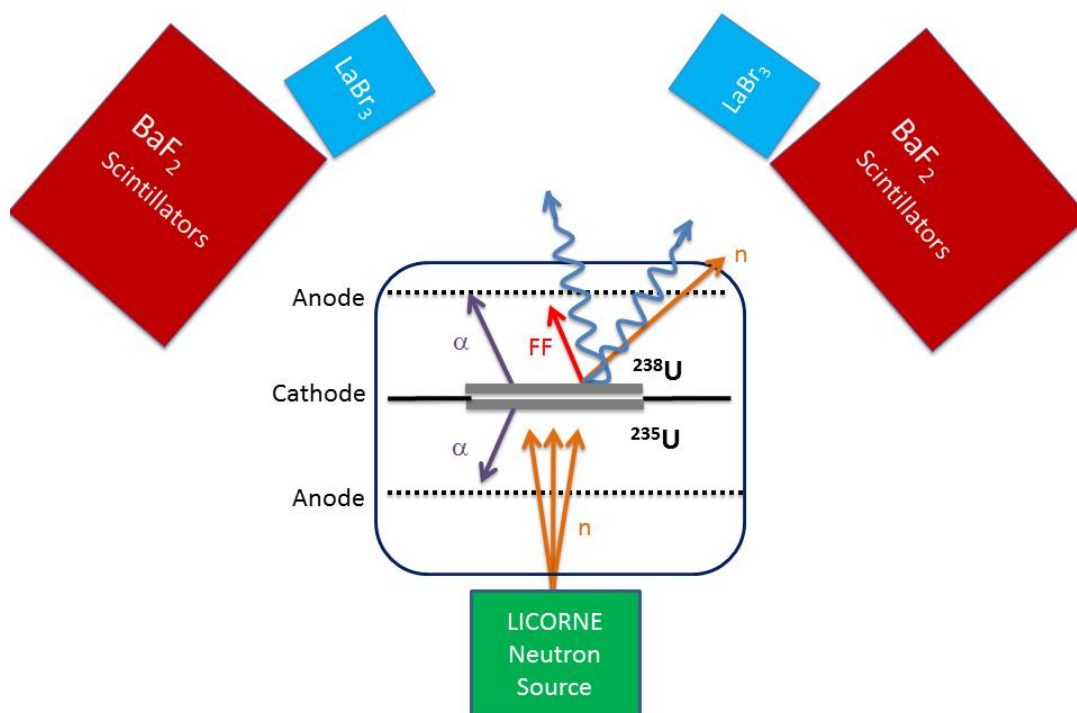
Fig. 2: Schematic diagram of the experimental setup for the first part of the experiment.

Neutrons of average energy 1.5 MeV from the LICORNE inverse kinematics neutron source were used to bombard the targets with estimated fluxes at the target position of up to 2×10^5 n/s/cm^2 . This gave maximum fission rates of around 0.3 fissions per second and 1.2 fissions per second for ^{238}U and ^{235}U targets respectively. In total 4.2×10^4 fission events of ^{238}U and 1.5×10^5 fission events for ^{235}U were recorded to disk over a period of around 3 days. Gamma rays detected in coincidence with the fission fragments were histogrammed into spectra. The analyses of the data are ongoing.

The second part of the experiment involved the same two clusters of 14 BaF$_2$ in a close packed geometry around thick samples of ^{238}U (38g) and ^{232}Th (50g), forming a calorimeter with a geometric efficiency of approximately 70%. The ^{238}U sample was a disc of 6.5cm diameter and the thorium sample a square of dimensions 5cm $\times$ 5cm. The cone of neutrons was produced from a ^{7}Li beam of 15 MeV bombarding energy was emitted at a maximum opening angle of 20 degrees and passed through the centre of the calorimeter to irradiate the thick samples placed at 14 cm from the neutron source. It was estimated that fission rates of ~500 and ~150 fissions per second were produced in the ^{238}U and ^{232}Th samples respectively. Neutron beams were pulsed at 2.5 MHz rate (400 ns between bunches) and bunch width of around 2 ns. This allowed timing information from

the beam buncher to be used as a reference with which to measure event detection times relative to the bunch. Fission events can be discriminated from background by looking for high sum-energy and multiplicity events in the calorimeter that occurred within a short time window. The background is complex and arises from several sources: ^{7}Li+^{12}C fusion evaporation reactions in the polypropylene giving rise to high energy gammas and neutrons, intrinsic activity of the target itself, parasitic neutrons from the ^{7}Li+^{12}C reactions provoking (n,n') reactions in the scintillators, (n,n') reactions in the detectors from scattering of the primary neutron beam on the target, intrinsic activity of the scintillator crystals, and gammas from the room. Once fission events are identified, the spectrum in the LaBr$_3$ detectors in coincidence can be projected. The technique has been demonstrated to work well for a ^{252}Cf source in circumstances where the relative background is quite low. Figure 3 shows the 2D histogram of the multiplicity and sum energy of events detected in the calorimeter. The fission events are selected to the right of the black line, eliminatingbackgrounds from intrinsic activity of the BaF$_2$ detectors and the room.
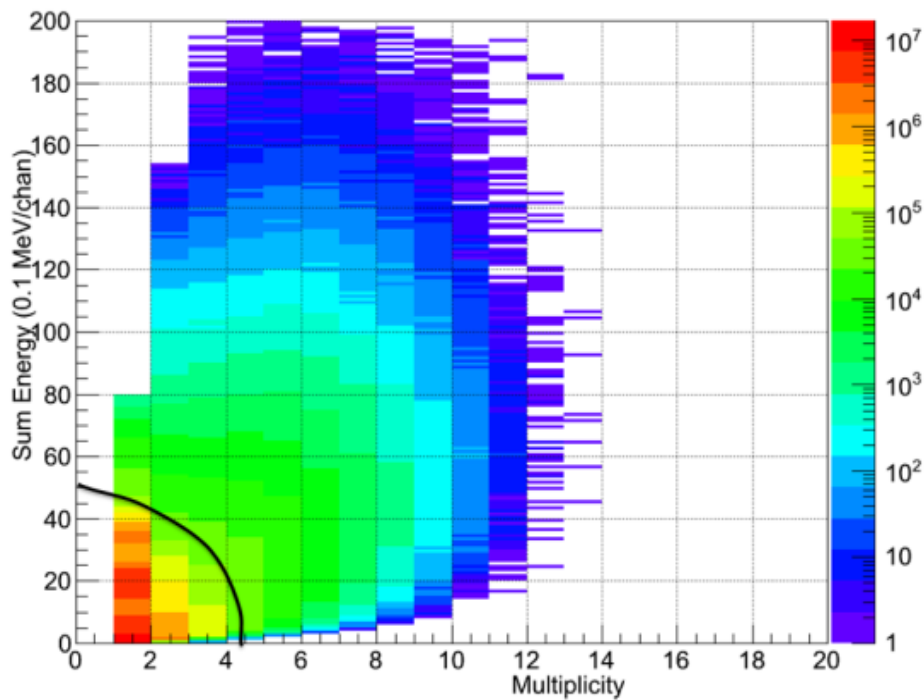
Fig. 3: Sum energy vs multiplicity of events detected in the BaF$_2$ calorimeter when a ^{252}Cf source is placed inside. Fission events are selected to the right of the black line.

The analysis of the in-beam data is ongoing and it remains to be seen if fission events can be discriminated from background without having to place a severe cut on the multiplicity, sum-energy and event time. Too severe selection criteria have the potential to introduce a bias in the resulting prompt fission gamma ray spectrum.

3   Conclusion

LICORNE is a dedicated facility to produce intense, naturally collimated, quasi-mono-energetic neutron beams at the IPN Orsay. The kinematic focusing of the neutron allows gamma detectors to be placed near the irradiate sample and opens up a whole host of new possibilities for the study of

neutron-induced reactions, in particular nuclear fission. A first experiment, financed by ERINDA, was carried out with LICORNE in July 2013 ot measure the prompt fission gamma ray emission in fast neutron induced fission of ^{235}U, ^{238}U and ^{232}Th via two different techniques. Analysis of the in-beam data is ongoing.
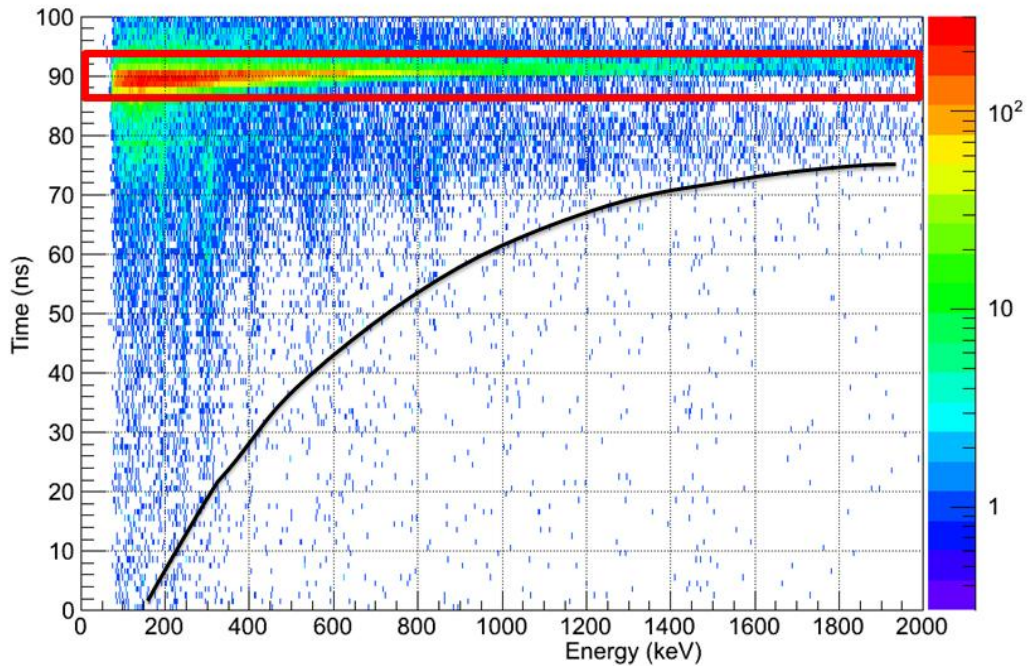
Fig. 4: Relative arrival time vs energy of gamma rays detected in the LaBr$_3$ detector in coincidence with fission events tagged in the calorimeter. Time on the y-axis goes backwards. Prompt fission gamma rays can be seen selected in the red box. The black line indicates the locus of gamma rays which can originate from (n,n') events caused by prompt fission neutrons.

References

[1] M. Lebois, J.N. Wilson et al., Development of a kinematically focused neutron source using the p(7Li,7Be)n inverse reaction. Nuc. Instr. Meth A. 735, 145 (2014)

Strength function from the ^{113}Cd(n,γ) reaction

T. Belgya[1], L. Szentmiklósi[1], R. Massarczyk[2], R. Schwengner[2], G. Schramm[2], E. Birgersson[2], A. Junghans[2]

[1]Nuclear Analysis and Radiography Department, Institute for Energy Security and Environmental Safety, Centre for Energy Research H-1525 POB 49, Budapest, Hungary

[2]Helmholtz-Zentrum Dresden-Rossendorf, Institute of Radiation Physics

Abstract

GENAT4 Monte Carlo simulations of the Budapest PGAA detector system are presented. The obtained response functions were used to unfold the spectrum from ^{113}Cd(n,γ) reaction – measured at the Budapest PGAA – in order to determine the γ-ray strength function. Preliminary results for the total radiative neutron capture cross sections for the ^{14}N(n,γ) and the ^{113}Cd(n,γ) reactions based on the unfolding approach are presented.

1   Introduction

Radiative capture of neutrons is a nuclear process of special importance for projects on the transmutation of radioactive waste. As capture channels compete with fission their knowledge is essential for the design of transmutation scenarios. For respective calculations performed on the basis of the Hauser-Feshbach formalism one needs the photon strength function governing the γ-decay to low lying final states from the capturing resonances in the continuum. As shown recently [1], photon scattering experiments performed at the ELBE facility have delivered data which can be described with a surprisingly successful parameterization of the electric dipole strength function in heavy nuclei using the so-called triple Lorentzian (TLO) strength function.

This triple Lorentzian concept [1] also describes various radiative neutron capture data hitherto interpreted in a different way [2]. Disagreeing predictions for photon strength functions have been in use by the two communities of neutron and photon beam experimenters – as documented in the IAEA reference input parameter library RIPL2 [2], where six different propositions based on capture data are listed for the calculation of E1-strengths. As also the microscopically calculated E1-strength function given there is at variance to many neutron capture as well as photon data [1] further investigations are urgently needed. In the recently started RIPL3-initiative [3] some of these deficiencies have been worked on, but the correlation between GDR width and nuclear triaxiality [1] is not properly accounted for.

One reason for the antagonism between the parameterizations resulting from photon respectively neutron capture data may be the fact that often different spins are populated making a direct comparison of data difficult. This difference can be minimized by using spin ½⁻ nuclei with A,Z for neutron capture to be compared to photo effect data in A+1,Z. Unfortunately, only very few pairs of stable isotopes A,Z and A+1,Z are available as targets for these comparative experiments.

A collaboration within the EU-EFNUDAT consortium, formed by the Centre for Energy Research (formerly Institute of Isotopes), Charles University and Helmholz Zentrum Dresden-Rossendorf, has investigated first the ^{77}Se(n,γ) and the ^{78}Se(γ,γ') reactions. Both data sets have already been analysed and published [4]. The other favourable pair ^{195}Pt/^{196}Pt – belonging to a clearly different mass region – has also been evaluated and published [5]. It has been shown that

both the experimentally measured (n,γ) and (γ,γ') spectra can be described with a common strength function [4, 5].

In addition to the E1 strength the magnetic dipole (M1) strength also contribute to radiative capture. The study of complete gamma spectra following the capture of thermal neutrons in a spin ½+-target may yield independent, interesting information for this case. It is thus proposed to extend the EFNUDAT-study for capture in spin ½+-targets by also looking at the pair of [113]Cd(n,γ) and [114]Cd(γ,γ') reaction spectra. In this case the capture of thermal neutrons on [113]Cd was studied by the Compton suppressed HOGe-detector at the Budapest PGAA facility

To analyse the data the Budapest group had to improve the response function description of the PGAA detector. The group has already spent a substantial amount of efforts for calculating the response functions [6-8] with MCNP-CP and GEANT4. After making fine adjustment of the detector model in the GEANT4 Monte Carlo calculations, the response function simulation has reached a satisfactory degree of agreement between the calculations and experiments only recently and therefore we could use the current set of GEATN4 response function data modelled by GEANT4 for unfolding or stripping of experimental spectra. In this article we provide details on the PGAA response function modelling and about our methodology of unfolding, and some results, This work will facilitate the strength function determination of [114]Cd in collaboration with the Dresden group.

2   Experiments

The latest description of the Budapest PGAA facility has been published recently [9]. The experiments related to the detector response function utilized the PGAA sample chamber. This chamber can be evacuated to suppress the signals coming from the activation of the air in the sample chamber. Polymer sheets loaded with [6]Li-enriched LiF were used to cover the interior of the flight tube and the target chamber to shield against the neutrons scattered by the target. The gamma-rays emitted by the irradiated samples or by the calibration sources were measured with a 27% relative efficiency HPGe detector which is surrounded by a BGO guard annulus and heavy lead shielding. The gamma-ray spectra were accumulated in an acquisition computer with 16 K channel resolution, covering the 45 keV-12 MeV energy range.

The low energy detector response function were measured with a number of γ-ray standard sources, including ^{60}Co, [207]Bi, [133]Ba, [152]Eu. For higher energies, gamma-sources utilizing the neutron capture reactions of H(n,γ)D and [14]N(n,γ)[15]N in form of suitable H_2O and Urea-D targets were used.

The [113]Cd(n,γ) experiments were performed on enriched as well as on a high purity natural metal samples. The highly enriched sample was obtained from the USSR and its composition is given in Table 1.

Mass number								
106	108	110	111	112	113	114	115	Other elements
-	-	0.4	0.7	3.4	90.2	4.9	0.4	< 0.001

Table 1: Composition of the enriched [113]Cd sample in % of atom numbers

The natural sample was 50 μm thick, 99.99% pure cadmium metal sheet obtained from Goodfellow. The radiative neutron capture cross section of cadmium is so high that a pencil-beam with 1 mm^2 cross section could already provided sufficient to induce 1 k (suppressed) and 3 k (unsuppressed) counting rates. We measured both samples for about one day. The detector signal was split and acquired in both Compton-suppressed and unsuppressed modes. The dead time in the unsuppressed mode was 3.6% for the enriched sample and 3.2% for the natural sample. The visual comparison of the enriched and natural samples shows no significant difference between them. The dead time for the natural target measurements was 7.8% in the Compton-suppressed case and 7.2% for the enriched sample.

3   GEANT4 calculations for the response functions of the Budapest PGAA HPGe detector

The GEANT4 Monte Carlo simulation code[10] was used to generate the response functions of the Budapest PGAA detector. Several experimental conditions and X-ray radiographies for understanding the internal geometry of the detectors were used to study responses of HPGe detectors, including the Budapest PGAA detector [6], which were the starting point to build the more complex shielded geometry. The methodology of the calculation was to describe the measured response of our ^{60}Co point source as accurate as possible by making minor changes in the geometry obtained from the manufacturers and from the X-ray radiography of the HPGe detector. Drawings of the geometry are show in Figure 1.
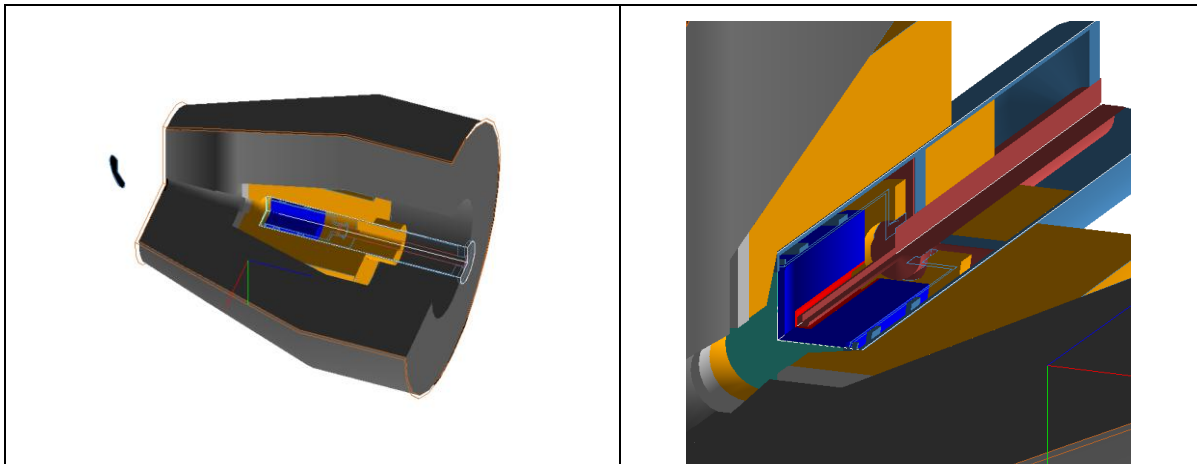
Figure 1: Drawing of the modelled detector geometries. Darker dray colour is the outer lead shielding, light gray is the main and catcher guard BGO detectors, and black is the Ge crystal. Many other details are not shown for the clarity.

The calculations were done in unsuppressed mode. We produced a list mode data file from the Monte Carlo code for the HPGe and BGO detectors to build up Compton suppression mode in separate replay calculations because the perfect anticoincidence did not provided satisfactory agreement with the experiment. The result of the Compton suppressed calculations will be presented in a separate paper. Here we concentrate only on results that can be obtained from the unsuppressed mode spectrum.

The calculated ^{60}Co spectrum was composed of the two gamma lines at 1173 keV and 1332 keV energies, by normalising them to the measured full energy peak areas. Figure 2 presents the agreement achieved for the ^{60}Co source measurement.

As it can be seen there is still some deviations below 400 keV, however this will not crucially influence the conclusions for higher energies. We achieved this quite satisfactory agreement after a long iteration procedure. At this point we decided to produce the response function as a function of the energy from 250 keV up to 12 MeV with a step of 250 keV with 1 keV binning. We call them as node spectra. The calculations took about 60 days of processor time on i5 Intel processors. All of our measured spectra were transformed to the 1 keV binning by a suitable algorithm to be able to compare them directly with the calculations.
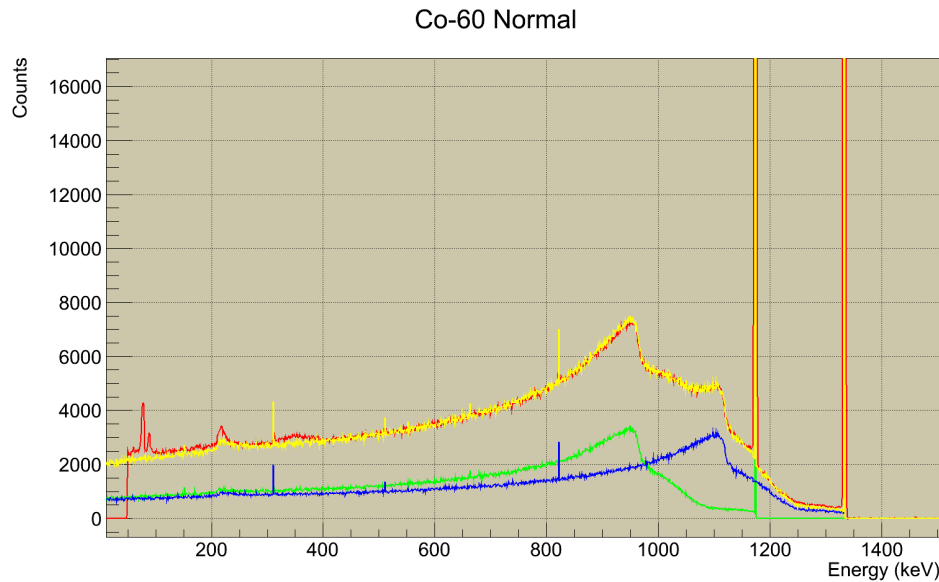
Figure 2. : The upper two curves are the simulated (black) and measured (grey) spectra of ^{60}Co calibration source. The two curves below are the simulated 1173 keV and 1332 keV full energy spectra; their weighted sum is the simulated curve.

We also decided to follow the treatment of the response functions according to the Oslo prescription [11]. We normalized all of the node spectra to one to form probability distributions. After the normalization, we removed the full energy, the single escape, the double escape and the Annihilation peaks. At the same time these event probabilities were fit with Cardinal-splines [12] for later use. Figure 3 shows the stripped node distributions that are suitable for interpolation.

122
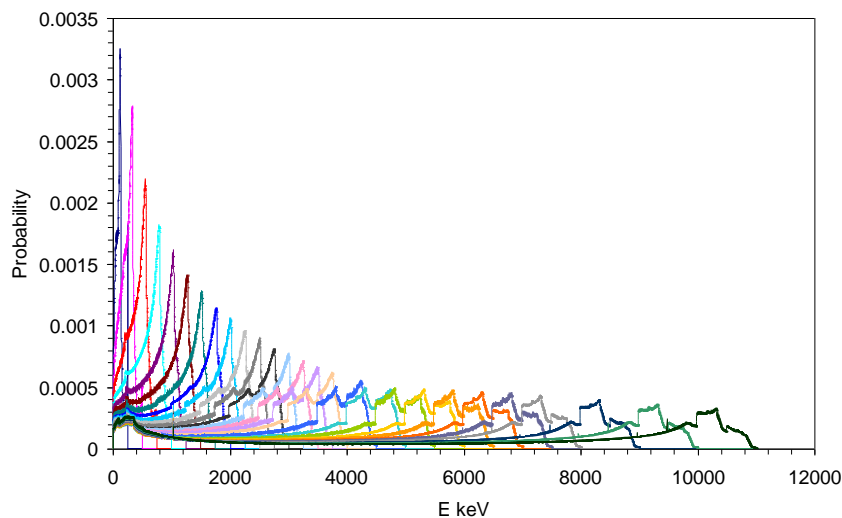
Figure 3.: The node response functions prepared for interpolation.

According to the Oslo prescription the interpolation for energy E of the Compton scattering part of the response function $c(E,E_\gamma)$ – belonging to the full energy peak of E_γ – can be done in the angle space θ using the two neighbouring node spectra between the Compton-edge and the backscattering peak.

$$c(E,E_\gamma) = \left(\frac{dE}{d\theta}\right)^{-1}_{E_\gamma} \left[c_1(E_1)\left(\frac{dE_1}{d\theta}\right)_{E_{\gamma 1}} + \frac{E_\gamma - E_{\gamma 1}}{E_{\gamma 2} - E_{\gamma 1}} \times \left(c_2(E_2)\left(\frac{dE_2}{d\theta}\right)_{E_{\gamma 2}} - c_1(E_1)\left(\frac{dE_1}{d\theta}\right)_{E_{\gamma 1}} \right) \right] \quad (1)$$

This is of course not true for the continuum belonging to the escape peaks; however we will neglect this here. Above the Compton-edge simple stretching and constriction interpolation is used similar to the one shown in Eq. (1). The quality of the interpolation is checked by direct comparison of the interpolated and simulated spectra. This is shown in Figure 4. As it can be seen in Figure 4 the interpolation is almost perfect with the Oslo method [11]. There seems to be a minor disagreement around the back scattered peak at about 220 keV for which the interpolation does not work well. This can also be treated by interpolating the back scattered peak as suggested but we neglected it since it does not contribute to our major goal of unfolding the ^{114}Cd spectrum significantly.
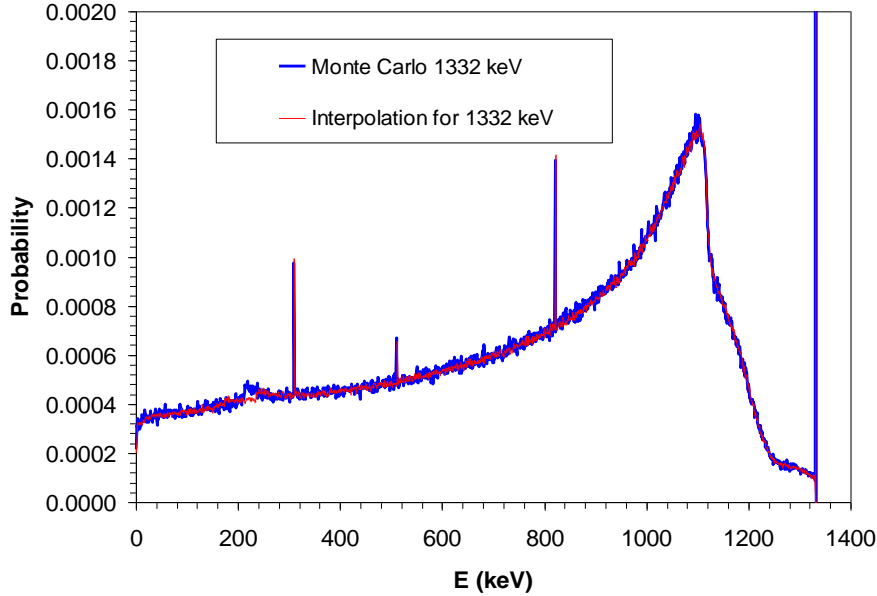
Figure 4: Comparison of the interpolated continuum and the GEANT4 Monte Carlo simulated spectra.

4 Unfolding of measured spectra, determination of capture cross sections

4.1 Unfolding procedure and results

Unfolding of spectra can be performed different ways. The simplest way is to start at the highest full energy peak that is detectable in the spectrum and consider its highest energy channel content

as a result of full energy deposition. Subtracting the corresponding full-energy point normalised response function from the whole spectrum will result in also a full energy point in the previous channel. This procedure can be repeated till the lowest channel for which response function was calculated. Of course any difference between the model and true response will accumulate bias in the process. In this study we neglect the calculation of the accumulated uncertainties and the effect of the peak width, which due to the small width do not influence the result much. In Figure 5 unfolding results for the ^{60}Co and ^{152}Eu calibration sources are shown.
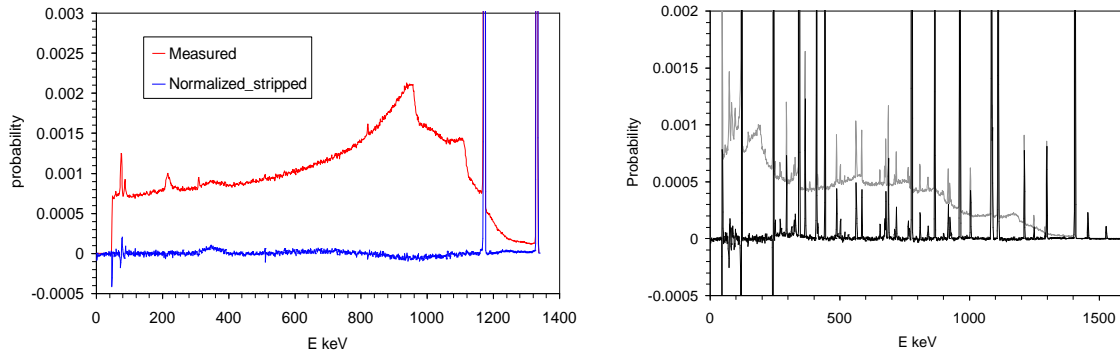
Figure 5: Unfolded ^{60}Co (left chart, black) and ^{152}Eu (right chart, black) calibration source spectra. The measured spectra (gray) were normalized to 1.

It can clearly be seen that the subtraction result in small differences where the continuum part of the response function is. The deviation form zero difference is smaller than 10% for most of the continuum and is positive and negative as well. The sum of differences is 0.0029 for the continuum and the summed peak area is 0.3618, the percentage of the continuum per peak area is 0.8%. For more complicated spectra it is more difficult to quantify.

Finally, we present the unfolding result for the ^{14}N(n,γ) and ^{113}Cd(n,γ) spectra in Figure 6.
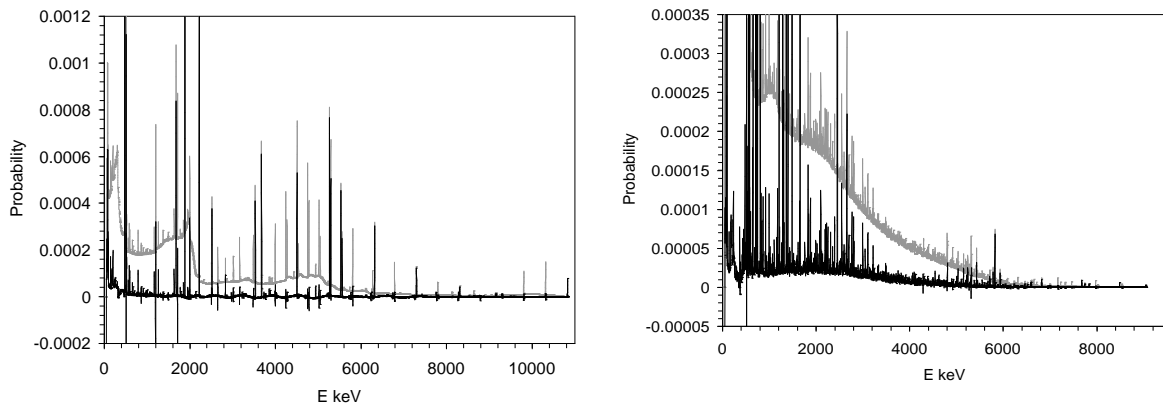
Figure 6: Unfolded ^{14}N(n,γ) (left chart, black) and ^{113}Cd(n,γ) (right chart, black) spectra. The measured spectra (gray) were normalized to 1.

It is clearly visible that the unfolding of relatively simple ^{14}N(n,γ) spectrum removed a large percentage of the continuum while the residuum has a periodic change between positive and negative values around zero. Peaks in the negative region are due to the difference of the full energy peak width and the escape peak width. The periodicity of the residuum can be correlated with the escape peak distances; however this statement has to be studied in detail. The unfolding of the far more complicated ^{113}Cd(n,γ) spectrum provides a significant bump with a centre of 2.2 MeV of positive values that can be associated with the expected quasi-continuum of full energy

peaks. It is important to note that the bump does not go to zero down to about 400 keV which means a large number of low energy transitions in the quasi-continuum.

4.2   Calculation of radiative capture cross sections

Before using the unfolded $^{14}N(n,\gamma)$ and $^{113}Cd(n,\gamma)$ spectra for total capture cross section calculation, they have to be corrected for full energy peak efficiency for which the measured and fitted efficiency curve was used. Since the unfolded spectra contain only full energy events they can be corrected with measured full energy efficiency for each channel. The efficiency-corrected unfolded $^{113}Cd(n,\gamma)$ spectrum and, the calculated and measured efficiency curves are shown in Figure 7.

Using the energy weighted sum rule [13] with internal calibration

$$\sigma_{th} = \sum_i \sigma_{\gamma i} E_i / B_n ,$$

(2)

we can obtain the thermal capture cross section σ_{th}. In Eq. (2) $\sigma_{\gamma i}$ is the partial γ-ray production cross section for the ith channel, E_i is its energy and B_n is the binding energy. In this formula there is no account for the possible conversion electron and internal pair-production [13] contributions.
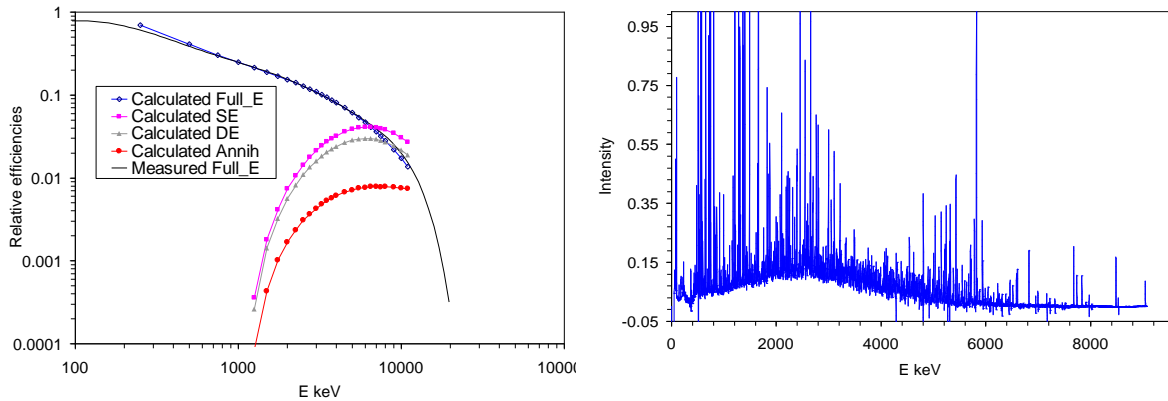
Figure 7: Measured and calculated relative efficiencies (left chart) and the full energy efficiency corrected $^{113}Cd(n,\gamma)$ spectrum (right chart).

For the $^{14}N(n,\gamma)$ thermal capture cross section Eq. (2) yields 90 mb, while the measured literature value is 80.3(8) mb [14]. This value contains the contribution from capture of ^{12}C from Urea-D, Cl and B impurities. The elimination of these impurity contributions requires more work. In the case of $^{113}Cd(n,\gamma)$ reaction the impurities can be neglected and the thermal capture cross section is 21640 b, while the literature value is 20600(400) b [15]. The agreement between the measured and literature values is quite good taking into the account that about 5-10% uncertainty can be assigned to the unfolding procedure. This agreement suggests that the procedure works rather well.

5   Conclusions

GENAT4 Monte Carlo simulations for the Budapest PGAA detector system were presented. It was shown that they can be adequately used to approximate measured spectra of various complexities.

The obtained response functions were used to unfold simple, as well as complicated spectra, including the measured ^{113}Cd(n,γ) spectrum which is our goal in the EFNUDAT and ERINDA collaborations. To check the quality of the procedure total thermal capture cross sections of the ^{14}N(n,γ) and ^{113}Cd(n,γ) reactions have been calculated and compared to the literature. The unfolded ^{113}Cd(n,γ) spectrum contains a broad bump of continuum centred around 2.2 MeV. It will be used to deduce the gamma ray strength function based on simulation of the decay scheme.

Acknowledgement

References

[1] Junghans, A. R., G. Rusev, R. Schwengner, A. Wagner, and E. Grosse, Phys. Lett. **B 670**(3) (2008) 200.

[2] Belgya, T. et al., *Handbook for calculations of nuclear data, RIPL-2*, M. Herman, Editor. IAEA-TECDOC-1506: Vienna (2006)

[3] Capote, R., M. Herman, P. Oblozinsky, P.C. Young, S. Goriely, T. Belgya, A.V. Ignatyuk, A.J. Koning, S. Hilaire, V.A. Plujko, M. Avrigeanu, O. Bersillon, M.B. Chadwick, T. Fukahori, Z.G. Ge, Y.L. Han, S. Kailas, J. Kopecky, V.M. Maslov, G. Reffo, M. Sin, E.S. Soukhovitskii, and P. Talou, Nuclear Data Sheets, **110**(12) (2009) 3107-3213.

[4] Schramm, G., R. Massarczyk, A.R. Junghans, T. Belgya, R. Beyer, E. Birgersson, E. Grosse, M. Kempe, Z. Kis, K. Kosev, M. Krticka, A. Matic, K.D. Schilling, R. Schwengner, L. Szentmiklosi, A. Wagner, and J.L. Weil, Phys. Rev. **C 85**(1) (2012) 014311 1-14.

[5] Massarczyk, R., G. Schramm, A.R. Junghans, R. Schwengner, M. Anders, T. Belgya, R. Beyer, E. Birgersson, A. Ferrari, E. Grosse, R. Hannaske, Z. Kis, T. Kögler, K. Kosev, M. Marta, L. Szentmiklósi, A. Wagner, and J.L. Weil, Phys. Rev. **C 87** (2013) 044306.

[6] Szentimiklosi, L., T. Belgya, B. Maroti, and Z. Kis, J. Nucl. Radioanal. Chem. (2014) submitted.

[7] Szentimiklosi, L., Z. Kis, T. Belgya, and A.N. Berlizov, J. Radioanal. Nucl. Chem. **298** (2013) 1605.

[8] Szentmiklósi, L., Berlizov, A.N., Nucl. Instr. Meth. **A 612** (2009) 122-126.

[9] Szentmiklósi, L., T. Belgya, Z. Révay, and Z. Kis, J. Radioanal. Nucl. Chem. **286** (2010) 501-505.

[10] Agostinelli, S.e.a., Nucl. Instrum. Methods Phys. Res. **A 506** (2003) 250.

[11] Guttormsen, M., T.S. Tveter, L. Bergholt, F. Ingebretsen, and J. Rekstad, Nucl. Instr. Meth. **A 374** (1996) 371.

[12] Belgya, T., J. Nucl. Radioanal. Chem. **265**(2) (2005) 175-179.

[13] Belgya, T., J. Nucl. Radioanal. Chem. **276**(3) (2008) 609-614.

[14] Belgya, T., Phys. Rev. **C 74** (2006) 024603-1-8.

[15] Mughabghab, S.F., IAEA INDC(NDS)-440 (2003).

Measurement of the neutron capture cross section of the fissile isotope [235]U with the CERN n_TOF Total Absorption Calorimeter and a fission tagging based on micromegas detectors

E. Mendoza[1], J. Balibrea[1], D. Cano-Ott[1], C. Guerrero[2], E. Berthoumieux[3], S. Altstadt[4], J. Andrzejewski[5], L. Audouin[6], M. Barbagallo[7], V. Bécares[1], F. Bečvář[8], F. Belloni[3,2]C, J. Billowes[9], V. Boccone[2], D. Bosnar[10], M. Brugger[2], M. Calviani[2], F. Calviño[11], C. Carrapiço[12], F. Cerutti[2], E. Chiaveri[3,2], M. Chin[2], N. Colonna[7], G. Cortés[11], M.A. Cortés-Giraldo[13], M. Diakaki[14], C. Domingo-Pardo[15] I. Duran[16], R. Dressler[17], N. Dzysiuk[18], C. Eleftheriadis[19], A. Ferrari[2], K. Fraval[3], S. Ganesan[2], A.R. García[1], G. Giubrone[15], M.B. Gómez-Hornillos[11], I.F. Gonçalves[12], E. González-Romero[1], E. Griesmayer[21], F. Gunsing[3], P. Gurusamy[20], D.G. Jenkins[22], E. Jericha[21], Y. Kadi[2], F. Käppeler[23], D. Karadimos[14], T. Kawano[24], N. Kivel[17], P. Koehler[25], M. Kokkoris[14], G. Korschinek[26], M. Krtička[8]C, J. Kroll[8], C. Langer[4], C. Lampoudis[3], E. Leal-Cidoncha[16], C. Lederer[27,4], H. Leeb[21], L.S. Leong[6], R. Losito[2], A. Manousos[19], J. Marganiec[5], T. Martínez[1], P.F. Mastinu[18], M. Mastromarco[7], C. Massimi[28], M. Meaze[7], A. Mengoni[29], P.M. Milazzo[30], F. Mingrone[28], M. Mirea[31], W. Mondelaers[32], C. Paradela[16], A. Pavlik[27], J. Perkowski[5], M. Pignatari[33], A. Plompen[32], J. Praena[13], J.M. Quesada[13], T. Rauscher[33], R. Reifarth[4]J, A. Riego[11], F. Roman[2,31], C. Rubbia[2,34], R. Sarmento[12], P. Schillebeeckx[32], S. Schmidt[4], D. Schumann[17], I. Stetcu[24], M. Sabaté[13], G. Tagliente[7], J.L. Tain[15], D. Tarrío[16], L. Tassan-Got[6], A. Tsinganis[2], S. Valenta[8], G. Vannini[28], V. Variale[7], P. Vaz[12], A. Ventura[29], R. Versaci[2], M.J. Vermeulen[22], V. Vlachoudis[2], R. Vlastou[14], A. Wallner[27], T. Ware[9], M. Weigand[4], C. Weiß[21], T.J. Wright[9], P. Žugec[10]

[1]Centro de Investigaciones Energeticas Medioambientales y Tecnológicas (CIEMAT), Madrid, Spain
[2]European Organization for Nuclear Research (CERN), Geneva, Switzerland
[3]Commissariat à l'Énergie Atomique (CEA) Saclay - Irfu, Gif-sur-Yvette, France
[4]Johann-Wolfgang-Goethe Universität, Frankfurt, Germany
[5]Uniwersytet Łódzki, Lodz, Poland
[6]Centre National de la Recherche Scientifique/IN2P3 - IPN, Orsay, France
[7]Istituto Nazionale di Fisica Nucleare, Bari, Italy
[8]Charles University, Prague, Czech Republic
[9]University of Manchester, Oxford Road, Manchester, UK
[10]Department of Physics, Faculty of Science, University of Zagreb, Croatia
[11]Universitat Politecnica de Catalunya, Barcelona, Spain
[12]Instituto Tecnológico e Nuclear, Instituto Superior Técnico, Universidade Técnica de Lisboa, Lisboa, Portugal
[13]Universidad de Sevilla, Spain
[14]National Technical University of Athens (NTUA), Greece
[15]Instituto de Física Corpuscular, CSIC-Universidad de Valencia, Spain
[16]Universidade de Santiago de Compostela, Spain
[17]Paul Scherrer Institut, Villigen PSI, Switzerland
[18]Istituto Nazionale di Fisica Nucleare, Laboratori Nazionali di Legnaro, Italy
[19]Aristotle University of Thessaloniki, Thessaloniki, Greece
[20]Bhabha Atomic Research Centre (BARC), Mumbai, India
[21]Atominstitut, Technische Universität Wien, Austria
[22]University of York, Heslington, York, UK
[23]Karlsruhe Institute of Technology, Campus Nord, Institut für Kernphysik, Karlsruhe, Germany
[24]Los Alalamos National Laboratory, Los Alamos, New Mexico 87545, USA
[25]Oak Ridge National Laboratory (ORNL), Oak Ridge, TN 37831, USA
[26]Technical University of Munich, Munich, Germany
[27]University of Vienna, Faculty of Physics, Vienna, Austria

[28]Dipartimento di Fisica, Università di Bologna, and Sezione INFN di Bologna, Italy

[29]Agenzia nazionale per le nuove tecnologie, l'energia e lo sviluppo economico sostenibile (ENEA), Bologna, Italy

[30]Istituto Nazionale di Fisica Nucleare, Trieste, Italy

[31]Horia Hulubei National Institute of Physics and Nuclear Engineering - IFIN HH, Bucharest - Magurele, Romania

[32]European Commission JRC, Institute for Reference Materials and Measurements, Retieseweg 111, B-2440 Geel, Belgium

[33]Department of Physics and Astronomy - University of Basel, Basel, Switzerland

[34]Laboratori Nazionali del Gran Sasso dell'INFN, Assergi (AQ),Italy

Abstract

Actual and future nuclear technologies require more accurate nuclear data on the (n,γ) cross sections and α-ratios of fissile isotopes. Their measurement presents several difficulties, mainly related to the strong fission γ-ray background competing with the weaker γ-ray cascades used as the experimental signature of the (n,γ) process. A specific setup has been used at the CERN n_TOF facility in 2012 for the measurement of the (n,γ) cross section and α-ratios of fissile isotopes and used for the case of the ^{235}U isotope. The setup consists in a set of micromegas fission detectors surrounding ^{235}U samples and placed inside the segmented BaF$_2$ Total Absorption Calorimeter.

1 Introduction

Nuclear data on neutron-induced capture and fission cross-sections are necessary for improving the design and performance of advanced nuclear reactors and transmutation devices for the incineration of radioactive nuclear waste [1, 2]. The actual nuclear data priorities are summarized in the High Priority Request List [3] of the Nuclear Energy Agency, where the capure cross sections of four fissile isotopes has been included: ^{233,235}U and ^{239,241}Pu. The difficulty of these measurements is that the detection of the capture reactions is performed by detecting the capture γ-rays, which in this case competes with the fission γ-ray background.

We have measured the ^{235}U(n,γ) cross section at the n_TOF facility [4, 5] with the Total Absorption Calorimeter (TAC) [6] and fission micromegas detectors (FTMGAS) [7]. Here we describe the experimental setup used and the first preliminary results.

2 The experimental setup

The CERN n_TOF neutron time-of-flight (TOF) facility delivers a neutron beam generated in spallation reactions induced by a 20 GeV/c pulsed proton beam of $7 \cdot 10^{12}$ protons per pulse and with 16 ns FWHM time resolution. The spallation target is a cylindrical lead block with 60 cm diameter and 40 cm length. The neutrons are moderated in a 4 cm thick borated water layer before traveling 185 m in vacuum until reaching the experimental area, where the measured samples and the detectors are placed.

We used 10 isotopically enriched samples of ^{235}U$_3$O$_8$ produced at IRMM Geel. They have around 300μg/cm^2 surface density, and are deposited on 20 μm thick aluminum backings. They have a diameter of 42 mm, thus covering the entire neutron beam profile.

The (n,γ) reactions were measured with the Total Absorption Calorimeter, which is a segmented array composed by 40 BaF$_2$ crystals of 15 cm in length and covering 95% of the 4π solid angle. This detector is used to measure neutron capture cross sections by detecting in coincidence (nearly) all the γ-rays forming the cascades de-exciting the compound nucleus after the neutron capture reactions. The

fission reactions were measured with micromegas detectors, operated with a gas mixture of Ar 88%, CF$_4$ 10% and isobutane 2% at 1 atm. All the sigals induced in the TAC and in the FTMGAS detectors were recorded by high-performance digitizers (Acqiris-DC270) with 8 bits resolution, operated at 250 MSamples/s and recording for each neutron pulse 32 ms long data buffers which contain the entire digitized electronic response of each individual detector [8].

The measurement was performed with the samples and the FTMGAS placed in the center of the TAC, surrounded by a 5 cm thick shperical neutron absorber shell made of borated polyethylene, used to reduce the background of scattered neutrons. This setup can be seen in Fig. 1. Two different fission configurations were used, based on 2 and 10 fission tagging micromegas detectors.
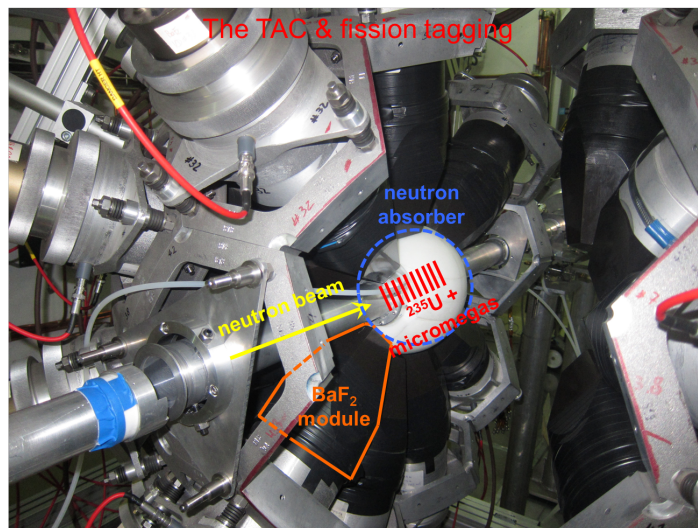
Fig. 1: Experimental setup of the ^{235}U(n,γ) cross section measurement. The ^{235}U samples and the FTMGAS are placed in the center of the TAC, which appears opened in two semispheres in the picture, surrounded by a neutron absorber.

The configuration with the 2 FTMGAS was dedicated to the ^{235}U(n,γ) cross section measurement. A stack of 8 bare ^{235}U samples and two samples encapsulated inside the FTMGAS were placed in the beam for improving the signal to background ratio (i.e. to minimize the amount of dead material from the fission tagging setup in the neutron beam). A low fission tagging efficiency of ∼20% was achieved. As it has been demonstrated in [9], it is possible to remove accurately the gated fission γ-ray background at low tagging efficiencies by selecting events with a high γ-ray multiplicity which correspond only to (n,f) γ-rays and for which the TAC has a nearly 100% detection efficiency. Indeed, a simplified version of this technique, without any fission tagging, has been used as well at LANL in a ^{235}U cross section measurement [10]. The option of having fission tagging capabilities at a low efficiency has been preferred for the measurement at n_TOF for deducing the normalization of the data strictly from experimental parameters, without the need of a using evaluated cross section data as an external reference.

The configuration with the 10 FTMGAS was dedicated the ^{235}U(n,f)/^{235}U(n,γ) ratio (α-ratio) for well resolved resonances, as a cross check for the 2 FTMGAS data and for the measurement of γ-ray energy distributions from the lowest lying resonances. Each sample was inserted in a FTMG for measuring the fission cross section with a high efficiency (∼90%) at the price of having a much larger dead material (i.e. background) than with the 2 FTMGAS configuration.

In both cases, dedicated background measurements with the same experimental setup but without the ^{235}U layers were performed, including all the dead material layers intercepting the neutron beam. Additional measurements with a ^{197}Au sample (capture cross section reference) and a carbon scatterer foil (for determining the neutron sensitivity) were also performed.

3 Preliminary analysis

The TAC measures in coincidence the γ-rays emitted after the capture reactions. The individual signals are grouped into TAC events, using a time coincidence window of 20 ns. Each TAC event is characterized by its time-of-flight, the total energy deposited (E_{sum}) and the crystal multiplicity (m_{cr}), which is the number of detectors contributing to the event above a given threshold. Conditions are applied to the detected events in E_{sum} and m_{cr} in order to improve the capture signal over background ratio. A coincidence analysis is also performed between the fission events detected by the FTMGAS and the TAC events. If a TAC event is in coincidence with a FTMGAS event, it is tagged as a fission event. The tagging efficiency can be calculated from the ratio of counts in the TAC in coincidence with the micromegas to the total number of counts in the TAC, for very restrictive conditions in the TAC events (high E_{sum} and high m_{cr}) which guarantee that the TAC event is a fission event. The preliminary values obtained for the tagging efficiency are 19.4(4)% and 90.0(3)%, for the 2 FTMGAS and the 10 FTMGAS configurations, respectively.

Examples of deposited energy spectra in the TAC are presented in Fig. 2, where two different backgrounds are presented. The one in blue ("Background") has been obtained from the dedicated background measurements (dummy assemblies and measurements without beam), and does not include the background due to fission reactions in ^{235}U. The one in magenta ("Fission") is the background due to fission in ^{235}U, and it has been obtained from the tagged events scaled by the inverse of the tagging efficiency.
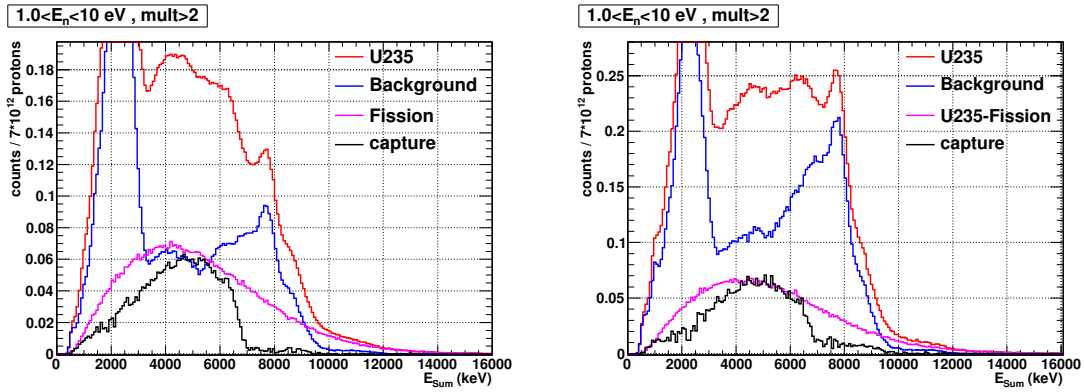
Fig. 2: Deposited energy spectra in the TAC corresponding to the ^{235}U(n,γ) measurement (red), the backround excluding fission (blue), the fission events (magenta), and the capture events (black). All the spectra correspond to TAC events with m_{cr}>2, and neutron energies between 1 and 10 eV. The results corresponding to the 2 FTMGAS configuration are presented in the left panel and the results corresponding to the 10 FTMGAS configuration in the right panel.

A preliminary experimental capture ($x = \gamma$) and fission ($x = f$) cross-sections have been calculated for each configuration with:

$$\sigma_{(n,x)} = \frac{1}{n_{at}} \frac{C_x(E_n) - B_x(E_n)}{\epsilon_x \cdot \Phi(E_n)}. \tag{1}$$

where C_x, B_x, and ϵ_x are the counting rate, background and detection efficiency of the TAC and the micromegas, respectively, and $\Phi(E_n)$ is the neutron energy fluence distribution.

A (very preliminary) cross sections have been obtained in this way, and are presented in Fig. 3 to Fig. 8. They have been normalized to the cross sections available in the ENDF/B-VII.0 library [11] in the 0.2-10 eV neutron energy range
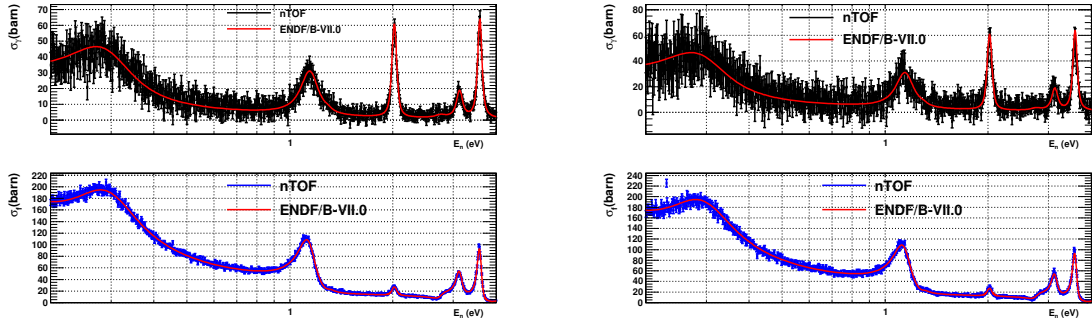
Fig. 3: Preliminary capture (top) and fission (bottom) cross sections obtained with the TAC and with the micromegas, calculated from the 2 FTMGAS (left) and 10 FTMGAS (right) configurations, in the 0.2-4 eV energy range.
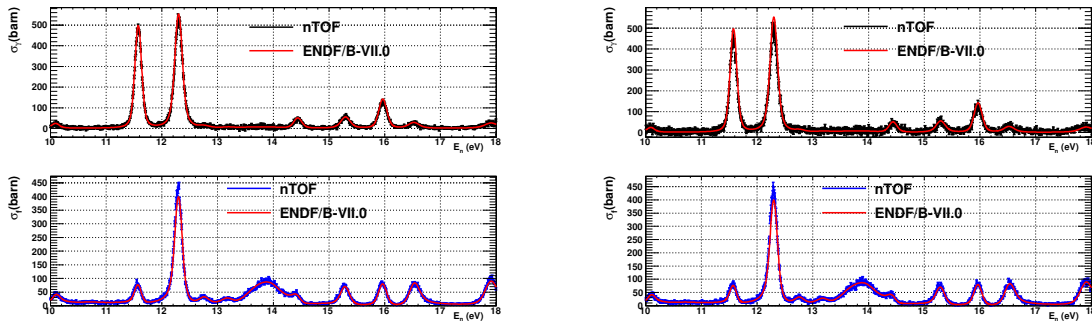
Fig. 4: Preliminary capture (top) and fission (bottom) cross sections obtained with the TAC and with the micromegas, calculated from the 2 FTMGAS (left) and 10 FTMGAS (right) configurations, in the 10-18 eV energy range.
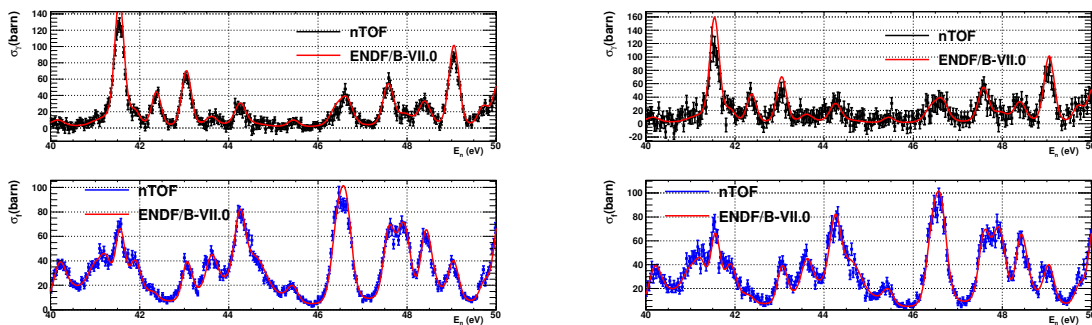
Fig. 5: Preliminary capture (top) and fission (bottom) cross sections obtained with the TAC and with the micromegas, calculated from the 2 FTMGAS (left) and 10 FTMGAS (right) configurations, in the 40-50 eV energy range.
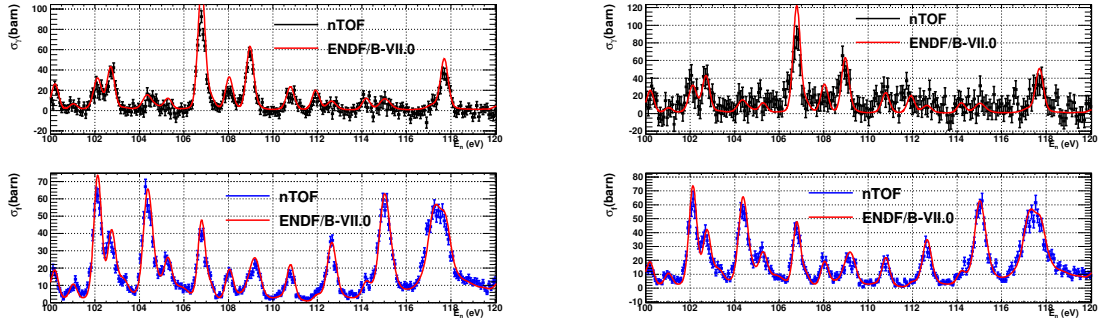
Fig. 6: Preliminary capture (top) and fission (bottom) cross sections obtained with the TAC and with the micromegas, calculated from the 2 FTMGAS (left) and 10 FTMGAS (right) configurations, in the 100-120 eV energy range.
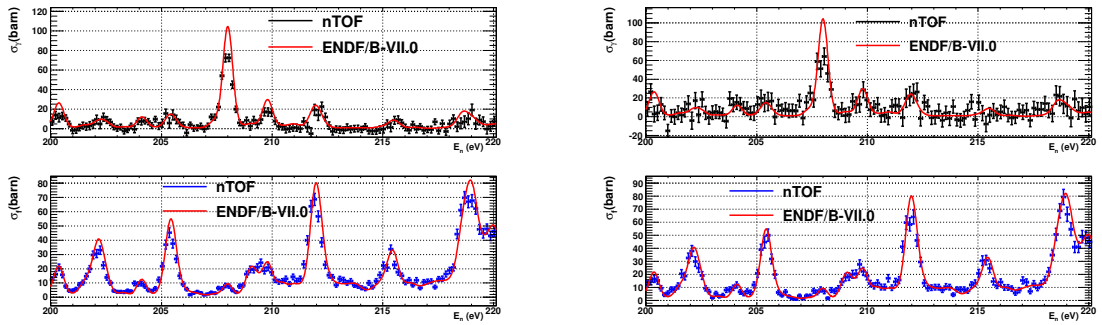
Fig. 7: Preliminary capture (top) and fission (bottom) cross sections obtained with the TAC and with the micromegas, calculated from the 2 FTMGAS (left) and 10 FTMGAS (right) configurations, in the 200-220 eV energy range.
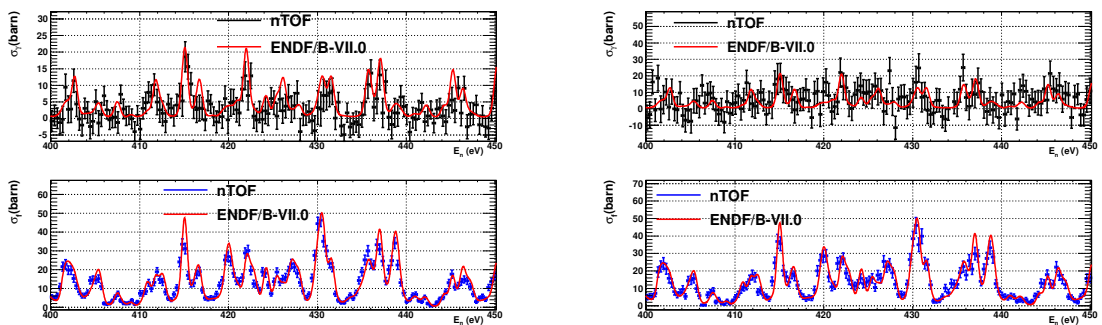
Fig. 8: Preliminary capture (top) and fission (bottom) cross sections obtained with the TAC and with the micromegas, calculated from the 2 FTMGAS (left) and 10 FTMGAS (right) configurations, in the 400-450 eV energy range.

4 Future Work

We have presented a brief description of the experimental setup and a very preliminary analysis of the measured data. At this moment, a detailed and complete analysis of the measurement is being performed.

Acknowledgments

References

[1] A.J. Koning *et al.*, CANDIDE: Nuclear data for sustainable nuclear energy EUR 23977 EN (2009).

[2] Working Party on International Evaluation Co-operation of the NEA Nuclear Science Committee, Uncertainty and target accuracy assessment for innovative systems using recent covariance data evaluations, ISBN 978-92-64-99053-1 (2008).

[3] NEA Nuclear Data High Priority Request List, http://www.nea.fr/dbdata/hprl/index.html.

[4] C. Guerrero *et al.*, Eur. Phys. J. A (2013) 49

[5] U. Abbondanno *et al.*, CERN n TOF Facility: Performance Report, CERN-SL-2002-053 ECT (2002).

[6] C. Guerrero *et al.*, Nucl. Instr. Meth. A 608 (2009)

[7] S. Andriamonje *et al.*, J. Korean Phys. Soc. 59 (2011).

[8] U. Abbondanno et al., Nucl. Inst. Meth A, 538 (2005) 692.

[9] C. Guerrero et al., Eur. Phys. J. A 48 (2012)

[10] M. Jandel *et al.*, Phys. Rev. Lett. 109 (2012)

[11] M.B. Chadwick *et al.*, Nuclear Data Sheets 107 (2006)

Importance of nuclear triaxiality for electromagnetic strength, level density and neutron capture cross sections in heavy nuclei

E. Grosse [2], *A.R. Junghans* [1] *and R. Massarczyk* [1,2]

[1] Institute of Radiation Physics, Helmholtz-Zentrum Dresden-Rossendorf, 01328 Dresden, Germany

[2] Institute of Nuclear and Particle Physics, TU Dresden, 01069 Dresden, Germany

Abstract:
Cross sections for neutron capture in the range of unresolved resonances are predicted simultaneously to level distances at the neutron threshold for more than 100 spin-0 target nuclei with A >70. Assuming triaxiality in nearly all these nuclei a combined parameterization for both, level density and photon strength is presented. The strength functions used are based on a global fit to IVGDR shapes by the sum of three Lorentzians adding up to the TRK sum rule and theory-based predictions for the A-dependence of pole energies and spreading widths. For the small spins reached by capture level densities are well described by only one free global parameter; a significant collective enhancement due to the deviation from axial symmetry is observed. Reliable predictions for compound nuclear reactions also outside the valley of stability as expected from the derived global parameterization are important for nuclear astrophysics and for the transmutation of nuclear waste.

1   Introduction

The radiative capture of neutrons in the keV to MeV range by heavy nuclei plays an important role in considerations for advanced systems aiming for the reduction of radioactive nuclear waste [1]. This process is of interest also for the cosmic nucleosynthesis, especially for scenarios with high neutron fluxes, where neutron capture processes lead to a production of nuclides beyond Fe [2]. Predictions for radiative neutron capture cross sections in the range of unresolved resonances are based on statistical model calculations. Their reliability depends not only on the proper characterization of the input channel, but more strongly on the details determining the decay of the intermediately formed compound nucleus. Here the strength of its electromagnetic decay is of importance as well as the open phase space in the final nucleus, i.e. the density of levels reached by the first photon emitted. The experimental studies forming the basis for parameterizations can mainly be performed on nuclei in or close to the valley of beta-stability, but in cosmic environments many radiative processes occur in exotic nuclei which are not easily accessible experimentally. Similarly the knowledge of radiative neutron capture cross sections in actinide and other unstable nuclei is of importance for the understanding of the competition between nuclear fission and the production of long-lived radionuclides by capture. It is thus desirable to derive a parameterization which is global as based on concepts accepted to be valid generally and thus expected to be applicable also away from the stable nuclei. As is well known [3], the variation of nuclear quadrupole moments over the nuclide chart is very significant. It thus is justified to investigate the influence of nuclear shapes on the extraction of strength functions from isovector giant dipole resonance (IVGDR) data as well as on nuclear level densities. If the restriction to axial symmetry is released, the contribution of collective rotation to level densities is significantly increased [3, 4], and Lorentzian fits to IVGDR data are improved [5].

Previously the results of various experiments on electromagnetic processes were often analysed [3] not regarding triaxiality. As demonstrated [6] one has to go considerably beyond the well documented [7] information on B(E2)-values and their relation *e.g.* to quadrupole moments.

Also theoretically the breaking of axial symmetry has often been disregarded, although it was shown [8] within the Hartree-Fock-Bogoliubov (HFB) scheme, that exact 3-dimensional angular momentum projection results in a pronounced triaxial minimum also for deformed nuclei. Various spectroscopic studies (*e.g.* [6, 9, 10, 11, 12]) have identified triaxiality effects in very many nuclei and especially in nuclei with small but non-zero quadrupole moments. The study presented in the following makes use of a constrained CHFB-calculation for more than 1700 nuclei [13], which predicts not only quadrupole transitions rather well, but also the breaking of axial symmetry, *i.e.* the triaxiality parameter γ. Predictions derived using these results in the parameterization for the energy dependence of photon strengths as well as of nuclear level densities will be compared to average radiative widths at the neutron separation energy S_n and of capture cross sections in the energy range of 30 keV. The present investigation tests a global prediction for 132 nuclides reached by neutron capture in spin-0 targets.

2   Dipole strength in triaxial nuclei

Electromagnetic processes play an important role not only in nuclear spectroscopy but also for the de-excitation processes following neutron capture or other nuclear reactions. Since decades the relation of the IVGDR to the nuclear radiative strength [14, 15] is considered the basis of its parameterization for heavy nuclei. Its mean position E_0 can be predicted using information from liquid drop fits to ground state masses [16] and for triaxial nuclei the three pole energies E_k are given by *a priori* information on the three axis lengths r_k : $E_k = r_0/r_k \cdot E_0$. A parameterization of the electromagnetic strength in heavy nuclei with mass number A>70, which considers their triaxial deformation, was shown to be in reasonable accordance to various data of photon strengths $f_1(E_\gamma)$ [5, 17]. This triple Lorentzian (TLO) approach [18, 19], combined to the axis ratios calculated by CHFB [13], describes the shapes of their IVGDR's as well as their low energy tail at energies below the neutron separation energy S_n. Using averages from the even neighbours this is the case also for odd nuclei as reached by capture from even target nuclei and Eq. (1) describes both cases (with the fine structure constant α):

$$f_{E1}(E_\gamma) = \frac{4\,\alpha}{3\pi\,g_{eff}\,m_N c^2} \frac{ZN}{A} \sum_{k=1}^{3} \frac{E_\gamma \Gamma_k}{\left(E_k^2 - E_\gamma^2\right)^2 + E_\gamma^2 \Gamma_k^2}; \quad g_{eff} = \sum_{r=1}^{2\cdot\min(\lambda,J_0)+1} \frac{2J_r + 1}{2J_0 + 1} = 2\lambda + 1 = 3. \quad (1)$$

To fix its low energy tail of importance for radiative capture processes only its widths Γ_k have to be known in addition to its full strength – fixed by the TRK sum rule for the nuclear dipole strength [18- 21]. Here the relation between GDR pole energy and width, well-established by hydrodynamics, can be generalized for triaxial shapes [22]: $\Gamma_k = c_w \cdot E_k^{1.6}$ with the proportionality factor $c_w \cong 0.45$ resulting from a fit to data for many nuclei with 70<A<240. For two nuclei often considered spherical the TLO sum for the IVGDR is compared in Fig. 1 to rescaled [24] data; the three poles are indicated as black bars. Obviously the fit is in accord to the prediction – in contrast to the single Lorentzian (SLO) ansatz [23], which clearly exceeds the TRK sum rule, and the difference between the two increases with decreasing photon energy. This feature is of large importance for radiative capture which populates an excitation energy region of high level density $\rho(E_x)$, when E_x is close to S_n, i.e. E_γ is small. At such small energy $f_1(E_\gamma)$ is determined for TLO solely by the width parameter; the use of axis ratios from CHFB supports the validity of the TRK sum rule. When account is made for instantaneous shape sampling (ISS) [24] due to the variance of the deformation parameters [13] TLO describes the IVGDR peak even better. In nearly all cases studied so far the TLO prediction is below experimental data [17, 19, 24] acquired by photon scattering or other radiative processes under adoption of the Axel-Brink hypothesis [15, 25]. Thus

clear experimental evidence is missing which would imply a need for energy dependent strength reductions proposed on the basis of IVGDR fits neglecting triaxiality [23, 26].

At energies below S_n photon strength components, which are not of isovector electric dipole character, contribute to radiative capture [23, 26-30]. Respective information from photon scattering [31-33] is of use, asserting equal integrated strength for collective modes based on nuclear ground states and those on top of excited states [15, 25]. Minor strength, partly of other multipolarity, may also be derived from the analysis of gamma-decay following nuclear reactions [34-36] and our analysis investigates its importance. Two such components, both depending on the deformation β, have considerable impact on the predictions for radiative capture, as shown in Fig. 1 and later in Ch. 4:

1. Orbital magnetic dipole strength (scissors mode [32, 36]), which is approximated to peak at $E_{sc} = 0.21 \cdot E_0$ with a maximum strength of $Z^2 \cdot \beta^2 / 45$ GeV^{-3}.
2. Electric dipole strength originating from coupled 2^+ and 3^--phonons [31] is assumed to peak around $E_{quad} + E_{oct} = E_{qo} \approx 2\text{-}4$ MeV with a height of $Z \cdot A \cdot \beta^2 \cdot E_{qo} / 200$ GeV^{-3}.

For both a Gaussian distribution with σ = 0.6 MeV is assumed and it is admitted, that the guesses as presented here can only serve as a very first hint on the eventual role of these strength components.
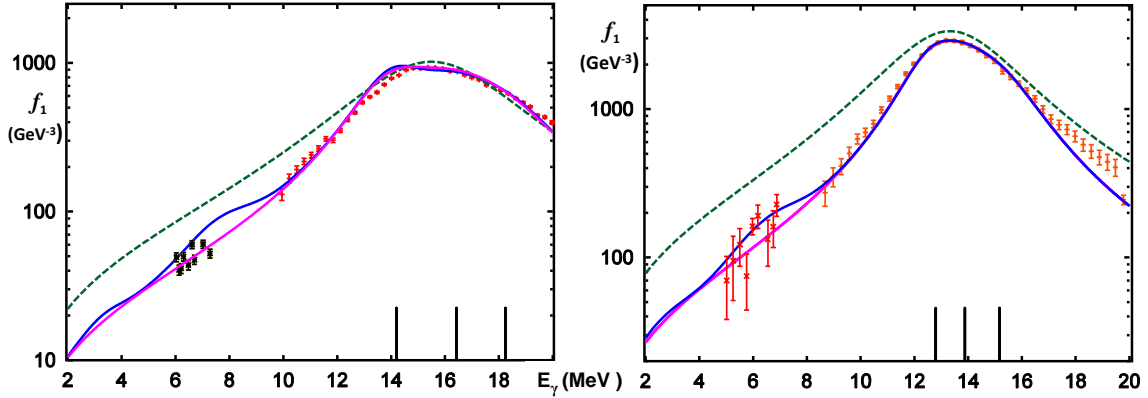
Fig. 1: The photon strength in comparison to a SLO-fit (dashed green) and TLO (magenta) with ISS, which is not included in the lines depicting the sum of 'minor' components and TLO (blue).
Left panel: The data above S_n are from photo-neutron data on ^{nat}Ag [34] and the ones below are derived from gamma decay subsequent to resonant neutron capture ^{105}Pd(n,γ) [26].
Right panel: Photon strength derived from the photo-neutron cross section (+, [34]) on ^{197}Au; also shown are photon scattering data (×, [15]) obtained with a quasi-monochromatic beam.

3   Level densities in triaxial nuclei

Since long the experimentally observable level density $\rho(E_x)$ is known to change strongly with nuclear deformation: An enhancement of $\rho(E_x)$ caused by allowing rotational bands on top of each intrinsic state was predicted [3, 4] to depend on axial symmetry and in the limit of low spin I one gets:

$$\rho(E_x, I) \longrightarrow \frac{2I+1}{\sqrt{8\pi}\ \sigma} \cdot \rho_{\text{int}}(E_x) \quad \text{for axial,}$$

$$\text{and } \rho(E_x, I) \longrightarrow \frac{2I+1}{4} \cdot \rho_{\text{int}}(E_x) \quad \text{for triaxial nuclei, assuming } \Re \text{ - symmetry} \tag{2}$$

Compared to the spherical case the enhancement is around 50 for one rotational degree of freedom (axial case) and this is considered 'standard' enhancement [23]. But, as obvious from Eq. (2), the effect of two extra rotational axes amounts to another factor of ≈ 6, when a typical spin dispersion (or cut off) factor of $\sigma \approx 5$ is assumed. But surprisingly such a large collective enhancement has not yet been included in comparisons to respective data. Seemingly a satisfying agreement was reached without this factor, such that the new finding of triaxiality being a very widespread property of heavy nuclei may require a compensating factor *e.g.* in the prediction for the intrinsic state density $\rho_{\text{int}}(E_x)$.

For $\rho_{\text{int}}(E_x)$ usually [23, 37] a distinction is made between a superfluid (Bosonic) phase below and a Fermi gas description above a critical temperature $t_c = \Delta_o \cdot e^C / \pi = 0.567 \cdot \Delta_0$, with the Euler constant C and the paring gap approximated by $\Delta_0 = 12 \cdot A^{-1/2}$. In both phases the level density ρ and the average level distance D are given by the nuclear entropy S with an additional term containing the determinant d of the matrix resulting from the use of the saddle point approximation [3, 23, 37]:

$$\rho_{\text{int}}(E_x) \approx \frac{e^S}{\sqrt{d}}; \quad D_{\text{int}}(E_x) \approx \frac{\sqrt{d}}{e^S} \tag{3}$$

In a Fermi gas the level density parameter "a" relates the temperature t to the entropy S. Its main component is proportional to the mass number A divided by the Fermi energy $\varepsilon_F = 37\ MeV$:

$$a = \frac{\pi^2 A}{4\ \varepsilon_F} + \frac{A^{2/3}}{7} \tag{4}$$

It corresponds to the expectation for nuclear matter [3]. For the only free parameter, the small surface term, an expression [3, 23] is used here, which agrees to an average yielding a reasonable agreement to fission data [37, 38]. The widespread habit to further modify a – proposed as phenomenological inclusion of shell effects or even taken as a free local fit parameter [23, 37] – is avoided here to suppress any mutual interference between the A and E-dependence of $\rho_{\text{int}}(E)$. The energy shift related to pairing is A-dependent and is usually [23] quantified by pairing gap Δ_0 and condensation energy $E_c = \frac{3a}{2\pi^2} \cdot \Delta_0^2$. As shown in Eq. 6 the zero energy for the Fermi gas is shifted from the excitation energy E_x by E_s, which we take as $E_s = E_c + n \cdot \Delta_0$. This shift exceeds values used previosly [23, 37], but it avoids the inconsistencies in the description of pairing effects, which appear for light nuclei in earlier work – as recently demonstrated [39]. Here the reduction resulting from the large shift counteracts the enhancement in level density due to triaxiality. Account for the ground state pairing is taken by setting n to 0, 1 and 2 for odd-odd, odd and even nuclei. This choice assigns $\rho_{\text{int}}(E)$ to odd-odd nuclei, as was also done for previous back-shifted Fermi-gas calculations [3, 23, 38].

The account of shell effects makes use of the shell correction δW_o already known from a liquid drop model fit to ground state masses [40] as compiled for RIPL-3 [23] in a table together

with the deformation energy calculated within the liquid drop model. This energy was subtracted here as correction to account for ground state deformations. A reduction of the shell correction is included at variance to previous work [23], but in a similar way as discussed years ago [3] and performed before [41]. It varies with temperature t (*i.e.* excitation) by

$$\delta W(t) = \delta W_0 \cdot \frac{\tau^2 \cosh \tau}{(\sinh \tau)^2} \quad \begin{array}{c} \xrightarrow{t \to \infty} 0 \\ \xrightarrow{t \to 0} \delta W_0 \end{array} \; ; \quad \tau = \frac{2\pi^2 t}{\hbar \varpi_{sh}} A^{1/3}; \quad \hbar \varpi_{sh} \cong \frac{1.4 \hbar^2}{r_0^2 m_N A^{1/3}} \tag{5}.$$

In the Fermi gas regime ($t > t_c$) one has correspondingly for entropy S, energy E_x and determinant d

$$S = 2at - \frac{\delta W(t)}{t} + \frac{\delta W_0}{t} \frac{\tau}{\sinh(\tau)} \quad \begin{array}{c} \xrightarrow{t \to \infty} 2at \\ \xrightarrow{t \to 0} 0 \end{array} \; ; \quad E_x = at^2 - \delta W(t) + E_s \quad \begin{array}{c} \xrightarrow{t \to \infty} E_s + at^2 \\ \xrightarrow{t \to 0} E_s - \delta W_0 \end{array} \; ; \quad d = \frac{18}{\pi} \cdot t^2 \cdot S^3 \tag{6}.$$

As obvious, the damping does not depend on any additional parameter as it is determined by the average frequency ω_{sh} of the harmonic oscillator determined by radius parameter r_0 and nucleon mass m_N alone. This reduction of the number of free parameters is an advantage over previous proposals for a generalized superfluid model [23, 37]. Additionally the limits for large and small t are determined separately for S and E_x (cf. Eq. (6)) and are thus under independent control.

Knowing δW_0 the intrinsic level density $\rho(E_x)$ can be calculated from Eqs. (3) to (7) for the Fermi gas regime as well as the values for S, E_x and d at the critical point of transition. Below $E_x(t_c)$ an interpolation to the ground state is used which complies with rules for a Bose gas, *i.e.* no zero point energy and thus no backshift are indicated. The rules $(S-S_0) \cdot t \propto E_x$ and $E_x \propto t^{2.5}$ result in $(S-S_0) \propto E_x^{0.6}$ with the proportionality factor adjusted to have a continuous transition at $E_x(t_c)$ and $S_0 = \Delta/t_c \cong 1.76$ for an odd nucleus [36]. With the additional setting of $d = d_c = const.$ an energy dependence of ρ close to previous work [37, 42] is obtained, characterized by a nearly constant logarithmic derivative of $\rho(E_x)$, the inverse of the 'spectral' temperature T. As was pointed out [3], T is usually somewhat larger than the parameter t. A comparison of the presented ansatz to the experimental data compiled in the database of RIPL-3 [23] is depicted in Fig. 2 for more than 100 nuclei with A>70. For the region below $E_x(t_c)$ calculated averages of T are compared to corresponding values extracted by various authors [23, 43, 44] from information on nuclear level schemes (Fig. 2(a)); in view of the scatter in these the agreement to the prediction is satisfactory. Another comparison uses the average distance of s-wave resonances seen with neutron capture in even target nuclei [45, 23]. As these all have spin ½$^+$, a comparison of these data to our prediction is free from spin cut-off ambiguities and it is worthwhile noting that for spin ½ the small J limit differs from a more complete approximation by a few % only. Fig. 2(b) shows the resulting level distances at S_n including the effect of triaxiality. The possible influence of parity on the level density is neglected here, but vibrational enhancement was investigated by inserting $\hbar\omega_{vib} = E_2(2^+)$ and $\hbar\omega_{vib} = E_3(2^+)$ in the respective expression [4] with the excitation energies $E_x(2^+)$ taken from the CHFB calculations; it would contribute less than 20%.
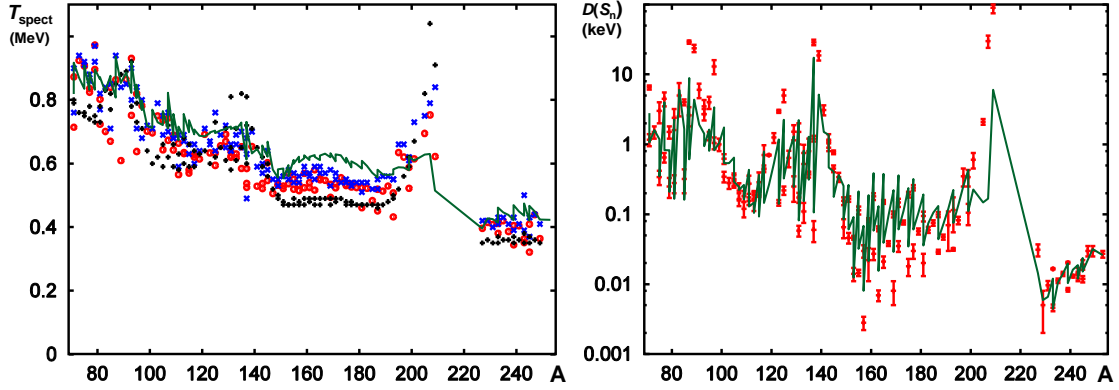
Fig. 2: Comparison of experimental level density information to predicted results presented as green line. **(a)**: Spectral temperature averaged between 1 MeV and S_n.   **(b)**: Average resonance distance near S_n.

Apparently nearly all of the measurements lie close to the prediction and an improved agreement may result from the inclusion of vibrational enhancement, as well as from parity effects. For A≈208 no agreement can be expected and it is of interest to find out, what reduction of collective enhancement near closed shells leads to an even better global fit. With respect to the intrinsic level density $\rho_{int}(E_x)$ an important influence on $\rho(E_x, J)$ was found to emerge from the choice made for δW_0: Replacing the shell effect from ref. [40] by one of the others also listed [23] modifies the level density for actinide nuclei by up to a factor of five. As this difference is less for smaller A the A-dependence of δW_0 may need further theoretical study.

4   Radiative neutron capture

The good agreement of the low energy slopes of the IVGDR to a 'triple Lorentzian' parameterization (TLO) as obtained by using independent information on triaxial nuclear deformation suggests the use of a corresponding photon strength function also for the radiative neutron capture, an electromagnetic processes alike. To test the influence of dipole strength functions on radiative neutron capture over a wide range in A the investigation of only even-even target nuclei has the advantage of offering a large sample with the same spin. For the ℓ-wave capture by spin 0 nuclei the assumption $\Gamma_\gamma \ll \Gamma_n$ and the neglect of any ℓ-dependent neutron strength enhancement leads to the cross section [46]   :

$$\langle \sigma_R(n, \gamma) \rangle \cong 2(2\ell+1)\pi^2 \lambda_n^2 \cdot \rho(E_R, \tfrac{1}{2}^+) \cdot \langle \Gamma_{R\gamma}(E_\gamma) \rangle; \qquad \langle \Gamma_{R\gamma}(E_\gamma) \rangle = \int M_t \rho_{int}(E_f, J_f) E_\gamma^3 f_1(E_\gamma) dE_\gamma. \qquad (7)$$

The factor M_t accounts for the number of magnetic sub-states reached by the γ-decay in comparison to the number of those populated by capturing the neutron. In view of Eq. (2) it is assumed here that for λ=1-transitions from $J_R = 1/2^+$ to $J_f = 1/2$ and $J_f = 3/2$ the quantum-statistical part of M_t is 5. In the region well above separated resonances Porter-Thomas fluctuations [14, 15], albeit reduced by averaging over a large number of neutron resonances R, a correction factor needs to be included. From statistical calculations a value of 0.85 was derived bringing M_t to 4.3. It was pointed out previously [26] that strength information can be extracted from capture data directly by regarding average radiative widths $\langle \Gamma_\gamma \rangle$. Equation (7) shows, that these are proportional to the photon strength, and depend in addition on the ratio between the level densities at the capturing resonances - included in $f_1(E_\gamma)$ - and the final states reached by the γ-decay. Consequently the

140

average radiative widths vary with the slope of $\rho(E_x)$ in the energy range reaching from E_f to E_R, equivalent to the spectral temperature T [3, 23, 43, 44], whereas capture cross sections also vary with the level density at S_n. A good agreement is found [18] between the $\langle\Gamma_\gamma\rangle$ predicted from TLO and average radiative widths as derived by a resonance analysis of neutron data taken just above S_n and tabulated [45] for over 100 even-odd nuclei with A > 70.

As shown in Fig. 3 (a) the agreement between predicted neutron capture cross sections for Th-, U- and Pu-nuclei and data is satisfactory on an absolute scale. As depicted for ^{238}U the minor photon strength as discussed in the end of Ch. 2 is important: The dashed curve corresponds to TLO alone and the drawn one has the orbital M1 strength included as well as the vibrational coupling E1. The dipole components other than isovector E1 known [24, 26-30, 35, 36] for higher E_γ are suppressed by the steep decrease of $\rho_{int}(E_x)$ and strength at low E_γ suffers from the factor E_γ^3 in Eq. (7) [28, 30]. The dotted curve indicates the predicted cross section when p-wave capture is approximately included. The good agreement to actinide data within ≈ 30 % as seen in Fig. 3 (a) gives a convincing impression for the validity of the parameterization presented and the approximations applied.
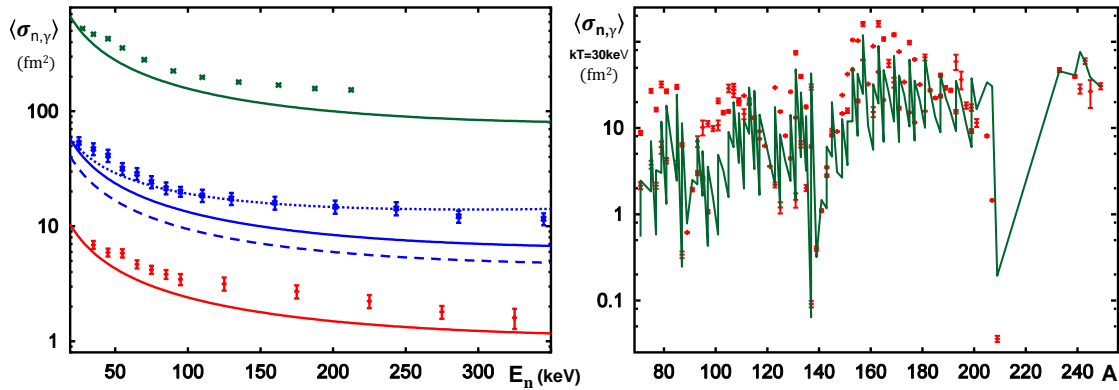
Fig. 3: Comparison of calculated neutron capture cross sections σ(n,γ) to experimental data (in fm²) [34]. **(a):** Dependence on E_n for targets of (bottom to top) **(b):** Maxwellian averaged cross sections vs. A ^{240}Pu (red, ×10), ^{238}U (blue) and ^{232}Th(green, ÷10). for $kT_{AGB} = 30$ keV.

To cover the full range of A>70 in the comparison to data Maxwellian averaged (MACS) neutron capture cross sections are shown in Fig. 3 (b) together with the prediction made by folding of the cross sections as given by Eq. (7) with a Maxwellian distribution of neutron energies [2]. MACS have been tabulated [47] covering many heavy nuclei as they are of use for the investigation of nuclear processes in cosmic objects like red giant (AGB) stars, where radiative neutron capture takes place at approximately $kT_{AGB} = 30$ keV. For several actinide nuclei equivalent data were compiled [48] and uncertainty bars were derived from the scatter as published. In view of the fact that D $\gg \Gamma_R \geq \Gamma_{R\gamma}$ the Maxwellian averages around 30 keV are formed incoherently and fluctuations (beyond the ones mentioned above) are neglected. By only regarding the radiative capture by spin-zero targets effects related to ambiguities of spin cut off parameter and angular momentum coupling are suppressed, but still the data vary by about 4 orders of magnitude in the discussed range of A – and they are well represented by the TLO-parameterization used here together with the schematic ansatz for ρ (A, E_x), as described by Eqs. (2) – (6). The discrepancy observed in the region of A≈90 may well be related to the omission of p-capture here, which is known to be especially important in that mass range [23, 37]. This and other local effects have no significance on the stated importance of triaxiality in heavy nuclei – the main topic here.

5 Conclusions

In agreement to various spectroscopic information available for a number of heavy nuclei [6, 9-12] two effects – hitherto not emphasised as such – indicate triaxiality for nearly all of them (with A > 70):

1) the scheme proposed for the prediction of level densities nicely reproduces observations for nuclei with $J_0 = \frac{1}{2}$, when the collective enhancement due to symmetry reduction by triaxiality is included and the recently detected [39] inconsistency is avoided by fixing the Fermi gas zero point energy, *i.e.* the backshift, to the sum $E_c + n \cdot \Delta_0$;

2) the triple Lorentzian photon strength (TLO) not only improves the fit to the shape of the IVGDR peak in accord to the TRK sum rule, but it also predicts its low energy tail – without additional modification – to match respective strength data as well as neutron capture cross section data in the energy range of unresolved resonances.

For the last-mentioned finding a combination of the points 1) and 2) is needed, which is easily performed by using axis ratios from a sufficiently global calculation like CHFB [13]. But actually the exact deformation parameters are unimportant for the low spins occurring in neutron capture by even targets as neither spin cut off nor moments of inertia are involved (cf. Eq. (2)). Beyond previous knowledge the triaxiality of most heavy nuclei is established by the fact that for more than 100 spin-0 target nuclei with 70<A< 244 experimental data on level distances and average capture cross sections are well predicted. The global ansatz as presented here may thus be considered a very good starting point for network calculations in the field of stellar element production as well as for simulations of nuclear power systems and the transmutation of radioactive waste. Here the applicability up to actinide nuclei is of importance and a non-negligible effect of 'minor' photon strength other than isovector electric is indicated. The literature study performed within this investigation on the available information from previous experimental data indicates that minor magnetic and electric dipole strength increase the radiative capture cross section by approximately up to 40%. The size of this enhancement calls for new experimental investigations of photon strength in the region of 3-5 MeV. The fact that TLO does not exceed data for (a) photon strength in the region below S_n [5, 17-19, 21, 24] and (b) radiative neutron capture cross sections [34] as depicted in Fig. 3 (and analysed in many other nuclei besides the actinides shown) can be considered a rather stringent test of the global parameterization proposed for electric isovector strength.

When previous investigations in this field [*e.g.* 26] have worked with a smaller strength in the IVGDR tail leading to a larger relative influence of 'minor' strength components this indicates the significant impact of a triple Lorentzian scheme in comparison to single or double IVGDR fits, which – as we believe – result in erroneous estimates of the corresponding E1-strength. Here the often assumed dependence of the resonance widths on gamma-energy plays an important role. This is especially so if theory-based modifications [26] are imposed to seemingly improve f_{E1} at small energies without much of a change in the peak region. In the TLO approach the variation of Γ_{E1} solely with the pole energy, its use of only two global parameters and the strict accord to the TRK sum rule result in a global dipole strength prediction for the tail region which has a regular A-dependence. This sheds some doubt on E1 strength predictions presented by RIPL-3 [23] which seem to imply such irregularities. TLO is based on assuming triaxial shapes of nearly all heavy nuclei away from [208]Pb and the good agreement to level distance data by a description of collective enhancement assuming non-axiality as well as well predicted radiative capture data confirms this finding. As also this level density description needs only one new global parameter the predictive power for compound nuclear reaction rates is clearly remarkable. Regarding the rather limited

theoretical work done so far [8, 13] the importance of broken axial symmetry already at low spin – as documented here – should induce further investigations.

Acknowledgements

References

[1]   M. Salvatores and G. Palmiotti, Prog. Part. Nucl. Phys. 66 (2011) 144; E. Sartori, Ann. Nucl. Energy E 34 (2007) 550.

[2]   F. Käppeler et al., Rev. Mod. Phys. 83 (2011) 157.

[3]   A. Bohr and B. Mottelson, Nuclear Structure ch. 2, 4 & 6, (Benjamin, Reading, Mass., 1975).

[4]   S. Bjornholm, A. Bohr, B. Mottelson, Rochester-conf., IAEA-STI/PUB/347 (1974) 367.

[5]   A.R. Junghans et al., Phys. Lett. B 670 (2008) 200.

[6]   K. Kumar, Phys. Rev. Lett. 28 (1972) 249.

[7]   S. Raman et al., At. Data and Nucl. Data Tables 78 (2001) 1.

[8]   A. Hayashi, K. Hara, P. Ring, Phys. Rev. Lett. 53 (1984) 337.

[9]   D. Cline, Ann. Rev. Nucl. Part. Sci. 36 (1986) 683.

[10]   W. Andrejtscheff and P. Petkov, Phys. Rev. C 48 (1993) 2531; id., Phys. Lett. B 329 (1994)1.

[11]   C. Y. Wu and D. Cline, Phys. Rev. C 54 (1996) 2356.

[12]   Y. Toh et al., Phys. Rev. C 87 (2013) 041304.

[13]   J.-P. Delaroche et al., Phys. Rev. C 81 (2010) 014303.

[14]   P. Axel et al., Phys. Rev. C 2 (1970) 689.

[15]   G. A. Bartholomew et al., Adv. Nucl. Phys. 7 (1972) 229.

[16]   W.D. Myers et al., Phys. Rev. C 15 (1977) 2032.

[17]   E. Grosse et al., AIP Conf. Proc. 1090, 308 (2009); //link.aip.org/link/doi/10.1063/1.3087034.

[18]   R. Beyer et al., Int. Journ. of Mod. Phys. E20 (2011) 431.

[19]   A.R. Junghans et al., Journ. Korean Phys. Soc. 59 (2011) 1872.

[20]   M. Gell-Mann et al., Phys. Rev. 95 (1954) 1612.

[21]   E. Grosse et al., Eur. Phys. Journ., Web of Conf. 21 (2012) 04003; http://dx.doi.org/10.1051/epjconf/20122104003.

[22]   B. Bush and Y. Alhassid, Nucl. Phys. A 531 (1991) 27.

[23]   R. Capote et al., Nucl. Data Sheets 110 (2009) 3107; id., //www-nds.iaea.org/RIPL-3/

[24]   M. Erhard et al, Eur. Phys. Journ. A 27 (2006) 135.

[25]   P. Axel, Phys. Rev. 126, 671 (1962); D. Brink, Ph.D. thesis, Oxford (1955).

[26]   J. Kopecky and M. Uhl, Phys. Rev. C 41 (1990) 1941.

[27]   M. Krticka et al., Phys. Rev. Lett. 92 (2004) 172501.

[28]   G. Schramm et al., Phys. Rev. C 85 (2011) 014311.

[29]   G. Rusev et al., Phys. Rev. C 87 (2013) 054603.

[30]   R. Massarczyk et al., Phys. Rev. C 86 (2012) 014319; id., Phys. Rev. C 87 (2013) 044306.

[31] U. Kneissl et al., J. Phys. G 32 (2006) R217; id., Nuclear Physics News 16 (2006) 27.

[32] K. Heyde et al., Rev. Mod. Phys. 82 (2010) 2365.

[33] E. Grosse and A.R. Junghans, Landolt-Börnstein, New Series I, 25 (2013) 4.

[34] NNDC database: http://www.nndc.bnl.gov/exfor/exfor00.htm and .exfor/endf00.jsp

[35] T.D. Poelhekken et al., Phys. Lett. B 278 (1992) 423.

[36] M. Guttormsen et al., Phys. Rev. Lett. 109 (2012) 162503; id., Phys. Rev. C 88, 024307; id., Phys. Rev. C 63 (2001) 044301.
37

[37] A.V. Ignatyuk et al., Phys. Rev. C 47 (1993) 1504; id., IAEA-INDC 0233 (1985) 40.

[38] A.R. Junghans et al., Nucl. Phys. A 629 (1998) 635.

[39] K.-H. Schmidt and B. Jurado, Phys. Rev. C 86 (2012) 044322.

[40] W.D. Myers and W.J. Swiatecki, Nucl. Phys. 81 (1966) 1; id., Ark. Fizik, 36 (1967) 343.

[41] S. K. Kataria, V. S. Rarnamurthy, and S. S. Kapoor, Phys. Rev. C 81 (10) 047302.

[42] S.F. Mughabghab and C.L. Dunford, Phys. Rev. Lett. 81 (1998) 1504.

[43] T. v. Egidy and D. Bucurescu, Phys. Rev. C 78 (2008) 051301.

[44] A. Koning et al., Nucl. Phys. A 810 (2008) 13.

[45] A.V. Ignatyuk, RIPL-2, IAEA-TECDOC-1506 (2006); www-nds.iaea.org/RIPL-3/resonances

[46] H. Feshbach et al., Phys. Rev. 71 (1947) 145; id., Phys. Rev. 87 (1952) 366.

[47] I. Dillmann et al., Phys. Rev. C 81, 015801 (2010); id., AIP Conf. Proc. 819, 123; //www.kadonis.org.

[48] B. Pritychenko et al., At. Data and Nucl. Data Tables 96 (2010) 645; www.nndc.bnl.gov/astro.

Status of the general description of fission observables by the GEF code

B. Jurado[1] and K.-H. Schmidt[1]
[1]CENBG, CNRS/IN2P3, Chemin du Solarium, B. P. 120, 33175 Gradignan, France

Abstract

The GEneral Fission (GEF) model treats spontaneous fission and fission up to an excitation energy of about 100 MeV of a wide range of heavy nuclei. GEF makes use of general laws of statistical and quantum mechanics, assuring a high predictive power. It is unique in providing a general description of essentially all fission observables in a consistent way while preserving the correlations between all of them. In this contribution we present some of the physical aspects on which the model is based, give an overview on the results that can be obtained with the code and show an example that illustrates how the GEF code can serve as a framework for revealing the sensitivity of the fission observables to some basic nuclear properties.

1   Introduction

During several short-term visits that were financed by the EFNUDAT and by the ERINDA projects, the semi-empirical GEneral Fission model GEF has been developed and continuously extended. The GEF code provides results for fissioning nuclei ranging from polonium to seaborgium up to excitation energies of 100 MeV including multi-chance fission. Contrary to most of the existing fission models, GEF gives also reliable results for nuclei where no experimental information is available. GEF is a Monte-Carlo code and calculates for each fission event all the properties of the two fission fragments at scission: mass, charge, excitation energy and angular momentum, as well as the fission-fragment kinetic energies. In addition, GEF treats the deexcitation of the fission fragments and provides the prompt-neutron and prompt-gamma multiplicities associated with each fragment, as well as the prompt-neutron and prompt-gamma kinetic energies and angles. All this information can be delivered by the code on an event-by-event basis and can serve as an event generator for simulation purposes. Because the model is based on robust physical concepts, one can also make use of the correlations between the different physical quantities given by GEF.

2   Physics behind GEF

GEF combines general laws of quantum and statistical mechanics with specific experimental information. A complete description of the code can be found in [1]. In this contribution we concentrate on the main ideas used to derive the global shape of the fission-fragment yields and the partition of the intrinsic excitation energy between the fragments.

2.1   Fission-fragment yields

The fission-fragment yields are determined by the potential energy landscape between the fission barrier and scission as a function of the mass-asymmetry degree of freedom. The microscopic-macroscopic approach has proven to be very useful for calculating nuclear properties, in particular in applications to fission [2]. According to this approach, the shape of the potential

energy on the way to scission is given by the combination of the macroscopic potential, as given by the liquid-drop model, and shell effects. When the two-centre shell model became available, it was possible to study the single-particle structure in a di-nuclear potential with a necked-in shape. Investigations of Mosel and Schmitt [3] revealed that the single-particle structure in the vicinity of the outer fission barrier already resembles very much the sequence of single-particle levels in the two separated fragments. They explained this result by the general quantum-mechanical feature that wave functions in a necked-in potential are already essentially localized in the emerging fragments. This finding means that the microscopic properties of the fissionning system are essentially determined by the shells of the fragments, and only the macroscopic properties are specific to the fissioning system [4]. This "separability principle" is exploited in the GEF code, which relies on empirical information to determine the stiffness of the macroscopic potential and the position and strength of the fragment shells. The latter are valid for all fissioning systems, which explains why the GEF code is able to give results for a very large number of fissioning nuclei with just one single set of parameters. The magnitudes of the shell effects that form the fission valleys and the stiffness parameters in mass-asymmetric distortions are deduced from a global fit of measured mass distributions.
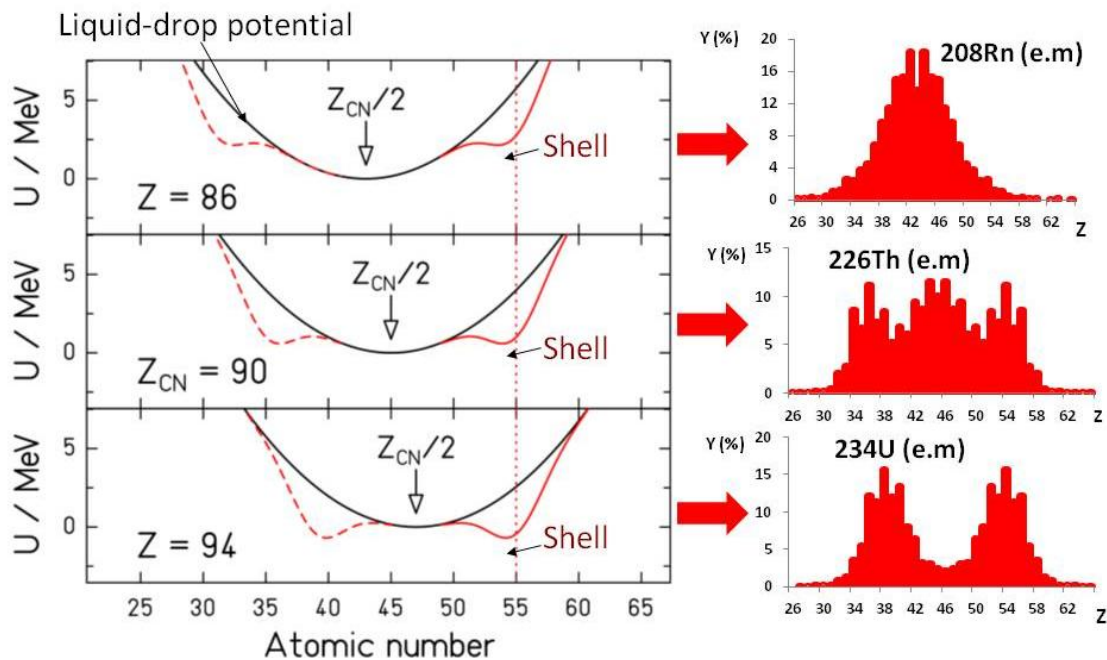
Fig. 1: (Left) Total potential energy (red lines) and macroscopic potential (black lines) as a function of the fragment charge for fissioning nuclei around Th with steps of $4Z_{CN}$ (schematic). The minimum of the macroscopic potential located at symmetry is indicated. One fragment shell located at Z=55 is assumed. (Right) Corresponding variation of the experimental charge distributions around [226]Th obtained in electromagnetic-induced fission [5].

Regarding shell effects, asymmetric fission was initially attributed to the influence of a deformed ($\beta \approx 0.6$) fragment shell at N=88 and the combined influence of the spherical shells at N=82 and Z=50 [6]. However, new data on fission-fragment Z distributions over long isotopic chains [7], reveal very clearly that the position in neutron number varies systematically over more than 7 units, while the position in proton number is approximately constant at Z=54. The rather short isotopic sequences covered in former experiments did not show this feature clearly enough and gave the false impression of a constant position in mass. This finding represents a severe

puzzle to theory, since shell-model calculations [6, 8] do not show any shell stabilization near $Z=54$ at a deformation of $\beta\approx0.6$, which is suggested by the mass-dependent prompt-neutron yields, see below. Therefore, the shell effect close to $Z=54$ is a key input information included in GEF that has a purely empirical origin. Fig. 1 illustrates how the observed transition from symmetric to asymmetric fission around $A=226$ can be explained by the interplay between the macroscopic potential and shell effects. The strength of the shell and its position is fixed for the three fissioning nuclei considered. However, the stiffness and the position of the minimum of the macroscopic potential increase with the mass of the fissioning nucleus. As a consequence, the minimum of the total potential moves from symmetric to asymmetric splits.

2.2   Partition of excitation energy between the fragments

The early manifestation of fragment shells on the fission path, mentioned above, indicates that the fragments acquire their individual characteristics already in the vicinity of the fission barrier. Therefore, at this position the fissioning nucleus consists of two well defined nuclei in contact through the neck. Before scission, the available intrinsic excitation energy E^*_{intr} (given by the sum of excitation energy above the barrier and the dissipated potential energy after the sadle) has to be divided between the fragments. In GEF the excitation-energy partition is determined according to statistical mechanics. It is assumed that the system formed by the two nuclei in contact reaches statistical equilibrium where all the configurations that are energetically possible have the same probability to be populated. Therefore, the partition of excitation energy is determined by a probability distribution that is given by the product of the level densities of the individual fragments. The average excitation energy of the light fragment $<E_L>$ at thermal equilibrium of the light fragment is given by :

$$< E_L > = \frac{\int_0^{E^*_{intr}} E_L \rho_L(E_L)\rho_H(E^*_{intr} - E_L)dE_L}{\int_0^{E^*_{intr}} \rho_L(E_L)\rho_H(E^*_{intr} - E_L)dE_L}. \tag{1}$$

where ρ_L and ρ_H are the level densities of the light and heavy fragment, respectively.
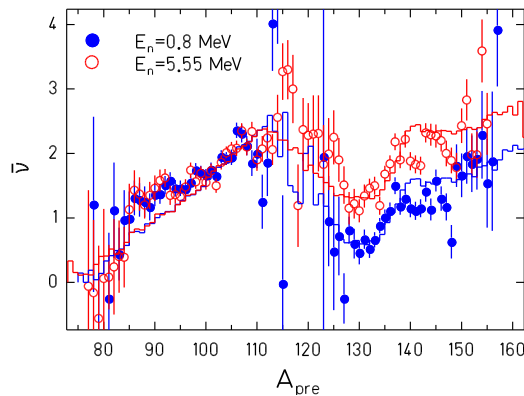
Fig. 2: Measured prompt-neutron yield in ^{237}Np(n,f) as a function of pre-neutron mass at two different incident-neutron energies [9] (data points) in comparison with the result of the GEF code (histograms).

There is increasing evidence [10, 11] that the nuclear level density in the regime of pairing correlations essentially deviates from the widely so-called Fermi-gas level-density formula that had been derived by Bethe [12] for a system of non-interacting Fermions. Due to the gradual

breaking of Cooper pairs, the effective number of degrees of freedom of the nucleus increases strongly, leading to a large heat capacity, and, therefore, the level density as a function of excitation energy is well approximated by an exponential function. This means that the nuclear temperature in the regime of pairing correlations is essentially constant. Thus, the fissioning nucleus represents a very interesting system of two microscopic objects that behave as coupled thermostats with a limited total energy. Because the logarithmic slope of the level densities in the constant-temperature regime is proportional to $A^{2/3}$, the most probable configurations are those where the available excitation energy concentrates in the heavy fragment. In other words, excitation-energy sorting takes place, where the thermal energy is transferred from the light to the heavy fragment [13-15]. The process of energy sorting is clearly reflected by experimental data on prompt-neutron yields. Fig. 2 shows the prompt-neutron yields of the system ^{237}Np(n,f) for two energies of the incoming neutrons. The additional energy introduced by the 5.5-MeV neutrons enhances the prompt-neutron yields in the heavy fission-fragment group, only, while the neutron yields in the light group remain unchanged. Of course, the energy-sorting process ends at scission, and the deformation energy of the individual fragments at scission, that is dissipated after scission, remains in the respective fragment and represents the main source of the saw-tooth like behaviour of the mean mass-dependent prompt-neutron fission yield. In [16] we show that the even-odd effect in fission-fragment elemental yields is the consequence of extreme excitation-energy sorting, i.e., the even-odd effect reflects the preferential population of the ground state of even-even light fragments.

3 Comparison with experimental data and evaluations

In the following figures the results obtained with GEF are compared with experimental data. All the GEF results have been obtained with the same parameter set. Fig. 3 shows the fission-fragment distributions for different systems ranging from the electromagnetic-induced fission of ^{226}Th to the spontaneous fission of ^{258}Fm. It is remarkable that fine structure effects such as the even-odd staggering of the elemental yields of ^{226}Th and the very fast transition from asymmetric to symmetric fission observed when going from ^{256}Fm to ^{258}Fm are very well reproduced by GEF.
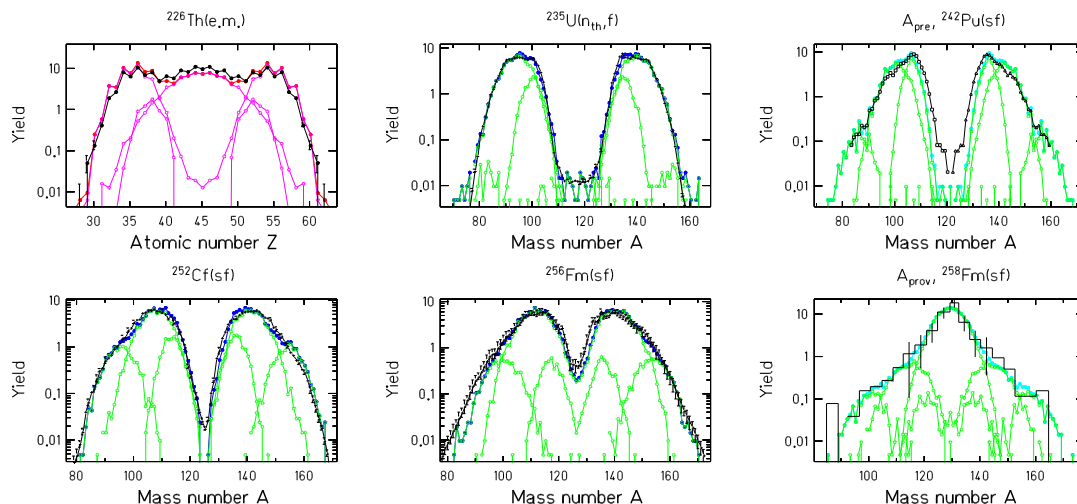
Fig. 3: Mass and Z distributions of fission fragments from spontaneous fission (sf), thermal-neutron-induced fission (n$_{th}$,f) and electromagnetic-induced fission (e.m.). (In most cases the post-neutron masses are shown. A_{prov} is the "provisional mass" that is directly deduced from the ratio of the kinetic energies of the fragments and, thus, it is not corrected for neutron emission.) Measured or evaluated data (black lines, respectively histogram) are compared with predictions of the GEF code (pink and green lines). The contributions of different fission channels are shown. (See [1] for references of the data.)

Fig. 4 shows the variation of the average prompt-neutron multiplicities with incident neutron energy for various fissionning nuclei. The differences between GEF results and the values given by ENDF/B-VII.1 amount to less than 0.2 neutrons for all systems. Note that the prompt-neutron multiplicity is a very complex quantity that strongly depends on the particular shape of the fragment yields and on the properties of the fragments at scission. It is not possible to simply extrapolate this quantity from one fissioning nucleus to another because the shapes of the yields can strongly vary for neighbouring fissioning nuclei, as shown for instance for ^{256}Fm and ^{258}Fm in Fig. 3. GEF results for the average number of neutrons as a function of the fragment mass for ^{237}Np at two incident neutron energies are presented in Fig. 2. The increase of the neutron yields of the heavy fragments when the incident energy increases is very well reproduced by GEF thanks to the inclusion of the energy-sorting process.
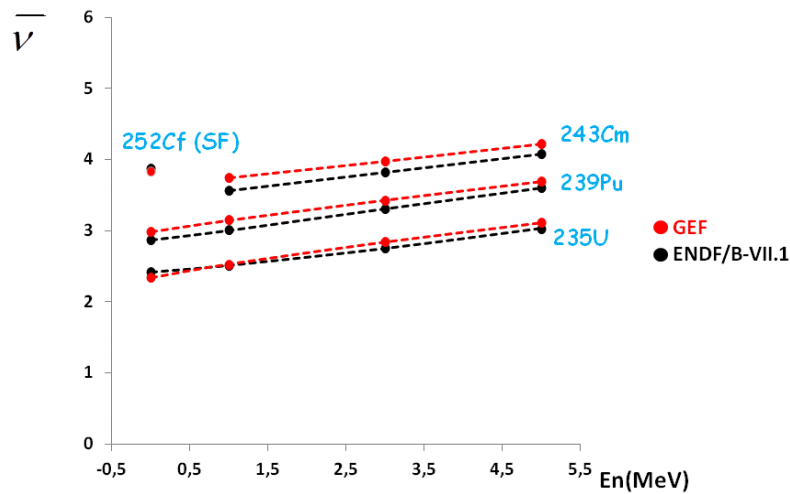
Fig. 4: Average prompt-neutron multiplicities as a function of neutron energy for different fissioning nuclei.

The experimental prompt fission-neutron spectrum for the system ^{235}U(n_{th},f) [17] is compared with results of the GEF code in Fig. 5. In order to better visualize the deviations, the right panel shows a reduced presentation with the spectrum normalized to a Maxwellian distribution with the parameter T= 1.32 MeV. The GEF code reproduces the data very well. Good agreement has also been found with the experimental fission-prompt-neutron spectra of ^{252}Cf(sf), ^{240}Pu(sf) and ^{239}Pu(n_{th},f) [1]. This qualifies the GEF code for estimating prompt-neutron spectra in cases where experimental data do not exist. It also seems to be a suitable tool for improving evaluations.

4   GEF: a useful tool for reactor physics

The previous figures show that GEF has acquired an accuracy that meets the requirements of technical applications. Indeed, GEF fission-fragment yields will be part of the next edition of the JEFF library. Moreover, different features have been developed to facilitate the use of GEF results in reactor physics. The most important ones are:

-The independent and cumulative yields of GEF are available in ENDF format (GEFY) [18].

-There is also a deterministic version of GEF in the form of a subroutine (GEFSUB) that can be linked to deterministic codes like e.g. TALYS or EMPIRE [1].

-Error bars for yields from perturbed model parameters including the covariance matrix for yields are available [1]. The covariance matrix is determined by the correlations between the yields of different nuclides according to the underlying physics of the model.

-GEF also calculates the production of isomers [1].

149
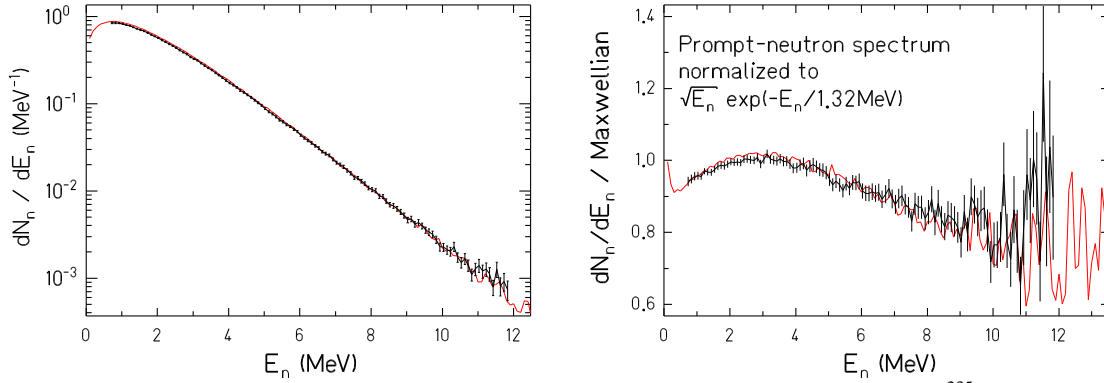
Fig. 5: Experimental prompt-fission-neutron spectra (black lines and error bars) for ^{235}U(n$_{th}$,f) [17] in comparison with the result of the GEF code (red lines). In the right panel the spectra have been normalized to a Maxwellian with $T = 1.32$ MeV.

5 GEF: a useful tool for fundamental physics

As has been shown above, the GEF model has been developed within a global approach where the same description is used for all fissioning nuclei. There is no local parameter adjustment and the tuning of the model parameters within a certain region of fissioning nuclei has naturally an impact also for fissioning systems located in a different region. This is a powerful feature that can help to reveal some basic nuclear properties. In this contribution we will illustrate how the GEF code has revealed the presence of a shell effect at Z=44. The accurate reproduction by GEF of the mass distribution for ^{239}Pu(n$_{th}$,f) and other neighbouring fissioning nuclei can only be obtained by the inclusion of a shell effect at Z=44 that increases the yields in the light-fragment side close to A~105 and the complementary heavy fragments. This shell has no mayor impact for lighter actinides. However, it has a significant influence on the yields of relatively light neutron-deficient fissioning nuclei like ^{180}Hg, where an asymmetric mass distribution has recently been measured [19]. As can be seen in Fig. 6, the mass distribution given by GEF changes from a symmetric to an asymmetric shape when the shell effect at Z=44 is included. The asymmetric distribution shown on the right part of Fig. 6 has been calculated assuming an excitation energy of 12 MeV. However, in the measurement the ^{180}Hg nuclei are populated after the beta decay of ^{180}Tl. They follow an excitation-energy distribution that is not well defined and can cover energies below and above 12 MeV. This can explain, at least partly, the differences found between GEF and the data on the right panel of Fig. 6.
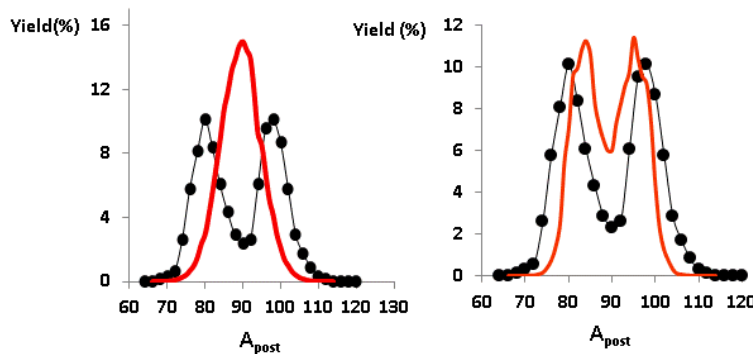
Fig. 6: Experimental post-neutron fission-fragment mass distribution of ^{180}Hg [19] (black dots) compared to GEF results (red lines). The shell effect at Z=44 is only included in the GEF calculation shown in the right panel.

6 Conclusions and perspectives

The GEF model gives reliable predictions for essentially all fission observables of a broad range of fissioning nuclei, including nuclei where no experimental data exist. The GEF model combines physical concepts from quantum mechanics and statistical mechanics with specific experimental information within a general approach where the same description is applied to all the fissioning systems. In this contribution we have shown that GEF results are in good agreement with experimental data on fission-fragment distributions, prompt-neutron yields and prompt-neutron energy spectra of different fissioning nuclei. The accuracy of GEF meets the requirements of technical applications. As a consequence, fission-fragment yields given by GEF will be included in the next edition of the JEFF library. GEF can also be very useful for investigating fundamental nuclear properties. As an example, GEF has revealed the existence of a shell effect at Z=44 that has some influence on the fission-fragment mass distributions of heavy actinides like ^{239}Pu and explains the asymmetric character of the mass distribution of light neutron-deficient nuclei such as ^{180}Hg.

GEF is constantly improved. Some of the foreseen developments are the inclusion of ternary fission, the treatment of proton-, electron- and photon-induced fission and the incorporation of more detailed nuclear-structure information of the fission fragments. We will also perform a quantitative assessment of the deviations between GEF and experimental and evaluated data.

Acknowledgement

References

[1] http://www.cenbg.in2p3.fr/GEF or http://www.khs-erzhausen.de/GEF (and references therein)

[2] M. Brack et al., Rev. Mod. Phys. **44**, 320 (1972)

[3] U. Mosel, H. W. Schmitt, Nucl. Phys. A **165,** 73 (1971)

[4] K.-H. Schmidt, A. Kelic, M. V. Ricciardi, Europh. Lett. **83**, 32001 (2008)

[5] K.-H. Schmidt et al., Nucl. Phys. A **665**, 221 (2000)

[6] B. D. Wilkins, E. P. Steinberg, R. R. Chasman, Phys. Rev. C **14,** 1832 (1976)

[7] C. Boeckstiegel et al., Nucl. Phys. A **802**, 12 (2008)

[8] I. Ragnarsson, R. K. Sheline, Phys. Scr. **29**, 385 (1984)

[9] A. A. Naqvi, F. Kaeppeler, F. Dickmann, R. Mueller, Phys. Rev. C **34,** 218 (1986)

[10] M. Guttormsen et al., Phys. Rev. C **68**, 034311 (2003)

[11] K.-H. Schmidt, B. Jurado, Phys. Rev. C **86**, 044322 (2012)

[12] H. A. Bethe, Phys. Rev. **50**, 332 (1936)

[13] K.-H. Schmidt, B. Jurado, Phys. Rev. Lett. **104**, 212501 (2010)

[14] K.-H. Schmidt, B. Jurado, Phys. Rev. C **83**, 014607 (2011)

[15] K.-H. Schmidt, B. Jurado, Phys. Rev. C **83**, 061601 (2011)

[16] K.-H. Schmidt, B. Jurado, submitted to Phys. Rev. Lett.

[17] N. V. Kornilov et al., Nucl. Science Engin. **165**, 117 (2010)

[18] http://www.cenbg.in2p3.fr/GEFY or http://www.khs-erzhausen.de/GEFY

[19] A. N. Andreyev et al., Phys. Rev. Lett. **105**, 252502 (2010)

Electromagnetic dipole strength distribution in ^{124,128,132,134}Xe below the neutron separation energy

R. Massarczyk[1,2], *R. Schwengner*[1], *F. Dönau*[1], *S. Frauendorf*[3], *D. Bemmerer*[1], *R. Beyer*[1,2],
M. Butterling[1,2], *R. Hannaske*[1,2], *A. Junghans*[1], *T. Koegler*[1,2] *G. Rusev*[4,5], *K.D. Schilling*[1],
G. Schramm[1,2] , *A . P. Tonchev*[4,5], *W. Tornow*[4,5], *A. Wagner*[1]

[1]Institute of Radiation Physics, Helmholtz-Zentrum Dresden-Rossendorf, 01328 Dresden, Germany
[2]Technische Universität Dresden, 01062 Dresden, Germany
[3]University of Notre Dame, Notre Dame, Indiana 46556, USA
[4]Duke University, Durham, North Carolina 27708, USA
[5]Triangle Universities Nuclear Laboratory, Durham, North Carolina 27708, USA

Abstract

Dipole strength functions in the chain of xenon isotopes are analyzed on the basis of photon-scatterde experiments with bremsstrahlung at the γELBE facility in Dresden, Germany, and at the HIγS facility in Durham, North Carolina, USA. The evolution of dipole strength with neutron excess and nuclear deformation is studied.

The results presented in this report are part of the work published in Ref. [1]. Electromagnetic strength functions are a suitable tool for describing the average transition strengths between nuclear states in the quasicontinuum. In connection with nuclear level densities the strength functions describe photo-excitation and -deexcitation of an excited states [2]. The dominant $E1$ strength is measured for a few nuclei so far. The prominent hump of the giant dipole resonance (GDR) can be approached with various phenomenological functions [3] resulting in different predictions for the strength function below the neutron-separation energy. However, for astrophysical calculations and simulations regarding reactor safety this part of the strength function is of crucial importance. As shown e.g. in Ref. [4, 5] one can describe the photon spectrum following neutron capture with an experimentally deduced strength function.

For most of the nuclei no information is available so far or may be ever available, because the majority of nuclides has very short lifetimes and the measurement is a challenging task. Nevertheless, these nuclides play an important role in the addressed calculations, because they occur as intermediate fission and fusion products, before decaying to stable nuclei. Therefore, global descriptions of strength functions are needed based on fundamental nuclear properties such as neutron and proton number. One important parameter is the nuclear deformation. For the GDR it was shown [6] that it changes the distribution of dipole strength around the resonance region.

With the goal to check the influence of deformation on the low-energetic part, experiments on several isotopes in the xenon chain have been performed at the bremsstrahlung facility of the Helmholtz-Zentrum Dresden-Rossendorf [7]. By measuring photoabsorption cross sections it is possible to deduce an electromagnetic strength function. Several steps of the analysis [9], such as simulations with GEANT4 [8] in to correct the spectra for background and detector response, as well as simulation with γDEX [4] to estimate inelastic scattering, are performed. This analysis ensures that the derived photoabsorption cross section includes not only information about visible peaks, but also the full information about the quasicontinuum of unresolved states.

Fig. 1 shows the experimental results in combination with predictions of various parametrizations. One can see that the description of the low-energy strength as the tail of a Lorentzian is not correct. It approaches the data in some cases, e.g. for the well deformed nucleus ^{124}Xe, but not for the almost spherical ^{134}Xe. A reason for this deviation may be the excess of neutrons in ^{134}Xe relative to ^{124}Xe,
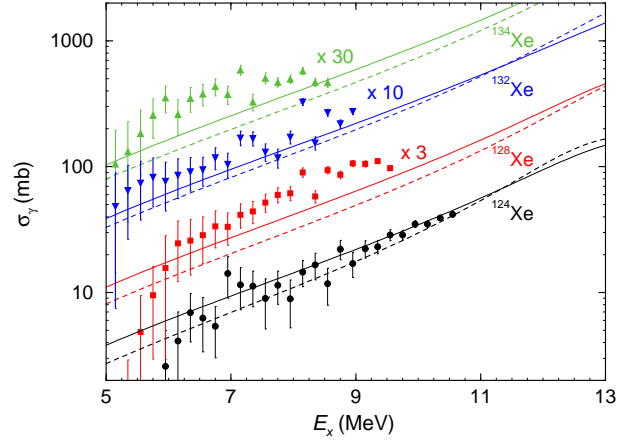
Fig. 1: Comparison of experimental deduced photo-absorption cross sections (colored circles) and predictions by the triple-lorentzian model ([6],solid lines) and the single-lorentzian description of RIPL3 ([3], dashed lines).
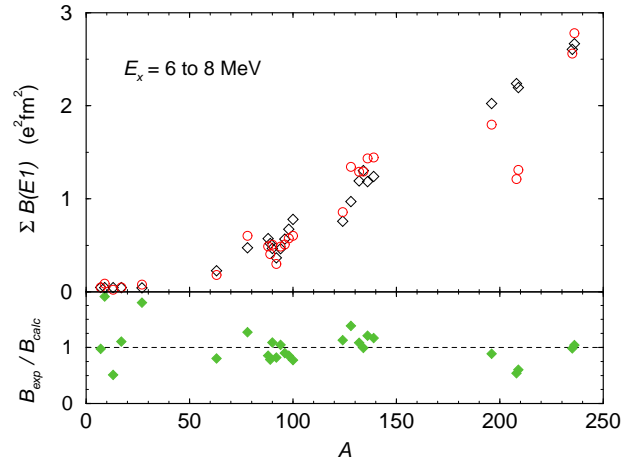
Fig. 2: Comparison of the prediction of the low-energetic strength with experimental information available in EXFOR [10].

as shown in Ref. [1]. It is possible to describe the strength below the neutron separation energy with the following equation:

$$\sum_{6-8\text{MeV}} B(E1) \approx 0.08 \frac{NZ}{A} \left(\frac{N}{Z} - 1 \right) \tag{1}$$

This formula is valid for a wide range of nuclei, as one can see in Fig. 2. It connects the fundamental properties such as neutron number N, proton number Z and mass number $A = N + Z$ with the strength. The formula shows that the distribution depends on the complete dipole strength, described with the Thomas-Reiche-Kuhn sum rule [11–13]. In addition, the neutron excess $(N/Z - 1)$ modifies the strength, whereas the nuclear deformation seems to be only of minor importance.

References

[1] R. Massarczyk *et al.*, Phys. Rev. Lett., in print, (2014).

[2] G. Bartholomew *et al.*, Advances in Nuclear Physics **7** 229 (1973).

[3] R. Capote *et al.*, Nuclear Data Sheets **110**, 3107 (2009).

[4] G. Schramm *et al.*, Phys. Rev. C **85**, 014311 (2012).

[5] R. Massarczyk *et al.*, Phys. Rev. C **87**, 044306 (2013).

[6] A.R. Junghans *et al.*, Phys. Lett. B **670**, 200 (2008).

[7] R. Schwengner *et al.*, Nucl. Instr. Meth. A **555**, 211 (2005).

[8] S. Agostinelli *et al.*, Nucl. Instr. Meth. A **506**, 250 (2003).

[9] R. Massarczyk *et al.*, Phys. Rev. C **86**, 014319 (2012).

[10] http://www.nndc.bnl.gov/exfor/exfor00.htm .

[11] W. Thomas, Naturwissenschaften **13**, 627 (1925).

[12] F. Reiche and W. Thomas, Z. Phys. **34**, 510 (1925).

[13] W. Kuhn, Z. Phys. **33**, 408 (1925).

^{241}Am: a difficult actinide for (n,γ) cross section measurement

M.Rossbach[1], C. Genreith[1]

[1]Institute of Energy and Climate Research, IEK-6: Nuclear Waste Management and Reactor Safety, Forschungszentrum Jülich GmbH, 52424 Jülich, Germany,

Abstract

Many attempts have been made in the past to determine accurate cross section data for neutron capture in ^{241}Am, however, the reported data for thermal neutron energies scatter by more than 25% around 680 b. The situation is complicated as the product of the capture reaction is twofold: ^{241}Am (n,γ)^{242g}Am,^{242m}Am. The production ratio for ground- and metastable state is uncertain but also ^{241}Am exhibits a very low first resonance at about 0.3 eV and this might influence the 1/v behaviour at thermal energy, 0.025 eV. In our experiments, we are using cold neutrons at the PGAA facilities of the Budapest and Garching Research Reactors, hence, we assume to be independent of the perturbations from possible non-1/v behaviour.

1   Introduction

^{241}Am is a key actinide in nuclear waste. It is produced by multiple neutron capture starting from ^{238}U and ^{239}Pu following by successive beta decay and alpha-decays with a half- life of 432 years forming ^{237}Np with a half-life of 2.1 My. Following ^{239}Pu it exhibits the second largest contribution to the radiotoxicity of nuclear waste after the initial decay of short lived fission products. Many attempts have been made in the past to propose dedicated Am-burners [1] or to reduce Am inventories in nuclear fuel by mixing it into MOX fuel for fast neutron reactors of the GEN IV type after careful partitioning of the actinides from used fuel [2].

In order to closely follow the behaviour of americium in the fuel cycle as well as in extracts from partitioning and fuel production sensitive analytical techniques are required to trace the actinide in highly radioactive environments. Non-destructive assays would be preferable if radiation hazards and secondary nuclear waste from analytical procedures are to be avoided. Apart from high energy alpha radiation (5.5 MeV) ^{241}Am emits a low energy gamma ray (60 keV) which hampers the quantification of the nuclide by direct gamma ray spectroscopy if any shielding is present. Active neutron interrogation making use of the relatively high capture cross section of ^{241}Am could drastically increase the sensitivity by determination of the induced prompt gamma ray emission. A prerequisite for accurate quantification of actinides in complex matrices using the prompt gamma activation approach, however, is precise knowledge of the thermal neutron capture cross section of the ^{241}Am(n,γ)^{242}Am reaction.

Prompt gamma neutron activation analysis (PGAA) is based on the measurement of prompt gamma radiation emitted after thermal neutron capture. The energy of the prompt gamma radiation ranges from a few keV up to several MeV and can therefore pass even through highly-absorbent waste matrices and shielding with a high level of transmission. However, for the identification and quantification precise data on the prompt gamma radiation of the isotopes in questions need to be provided. The most precise data on prompt gamma radiation were collected in the PGAA database, developed in Budapest [3] and evaluated by the IAEA [4]. But this prompt gamma data base provides information for elements up to uranium only. Energies and relative intensities of prompt gamma radiation of transuranic actinides like ^{241}Am can be found partially in

nuclear data reported in the ENSDF database [5]. However, the neutron capture data of some nuclides in the ENSDF consists of compilations of data from several individual experiments in separate energy regions and are based on very few experiments only. Using the PGAA approach, the incident neutron beam is well defined and the HPGe prompt gamma spectra cover the energy range from 50 keV up to 12 MeV. In addition to prompt gamma rays from which partial capture cross sections can be deduced, the activated short lived product nuclide can be used for thermal capture cross section evaluation. The use of cold neutrons, as available in Budapest and at FRM II in Garching, assures elevated sensitivities and prevents possible interference with low energy resonances of nuclides such as e.g. [241]Am.

2   Sample preparation for PGAA measurements

Samples used for cross section measurements in PGAA should be as pure as possible, preferably of stoichiometric composition, should not contain any hydrogen to avoid excessive scattering of neutrons, and should be homogeneously combined with an element of well-known thermal cross section to estimate the thermal equivalent neutron dose the sample was exposed to during irradiation.

Due to geometrical reasons – the sample must be positioned in the intersection of the neutron beam and the solid angle of the collimated HPGe detector – it is preferable to encapsulate the radioactive sample material such that positioning can be traced at any time.

2.1   Sample preparation between quartz slabs

After some initial experiments using aluminium foils and quartz ampules as encapsulation it was decided to use thin Suprasil[©] quartz blades (Heraeus Quarzschmelze, Hanau), 0.2 mm thick, 40 x 40 mm wide, to encapsulate the actinide samples. A 185 MBq [241]Am nitrate solution (0.5 ml) was purchased from Eckert & Ziegler and sent to PTB Braunschweig, the German Metrological Institute. A 3 mm diam. and 3 μm thick 99.9% pure gold foil (Alfa Aesar) was placed central to one quartz blade, a tiny drop of the activity solution was dried onto the gold and a second quartz blade was subsequently fixed with epoxy on top of the sandwich (see Figure 1). This procedure ensured a spot size sample, the possibility to closely inspect sample positioning and precisely determine the mass of material through the certified activity of the [241]Am (see table 1).

No.	Activity [MBq]	Au mass [mg]	Mass of [241]Am [μg]
1	4.67 ± 0.07	-	36.8 ± 0.9
2	4.33 ± 0.07	-	31.6 ± 0.9
3	4.63 ± 0.07	-	36.5 ± 0.9
4	3.87 ± 0.06	0.432 ± 0.005	30.5 ± 0.8
5	4.66 ± 0.07	0.434 ± 0.005	36.8 ± 0.9

Table 1: Specification of the [241]Am targets

Samples with and without Au were prepared for partial and integral neutron capture cross sections determination. Unfortunately, mass of americium was too low to determine a large number of prompt gamma lines under our current irradiation conditions. Further experiments will be carried out with samples of at least a factor of ten increased activity.
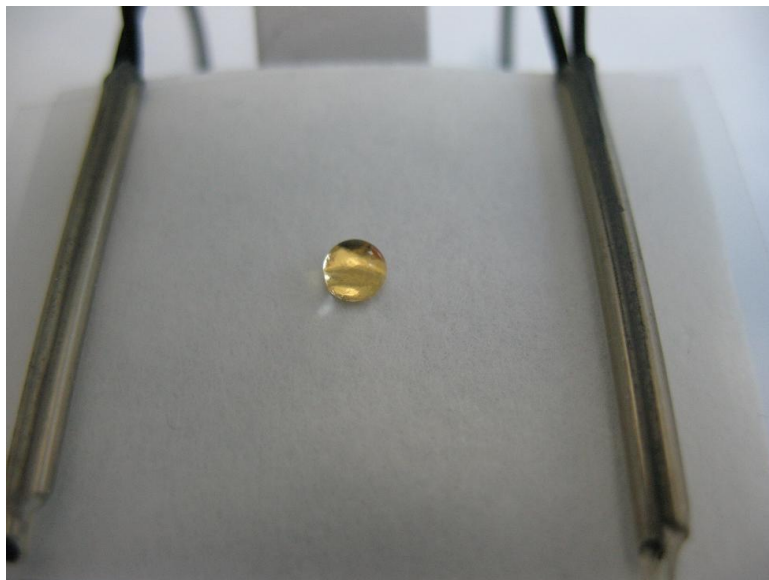
Fig. 1: A drop of [241]Am activity on top of a 3 mm diam. gold foil (courtesy by PTB Braunschweig)

3 Irradiation and counting

The PGAA facility at the Forschungsneutronenquelle Heinz Maier-Leibnitz, FRM II was used for our experiments as this Research Reactor is providing the highest external cold neutron flux worldwide. Preliminary experiments were carried out at the Budapest Research Reactor of the Centre for Energy Research, *MTA EK* providing a thermal equivalent cold neutron flux of 7×10^7 n cm^{-2} s^{-1} . The Compton suppressed 27% eff. HPGe detector is 23.5 cm away from the sample irradiation position. At FRM II in Garching the PGAA facility can provide 2×10^{10} n cm^{-2} s^{-1}, the detector system consists of a 60% eff. Compton shielded HPGe crystal and is about 30 cm away from the sample irradiation position. In view of the limited sample size we decided to use FRM II for our investigations. Still we were unable to detect most of the prompt gamma lines from our 4.6 MBq [241]Am samples after 6 to 12 hours of irradiation.

Hypermet-PC provided by the PGAA group in Budapest [6] was used for the evaluation of the complicated prompt gamma spectra. The same programme was used for the efficiency calibration of the detector, corrections for non-linearity of the energy calibration and for peak area calculation after multiplet analysis and background subtraction. Additionally, corrections for self-absorption of neutrons in the sample and housing as well as attenuation of low energy gammas in the same material were considered.

4 Results and Discussion

Results of our [241]Am experiments were reported at the ND2013 Conference held 04-08 March, 2013 in New York, USA and is documented in the proceedings of this Conference [7].

4.1 Evaluations

Neutron flux determination using the Au 411 keV gamma line considering the efficiency of the detector was done according to

$$\Phi_n = \frac{P_{411}}{N_{Au}} \cdot \sigma_{411} \cdot t_{irr}$$

for the thermal equivalent neutron flux, and neutron capture cross sections were calculated according to

$$\sigma_\gamma = \frac{P_\gamma}{N \cdot \Phi_n \cdot t_{irr}},$$

were Φ_n is the thermal equivalent neutron flux,

P_γ is the corresponding corrected peak area,

N is the number of atoms,

σ_γ is the thermal neutron capture cross section, and

t_{irr} is the irradiation time.

During the irradiation, mostly ^{242g}Am, but also ^{242m}Am is produced. Since the intensities of decays from both ^{242g}Am and ^{242m}Am are weak and not well known, the K_α x-rays of ^{242}Pu are used which originate from the electon capture-decay of the ^{242g}Am (16.02(2) h). These x-rays at energy of 99.5 keV and 103.4 keV are very close to the 98.97 keV and 102.98 keV γ-rays of ^{241}Am. Also they are very close to each other with respect to the energy resolution of the detector. Therefore a low energy detector (LED) would be desirable for this kind of measurement.

Following appropriate corrections for photon absorption and decay corrections the calculated neutron flux was used to calculate the ^{241}Am(n,γ)^{242g}Am capture cross section. Using the branching ratio of Fioni et al. (0.914(7)) [1] the thermal capture cross section of the reaction ^{241}Am(n,γ)^{242g,m}Am could be calculated (see Figure 2).
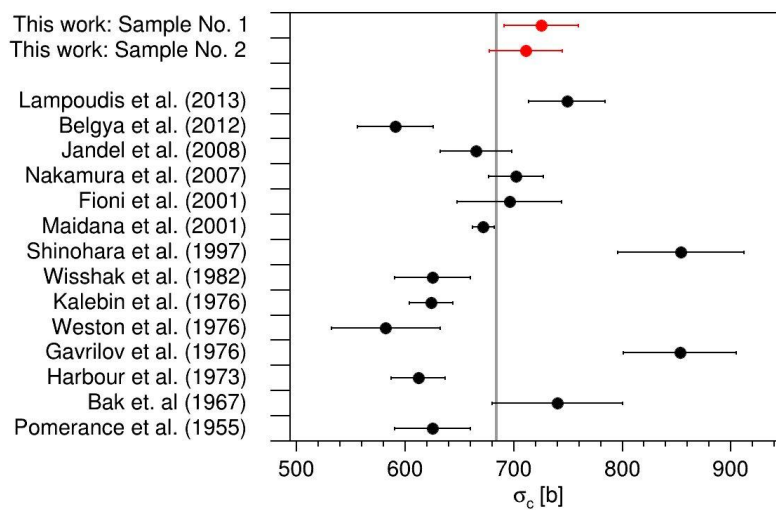
Fig. 2: The thermal neutron capture cross sections as calculated from the measurements described in this work (Garching) for both samples along values taken from literature [8-20]. The ENDF/B-VII.1 value is given for comparison (line at 684.3 b).

Our results of 711 ± 34 b and 725.4 ± 34.4 b compare well with the most recent results of Lampoudis et al. produced at the time-of-flight facility GELINA at IRMM, Geel (749 ± 35 b) [8].

4.2   Energy dependence of ^{241}Am cross section determination

The large scatter of results from ^{241}Am (n,γ) cross section determinations as shown in Figure 2 provoked a discussion on possible reasons for the discrepancies observed. As most of the values reported were based on thermal neutron irradiation experiments a Westcott correction factor for epithermal contributions had to be applied which was questioned to be correct. In addition, a low lying first resonance could have affected the 0.0253 eV capture cross section determination when thermal neutron irradiations are concerned. As our experiments were performed using sub-thermal neutrons we assume our values to be free from interferences of low energy resonances (see Figure 3).
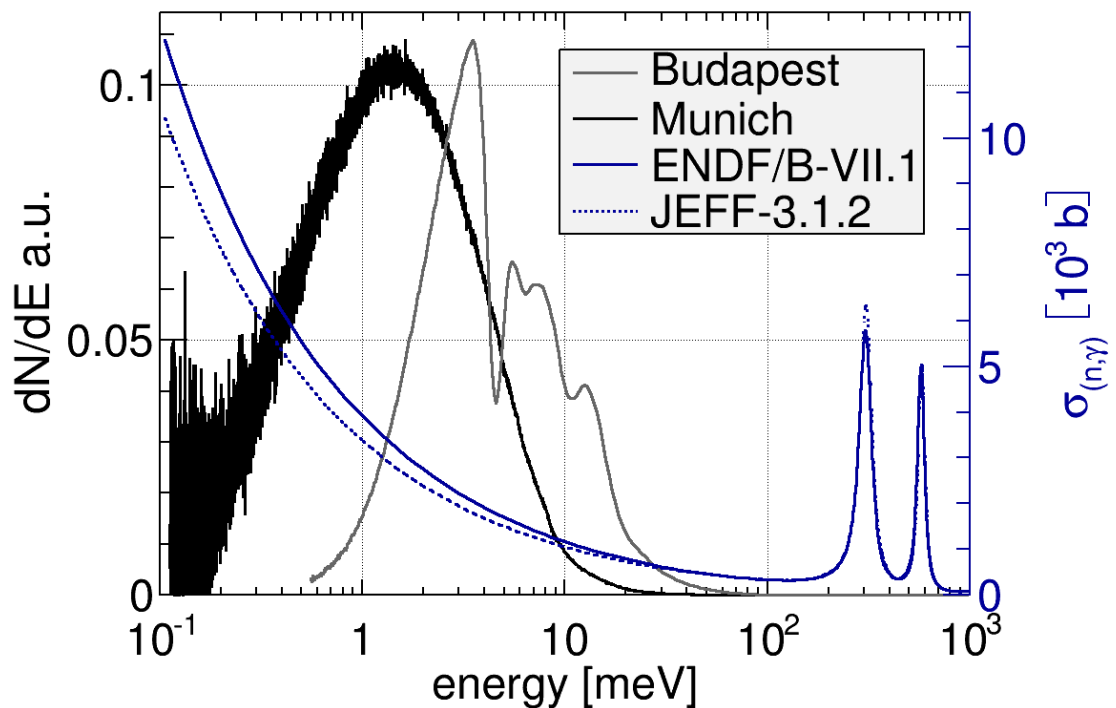
Fig. 3: Energy distribution of the cold beams at Budapest and at FRM II in München overlaid with the energy dependent capture cross section of ^{241}Am

As our ^{241}Am data are related to the well-known 0.0253 eV capture cross section of ^{197}Au (98.65 ± 0.01%) our values represent the thermal capture cross section of ^{241}Am(n,γ)^{242g,m}Am, if the 1/v-law is valid at the thermal point, otherwise it should be corrected for the different shape.

4.3   Uncertainty of the thermal capture cross section

Apart from the uncertainty of the production ration of ^{242g}Am and ^{242m}Am reported by Fioni et al. (2001) of 0.914(7) the uncertainty of the final PGAA result of the ^{241}Am(n,γ) thermal capture cross section is dominated by peak area determination of the low energy x-rays of the decay product ^{242}Pu at 99 and 103 keV following the decay of ^{242g}Am. The emission probability of the x-rays is

also associated with 2 to 3 % uncertainty, hence, the combined uncertainty of the overall cross section adds to < 5 %. A reduction of the uncertainty might be possible by using a low energy detector (LED) for gamma spectroscopy and/or by re-evaluation of the x-ray emission probability.

5   Conclusions

Sensitive and reliable determination of thermal capture cross section data of actinides is possible by applying prompt gamma activation analysis under carefully controlled conditions. If samples are combined with appropriate flux monitors of same shape, producing similar activity under irradiation, gamma spectra are recorded with well calibrated germanium detectors and spectra are being evaluated using sophisticated software with appropriate corrections for self-shielding of neutrons and attenuation of low energy gammas, the use of cold neutron beams at high flux research reactors can offer a valuable research tool for cross section measurements. Our results for ^{241}Am$(n,\gamma)^{242g,m}$Am neutron capture cross sections of 711 ± 35 b and 725.4 ± 34.4 b compare well with the most resent time-of-flight measurement from IRMM, Geel of 749 ± 34 b.

References

[1] Fioni, G. et al. (2001) Nucl. Phys. A **693** 546-564
[2]   Salvatores M., A. Zetta, C. Girard, M. Delpech, I. Slessarev, and J. Tommasi (1995) Appl. Radiat. Isot. **46** 6/7 681-687
[3] Révay Z., T. Belgya, R. Lindstrom, C. Yonezawa, D. Anderson, Z. Kasztovszky, R. Firestone, G. Molnár (2004) Handbook of Prompt Gamma Activation Analysis with Neutron Beams, Kluwer Academic Publishers
[4] IAEA (Ed.) (2007) Database of Prompt Gamma Rays from Slow Neutron Capture for Elemental Analysis, volume STI/PUB/**1263**
[5]   Capgam, Website of the National Nuclear Data Center (2011) http://www.nndc.bnl.gov/capgam/.
[6] Revay Z., T. Belgya, G. Molnar (2005) J. Radioanal. Nucl. Chem. **265** 261-265
[7] Genreith G., M. Rossbach, Zs. Revay, P. Kudejova (2013) accepted for publication in: Nuclear Data Sheets
[8] Lampoudis C., S. Kopecky, O. Bouland, F. Gunsing, G. Noguerre, A.J.M. Plompen, C. Saga, P. Schillebeeckx, and R. Wyants (2013) Eur. Phys. J. Plus **128** 86
[9]   Belgya T.et al., (2012)IAEA Prog. Rep. INDC(HUN).
[10]   Jandel M.et al., (2008) Phys. Rev. C **78** 034609.
[11]   Nakamura et al., (2007)J. of Nucl. Sci. and Techol. **44** 1500-1508.
[12]   Maidana N.L., M.S. Dias, M.F. Koskinas (2001) Radiochim. Acta **89** 419-423.
[13]   Shinohara N., Y. Hatsukawa, K. Hata, N. Kohno, (1997) J.Nucl. Sci. and Techol. **34** 613-621.

[14]   Wisshak K.et al. (1982), Nucl. Sci. and Eng. **81** 396-417.
[15]   Froehner F.H. et al. (1982).Proc. of 1982 Intern. Con. in Nucl. Data for Sci. and Techn. **265** 211
[16]   Kalebin S.M.et al. (1976), J. Atomic Energy **40** 373-377.
[17]   Weston L.W., J.H. Todd (1976) Nucl. Sci. and Eng. **61** 356-365
[18]   Harbour R.M., K.W. MacMurdo, F.J. McCrosson (1973) Nucl. Sci. Eng. **50**,364-369.
[19]   Dovbenko A.et al. (1971) Los Alamos National Laboratory Rep. **265**,LA-TR-71-74.
[20]   Pomerance H. (1955) Oak Ridge National Laboratory Rep. ORNL-**1879**,50-51

Nuclear Fission Reactor Safety Research in FP7 and future perspectives

Roger Garbil[1], Ivelina Ivanova[2]
[1] European Commission, DG Research and Innovation, Euratom Fission, Brussels, Belgium
[2] Ministry of Economy and Energy, Sofia, Bulgaria

Abstract
The European Union (EU) has defined in the Europe 2020 strategy and 2050 Energy Roadmap its long-term vision for establishing a secure, sustainable and competitive energy system and setting up legally binding targets by 2020 for reducing greenhouse emissions, by increasing energy efficiency and the share of renewable energy sources while including a significant share from nuclear fission. Nuclear energy can enable the further reduction in harmful emissions and can contribute to the EU's competitive energy system, security of supply and independence from fossil fuels. Nuclear fission is a valuable option for those 14 EU countries that promote its use as part of their national energy mix. The European Group on Ethics in Science and New Technologies (EGE) adopted its Opinion No.27 'An ethical framework for assessing research, production and use of energy' and proposed an integrated ethics approach for the research, production and use of energy in the EU, seeking equilibrium among four criteria – access rights, security of supply, safety, and sustainability – in the light of social, environmental and economic concerns. The European Commission Symposium on 'Benefits and Limitations of Nuclear Fission for a Low Carbon Economy', held on 26-27 February 2013 in Brussels, also confirmed the need to pursue nuclear fission safety research. Overall, the 'Euratom experience' within the Framework Programmes (FPs) has been one of consistent success in pursuing excellence in research and facilitating pan-European collaborative efforts across a broad range of nuclear science and technologies and associated education and training activities.

1. European research activities supporting nuclear reactor safety

European reactor safety research activities are supporting, among others, projects on severe accident management coupled with numerical simulation codes (e.g. core physics and thermal hydraulics for reactor safety; multi-scale modeling of irradiation effects on reactor vessels and internals) and plant lifetime management. Since 1992, around 80 shared-cost research projects on severe accidents have been funded in part by the Euratom Fission Research Directorate (DG RTD) with a total EC contribution of EUR 66 million. The research performed is supporting a continuous and better understanding of the phenomenology of severe accidents and helping to reduce uncertainties that surround nuclear reactor safety.

1.1 Severe accident management research

The Network of Excellence (NoE) for a Sustainable Integration of European Research on Severe Accident Phenomenology (SARNET2 following FP6 EC-SARNET) has 42 European, Canadian,

Korean and American research and development organizations. These include Technical Support Organizations (TSOs) from safety authorities, industry, utilities and universities, with a total budget of EUR 38 million and EUR 5.8 million EC Euratom contribution. The NoE started in April 2009 and will run for four and half years. SARNET aims to: a) tackle the existing fragmentation in defining and/or carrying out research programmes; b) harmonize and improve Level 2 Probabilistic Safety Assessment (PSA) methodologies; c) disseminate the knowledge more efficiently to associated candidate countries; and d) bring together top scientists in the severe accident research field in order to become a world leader in advanced computer tools for severe accident risk assessment. The backbone of the integration is provided using the integral severe accident analysis code ASTEC (Accident Source Term Evaluation Code), the latest being adapted for use in any water-cooled reactor application in Europe.

Severe accident management research benefited greatly from the PHEBUS-FP (Fission Products) international research programme conducted between 1988 and 2010. The EC was strongly involved in the management and scientific cooperation of PHEBUS with a total EC contribution of EUR 40.5 million.

One of the most important contributions to severe accident research experiments, and one of the most important aspects of nuclear power plant safety operations concerns the ability to carry out a reliable and comprehensive safety assessment, taking into account all details related to siting, design, construction and operation of a reactor facility. Level 2 Probabilistic Safety Assessment (PSA) is a structured methodology aimed at assessing the risk of radioactive release into the environment in the case of an accident at a nuclear power plant.

The ASAMPSA2 project (Advanced Safety Assessment Methodologies Level 2 PSA) involved 21 European partners from 12 European countries and developed best practice guidelines for advanced severe accident probabilistic safety assessments, contributing significantly to harmonizing existing methodologies at EU level. Follow-up actions are being considered within the European framework to complete these guidelines with the assessment of specific risks induced by beyond-design extreme events, in relation to lessons learned from the Fukushima accident and following verification of the efficiency of nuclear power plant severe accident management measures within the framework of the stress tests.

The ERCOSAM project (Containment thermal-hydraulics of current and future LWRs for severe accident management) is looking at the presence of stratification in a nuclear power plant's containment, such as pockets of hydrogen in high concentrations that could lead to a deflagration or detonation, and how this stratification can be broken down by the operation of severe accident management systems, such as sprays, coolers and passive auto-catalytic recombiners. Experiments are being performed on a smaller scale at TOSQAN (IRSN, Saclay, France), and on a medium scale at MISTRA (CEA, Saclay, France) and PANDA facilities (PSI, Villigen, Switzerland). Test specifications at the Russian KMS facility (NITI, St Petersburg, Russian Federation) will also provide a basis for a code benchmarking at nearly prototypical scale, development of state-of-the-art tools and computational fluid dynamics codes, calculations and analyses of scenarios. The ERCOSAM research is being conducted by two parallel projects comprising one project consortium composed of PSI (Switzerland), IRSN and CEA (France), KIT (Germany), NRG (the Netherlands) and AECL (Canada), and the other comprising the following Russian organizations: IBRAE, SPbAEP, IPPE, and NITI (Russian Federation).

Euratom has also supported experimental facilities, namely PLINIUS and LACOMECO which are experimental platforms located at the CEA Cadarache in France and at the Karlsruhe Institute of Technology (KIT) in Germany, where large-scale infrastructures offered transnational access activities under FP6 Integrated Infrastructure Initiatives (I3) and FP7 Coordination and Support Actions (CSA) funded schemes.

Nuclear safety of existing reactors and advanced nuclear systems is being maintained and achieved thanks to the availability of the necessary supporting research infrastructures, as mentioned above as facilities for illustration, but also numerical and simulation research facilities and tools, as follows.

1.2 Numerical simulation research tools for light water reactors

Since 2005, Euratom has supported four major shared-cost research projects in the establishment of such a simulation platform. The contribution from EC Euratom Fission (DG RTD) is EUR 16.5 million of the total cost of EUR 28.2 million. Complementary research topics include the improved prediction of irradiation or corrosion effects on a reactor's internal structures and fuel cladding, and increasing the existing accuracy when forecasting any extension to safe reactor lifetime.

The FP6 NURESIM Integrated Project (European Platform for Nuclear Reactor Simulations) has provided the initial steps towards a common European standard software platform for modeling, recording and recovering computer data for nuclear reactor simulations. The common platform has facilitated the exchange of data across sites, codes of application and computing platforms. From 2009, the follow-on FP7 NURISP Collaborative Project (Nuclear Reactor Integrated Simulation Project) made significant steps towards a European reference simulation platform for applications relevant to present PWR, BWR and future reactors. The project also developed significant capacities for multi-scale and multi-physics calculations, for deterministic and statistical sensitivity and uncertainty analysis, facilitating their use in a generic environment. The individual models, solvers and codes integrated into the platform were verified, validated and demonstrated through benchmarks, using mainly OECD/NEA or IAEA centralized databanks, corresponding to present Generation-II, Generation-III PWR, VVER and BWR challenging applications, while care has also been taken to use generic methods to enable future extension to Generation-IV reactors.

Most of the existing tools are based on a number of approximations, while the Monte Carlo method for neutron calculations avoids some approximations. In HPMC (High Performance Reactor Core Design) this method is combined with thermal hydraulics and fuel burn-up calculations for reactor safety analysis. The advantage of this method is that it relies on Monte Carlo safety-related nuclear reactor full core analysis while taking into account the time dependence, thermal hydraulic feedback and burn-up of the system.

Improvements in and optimization of the simulation and numerical codes is not enough to improve reactor safety. It is also important to predict reactor core behavior to the highest possible evaluation degree by using the latest accurate nuclear data cross-sections and libraries, materials radiation resistance and thermal-hydraulic databases. This is made possible by supporting infrastructure experiments and measurement activities through projects such as EFNUDAT (European Facilities for Nuclear Data Measurements), ANDES (Accurate Nuclear Data for Nuclear Energy Sustainability), EUFRAT (European Facility for Innovative Reactor and Transmutation Neutron data) and ERINDA (European Research Infrastructures for Nuclear Data Applications). Overall, through FP6 and FP7, the contribution to nuclear data activities from EC Euratom Fission (DG RTD) is EUR 10.1 million of the total cost of EUR 14.2 million.

After the 2011 Fukushima Daiichi accident in Japan, improving nuclear safety has become even more paramount in further developments in the nuclear industry. From 2013, the NURESAFE project has been addressing the engineering aspects of nuclear safety, especially those related to design basis accidents (DBA). Although the Japanese accident was severe, in a process of defense-in-depth, prevention and control of DBAs is obviously one of the priorities for safety improvement. By 2015, FP7 NURESAFE should deliver multi-physics and fully integrated applications to support this European simulation platform on reactor computation safety, which has been promoted over the last few years by means of a roadmap which is fully integrated into the Strategic Research and Innovation

Agenda (SRiA) of the Sustainable Nuclear Energy Technology Platform (SNETP), published in February 2013.

1.3 Plant life prediction and residual lifetime evaluation research

As the result of feedback and improvements through targeted research and development, future Generation-III reactors should deliver improved performances and enhanced safety features. The long-term operation as a key driver of applied research and development, technological innovation has led to the creation of the FP6 NULIFE NoE (Nuclear Plant Life Prediction) and developed the basis for joint programming research activities on safety issues of common interest. NULIFE started as a European NoE with a total EC Euratom Fission (DG RTD) contribution of EUR 5 million towards a total cost of EUR 8.4 million, and has evolved since March 2012 as an independent international non-profit association under Belgian law (AISBL) called NUGENIA (Nuclear Generation II and III Association) and mandated by SNETP. Most countries have already launched initiatives to confirm the possible extension design lifetime of their nuclear power plants. Assessments of systems, structures and components' residual lifetime are important European research activities, including: a) integrity assessment for metallic components and concrete; b) materials performance and ageing, covering metallic structures and components, material properties, ageing and degradation mechanisms, and modelling of ageing. A total EC Euratom Fission contribution (DG RTD) of EUR 16.6 million has been provided towards a total cost of EUR 32.7 million in support of the following projects.

Within the PERFORM 60 project (Prediction of the effects of radiation for reactor pressure vessel and in-core materials using multi-scale modelling towards a 60 years foreseen plant lifetime), effects of radiations on reactor vessels and in-core materials are predicted. Treatment of long-term irradiation effects in reactor pressure vessel safety assessment are also explored in the LONGLIFE project aimed at achieving an improved understanding of irradiation effects in the vessel steels under conditions representative of a long-term operation. The objectives of the STYLE project were to estimate, optimize and develop the use of advanced tools to assess the structural integrity of piping, using theoretical and experimental results, performance assessment and further development of micromechanical models, and to carry out simplified engineering assessment methods. The MULTIMETAL project has been extending previous research activities carried out in Euratom fission projects, such as BIMET (Structural integrity of bi-metallic components) and ADIMEW (Assessment of aged piping dissimilar metal weld integrity) in the structural performance of dissimilar multi-metal welds. Lifetime safety research on instrumentation and technological control systems is also performed in the following collaborative projects. The project ADVANCE (Ageing diagnostics and prognostics of low-voltage instrumentation and control cables) is related to determination of the existing conditions of installed electric cables over their entire length. The project HARMONICS (Harmonized assessment of reliability of modern nuclear instrumentation and control software) is looking at the reliability and safety of computer-based systems that implement safety functions to ensure that the nuclear industry has well-founded, up-to-date methods and data for assessing the software of safety systems at Generation-II and Generation-III nuclear power plants.
Euratom research is supporting research activities into highly complex technological systems, and research into their operational safety is obviously multifaceted.

1.4 Human factors, education, training and safety culture

The Euratom Framework Programmes have a strategic role to play in this perspective. Education and training (E&T) is being fostered through dedicated projects, or by including a specific education and

training activity in the largest projects in FP6 and FP7, with at least 5 % of the total project budget being dedicated to these activities. The goal is to offer the EU nuclear community a list of high-quality teaching modules that can be assembled either into Euro-Master programmes (university level education) or into training packages requested by industry or regulatory bodies.

The European Credit System for Vocational Education and Training (ECVET), making lifelong learning and borderless mobility for students and the scientific community a reality, is a priority for EU research and education policy. The ECVET was launched in Copenhagen in 2002 and successfully tested across a wide range of industrial sectors. There are some similarities between the ECVET system and European Credit Transfer and accumulation System (ECTS) initiated by the Bologna Process in 1999 for academic education. The main objective of ECVET is to promote mutual trust, transparency and recognition of learning outcomes that refer not only to knowledge but also to skills and competences. ECVET and ECTS training schemes are at the heart of the EFTS (Euratom Fission Training Schemes) and consist of portfolios of learning outcomes that are needed to perform a number of identified jobs or functions.

In September 2003, the European Nuclear Education Network (ENEN) Association was established by the partners of the FP5 European Nuclear Engineering Network ENEN project with a legal status as a non-profit international organization under French law.

A total EC Euratom Fission (DG RTD) contribution of EUR 14.5 million towards a total cost of EUR 22.3 million, some of which is supporting education and training actions through the ENEN Association, and for the following projects: a) TRASNUSAFE, Nuclear Safety Culture, addressing mainly the health physics sector (e.g. ALARA principle in industry and medical field); b) ENEN III Training schemes on Generation III and IV engineering, addressing mainly the nuclear systems suppliers and engineering companies; c) ENETRAP II, European Network on E&T in Radiological Protection, addressing mainly the nuclear regulatory authorities and TSOs; d) PETRUS II and III, Programme for Education, Training, Research on Underground Storage addressing mainly the radiation and waste agencies; e) CINCH I and II, Cooperation in education In Nuclear Chemistry addressing mainly the sectors of the nuclear fuel cycle and site rehabilitation; f) CORONA, Regional Centre of Competence for VVER Technology and Nuclear Applications, with a focus on VVER personnel; g) EURECA!, Cooperation between EU and Canada in Education, Training and Knowledge Management on Super-Critical Water Reactors; h) GENTLE, Graduate and Executive Nuclear Training and Lifelong Education with a focus on synergies between industry and academia; i) NUSHARE, Project for sharing and growing nuclear safety competence, focused on three target groups (policy-makers, nuclear regulatory authorities and industry); j) EUTEMPE-RX, European Training and Education for Medical Physics Experts in Radiology, with a focus on Council Directive 97/43/Euratom on Medical Exposures.

The project MMOTION (Man machine organization (MMO) through innovative orientations for nuclear) analyzed the current and future trends concerning man-machine organizations and safety-related aspects. A single consolidated European research roadmap for the period 2010-2015, designed to comprehensively address the recognized issues, was the project's main deliverable and has been integrated into SNETP's updated SRiA. The project CORONA (Establishment of a regional center of competence for VVER technology and nuclear applications) should provide a dedicated structure for the training and qualification of personnel serving VVER technology. Such an approach should allow for unifying the existing VVER-related training schemes according to IAEA standards and commonly recognized criteria within the EU.

Finally, with regard to the need for a better understanding of the skills gaps in both the nuclear industry and research organizations, the working group on Risks of European Nuclear Energy Forum (ENEF) was active in the creation of the European Human Resources Observatory – Nuclear Energy (EHRO-N) in October 2009: The implementing agent of EHRO-N is the EC's Joint Research Centre

DG in Petten, the Netherlands. For example, in May 2012, the EHRO-N published an authoritative report about the shortage of nuclear skills, entitled 'Putting into Perspective the Supply of and Demand for Nuclear Experts by 2020 within the EU-27 Nuclear Energy Sector'.

1.5 Following Fukushima, immediate actions have been undertaken at international level

A number of initiatives have been undertaken immediately in most countries and at international level in order to take into account the lessons learned from this accident concerning the improvement of nuclear reactor safety design and established organizations to manage radiological accidents, at EC and OECD/NEA ministerial meetings, a safety authorities' forum, and at a ministerial conference organized by the IAEA in June 2011 which resulted in the Action Plan on Nuclear Safety, which was endorsed by an IAEA general conference. Most of the countries operating nuclear reactors have launched a systematic reassessment of the safety margins of their nuclear fleet under severe natural hazards, and comprehensive stress tests have been launched by the European Council under the coordination of the European Commission in collaboration with peer reviews organized by the European Nuclear Safety Regulators Group (ENSREG).

A few months after the Fukushima event, the Sustainable Energy Technology Platform SNETP published a report at the end of 2011 entitled 'Identification of Research Areas in Response to the Fukushima Accident'. In February 2013, SNETP also issued a revised version of the Strategic Research Agenda, the 2013 Strategic Research and Innovation Agenda (SRiA), focusing on nuclear safety and taking into account lessons learned from the event.

The Euratom work programmes for 2012 and 2013 also placed a total emphasis on nuclear safety, in particular on the management of a possible severe accident at the European level. Two priority topics emerged: a) impact of the nuclear accident in Japan on severe accident management; and b) consequences of a combination of extreme external events on the safety of nuclear power plants.

As a result, three collaborative projects addressing the lessons learned from Fukushima were funded on: a) an investigation of passive and active systems on severe accident mitigation and enhanced safety of future reactors (PASSAM); b) the upgrade of computer codes for European severe accident management (CESAM); and c) the establishment of best practice guidelines for the identification of consequences of a combination of extreme external events on the safety of nuclear power plants (PREPARE). Another project was funded to complete the roadmap of a European simulation platform to perform multi-scale and multi-physics computation for the safety of existing reactors (NURESAFE). A total EC Euratom Fission (DG RTD) contribution of EUR 26.3 million has been provided towards a total cost of EUR 48 million in support of the above-mentioned projects as an early reaction and follow-up research actions. In addition, the NUSHARE coordination action (NUclear culture SHARing amongst the EU Member States) is a training and information programme drawing lessons from Fukushima in a four-year action under the leadership of ENEN.

The European Commission is committed to a structured dialogue on research policy and priorities within the framework of H2020, with European technology platforms and fora, including OECD/NEA and IAEA, and relevant to the field of activities to tackle European societal challenges and acknowledge the role and participation of civil society in its decision-making.

To illustrate such a commitment from the nuclear community, it is important to recall – as requested by the EU Council in June 2011 and in response to Fukushima – the 2013 symposium co-organized by the European Commission and the European Economic and Social Committee (EESC) on 'Benefits and limitations of nuclear fission for a low-carbon economy'. Held in Brussels on 26 and 27 February 2013, it was attended by about 350 people from research organizations, industry, politics, government representatives, science and civil society. Special emphasis was given to the research needs for a

sustainable, secure, reliable and competitive energy mix, including nuclear fission. The outcome also confirmed the need to strengthen the links between science, civil society, industry and policy-makers in order to maintain a sustained focus on increased safety, risk-mitigation, safeguards and security.

Two studies contributed to the symposium: a) the first 2012 interdisciplinary study on 'Benefits and Limitations of Nuclear Fission for a Low-Carbon Economy/Defining priorities for Euratom fission research and training (Horizon 2020)'; b) a second study requested by President José Manuel Barroso in December 2011, which was carried out by the European Group on Ethics (EGE) on 'An ethical framework for assessing research, production, and use of energy', and adopted unanimously on 16 January 2013. The EGE recommends an integrated ethical approach to achieving equilibrium between four criteria: 1) access rights; 2) security of supply; 3) safety; and 4) sustainability in the light of social, environmental and economic concerns. The proposed activities fit well with the activities planned within H2020, in particular energy challenge number 3 and the fission part of the Euratom programme – the latter had already called for socio-economic research activities within its 2013 Call for proposals.

Finally, the crucial participation of civil society is acknowledged in the area of nuclear energy and underlined in this context in the following initiatives: a) regular meetings since 2007 of the European Nuclear Energy Forum (ENEF) and its specific working group on transparency issues; b) round tables organized from 2009 onwards by the European Commission and the French National Association of Local Information Commissions and Committees (ANCCLI) to open a dialogue on the practical implementation of the United Nations' Aarhus Convention in the nuclear field supporting the rights of the public with regard to the environment, in partnership with the ENEF and the French Ministry of Ecology and Sustainable Development; and c) the supporting role of the European Economic and Social Committee (EESC) in helping EU institutions to involve civil society in its decision-making, including on research and energy policy.

1.6. European technology platforms, SNETP and NUGENIA Generation II-III Associations

Under the Euratom Framework Programme, the European Commission should promote and facilitate nuclear safety research activities in EU Member States and complement them through specific Community research and training activities. Within this scope, it should help to stimulate joint funding from Member States and/or enterprises, and benefits should be drawn from the increasing interaction between technology platforms, the 'Sustainable Nuclear Energy Technology Platform' (SNETP), the 'Implementing Geological Disposal of Radioactive Waste Technology Platform' (IGDTP), the 'Multidisciplinary European Low Dose Initiative' (MELODI) and other stakeholder fora (ENEF, ENSREG, FORATOM), OECD/NEA and IAEA at the international level.

The successful European Nuclear Energy Forum (ENEF) was set up in 2007 as a pan-European forum on transparencies issues, opportunities and risks of nuclear energy, gathering together all relevant stakeholders in the nuclear field, such as representatives from EU Member States, EU institutions, European Parliamentarians, the nuclear industry, electricity consumers, research organizations, non-governmental organizations, and civil society. The European Nuclear Safety Regulators Group (ENSREG), established in 2007, gathers together EU high-level independent and authoritative experts on nuclear safety, radioactive waste safety or radiation protection regulatory authorities from 27 Member States and representatives from the European Commission. ENSREG fosters the continuous improvement and understanding of nuclear safety in Europe and their prominent role should be acknowledged in support for the coordination of peer reviews during the latest stress test exercise undertaken following the 2011 Fukushima accident.

The Sustainable Nuclear Energy Technology Platform (SNETP) is the European technology platform aimed at promoting the research, development and demonstration of European nuclear fission technologies, covering current and future nuclear systems, including safety research, fuel cycle, appropriate research and development infrastructure, and human resources. Since its launch in 2007, SNETP has become a recognized platform in Europe for the identification of common research activities within the nuclear fission safety domain. Today, SNETP has gathered more than 110 members from research organizations and industry. It has achieved an efficient collaboration with its stakeholders, acting as a reliable supporting partner to the European institutions, Euratom and other co-operation frameworks such as the SET-Plan. Since its launch, SNETP has been able to develop a common vision on the future contribution of nuclear fission energy in Europe through the publication of the 'Vision Report, SRiA and Deployment Strategy', including a public consultation for the SRiA. Several working groups have been established: for example, one of these is related to education, training and knowledge management with the aim of identifying education and training gaps and recommending actions at appropriate levels. An open and transparent governance process is in place supported by a secretariat. Public communication is assured continuously. SNETP has structured its nuclear fission research, development and demonstration activities around three technological pillars with the following objectives: a) to maintain the safety and competitiveness of today's Generation II-III technologies (NUGENIA); b) to develop a new generation of more sustainable Generation-IV reactor technologies, the so-called fast neutron reactors with closed fuel cycles (ESNII); and c) to develop new nuclear power applications, such as the industrial scale production of hydrogen, desalination or other industrial process heat applications (NC2I).

As a result of all the above-mentioned initiatives, the European Commission is committed to a structured dialogue on research policy and priorities with European technology platforms and fora within the framework of H2020 and relevant to the field of activities to tackle European societal challenges.

2. Conclusions and perspectives

The EU Euratom Framework Programmes are making a significant contribution to establishing a common European view on scientific issues and towards integrating and establishing the European Research Area in nuclear science and technology: FP6-FP7 collaborative projects, FP6 Networks of Excellence, FP6 integrated infrastructure initiatives, FP7 coordination and support actions, actions to promote and develop human resources and mobility and international cooperation. They are being implemented to reinforce Euratom R&D programmes, to develop supporting research infrastructures, to foster networking, transnational access and joint research activities. This research effort is needed primarily to retain then improve competences and know-how, and to enhance the efficiency and effectiveness of a true European Research Area which can contribute to maintaining high levels of nuclear knowledge, capabilities and competiveness of the industry in the nuclear field.

As promoted by the EU under FP7, the establishment of industry-driven technology platforms by the research community in the areas of sustainable nuclear energy, waste management and low-dose research are being capitalized on by SNETP, NUGENIA, IGDTP, and MELODI, respectively. Mapping is being carried out of the capacity of research centers and other research infrastructures that need more support to coordinate across the European Union and beyond, together with implementation of the SET-PLAN European Sustainable Nuclear Industrial Initiative.

Close collaboration is also being maintained with ENEF, ENSREG as well as OECD/NEA and IAEA on very a regular basis.

Since 1988, the European Commission has supported nuclear fission safety research starting from severe accident management, numerical simulation tools for current light water reactors, residual lifetime evaluation, human factors, education and training, and the international dimension of FP7 actions leading to the wide dissemination of a safety culture both inside and outside Europe. Projects dedicated to safety and emergency management have been and are still being funded from the available EC budget. Research into safety of the present and future light water reactors will be continued and supported, as indicated in the updated roadmap within the framework of the SNETP NUGENIA association encompassing all aspects of the safety of Generation II and III reactors, as referred to in one of the general objectives of the Horizon 2020 Euratom Framework Programmes: to improve nuclear safety, security and radiation protection and to support the safe operation of nuclear systems.

An overview of several projects has been given above together with an analysis of key results delivered to date, including first lessons learned from the Fukushima accident. In addition, new projects are being launched and capitalizing on previous research, fostering integration of European infrastructures and responding to key identified research needs.

The European Group of Ethics on 'An ethical framework for assessing research, production, and use of energy' recommended an integrated ethical approach to achieving equilibrium between four criteria: 1) access rights; 2) security of supply; 3) safety; and 4) sustainability in the light of social, environmental and economic concerns. The study raises a number of questions to be tackled by R&D, in particular in the areas of socio-economics, energy-system modelling and environmental impacts. Most of the proposed topics cover non-nuclear technologies as well as nuclear energy. In general, the proposed activities fit well with the activities planned within H2020, in particular third energy challenge and the fission part of the Euratom Programme – the latter having already called for socio-economic research activities.

The 'Euratom experience' with Framework Programmes has been one of consistent success in pursuing excellence in research and facilitating pan-European collaborative efforts across a broad range of nuclear science and technologies and associated education and training activities in line with Horizon 2020 key priorities: excellent science, industrial leadership, and societal challenges, one of which being the secure, clean and competitive energy challenge for Europe in the context of the EU energy mix.

Acknowledgements and references

Acknowledgements go to all colleagues and collaborators from the European Commission, research organisations, universities, industry, fora and international organisations involved in the follow-up and successful development of the projects within the Euratom Framework Programmes.

Europe 2020 http://ec.europa.eu/europe2020/
EU Energy Roadmap 2050 http://ec.europa.eu/energy/energy2020/roadmap/index_en.htm
EGE Opinion http://ec.europa.eu/bepa/european-group-ethics/docs/publications/opinion_no_27.pdf
2013 Symposium http://www.eesc.europa.eu/?i=portal.en.events-and-activities-symposium-on-nuclear-fission
EU Energy research: http://ec.europa.eu/research/energy/index_en.cfm
Euratom Seventh Framework Programme: http://cordis.europa.eu/fp7/euratom/home_en.html
Information on FP7 and access to programmes and calls: http://cordis.europa.eu/fp7/home_en.html
Research Participant Portal http://ec.europa.eu/research/participants/portal/page/home
Euratom FP6 Research Projects and Training Activities, Volume I-II and III (PDF)
Volume I ftp://ftp.cordis.europa.eu/pub/fp6-euratom/docs/nuclear_fission_eur21228_en.pdf
Volume II ftp://ftp.cordis.europa.eu/pub/fp6-euratom/docs/nuclear_fission_eur21229_en.pdf

Volume III ftp://ftp.cordis.europa.eu/pub/fp7/docs/euratom-fission_eur22385_en.pdf
Euratom FP7 Research and Training Projects, Volume I (PDF)
Volume I ftp://ftp.cordis.europa.eu/pub/fp7/docs/fin-266-euratom-web-jun09v02_en.pdf
Volume II http://ec.europa.eu/research/energy/pdf/euratom-fp7-vol-2.pdf
Volume III
http://ec.europa.eu/research/energy/euratom/publications/pdf/euratom_fp7_research_&_training_projects_volume_3.pdf
Strategic Energy Technology Plan SET-Plan http://ec.europa.eu/energy/technology/set_plan/set_plan_en.htm
Implementing Geological Disposal of Radioactive Waste Technology Platform http://igdtp.eu/
Sustainable Nuclear Energy Technology Platform http://www.snetp.eu/
Nuclear Generation II & III Association http://nugenia.org/
Multidisciplinary European Low Dose Initiative http://melodi-online.eu/
European Atomic Forum http://www.foratom.org/
European Nuclear Energy Forum http://ec.europa.eu/energy/nuclear/forum/forum_en.htm
European Nuclear Safety Regulator Group http://www.ensreg.eu/
European Economic and Social Committee http://www.eesc.europa.eu
European Human Resources Observatory for the Nuclear Energy Sector (EHRO-N) http://ehron.jrc.ec.europa.eu/

Transmutation of high-level radioactive waste - Perspectives

Arnd Junghans[1], Roland Beyer[1], Eckart Grosse[2], Roland Hannaske[1,2],
Toni Kögler[1,2], Ralf Massarczyk[1,2], Ronald Schwengner[1], Andreas Wagner[1]
[1]Helmholtz-Zentrum Dresden-Rossendorf, Bautzner Landstrasse 400, 01328 Dresden, Germany
[2] Technische Universität Dresden, 01062 Dresden, Germany

Abstract

In a fast neutron spectrum essentially all long-lived actinides (e.g. Plutonium) undergo fission and thus can be transmuted into generally short lived fission products. Innovative nuclear reactor concepts e.g. accelerator driven systems (ADS) are currently in development that foresee a closed fuel cycle. The majority of the fissile nuclides (uranium, plutonium) shall be used for power generation and only fission products will be put into final disposal that needs to last for a historical time scale of only 1000 years. For the transmutation of high-level radioactive waste a lot of research and development is still required. One aspect is the precise knowledge of nuclear data for reactions with fast neutrons. Nuclear reactions relevant for transmutation are being investigated in the framework of the european project ERINDA. First results from the new neutron time-of-flight facility nELBE at Helmholtz-Zentrum Dresden-Rossendorf will be presented.

1 Motivation for nuclear transmutation

In the European Union a significant share of the gross electricity generation (27.6% in 2011) [1] comes from its 136 nuclear power reactors (incl. Switzerland) with a total electric power of about 125 GW. For example, France has 58 operational power reactors, the United Kingdom 16 and Sweden 10. The spent nuclear fuel constitutes the high-level radioactive waste that is produced with a rate of approximately 2500 tons per year.

In a once-through fuel cycle the nuclear waste management has to rely on direct final disposal of spent nuclear fuel after a certain time of intermediate storage to reduce the decay heat. By nuclear reprocessing the uranium and plutonium can be separated and reused for power generation, while the fission products and minor actinides are vitrified and conditioned for final disposal in a deep geological site. The repeated use of mixed oxide fuel in current power reactors can lead to a reduction of the plutonium inventory by about 25-45% [2].

In order to assess the radiological threat of spent nuclear fuel, we will now compare it with natural uranium. The ingestion radiotoxicity of 1 ton of spent nuclear fuel (4.5% UOX PWR with a burn up of 55 MWd/kg) is shown in Fig. 1. The long-lived radiotoxicity (> 10000 years is dominated by plutonium while below minor actinides are important. The short-lived radiotoxicity < 60 yrs is dominated by fission products. A common reference level is the ingestion radiotoxicity of the natural uranium required to produce 1 ton of enriched U-nuclear fuel (4.2% ^{235}U, 7.83 t nat. U) in equilibrium with its decay products: $1.47 \cdot 10^5$ Sv / tHM.

The mobility in the environment depends among other factors on the volatility of the chemical elements e.g. Cs, Sr, Tc, I, Se having a high volatility. This aspect is not included in Fig.1 but it is taken into account in the safety analysis of final repository concepts. The radiotoxicity of the long-lived fission products is lower than that of the long-lived actinides, but their activity is in the same order of magnitude.

From Fig. 1 the potential of partitioning and transmutation (P&T) as an alternative strategy to direct disposal of the long-lived waste is obvious: The long-term radiotoxicity will be reduced from geological to historical time scales of about 1000 years if all long-lived nuclides can be transmuted
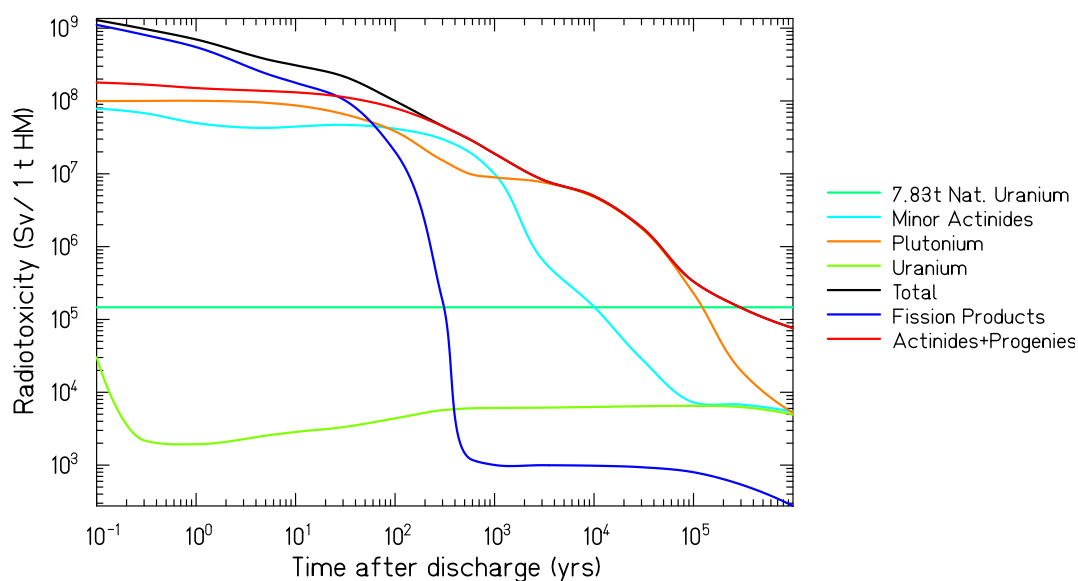
Fig. 1: Radiotoxicity of spent nuclear fuel in Sv per 1 ton of heavy metal as a function of time after discharge from the reactor. The radiotoxicity of plutonium and other (minor) actinides decay to the natural level of the uranium ore required to produce the fuel after 10-100 thousand years and thus their removal by transmutation is especially important. The reference level of the natural uranium required to produce 1 ton of enriched U-nuclear fuel is a horizontal line at $1.47 \cdot 10^5$ Sv / tHM.

into shorter lived fission products. The physics of transmutation is discussed in many review articles, e.g. [3,4]. Among the expected benefits of P&T the transuranium elements in the waste will be strongly reduced. The long term radioactive inventory, decay heat and peak dose rate from the final repository will be strongly reduced, see [5] and references therein.

2 Transmutation technologies and options

The development and safety of Partitioning and Transmutation is a subject of current research in many european and national projects [6]. In Generation IV reactor concepts a closed nuclear fuel cycle is foreseen that will also include nuclear transmutation to significantly reduce the amount of long-lived actinides. The reactor design can be based on modern supercomputers where detailed thermo hydraulic and neutron-transport coupled simulations in realistic geometry are to be done. Fundamental simulation of the processes on the atomic level in parts of the reactor core are possible. Especially in the fast neutron range precise nuclear data for neutron induced reactions are required. Many such nuclear data experiments have been supported by the FP6-EFNUDAT, FP7-ERINDA and FP7-CHANDA projects. In the following paragraphs different technologies for transmutation are introduced, this is done on a basic level, that must be incomplete due to the limited space. References for further information are included. From the arguments given, one should not be tempted to give preference to either one technology, because this will mostly depend on the waste management or nuclear fuel cycle strategy the technology is being developed for.

Based on french legislature from 2006 the Advanced Sodium Technological Reactor for Industrial Demonstration (ASTRID) is being developed by a consortium lead by CEA. ASTRID is planned to be a 600 MWe sodium-cooled fast reactor and it is the most advanced generation IV reactor project. The preliminary design phase II has already been started. Sodium cooled breeder reactors have been developed and operated over many decades giving this technology a solid basis. The main motivation of

ASTRID is to recycle plutonium without limitation. A fuel cycle to transmute and manage americium is also an important topic under study. Homogeneous fuel with a content of 2% Am or heterogeneous fuel with up to 10 % Am in a blanket can be used for transmutation [7]. In principle, the minor actinide content in a fast reactor fuel is limited by the criticality control. The criticality is influenced by the delayed neutron fraction and by the Doppler broadening of the neutron resonances. The corresponding reactivity coefficients get less favourable for fuels containing high concentration of minor actinides.

In an accelerator driven system (ADS) a high-power proton accelerator is coupled to a spallation target that is surrounded by a subcritical reactor core. To allow for a fast neutron spectrum for transmutation the ADS needs to be liquid-metal cooled. If the effective neutron multiplication factor of the reactor core (k_{eff}) is kept below 1 the system cannot have a self-sustained chain reaction. The spallation target is a strong source of neutrons that leads to fission reactions in the reactor core. The accelerator driven system concept was developed at Los Alamos [8] for a thermal spectrum and at CERN [9] for a fast spectrum nearly 20 years ago.

To demonstrate the accelerator driven system technology, i.e. the coupling of the three components (accelerator, spallation target and subcritical reactor) at realistic power level to draw conclusions on the industrial realisation the Multi-purpose hYbrid Research Reactor for High-tech Applications (MYRRHA) project has been established at SCK-CEN, Mol Belgium [10]. A Pb-Bi eutectic cooled fast reactor shall be built that can be operated in critical and subcritical mode. The thermal power is in the range of 65-100 MW. With a high-power proton linac of 600 MeV, 4mA and a subcritical core configuration ($k_{eff} = 0.95$) MYRRHA shall operate with mixed oxide U/Pu fuel. The subcritical layout of the ADS removes limitations due to the reduced fraction of delayed neutrons from fuels rich in minor actinides.

In order to achieve nearly full transmutation of all long-lived actinides several fuel cycles are required in solid fueled nuclear reactors, as the change in reactivity in the core during the operation and also radiation damage to the fuel elements limits the achievable burn up. Partitioning of the spent nuclear fuel, i.e. chemical separation of minor actinides and fission fragments from uranium and plutonium will be necessary as well as refabrication of fuel elements that will be much more radioactive than conventional unirradiated enriched uranium oxide fuel elements. The neutron rate of curium is rather high and it can be advantageous to first transmute Pu, Am and let the curium decay first [3].

Using molten salt technology, e.g. ^{7}LiF or NaF, ZrF_4 together with (U,Pu,M.A.)F_4 a nuclear fuel is produced that is transparent and liquid at high temperatures $T \approx 600°C$. The chemical reprocessing can be simplified as solid fuel fabrication and refabrication does not occur. Also radiation damage in the solid fuel is not a limiting factor. A molten salt reactor exhibits large negative temperature and void coefficients of reactivity that improve the operational safety due to the thermodynamical properties of its liquid fuel. The technology has been realized once in the molten salt reactor experiment at Oak Ridge in the 1960s, where a Thorium fuel cycle was envisioned to breed ^{233}U in a thermal spectrum. In a molten salt reactor volatile fission products are continuously emitted from the fuel and need to be treated, e.g. gaseous fission products must be extracted with an off-gas system. The Molten Salt Fast Reactor (MSFR) is one of the generation IV concepts [11,12]. Fuel Salt chemistry for high burn up of actinides and online reprocessing as well as structural material aspects at high temperatures and neutron irradiations are being investigated, e.g. in the FP7-EVOL project. The transmutation potential has been investigated e.g. for the German phase out of nuclear power and more than 90% transmutation efficiency has been found by simulations [13].

3   nELBE A new time-of-flight facility for nuclear data

For the development of nuclear waste management strategies and technologies for transmutation precise nuclear data especially in the range of fast neutrons are required. Important reactions to be studied are for example the neutron-induced fission of plutonium isotopes and minor actinides as well as the inelastic
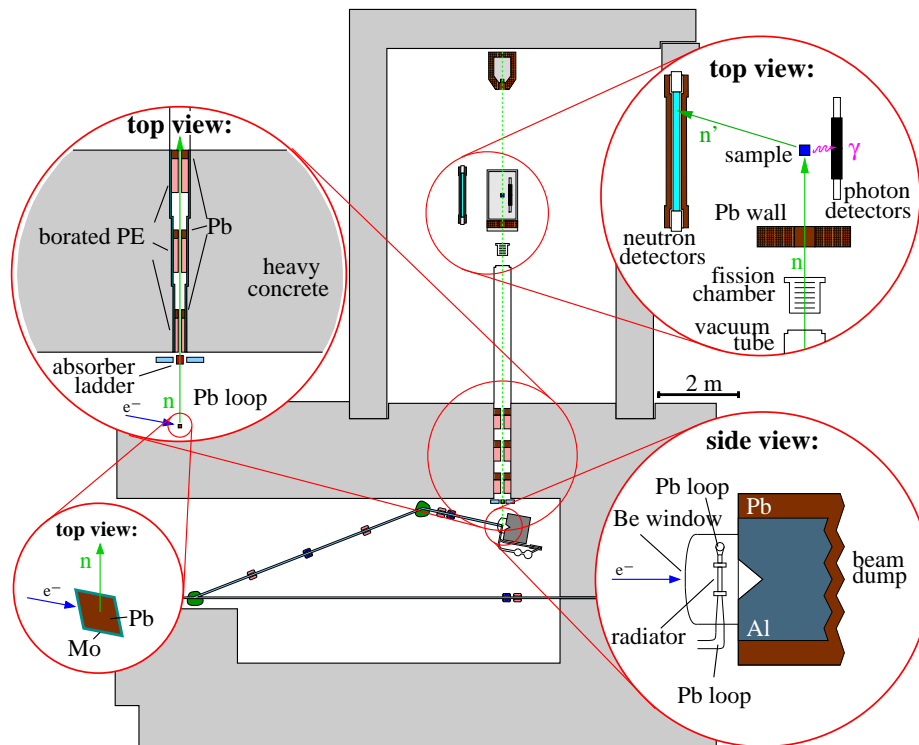
Fig. 2: Floorplan of the new nELBE facility at Helmholtz-Zentrum Dresden-Rossendorf. Insets show the neutron producing target, the collimator and the experimental setup in the time-of-flight hall. The maximum flight path is 11 m.

neutron scattering on structural, fuel and coolant materials, see e.g. [14].

The nELBE time-of-flight facility at Helmholtz-Zentrum Dresden-Rossendorf (HZDR) which – based on a superconducting electron accelerator – is dedicated to measurements in the fast neutron range has been extensively rebuilt. The time-of-flight path is now between 4 and 11 m. A much larger time-of-flight experimental hall allows us to reduce the background from scattered neutrons as all walls including ceiling and floor are at least 3 m away from the evacuated neutron beam line. The liquid lead circuit used as a neutron producing target has also been redesigned and rebuilt. Through the liquid-lead technology the neutron beam intensity is not limited by the heat dissipation inside the target. The technical design including thermomechanical parameters of the liquid lead circuit and the beam dump has been discussed in [15]. The neutron source strength at the nominal beam current of 1 mA has been calculated to be 10^{13} neutrons/s, [16]. The accelerator produces high brilliance electron beams with variable micropulse repetition rates and duty cycles. The electrons are accelerated up to 40 MeV in continuous wave-mode by superconducting radio frequency cavities. The maximum average beam current at a micropulse rate of 13 MHz is 1 mA. For typical time-of-flight measurements the repetition rate is reduced to 100-200 kHz resulting in a source strength of about 10^{11} n/s. The bunch length is about 5 ps, so that the time-of-flight resolution is not degraded and short flight paths can be used with a high resolution detection system. Figure 2 shows the floor plan of the new neutron time-of-flight facility in the Center for High Power Radiation Sources of HZDR.

The electron beam passes through a beryllium window mounted on a stainless-steel vacuum chamber and hits the radiator, consisting of a molybdenum channel confining the liquid lead. The channel has a rhombic cross section with 11 mm side length. The electrons generate bremsstrahlung photons which release neutrons in secondary (γ,n) reactions on lead. These leave the radiator almost isotropically, while
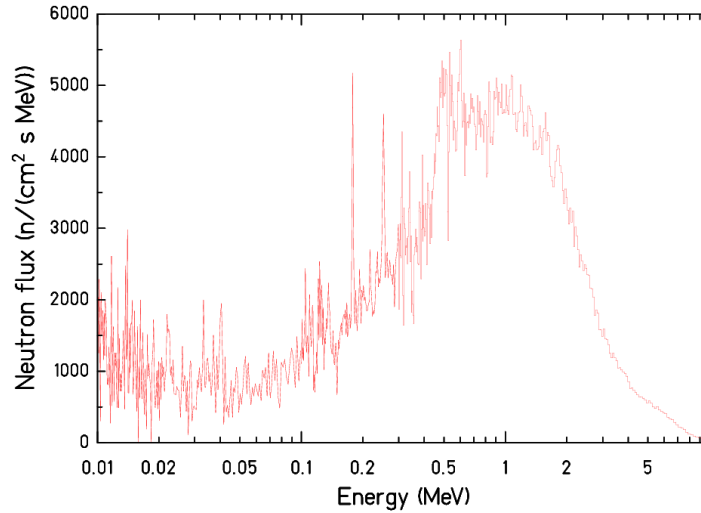
Fig. 3: Neutron spectrum measured with a ^{235}U fission chamber (H19, PTB Braunschweig) at a flight path of 815 cm. The electron beam energy was 30 MeV and the average current 6 μA with a measurement live time of 15 hours.

the angular distributions of electrons and photons are strongly forward-peaked. The collimator and the resulting neutron beam properties at the experimental area have been optimized using MCNP in order to maintain the correlation of time-of-flight and neutron energy. The collimator of 2.6 m length contains three replaceable elements of lead and borated polyethylene that are mounted inside a precision steel tube [16].

The redesigned neutron producing target and collimator have the same dimensions as before the extension of the facility, consequently a very similar neutron spectrum and spatial beam profile is expected. In a first beam time, the neutron spectral rate and the beam profile has been measured. In Fig. 3 the neutron spectral rate measured with a ^{235}U fission chamber is shown. At 30 MeV electron energy the usable neutron energy range extends from ca. 100 keV to 10 MeV. Absorption dips at 78,117, 355, 528, 722, 820 keV are due to ^{208}Pb scattering resonances. Pb is used as the neutron producing target, as collimator material and as bremsstrahlung absorber at the collimator entrance. Emission peaks at 40,89,179, 254, 314, 605 keV come from the near threshold photoneutron emission of ^{208}Pb (strong capture resonances of ^{207}Pb) [17]. The beam profile shown in Fig. 4 was measured by moving a plastic scintillator (length: 1 m, width: 11 mm) through the beam. The scintillator was read out on both ends by high gain photomultiplier tubes. By setting a gate on the time-of-flight spectrum the bremsstrahlung and neutrons can be separated. A fit assuming a rectangular beam profile with a sharp edge shows that the beam has some halo that might be attributed to a too small window at the exit of the neutron beam line. The beam profile measurement technique is described in [17].

To study the inelastic scattering a first test with LaBr$_3$ scintillators has been made. The target was a disk of ^{nat}Fe with a diameter of 7 cm and thickness 0.80 cm. The LaBr$_3$ detector was 30 cm away from the target under an angle of 159 degrees. Despite the short measurement time the 847 keV and 1238 keV gamma rays from the inelastic scattering ^{56}Fe(n,n') are clearly visible. Fig. 5 shows the time-of-fight to gamma-ray energy correlation matrix measured with the LaBr$_3$ scintillator. The time-of-flight was calibrated using the bremsstrahlung peak shown as a horizontal line. The gamma ray line at 1468 keV is from intrinsic radioactivity of the ^{138}La and can be used to monitor the PMT gain. It is planned to study the inelastic scattering with several LaBr$_3$ scintillators under different angles
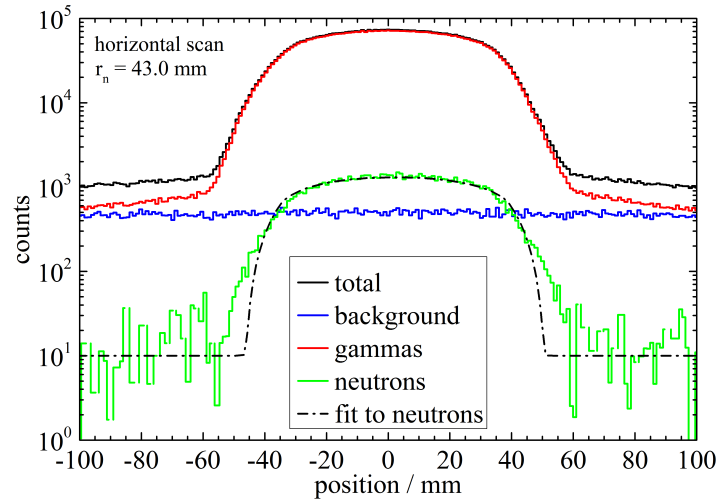
Fig. 4: Time-of-flight beam profile measured with a plastic scintillator moved through the beam in horizontal direction. A time-of-flight gate was used to determine the bremsstrahlung and neutron beam profile separately.
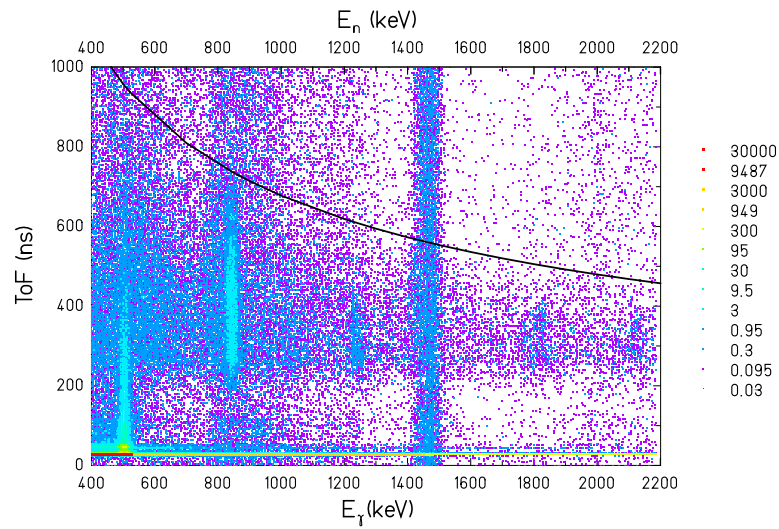
Fig. 5: Energy vs. time-of-flight spectrum of gamma rays emitted from ^{56}Fe(n,n') measured with a 3*3" LaBr$_3$ scintillator with an angle of 159 degrees to the beam direction. The flight path is $\approx$ 936cm. The black line corresponds shows the time-of-flight curve of neutrons with kinetic energy E_n (upper abscissa). The live time of the measurement is 1291 s.

4 Acknowledgments

References

[1] Statistical pocketbook Energy 2013 of the European Commission

[2] B. Merk, C. Broeders, atw 53. Jg. (2008) Heft 6 Juni 404

[3] Physics and Safety of Transmutation Systems A Status Report, OECD 2006, NEA No. 6090

[4] Salvatores, G. Palmiotti, Progress in Particle and Nuclear Physics 66 (2011) 144.

[5] Potential Benefits and Impacts of Advanced Nuclear Fuel Cycles with Actinide Partitioning and Transmutation, OECD 2011, NEA No. 6894

[6] 8th European conference on Euratom research and training in reactor systems, 14-17 October 2013,Vilnius, Lithuania

[7] International Conference on Fast Reactors and Related Fuel Cycles: Safe Technologies and Sustainable Scenarios (FR13), 4-7 March 2013, Paris, France, presentations by C. Behar and J. Grouiller.

[8] C.D. Bowman et al., NIM A320 (1992) 336; C.D. Bowman, Annu. Rev. Nucl. Part. Sci. 1998. 48:505

[9] C. Rubbia et al., Cern Report (1995) CERN/AT/95-44 (ET)

[10] H. Ait Abderrahim, Int. Jour. of Energy Research, 36 (2011) 1331

[11] C.W. Forsberg, Thermal- and Fast-Spectrum Molten Salt Reactors for Actinide Burning and Fuel Production, Paper in "Global 07: Advanced Nuclear Fuel Cycles and Systems", 2007, American Nuclear Society.

[12] SNETP strategic research agenda, Annex, January 2012, Molten Salt Reactor Systems.

[13] International Conference on Fast Reactors and Related Fuel Cycles: Safe Technologies and Sustainable Scenarios (FR13), 4-7 March 2013, Paris, France, presentation by B. Merk.

[14] Uncertainty and target accuracy assessment for innovative systems using recent covariance data evaluations, NEA/WPEC-26, Report NEA No. 6410, 2008

[15] E. Altstadt *et al.*, Ann. Nucl. Energy **34**, 36 (2007).

[16] J. Klug *et al.*, Nucl. Inst. Meth. **A 577**, 641 (2007).

[17] R. Beyer *et al.*, Nucl. Inst. Meth. **A 723**, 151 (2013).

The high intensity neutron source FRANZ

Claudia Lederer, René Reifarth[1]
[1]Johann-Wolfgang Goethe University Frankfurt, Germany

Abstract

The Frankfurt neutron source of Stern Gerlach Zentrum FRANZ is currently under construction at the University of Frankfurt. At FRANZ, a high intensity neutron beam in the keV energy region will be produced by bombarding a ^{7}Li target with a proton beam of several mA. These unprecedented high neutron fluxes will allow a number of neutron induced cross section measurements for the first time. Measurements can be performed by the time-of-flight and by the activation technique.

1 Introduction

About half of the solar abundances of elements heavier than Fe are produced by the slow neutron capture process (s process). The s process takes place in He burning stages of stars at moderate neutron densities of typically 10^8cm^{-3}. Neutrons are captured on seed nuclei in the Fe region and heavy elements up to Bi are built up by a sequence of neutron captures and radioactive β decays. In general, β decays are faster than neutron capture on unstable species and the reaction path goes along the valley of stability. There are, however, a number of long lived radionuclides where β decay competes with neutron capture, the so-called branching points. The main nuclear physics input to calculate abundances produced in the s process are Maxwellian averaged cross sections (MACS), defined as

$$< \sigma >= \frac{2}{\sqrt{\pi}} \frac{1}{(k_B T)^2} \int_0^\infty \sigma(E) E \exp(-\frac{E}{k_B T}) dE, \tag{1}$$

where T is the stellar temperature, and $\sigma(E)$ the energy dependent cross section. Since the s process takes place at stellar temperatures between 0.1 and 1 GigaKelvin, the Maxwellian neutron energy distribution peaks in the keV region. Depending on the stellar burning stage where the s process takes place, temperatures correspond to kT values of 8, 25 and 90 keV, respectively. Maxwellian averaged cross sections of branching point nuclei are of special interest since they give information about temperature, neutron density and mass density of s process environments [**?**].

Neutron induced cross sections are not only of interest for element synthesis in stars, but also for technological applications. They are, for example, important for calculating the neutron budget or estimating radioactive waste production in conventional reactors, as well as for innovative systems, such as accelerator driven systems and Generation IV power reactors.

In both areas, there is a special need for measuring cross sections of radioactive species. Such measurements require high neutron fluxes, since often only small amounts of sample material are available or the intrinsic sample activity is high. These nuclear data needs will be addressed at the high intensity neutron source FRANZ (Franz Neutron Source at Stern-Gerlach Zentrum), which is currently under construction at the Goethe University Frankfurt, Germany.

2 FRANZ

At FRANZ, neutrons will be produced by the ^{7}Li(p, n) reaction, which is the most prolific nuclear reaction to produce neutrons in the keV region. Neutron cross sections can be measured in time-of-flight, and in activation mode. A high intensity proton beam of 200 mA DC will be produced in a Volume type ion source. The proton beam of initially 150 keV is then accelerated to 2 MeV in an RFQ element. A drift tube cavity installed afterwards adjusts the proton energy to values between 1.8 and 2.2 MeV. The

accelerator can be operated in continuous and pulsed mode. In continuous mode, nominal proton currents are 20 mA, resulting in a neutron yield of 10^{12} neutrons per second available for activation experiments. For a pulsed proton beam, a chopper at the entrance of the RFQ will create bunches 100 ns in length with a frequency of 250 kHz. A bunch compressor of Mobley type will further compress the proton pulse to 1 ns width. In pulsed mode, proton beam currents will amount to about 2 mA on average. The pulse mode is required for time-of-flight experiments. Neutron captures are measured by detecting the prompt γ cascade emission with a 4π BaF$_2$ array. A sketch of the FRANZ accelerator is shown in Figure 1. More Details on the accelerator and its components can be found in [**?**].
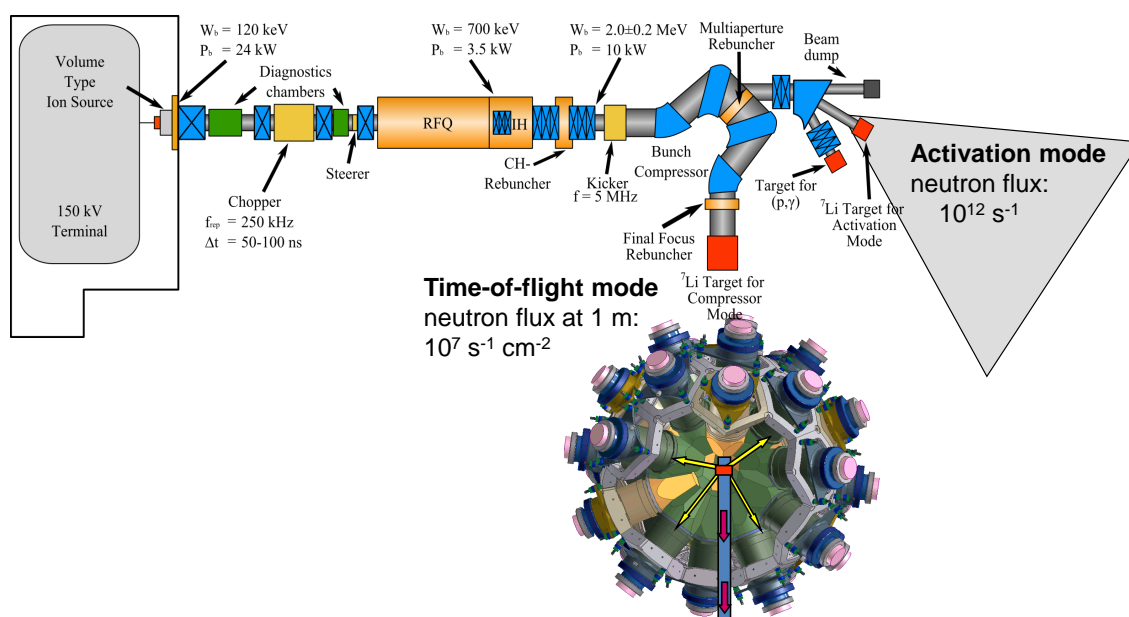

Fig. 1: Scheme of the future FRANZ neutron source. See text for details.

3 Neutron induced cross section measurements

3.1 Activation Measurements

For activation experiments, the neutron spectrum should be well known and extend only over a limited neutron energy range. The ^{7}Li(p,n) reaction at proton energies around 2 MeV is especially well suited for measuring Maxwellian Averaged Cross Sections. By choosing a proton energy of 1912 keV, not far above the reaction threshold of 1881 keV, the neutron energy spectrum approximates a Maxwellian distribution around 25 keV. This feature has already been extensively used at the former Van-de-Graaff accelerator at Forschungszentrum Karlsruhe (FZK, now Karlsruhe Institute of Technology) to measure stellar cross sections across the nuclear chart [**?**]. Additionally, the neutrons are emitted in a forward peaked cone due to kinematic reasons, which enables a sample to cover the entire neutron beam. A calculation of the neutron spectrum with the beam parameters that will be available at FRANZ (1912 $\pm$ 20 keV) is compared to a neutron spectrum of the form $\phi(E) \propto E \times \exp(-E/kt)$ with $kT = 24$ keV, required for obtaining Maxwellian averaged cross sections (see Eq. 1), in Figure 2.
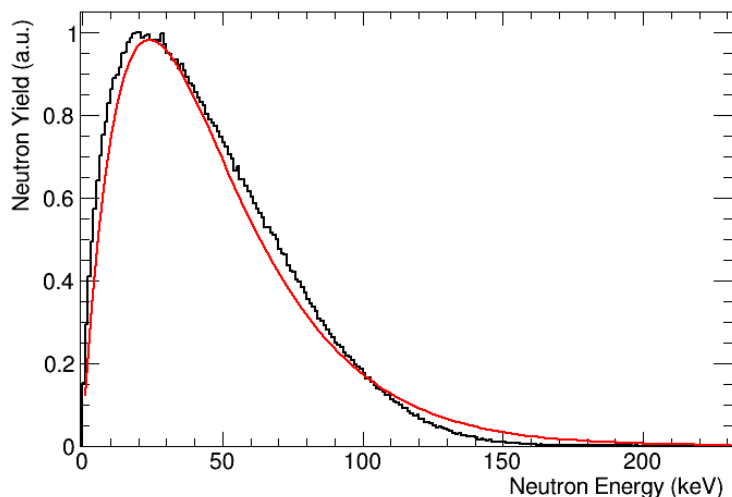
Fig. 2: Neutron spectrum for the ^{7}Li(p,n) reaction calculated with the code PINO [**?**], assuming a proton energy of 1912 ± 20 keV and a Li target thickness of 30 μm. The calculated spectrum (black) is compared to a spectrum of the form $\phi(E) \propto E \times \exp(-E/24\text{keV})$ (red), required to measure MACSs for the s process.

The Figure demonstrates that the produced neutron spectrum is perfectly suited for MACS measurements for the s process. Besides this favorable behaviour at 1912 keV, neutron spectra can also be tailored towards higher energies by increasing the proton energy. With the maximum proton energy of 2.2 MeV, neutron energies range up to 500 keV.

At FRANZ, final neutron yields in activation mode will reach around 10^{12} neutrons per second, which is a factor 1000 higher than what was possible at Karlsruhe. These high neutron fluxes will enable a number of new (n,γ) measurements of very small cross sections and of very small sample material, which is usually the case, when the sample is radioactive. One interesting example is neutron capture on the s process branch point isotope ^{59}Fe, which has a half life of only 45 days. The stellar ^{59}Fe(n,γ) cross section is crucial for understanding the abundances of the long lived ^{60}Fe (lifetime 1 My), which is produced in supernova explosions, in our galaxy. Using the high neutron flux available at FRANZ, ^{60}Fe can be produced via double neutron capture on ^{58}Fe. The number resulting of ^{60}Fe atoms can then be measured by Accelerator Mass Spectrometry.

3.2 Time-of-flight Measurements

For cross section measurements with the time-of-flight technique, the proton beam needs to be pulsed in order to accurately define the time when the neutrons were produced. At FRANZ, proton pulses will have a width of about 1 ns, which enables measurements with high neutron energy resolution even close to the Li target. At a flight path of 1 m for example, the neutron energy resolution at 10 keV neutron energy is 30 eV. Neutron capture cross sections will be measured by detection of the prompt γ-ray cascade with a 4π BaF$_2$ array, consisting of 42 crystals. This detector, which offers high efficiency combined with low sensitivity to reactions with neutrons, was already successfully used at FZK and transported to Frankfurt after shut down of the Van de Graaff accelerator. Additionally, it is planned to build a detector, especially suited for measuring samples at ultra-short flight paths ($\approx$10 cm) [**?**]. A first (n,γ) measurement with this novel setup is planned for the radioactive ^{85}Kr, which has a half-life of only 10 years.

4 Summary

The Frankfurt Neutron Source at Stern Gerlach Zentrum FRANZ is currently under construction at the Goethe University Frankfurt. At FRANZ, a highly intense neutron beam will be produced by the

^{7}Li(p, n) reaction using a proton beam energy between 1.8 and 2.2 MeV. Neutron fluxes will be a factor of 100-1000 higher than at present facilities. The neutron spectrum extend over energies from 1-500 keV, which is perfectly suited for measuring neutron cross sections of astrophysical, but also technological interest. Neutron cross sections can be measured via the activation, and via the time-of-flight technique. The unprecedented neutron fluxes will allow for the first time to measure cross sections on isotopes with half lives of only months.

References

[1] F. Käppeler, R. Gallino, S. Bisterzo, W. Aoki, Rev. Mod. Phys. 83 (2011) 157.

[2] C.Wiesner, L. P. Chau, H. Dinter, M. Droba, M. Heilmann, N. Joshi, D. Mäder, A. Metz, O. Meusel, I. Müller, D. Noll, H. Podlech, U. Ratzinger, H. Reichau, R. Reifarth, A. Schempp, S. Schmidt, W. Schweizer, K. Volk, C. Wagner, AIP Conf. Proc. 1265 (2010) 487.

[3] Z. Y. Bao, H. Beer, F. Käppeler, F. Voss, K. Wisshak, At. Data Nucl. Data Tab. 76 (2000) 70.

[4] R. Reifarth, M. Heil, F. Käppeler, R. Plag, Nuc. Instr. Meth. Phys. Res. A 608 (2009) 139.

[5] R. Reifarth, R. C. Haight, M. Heil, F. Käppeler, D. J. Vieira, Nucl. Instr. Meth. A 524 (2004) 215.

Measurement of the differential neutron-deuteron scattering cross section in the energy range from 100 keV to 600 keV using a proportional counter

R. Nolte[1], J. Beyer[1], A. Plompen[2], S. Röttger[1]
[1]Physikalisch-Technische Bundesanstalt (PTB), Bundesallee 100,
38116 Braunschweig, Germany
[2]Institute for Reference Materials and Measurements (IRMM), Retieseweg 111, 2440 Geel,
Belgium

Abstract

The angular distribution of neutron-deuteron scattering was investigated using the proportional counter P2 simultaneously as scattering target and detector for the recoil deuterons. The measurements were carried out using monoenergetic neutrons in the energy range from 150 keV to 500 keV. Various techniques were employed to reduce distortions of the experimental pulse-height distribution by photon-induced events. The experimental data were compared with realistic simulations which were carried out using different evaluated data sets. This comparison allows to conclude on inconsistencies in the evaluations.

1   Introduction

Next to the neutron-proton (n-p) scattering ($N = 2$), neutron-deuteron scattering ($N = 3$) is the most fundamental interaction process in a few-body quantum system consisting of N nucleons. It can be described by the re-formulated Fadeev three-body equations [1] using the well-developed nucleon-nucleon potentials for the interaction between the three nucleons involved. These calculations covered the energy range from 3 MeV to 19 MeV which were later extended to a lower limit of 50 keV [2].

In addition to its relevance for understanding quantum mechanical few-body systems, the differential neutron-deuteron (n-d) scattering cross section is also relevant for nuclear technology, in particular for the design and safe operation of heavy-water moderated reactors, e.g. of the CANDU design. Several critical and subcritical benchmark experiments for heavy-water moderated configurations demonstrated the sensitivity of the effective neutron multiplication factor k_{eff} and the coolant void reactivity (CVR) to the angular distribution of the neutron-deuteron scattering cross sections [3]. In particular, significant changes in the calculated k_{eff} and CVR values were observed when the data of the ENDF/B-VI.3 [4] library were replaced by data from later releases

It is very striking to see that the experimental data base supporting the evaluations are rather scarce and partially inconsistent, with some of the measurements dating back to the 1950's and 1960's. As an example, Figure 1 shows the experimental data available from EXFOR [5] for the energy range from 100 keV to 2 MeV. The data are grouped into four narrow energy intervals and compared with angular distributions from ENDF/B-VII.0 [6] calculated for the mean energy of each energy interval. The inconsistency of the available experimental data and, in particular, the difficulty to reproduce the results of benchmark experiments have prompted the inclusion of the differential neutron-deuteron scattering cross section in the OECD high-priority request list (HPRL) [7] for urgent nuclear data measurements.

As for neutron-proton scattering, the differential neutron-deuteron scattering cross sections can be measured either by detecting the scattered neutron or the recoiling deuteron. While the first approach is most suited for higher neutron energies, it poses difficulties at lower energies because efficient and well-characterized neutron detectors are difficult to find in the energy range below a few hundred keV. The present contribution reports results of new measurements using a proportional counter simultaneously as target and detector for the recoiling deuterons. This technique was already used for the measurements of some of the earlier data available from EXFOR. Therefore, the present work also aims at improving the potential of the method by proper modelling of deteriorating experimental influences.
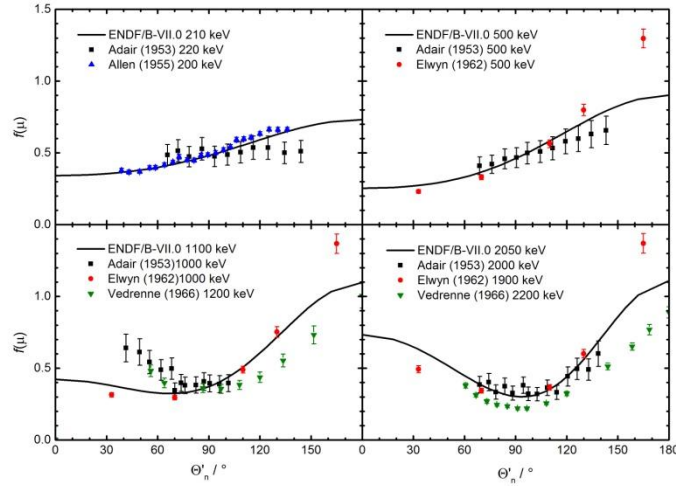
Fig. 1: Experimental angular distributions (symbols) for neutron-deuteron scattering for the energy range from 100 keV to 2000 keV compared with evaluated angular distributions from ENDF/B-VII.0 (solid lines) calculated for the mean neutron energy of the data sets.

2   Experimental Technique

For elastic neutron scattering in non-relativistic approximation a simple relation exists between the energy E_R of the recoil nucleus in the laboratory (LAB) system and the scattering angle Θ'_n in the centre-of-mass (CM) system,

$$E_R = E_n \frac{4A}{(A+1)^2} \frac{1+\cos(\Theta'_r)}{2} \tag{1}$$

where $A = m_T/m_n$ denotes the ratio of the mass m_T of the target nucleus to the mass m_n of the neutron. Because of this relation the energy distribution of the recoil nuclei in the LAB system is directly related to the differential scattering cross section $(d\sigma_{el}/d\Omega'_n)$ in the CM system,

$$\left(\frac{d\sigma_{el}}{dE_R}\right) = \frac{4\pi}{E_R^{max}} \left(\frac{d\sigma_{el}}{d\Omega'_n}\right)(E_R) . \tag{2}$$

Here, $E_R^{max} = 4A/(A+1)^2 E_n$ is the maximum energy of the recoil nucleus in the LAB system. For neutron-proton and neutron-deuteron scattering the kinematical factor $4A/(A+1)^2$ is approximately 1 and 8/9, respectively. Hence the angular distribution in the CM system is directly proportional to

the distribution of energies deposited by the recoil nuclei. In an ideal detector for recoil nuclei, this distribution is identical to the pulse-height (PH) distribution.

In real detectors, however, several effects deteriorate this simple relation because the energy deposition is only the first step of the detection process and is followed by production and transport of scintillation light in case of scintillation detector or the electron-ion pairs in case of gas detectors. In a proportional counter, incomplete energy deposition by particles leaking out of the sensitive volume (wall effects), sensitivity of the counter to parasitic photons and a possible energy dependence of the mean energy W required to produce an electron-ion pair distort the PH spectra and have to be accounted for in the analysis of the measurements. This can be achieved by an iterative comparison of a realistic Monte Carlo simulation with the experimental PH spectra and an adjustment of the angular distributions.

The present measurements were carried out using the PTB recoil proton proportional counter (RPPC) P2. A sketch of the RPPC is shown in Fig. 2. P2 is routinely used to measure the total fluence for neutron energies below 1.2 MeV. The use of this type of detector was described in detail by Skyrme et al. [8]. The RPPC P2 was constructed in compliance with this reference, with only slight modifications of the mechanical details. It consists of a cylindrical stainless steel housing, 0.5 mm thick, 76 mm in diameter and 360 mm in length. The thickness of the stainless steel entrance window is 0.5 mm. The size of the sensitive volume within this housing, 55.5 mm in diameter and 193.3 mm in length is restricted and defined by a cylindrically shaped cathode made of aluminium, 0.3 mm thick, and by guard tubes arranged at both ends of the anode wire.
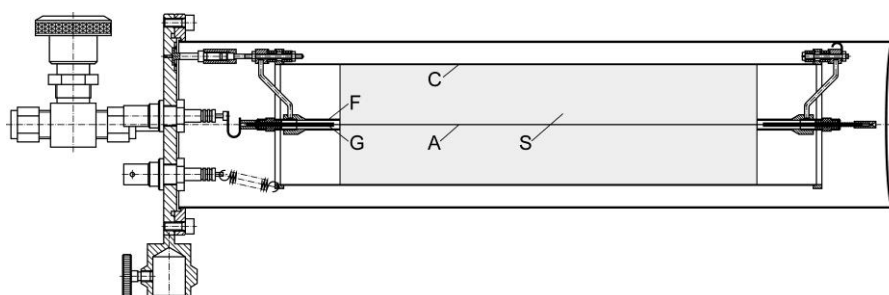
Fig. 2: Recoil proton proportional counter P2 used at the PTB as the primary reference instrument for fluence measurement of neutrons with energies up to 1.2 MeV. C: cathode cylinder, A: anode wire (gold-plated tungsten wire 100 μm in diameter), F: field tube, G: guard tube, S: sensitive volume (shaded in grey). The neutrons are usually incident along the axis of the counter.

The guard tubes are held at ground potential, while the potential of anode and cathode are selected such that the cylindrical equipotential surfaces extent undisturbed into the volumes before and behind the sensitive volume between the guard tubes. The gas of the RPPC must meet the requirements of a well-known hydrogen content and a high gas amplification. The optimal gas filling depends on the neutron energy. For neutron energies below 300 keV, P2 is operated with a mixture of H_2 (96.5 vol%) and CH_4 (3.5 vol%) while propane (C_3H_8) is used at higher energies to reduce the range of recoil protons and limit the influence of incomplete energy deposition by recoil particles escaping the sensitive volume through the annular or rear surface or entering it through the front surface. For deuterated gases the use of a D_2/CD_4 mixture can be extended to about 500 keV because of the smaller ranges of the deuterons at a given kinetic energy.

For the present experiments, P2 was operated with the D_2/CD_4 mixture at a pressure of 1000 hPa (965 hPa D_2 and 35 hPa CD_4). In addition, measurements were also carried out using a H_2/CH_4 mixture at the same pressure and C_3H_8 at 600 hPa to identify a possible distortion of the

PH spectra. The isotopic purity of the deuterium in the D_2 and CD_4 was 99.8% and 99.9%, respectively. The chemical purity of the D_2, H_2 and CH_4 gases were better than 99.999% while the purity of the CD_4 was only 99.9%. Therefore, oxisorb cartridges were used to remove traces of oxygen and water from the gas during the filling process.

The neutrons fields were produced in open geometry using the $^7Li(p,n)^7Be$ reaction. The measurements were carried out in the low scatter hall of the PTB ion accelerator facility PIAF using proton beams from the 3.7 MV Van-de-Graaff accelerator. Data were taken for mean neutron energies E_n of about 145 keV, 200 keV, 250 keV, 300 keV and 500 keV with and without a polyethylene shadow cone, 300 mm in length, for subtraction of room-return neutrons. The neutron fields had a 2% - 4% contribution of non-monoenergetic neutrons resulting from neutron scattering in the target. The spectral distribution of these neutrons was calculated using the TARGET code [9].

The proportional counter is also sensitive to photons. Hence, photon-induced events can deteriorate the determination of the angular distribution of neutron-deuteron scattering from the PH distributions. Therefore, several measures were undertaken to minimize photon interference as much as possible. The contamination of the neutron field with photons was reduced as much as possible by employing a metallic lithium target. The lithium mass per unit area was 70 µg/cm^2 and the target backing consisted of tantalum, 0.5 mm in thickness. The pressure in the counter was adjusted such that the energy deposition by Compton electrons directed parallel to the counting wire did not exceed 40 keV in case of the D_2/CD_4 mixture at 1000 hPa and 125 keV for the C_3D_8 gas at 600 hPa, while still keeping the wall effects for recoil particles below an acceptable level (see below).

For some neutron energies a cylindrical lead absorber, 21 mm in thickness and 82 mm in diameter, was placed between the target and the counter to further suppress the photon contamination. At the energies used in the present work, neutrons interact with lead only by elastic scattering which does not affect the spectral distribution of the field significantly. A PH distribution produced by photons only was measured at a proton energy of 1880 keV, i.e. below the $^7Li(p,n)^7Be$ threshold at 1881 keV. Assuming that the spectral distribution of the contamination photons has a weak energy dependence, this PH distribution was used to correct for the photon contribution for the neutron beams with energies between 145 keV and 250 keV, i.e. for proton energies between 1945 keV and 2021 keV. It should be noted here that a considerable fraction of the photon contamination is subtracted anyway by the shadow cone measurement. The residual photon interference is only caused because some photons are absorbed in the shadow cone which makes the subtraction of the photon component incomplete.

The sensitivity of the counter to the residual photons was suppressed by an analogue rise time discrimination scheme [10]. In a proportional counter the tracks caused by Compton electrons are much longer than those from recoil proton or deuterons. Hence, as shown in Fig. 3, the drift times of secondary electrons from a long electron track show a considerably larger spread than those from the short track of a recoil particle, unless the tracks are almost collinear with the counting wire. This spread in drift times is reflected in the rise time (RT) of the anode signal. In the present experiment, the rise time of the anode signal after shaping by a charge-sensitive preamplifier and a fast-filter amplifier was determined from the time difference between the outputs of a leading edge discriminator (LE) set just above the noise level and a constant-fraction discriminator (CFD) triggering at about 40% of the maximum signal amplitude ($f = 0.4$).

The events were sorted in a RT versus PH matrix. In this matrix the recoil events cluster on a ridge while the electron events have a wider distribution at low PH. Fig. 4 shows a RT vs. PH matrix for a neutron energy of 300 keV. The events contained in the shaded region are those effected by recoil deuterons. Of course, this RT discrimination cannot be perfect because at higher

energies the track length of recoil particles becomes similar to that of electrons in the sensitive volume.
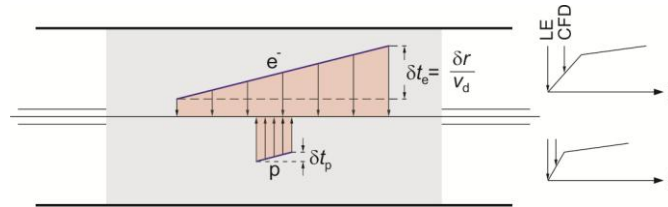

Fig. 3: Discrimination of recoil proton or deuteron events (short tracked labelled p) from those produced by Compton electrons (long track labelled e) using the different spread of the drift times of secondary electrons which is reflected in the rise time of the anode signal. The rise time is determined from the time difference of the outputs of two discriminators, one (LE) operating just above the noise level and one (CFD) at about 40% of the maximum signal amplitude.
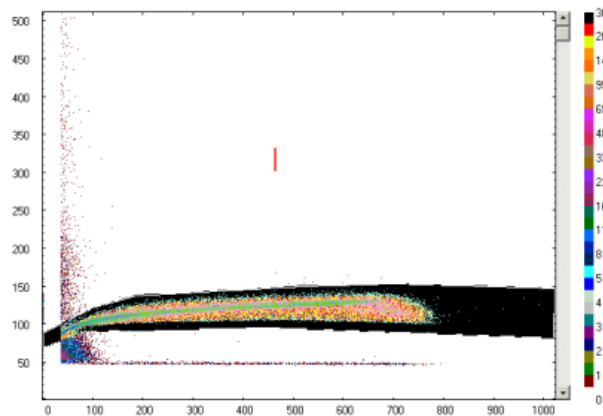
Fig. 4: RT (vertical axis) versus PH (horizontal axis) matrix for a neutron energy of 300 keV. The data points inside the shaded polygon are those produced by recoil deuterons.

Fig. 5 shows a comparison of the suppression of photon-induced events by the RT discrimination technique to that achieved using either the lead absorber (right panel) or the subtraction of a sub-threshold PH distribution (left panel). Obviously all techniques result in almost equivalent net PH distributions, except for very low pulse-height, where the lead-absorber seems to give slightly better results.
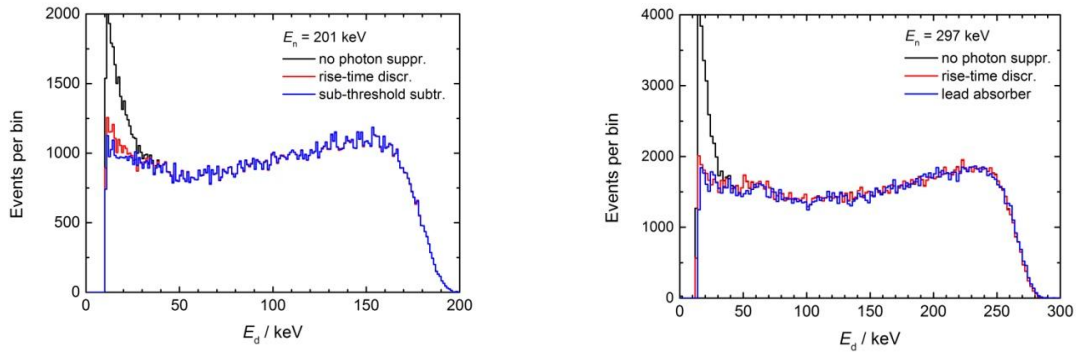
Fig. 5: PH distributions after subtraction of the shadow cone measurement. The black histograms are without further photon suppression. The red histograms show the effect of the RT discrimination. The blue histogram in the left panel was obtained by subtraction of a sub-threshold PH distribution from the black histogram. The blue histogram on the right panel shows the effect of using a lead absorber instead of applying the RT discrimination technique.

3 Results

The data analysis for the present experiment at PTB is based on a dedicated Monte Carlo code which simulates the scattering of neutrons on hydrogen (^{1}H), deuterium (^{2}H) and carbon (^{nat}C). The differential cross sections are sampled from Legendre expansions. For ^{1}H the coefficients from ENDF/B-VII.0 were used directly. For ^{2}H the coefficients were determined from fits to the tabulated angular distributions of the ENDF/B-VII.0, JENDL 4.0 [11] and ENDF/B-VI.3 libraries. For ^{nat}C data from ENDF/B-VII.0 were used. A logarithmic-linear interpolation scheme was used to obtain coefficients for all neutron energies. The recoil particles are tracked using range data calculated with the SRIM2013 code [12]. With the employed option of the code energy and angular straggling are not simulated. For H_2/CH_4 and D_2/CD_4 an energy-independent W value was used for protons and deuterons based on the data of Breitung [13]. A linear dependence of the W value for carbon ions on $\log(E / \text{keV})$ was assumed with a slightly modified slope compared with the data of Posny et al. [14] for propane. The neutron transport in the other counter materials was not modelled because calculations using MCNPX showed that neutron scattering on structural materials had a negligible effect on the shape of the PH distributions.

Figures 6 - 8 show a comparison of simulated and experimental PH distributions for the five neutron energies between 145 keV and 500 keV and for the two hydrogen isotopes. The simulated distributions were folded with a Gaussian response function of constant relative width to model the PH resolution of the instrument. The maximum order of Legendre polynomials used for fitting the angular distributions for ^{2}H was $l_{max} = 1$ below 500 keV and $l_{max} = 2$ at 500 keV.
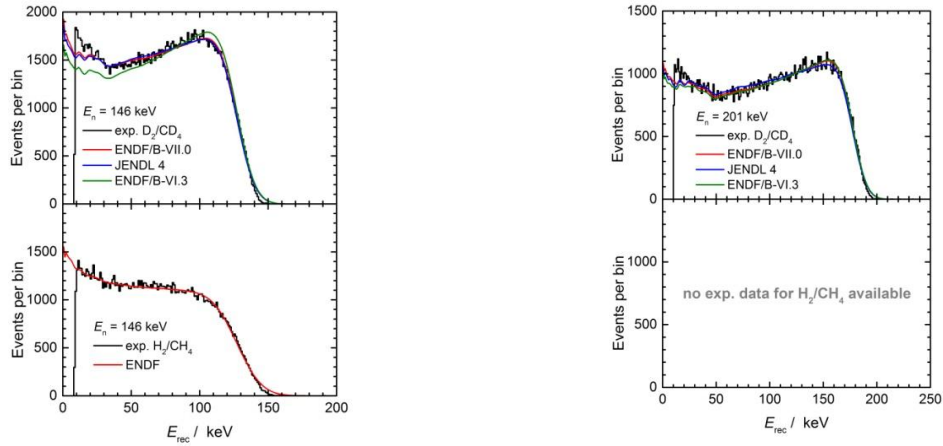
Fig. 6: PH spectra measured for 145 keV neutrons (left panels) and 201 keV neutrons (right panels) with D_2/CD_4 (upper panels) and H_2/CH_4 (lower panels) at a pressure of 1000 hPa (histograms). The solid lines show the calculated spectra obtained with the differential n-d and n-p cross sections from ENDF/B-VII.0 (red line), JENDL 4.0 (blue line) and ENDF/B-VI.3 (green line). The calculations were fitted to the experimental data in the recoil energies range above 35 keV (left panels) and 50 keV (right panels), corresponding to a neutron-deuteron scattering angle Θ'_n of 117.4° and 116.1°, respectively. The experimental data were obtained using rise time discrimination of photon-induced events. In addition a lead absorber was employed to reduce the photon contamination of the neutron field.

The good agreement of the measured pulse-height spectra with the calculations, except for the very low pulse heights, confirms the angular distributions from ENDF/B-VII.0 or JENDL 4.0 which are quite similar at these low neutron energies.
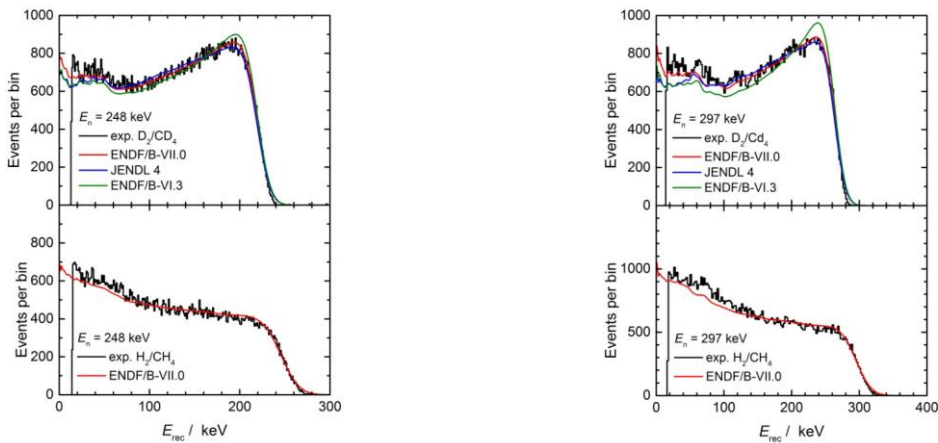
Fig. 7: Same as for Fig. 6 but for a neutron energy of 248 keV (left panels) and 297 keV (right panels). The calculations were fitted to the experimental data in the recoil energy range above 60 keV (left panels) and 100 keV (right panels), corresponding to a neutron-deuteron scattering angle Θ'_n of 117.1° and 104.1°, respectively.

193
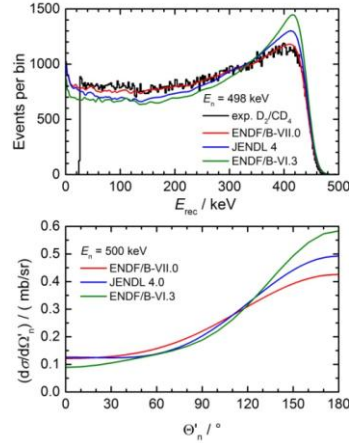
Fig. 8: The upper panel shows measured calculated PH spectra for 498 keV neutrons. The lower panel shows the angular distributions in the CM system from ENDF/B-VII.0 (red line), JENDL 4.0 (blue line) and ENDF/B-VII.3 (green line) for a neutron energy of 500 keV. The calculations were fitted to the experimental data in the recoil energies range above 120 keV, corresponding to a neutron-deuteron scattering angle Θ'_n of 117.3°.

At 300 keV, the fit of experimental and calculated spectra was restricted to recoil energies higher than 100 keV because there is a mismatch for smaller recoil energies for the data taken with both gases. Since the ranges of photons and deuterons differ by about a factor of about $\sqrt{2}$ for protons and deuterons of the same energy, it is not very likely that this mismatch is due to problems with the description of wall effects, but it could be due to a residual contribution of photon-induced events to the experimental spectra.

At 500 keV there is a clear difference in the angular distributions from ENDF/B-VII.0 and JENDL 4.0 as well as ENDF/B-VI.3. Only the ENDF/B-VII.0 distribution fits the measured spectra almost over the entire range of recoil deuteron energies. Unfortunately, it was not possible to obtain data for recoil protons stopped in H_2/CH_4 gas at this energy because the ranges already become too high so that wall effects would dominate the shape of the PH distribution.

4   Conclusions

From the present experiments it can be concluded that the angular distributions for $^2H(n,n)^2H$ at 500 keV are less backward peaked than predicted in JENDL 4.0 and are better represented by the ENDF/B-VII.0 distributions. The angular distribution from ENDF/B-VI.3 is considerably off for almost all neutron energies investigated. However, there are still open questions left about the influence of either a possible non-linearity in the PH response of the proportional counter or the incomplete discrimination of photon-induced events. Hence, further investigations are required.

Acknowledgment

References

[1] L. Canton, W. Schadow, and J. Haidenbauer, Eur. Phys. J. A **14** (2002) 225

[2] J.P. Svenne, L. Canton, K. Kozier, and L. Townsend, Proc. International Conference on Nuclear Data for Science and Technology 2007, Nice, April 22-27, 2007, DOI 10.1051/ndata:07208

[3] K.S. Kozier, Proc. International Conference on Nuclear Data for Science and Technology 2007, Nice, April 22-27, 2007, DOI 10.1051/ndata:07594

[4] P.G. Young, n + D Evaluation to 100 MeV, Release 3, ENDF/B-VI evaluation, distributed April, 1995

[5] Experimental Nuclear Reaction Data (EXFOR), available online: https://www-nds.iaea.org/exfor/exfor.htm

[6] M.B. Chadwick *et al*., Nucl. Data Sheets **107** (2006) 2931

[7] NEA Nuclear Data High-Priority Request List, available online: http://www.oecd-nea.org/dbdata/hprl/

[8] T.H.R. Skyrme, P.R.Tunnicliffe, A.G. Ward, Rev. Sci. Instr. **23** (1952) 204

[9] D. Schlegel, TARGET user's manual, PTB Laboratory Report PTB-6.42-05-2 (2005), Physikalisch-Technische Bundesanstalt Braunschweig, Germany

[10] E.F. Bennet, Nucl. Sci. Eng. **27** (1967) 16

[11] K. Shibata *et al*., J. Nucl. Sci. Technol. **48** (2011) 1

[12] J.F. Ziegler, SRIM-2013, available online: www.srim.org

[13] W. Breitung, Untersuchungen zur Energieabhängigkeit von *w* (Energieverlust/ Ionenpaar) für Protonen in Wasserstoff, Methan und H_2-CH_4 Gemischen im Hinblick auf Neutronenspektrumsmessungen mit Rückstoßprotonen-Proportionalzählrohren unterhalb 25 keV, KfK-Report KFK 1623 (1972), Kernforschungszentrum Karlsruhe, Germany

[14] F. Posny, J. Chary and V.D. Nguyen, Phys. Med. Biol. **32** (1987) 509